Charles University

Faculty of Science

Study programme: Molecular and Cell Biology, Genetics and Virology

Mgr. Katarína Vaškovičová

Changes in domain organization of the plasma membrane in the stress response

Změny doménového uspořádání plasmatické membrány v odpovědi na stres

Ph.D. thesis

Supervisor: doc. RNDr. Jan Malínský, Ph.D.

Prague, 2019

Prohlášení

Prohlašuji, že jsem závěrečnou práci zpracovala samostatně a že jsem uvedla všechny použité informační zdroje a literaturu. Tato práce ani její podstatná část nebyla předložena k získání jiného nebo stejného akademického titulu.

V Praze, 5.11.2019

Mgr. Katarína Vaškovičová

My contribution to the publications that are the basis of this Ph.D. thesis

Vaskovicova K., Stradalova V., Efenberk A., Opekarova M., and Malinsky J. (2015) **Assembly of fission yeast eisosomes in the plasma membrane of budding yeast: import of foreign membrane microdomains.** Eur J Cell Biol 94(1): 1-11.

I contributed to preparation of most of the plasmids and yeast strains used in the study. I contributed to a large portion of laser scanning microscopy experiments. I performed some of the data analysis. I participated in the writing of the manuscript and in the revision of the manuscript.

Vaškovičová K., Awadová T., Veselá P., Balážová M., Opekarová M., and Malinsky J. (2017) **mRNA decay is regulated via sequestration of the conserved 5'-3' exoribonuclease Xrn1 at eisosome in yeast.** Eur J Cell Biol 96(6) 591-599.

I designed the experiments and prepared all the plasmids and yeast strains that were constructed for the study. I performed substantial portion of laser scanning microscopy experiments. I performed all the qPCR analysis and all Western blot analysis and I analyzed most of the data. I prepared the manuscript draft and participated in the editing process. I also prepared all of the figures. I worked on the revision of the manuscript.

I confirm that the contribution of Mgr. Katarína Vaškovičová to the presented manuscripts, as stated above, is true.

Prague, 5.11.2019

doc. RNDr. Jan Malínský, Ph.D.
supervisor

Acknowledgements:

I would like to thank to my supervisor, doc. RNDr. Jan Malínský, Ph.D., for his guidance during my work in his laboratory. Thanks also for his useful suggestions regarding this dissertation thesis.

I would also like to thank to my colleagues and friends from the lab for their support and pleasant working atmosphere. Thank you to Petra Veselá, Dáša Folková, Martin Oškera and Suri Drápelová for all your help with the experiments and with everything else. Thank you to Vendy Strádalová for showing me what it means to be a great Ph.D. student. Thank you to Miri Opekarová for being extremely supportive in the hard times.

Rada by som tiež poďakovala svojej rodine a Rostíčkovi, ktorí vždy stáli pri mne a verili, že to všetko zvládnem.

Contents

Abstract

MCC/eisosomes are yeast plasma membrane microdomains that respond to changes in both extracellular and intracellular conditions and activate important stress-related signaling pathways. In this study, we investigated the function of MCC/eisosomes under the conditions of chronic glucose depletion. We found that MCC/eisosomes regulate mRNA decay under these conditions. Specifically, we demonstrated that the sequestration of the evolutionarily conserved Xrn1 exoribonuclease at MCC/eisosomes leads to the attenuation of its enzymatic activity. Modulation of activity by the enzyme localization may represent a novel and effective mechanism in regulation of biochemical pathways. Moreover, our results suggested that an MCC protein Nce102 might play a role in vacuolar fusion and lipid droplets degradation. We demonstrated that prolonged chronic glucose depletion induces the translocation of Nce102 from MCC to sterol-enriched microdomains in the vacuolar membrane. Deletion mutants lacking Nce102 and its functional homologue Fhn1 exhibited significant delay in vacuole maturation and in turnover of a lipid droplet marker Erg6.

The function of MCC/eisosomes in the stress response have been demonstrated in many fungal species. Similar to the microdomain function, also individual protein components of MCC/eisosomes are widely evolutionarily conserved. To further characterize this phenomenon, we tested the compatibility of *Saccharomyces cerevisiae* (*S. cerevisiae*) MCC/eisosome with MCC/eisosomal proteins from phylogenetically distant species *Schizosaccharomyces pombe* (*S. pombe*; *Sp*). We found that *S. cerevisiae* Pil1 and its homologue *Sp*Pil1 compete with each other and *Sp*Pil1 is able to substitute for Pil1 function in organizing *S. cerevisiae* MCC/eisosomes in cells lacking endogenous Pil1 protein. Similarly, Nce102 and its homologue *Sp*Fhn1 are competitors, albeit Nce102 is more effective than *Sp*Fhn1 in binding both Pil1- and *Sp*Pil1-organized eisosomes. In contrast, *S. pombe* homologue of the eisosome stabilizer Seg1, *Sp*Sle1, did not recognize Pil1 at the plasma membrane of *S. cerevisiae*, while it strongly interacted with its natural interaction partner *Sp*Pil1 under the same conditions. These observations shed not only the new light on principles of the MCC/eisosome organization, but also allowed us to reconstitute *S. pombe* MCC/eisosome in the plasma membrane of *S. cerevisiae*, which was capable to attract endogenous MCC proteins. Further tests would be necessary to prove whether the imported *S. pombe* microdomain preserves also its function in the stress response.

Abstrakt

MCC/eisosomy jsou mikrodomény kvasinkové plasmatické membrány. MCC/eisosomy vnímají změny extracelulárních a intracelulárních podmínek a aktivují důležité signální dráhy, které odpovídají na stres. V této studii jsme zkoumali funkci MCC/eisosomů za podmínek chronického nedostatku glukózy. Ukázali jsme, že za těchto podmínek MCC/eisosomy regulují degradaci mRNA. Konkrétně, sekvestrace evolučně konzervované exoribonukleázy Xrn1 na MCC/eisosomech vede ke snížení její enzymatické aktivity. Modulace enzymatické aktivity pomocí lokalizace enzymu může představovat nový a efektivní způsob regulace biochemických drah. Naše výsledky také naznačují, že MCC protein Nce102 může hrát úlohu ve fúzi vakuol a v degradaci lipidových partikulí. Odhalili jsme, že dlouhodobý nedostatek glukózy indukuje translokaci proteinu Nce102 z MCC mikrodomény do vakuolárních membránových mikrodomén bohatých na steroly. Mutanty, kterým chybí protein Nce102 a jeho funkční homolog Fhn1, vykazují signifikantní zpoždění v maturaci vakuol a v turnoveru markeru lipidových partikul, proteinu Erg6.

Funkce MCC/eisosomů v stresové odpovědi jsou zdokumentované ve velkém množství kvasinkových druhů. Podobně jako funkce těchto mikrodomén jsou i jednotlivé proteinové komponenty MCC/eisosomů evolučně konzervované. Abychom hlouběji charakterizovali tento jev, otestovali jsme kompatibilitu MCC/eisosomů v *Saccharomyces cerevisiae* (*S. cerevisiae*) s MCC/eisosomálními proteiny z fylogeneticky distantního druhu *Schizosaccharomyces pombe* (*S. pombe*, *Sp*). Zjistili jsme, že Pil1 a jeho homolog *Sp*Pil1 spolu kompetují a *Sp*Pil1 je schopný nahradit funkci endogenního Pil1 proteinu a organizovat MCC/eisosomy v *S. cerevisiae*. Podobně i Nce102 a jeho homolog *Sp*Fhn1 jsou kompetitory, i když Nce102 asociuje lépe než *Sp*Fhn1 jak s Pil1 tak s *Sp*Pil1 proteinem. Naproti tomu, homolog stabilizujícího proteinu Seg1 v *S. pombe*, *Sp*Sle1, nedokáže interagovat s Pil1 proteinem v plasmatické membráně *S. cerevisiae*, i když za stejných podmínek dokáže interagovat s jeho přirozeným interakčním partnerem, *Sp*Pil1 proteinem. Tato pozorování objasnila nejenom základní principy organizace MCC/eisosomů, ale také nám umožnila rekonstituovat *S. pombe* MCC/eisosomy v plasmatické membráně *S. cerevisiae*. Tyto eisosomy tvořené proteiny z *S. pombe* přitom byly schopné atrahovat endogenní MCC/eisosomální proteiny. Bude zajímavé zjistit, jestli si přenesená mikrodoména z *S. pombe* zachovává i svou funkci v stresové odpovědi u *S. cerevisiae*.

List of abbreviations

A. gossypii	*Ashbya gossypii*
A. fumigatus	*Aspergillus fumigatus*
A. nidulans	*Aspergillus nidulans*
ABA	benzamidine
arg	arginine
B. bassiana	*Beauveria bassiana*
BAR	Bin-Amphiphysin-Rvs
C. albicans	*Candida albicans*
CHX	cycloheximide
exp	exponential
F-BAR	FCH-BAR
FLPs	flavodoxin-like proteins
FM4-64	N-(3-triethylammoniumpropyl)-4-(6-(4-(diethylamino) phenyl) hexatrienyl) pyridinium dibromide, Fei-Mao™
glc	glucose
h	hours
his	histidine
I-BAR	inverse BAR
KanMX	kanamycin
LCBs	long chain bases
LDs	lipid droplets
leu	leucine
log	logarithmic
lys	lysine
MAP	mitogen-activated protein
MCC	membrane compartment of Can1
MCP	membrane compartment of Pma1
MCT	membrane compartment of TORC2
met	methionine
MFα2	mating factor α 2
min	minutes

clonNAT	nourseothricin
ON	overnight
P-bodies	processing bodies
PCR	polymerase chain reaction
PDK1	phosphoinositide-dependent protein kinase-1
PH	pleckstrin homology
$PI(4,5)P_2$	phosphatidylinositide(4,5)bisphosphate
PMSF	phenylmethylsulfonyl fluoride
PROM	promoter
qPCR	quantitative PCR
RT	room temperature
r.u.	relative units
S. cerevisiae	*Saccharomyces cerevisiae*
S. pombe	*Schizosaccharomyces pombe*
ser	serine
SPT	serine palmitoyltransferase
thr	threonine
TMD	transmembrane domain
TORC2	target of rapamycin complex 2
trp	tryptophan
ura	uracil
vac	vacuoles / vacuolar
wt	wild type

1. Introduction

The plasma membrane ensures various biological functions – it not only delimits the cell interior, but acts as a semipermeable barrier that plays crucial roles in secretion, nutrient transport, sensing and responding to external stimuli, signal transduction and is also important for pathogen defense (Alberts et al., 2008a, 2008b; Douglas and Konopka, 2016; Karp et al., 2016). As plasma membrane has to fulfill many different functions, the components of the plasma membrane are not distributed homogeneously; rather, plasma membrane is compartmentalized into distinct microdomains (Fig. 1). In fact, plasma membrane is thought to be a mosaic of microdomains (Spira et al., 2012).

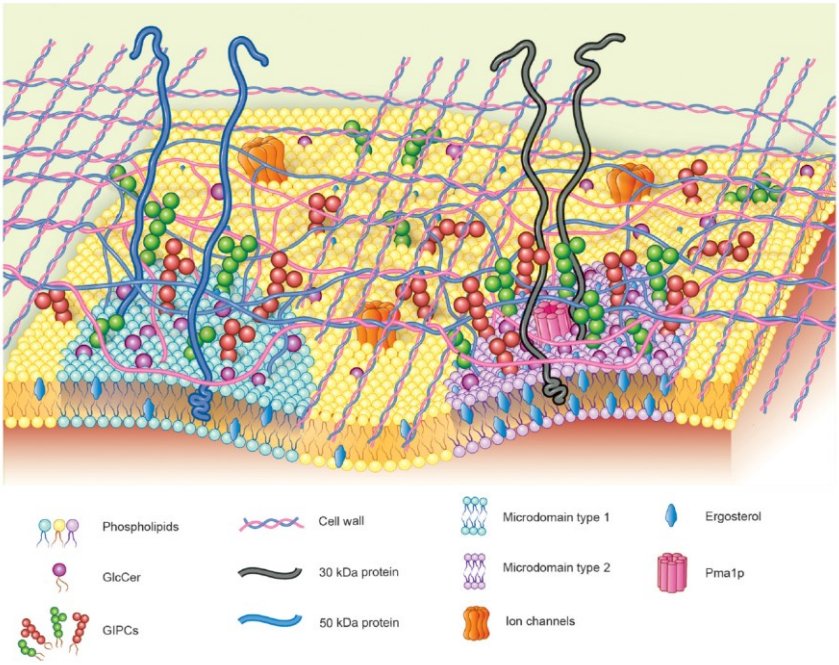

Figure 1. Plasma membrane compartmentalization.
The figure is adapted from (Guimarães et al., 2014).

The specific protein and lipid composition, dynamics and size of plasma membrane microdomains can vary greatly according to the specialized function of each microdomain. For example, the whole plasma membrane of epithelial cells is divided into two parts: the apical and the basolateral part that are separated by tight junctions (Fig. 2A). This ensures directed nutrient flow from the gut lumen to blood vessels (Lodish et al., 2008). Neuron plasma

membrane has specific composition on neuronal synapses that can have up to few µm in diameter (Fig. 2B). Synaptic vesicles fuse specifically with the pre-synaptic membrane regions to release neurotransmitter and specific receptors that detect the signal are found concentrated in post-synaptic membrane regions (Alberts et al., 2008c). Another example of specialized plasma membrane microdomains are caveolae, 50-80nm invaginations of plasma membrane of endothelial cells and adipocytes (Fig. 2C). They are able to sense mechanical stress and it is believed that they play a role in non-canonical endocytosis (Parton, 2018).

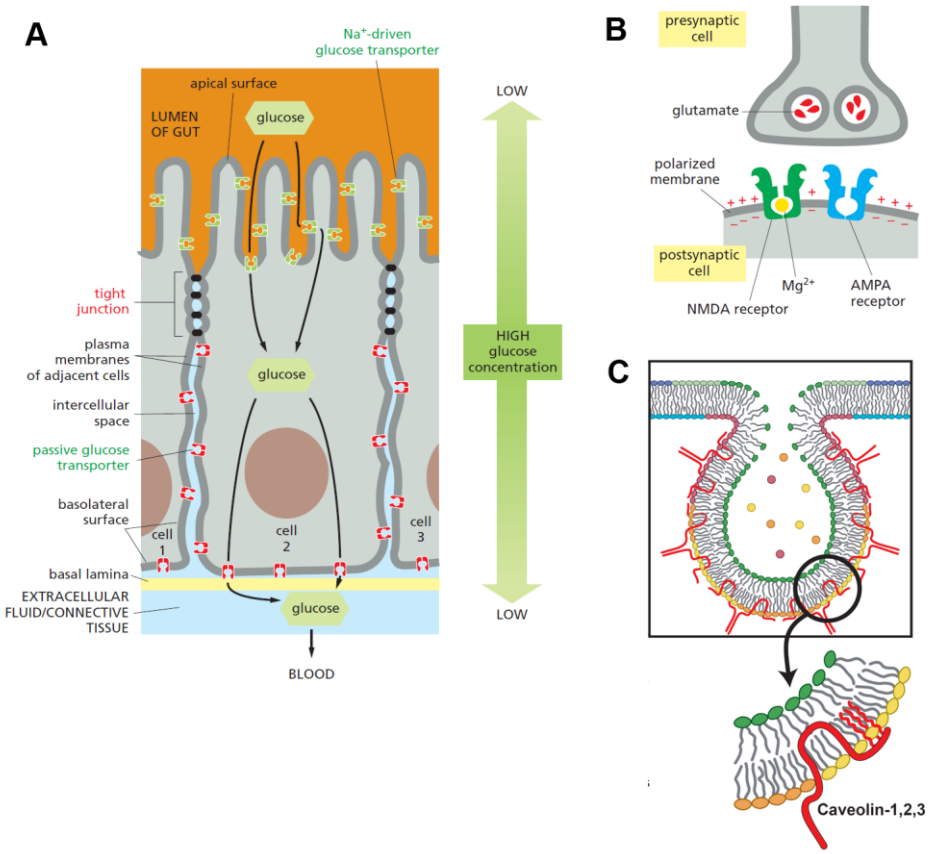

Figure 2. Examples of specific plasma membrane microdomains.

Intestinal epithelial cells with apical and basolateral membranes (A) (Alberts et al., 2015a).

Neuronal synapse with pre-synaptic cell with synaptic vesicles and post-synaptic cell with specific receptors in the membrane (B) (Alberts et al., 2015b).

Caveolae (C) (Parton, 2001).

In nature, yeast cells encounter with a wide range of environmental stresses – such as dehydration, hot and cold temperatures, lack of essential nutrients and even exposure to harmful substances. In order to survive, yeast cells have to sense these conditions and adapt to them. In *Saccharomyces cerevisiae* (*S. cerevisiae*), plasma membrane microdomain called membrane compartment of Can1 (MCC) (Malinska et al., 2003) supported by the complex of cytosolic proteins called eisosome (Walther et al., 2006) was shown to play an important role in this process. MCC/eisosomes accommodate many transmembrane as well as cytosolic proteins and act as signaling hubs in the plasma membrane that sense stress conditions, integrate them and transmit them to evoke an appropriate response (Foderaro et al., 2017; Malinsky and Opekarová, 2016). Importantly, although the variability of yeast species is extremely diverse, and their surviving techniques as well, MCC/eisosomes are widely conserved in fungi kingdom. This strongly suggests that MCC/eisosomes play a crucial role in stress response.

In my thesis, we investigated the changes in the MCC/eisosome microdomain during the specific stress conditions –upon the chronic glucose depletion. We focused on two proteins that change their localization upon the drop in glucose concentration in the medium. The exoribonuclease Xrn1 localizes to cytoplasm in logarithmic cells (which have glucose in the medium) and accumulates at MCC/eisosomes in post-diauxic cells (which lack glucose in the medium). We aimed to determine the effect of changed Xrn1 localization on Xrn1 enzymatic function. In contrast to Xrn1, Nce102 protein accumulates at MCC/eisosomes in logarithmic cells (with glucose in the medium) and upon chronic glucose depletion, it partially translocates from MCC/eisosomes into the cell interior. We investigated this intracellular localization in detail and aimed to identify the role that Nce102 might play in the inner membranes.
MCC/eisosomal proteins are widely conserved across fungi kingdom and Xrn1 enzyme is conserved from yeast up to mammals and humans. Moreover, MCC/eisosome function in stress response seems to be conserved as well. Therefore, we were interested whether also the structural abilities of the MCC/eisosome proteins are preserved in evolution. To reach this aim, we investigated the compatibility of *S. cerevisiae* and *S. pombe* MCC/eisosomal proteins in the plasma membrane of *S. cerevisiae*.

2. Current state of knowledge

2.1 Plasma membrane microdomains in yeast

The first described and so far, the most studied yeast plasma membrane compartment is called **membrane compartment of Can1** (**MCC**). It was discovered in 2003, when it was shown that fluorescently labeled arginine permease Can1 localizes to distinct foci in the yeast plasma membrane (Malinska et al., 2003) (Fig. 3). These foci are stable in time and are not disturbed upon disruption of actin cytoskeleton, microtubules or cell wall (Malinska et al., 2004, 2003; Walther et al., 2006). MCC microdomains are organized by cytoplasmic protein complexes called **eisosomes** (Walther et al., 2006) into furrow-like invaginations visible using electron microscopy (Stradalova et al., 2009). MCC/eisosomes play various crucial functions in cells. MCC/eisosomes organize plasma membrane and ensure balance of sphingolipid and phospholipid composition in cells. They accumulate many stress-responsive proteins and play a role in the cellular response to various stresses. They represent sensing and signaling hubs at the plasma membrane (Malinsky and Opekarová, 2016).

Importantly, other yeast plasma membrane compartments were visualized using fluorescence and confocal microscopy. Plasma membrane H^+ ATPase Pma1 was shown to be accumulated in domain called the **membrane compartment of Pma1** (**MCP**) (Malinska et al., 2003) (Fig. 3). In 2003, it appeared that Pma1 resides in all the areas of the plasma membrane except MCC/eisosomes, forming "network-like" microdomain (Fig. 3A). Later on, however, the stimulated emission depletion (STED) microscopy, which provides higher spatial resolution, followed by the image deconvolution showed that MCP, similarly to MCC, consists of isolated plasma membrane patches (Malinsky and Opekarová, 2016). Although Pma1 is an essential and in plasma membrane abundant protein (forming the driving force for nutrient uptake and regulation of cytoplasmic pH), the exact reason of the Pma1 compartmentalization into a microdomain is currently unknown.

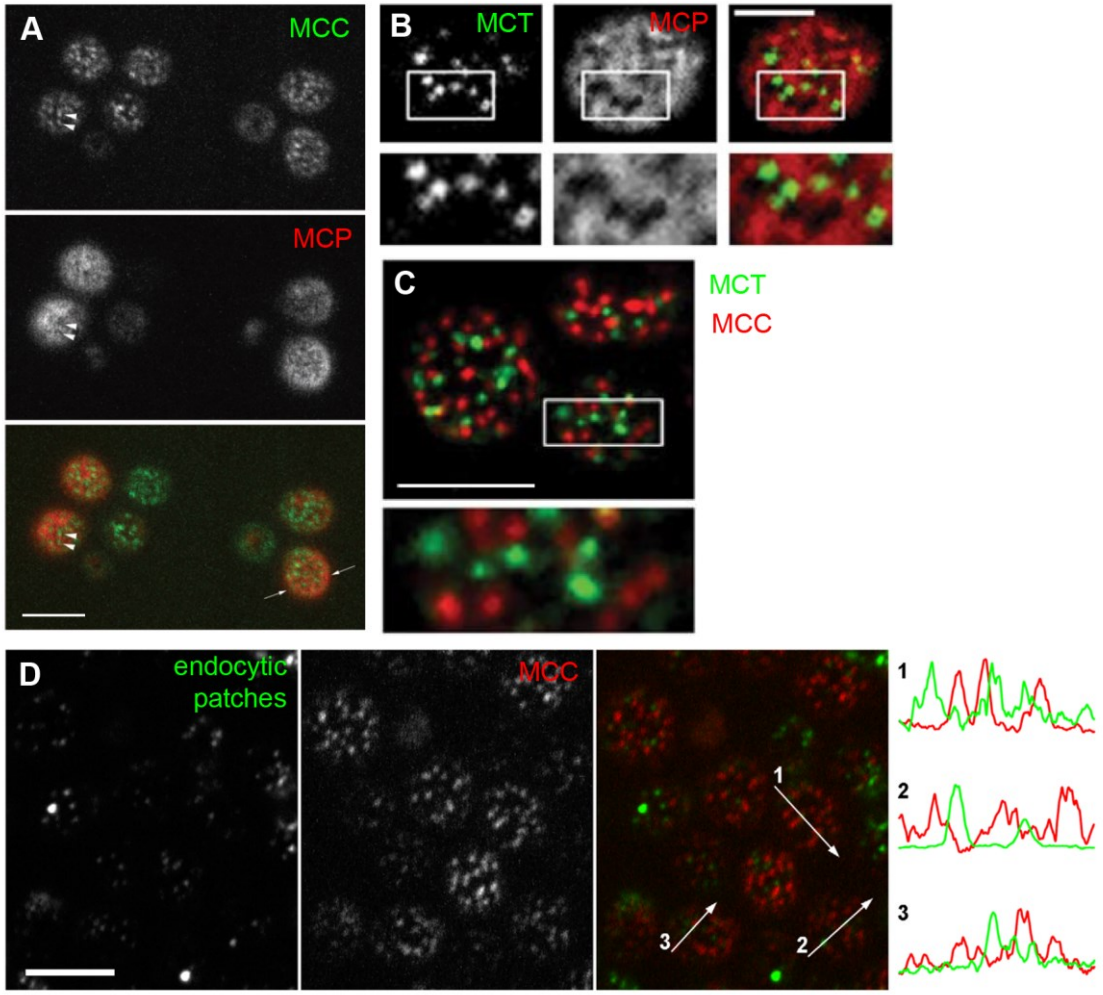

Figure 3. *S. cerevisiae* plasma membrane domains.

Membrane compartment of Can1 (MCC) marked by Can1-GFP does not overlap with membrane compartment of Pma1 (MCP) marked by Pma1-mRFP (A). Bar: 5 μm.

Membrane compartment of TORC2 (MCT) marked by Bit61-GFP does not overlap with MCP (marked by Pma1-RFPmars) (B) or MCC (marked by Lsp1-mRFP) (C). Bars: 2.5 μm (B), 5 μm (C).

Endocytic patches marked by Ede1-GFP do not overlap with MCC (marked by Sur7-mRFP (D). Bar: 5 μm.

The figures are adapted from (Berchtold and Walther, 2009; Malinska et al., 2003; Stradalova et al., 2012).

The components of the target of rapamycin complex 2 (TORC2) were found to localize in microdomain called **membrane compartment of TORC2** (**MCT**) (Berchtold and Walther, 2009) (Fig. 3). Bit61 and Avo1-3 proteins colocalize in distinct patches that do not overlap with either MCC or MCP (Fig. 3B, C). As shown by FRAP experiments, MCT patches are highly dynamic. The plasma membrane targeting of MCT components is dependent on the C-terminal pleckstrin homology (PH)-like domain of Avo1 that directly interacts with phosphatidylinositol(4,5)bisphosphate ($PI(4,5)P_2$) in the plasma membrane. The proper plasma

membrane targeting of TORC2 is essential for cell survival under plasma membrane stress conditions (Berchtold et al., 2012).

Endocytic sites can also be regarded as a specific type of a highly dynamic and transient plasma membrane microdomain where proteins of clathrin-mediated endocytosis are assembled (Fig. 3). Endocytic machinery comprises of more than 50 specific proteins that sequentially bind to and unbind from the endocytic sites and promote formation of endocytic vesicles (Kukulski et al., 2012). This process also involves the plasma membrane bending that is supported by the actin polymerization of Abp1-3 proteins and N-BAR (Bin, Amphiphysin, Rvs) domain-containing amphiphysins Rvs161/167 that cause the neck tubulation and vesicle scission. Still, only a little is known about the endocytic site selection. Most probably, early protein Ede1 is involved in this process (Stimpson et al., 2009). Importantly, endocytic sites are not homogeneously distributed throughout the plasma membrane, they do not occur at sites of plasma membrane with underlying cortical endoplasmic reticulum and at MCC/eisosomes (Fig. 3D) (Stradalova et al., 2012).

The examples above document only few examples of distinct plasma membrane microdomains. Presumably, no protein of the plasma membrane spreads over the entire plasma membrane homogeneously; it seems that there is always a specific microdomain in which the protein resides. Therefore, the plasma membrane is considered to be a patchwork of coexisting microdomains encompassing different sets of proteins (Spira et al., 2012). The domains may have different kinds of morphology – ranging from distinct patches to nearly continuous networks. Importantly, the protein transmembrane domains (TMD) define the protein localization within the plasma membrane and consequently affect also protein functionality (Spira et al., 2012).

2.2 MCC/eisosome structure

MCC is the plasma membrane compartment accumulating many different transmembrane proteins - nutrient transporters and proteins of Sur7- and Nce102-families (Grossmann et al., 2008; Malinska et al., 2004). When a protein accumulating at MCC is observed under fluorescence microscope, MCC appears as distinct patches in the plasma membrane (Fig. 4A). One cell forms approximately 50-80 MCC patches (Malinsky et al., 2010).

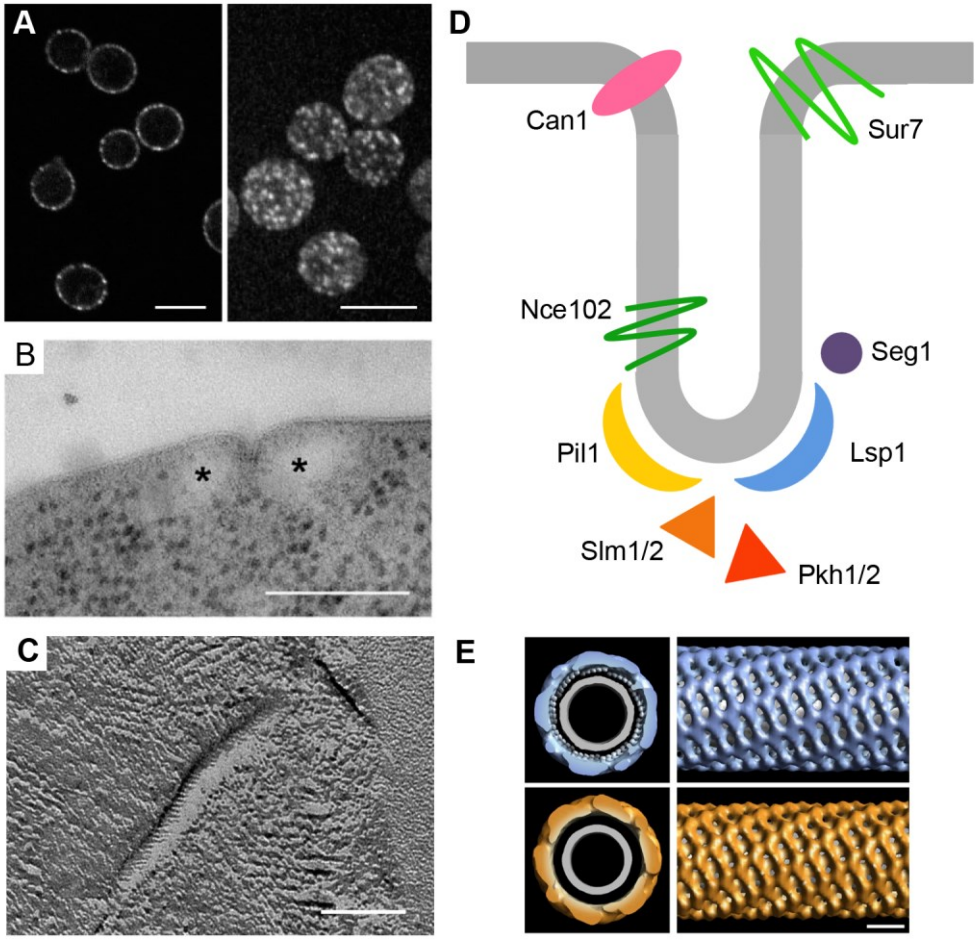

Figure 4. Different types of *S. cerevisiae* MCC/eisosome visualization, theoretical model of MCC/eisosome structure and 3D reconstruction of tubular filaments formed by Pil1 and Lsp1 proteins.

Confocal fluorescence image of Can1-GFP localizing to MCC/eisosomes (A). Bar: 5 µm.

Transmission electron microscopy image of furrow-like plasma membrane invagination at the site of MCC/eisosome (B). Bar: 500 nm.

Freeze-fracture replica image of single furrow-like invagination (C). Bar: 100 nm.

The model of MCC/eisosomes (D).

The 3D reconstruction of Lsp1 (blue) and Pil1 (yellow) filaments that are formed by binding of the respective protein to the membrane of liposomes. Based on the cryo-electron microscopy tomography. Bar: 10 nm.

The figures are adapted from (Karotki et al., 2011; Malinska et al., 2003; Stradalova et al., 2009).

Main structural proteins of eisosomes are Pil1 and Lsp1 proteins – BAR-domain proteins that are able to bind the membrane and bend it (Olivera-Couto et al., 2011; Ziółkowska et al., 2011). Pil1 and Lsp1 can tubulate the membrane of vesicles into tubular filaments *in vitro* (Fig. 4D) (Karotki et al., 2011). At the sites of MCC, Pil1 and Lsp1 oligomerize and form hemi-tubular scaffolds that help to bend the membrane of MCC into 200-300nm long, 50-100nm deep

furrow-like invaginations that can be observed using electron microscopy (Fig. 4B, C) (Stradalova et al., 2009). Interestingly, immuno-electron microscopic study revealed that Sur7 localizes to positively curved boundary of MCC/eisosome invaginations, whereas Pil1 was visualized at the bottom of these invaginations (Fig. 4D) (Stradalova et al., 2009). On the concave surface of the invaginations, fine striations can be observed (Fig. 4C) (Gross et al., 1978; Karotki et al., 2011). It was proposed that these striations result from binding of eisosome scaffold proteins Pil1 and Lsp1 to the plasma membrane (Karotki et al., 2011). The cryo-fluorescence microscopy combined with electron cryo-tomography showed that Pil1 binds to membrane invaginations of various depths, but only in the highly curved invaginations, Pil1 creates a dense protein coat (Bharat et al., 2018).

In addition to the core proteins, numerous cytosolic or plasma membrane proteins interact with MCC/eisosomes in dependence on the physiological conditions of the cell – e.g. Slm1, Pkh1/2, Xrn1 (Berchtold et al., 2012; Fröhlich et al., 2009; Grousl et al., 2015; Walther et al., 2007) (Fig. 4C).

2.3 MCC/eisosome composition

The list of proteins that were shown to localize to or physically interact with *S. cerevisiae* MCC/eisosomes is shown below (Table 1). Where known, the functions of the proteins and the presence of the conserved domains or motifs in the proteins are described (Table 1).

Table 1. Components of *S. cerevisiae* MCC/eisosomes.

Protein	Function	Domains, characteristics	Localization reference
MCC			
Can1	Arg permease		(Malinska et al., 2003)
Fur4	Ura permease		(Malinska et al., 2004)
Tat2	Trp permease		(Grossmann et al., 2007)
Lyp1	Lys permease		(Bianchi et al., 2018)
Mup1	Met permease		(Busto et al., 2018; Moharir et al., 2018)
Sur7		Sur7-family tetraspan	(Malinska et al., 2003; Young et al., 2002)
Fmp45		Sur7-family tetraspan	(Young et al., 2002)
Pun1		Sur7-family tetraspan	(Grossmann et al., 2008)
Ynl194c		Sur7-family tetraspan	(Young et al., 2002)
Nce102	SL sensing	Nce102-family tetraspan	(Grossmann et al., 2008)
Fhn1		Nce102-family tetraspan	(Grossmann et al., 2008)
Eisosome			
Pil1	Core eisosome protein	BAR domain	(Walther et al., 2006)
Lsp1	Core eisosome protein	BAR domain	(Walther et al., 2006)
Seg1	MCC/eisosome structure		(Moreira et al., 2012)
Pkh1	Ser/Thr protein kinase involved in SL signaling		(Luo et al., 2008; Roelants et al., 2002; Walther et al., 2007; Zhang et al., 2004)
Pkh2	Ser/Thr protein kinase involved in SL signaling	PH domain	(Luo et al., 2008; Roelants et al., 2002; Walther et al., 2007; Zhang et al., 2004)
Slm1		F-BAR domain, PH domain, glutamine and asparagine rich domain	(Fadri et al., 2005; Grossmann et al., 2008)
Slm2		F-BAR domain, PH domain, glutamine and asparagine rich domain	(Fadri et al., 2005)
Eis1		Coiled-coil	(Aguilar et al., 2010; Deng et al., 2009; Grossmann et al., 2008)
Mdg1		Carbohydrate binding	(Grossmann et al., 2008)
Ygr130c		Coiled-coil	(Deng et al., 2009; Grossmann et al., 2008)
Pst2		Similar to flavodoxin-like proteins (FLPs)	(Grossmann et al., 2008)
Rfs1		Similar to flavodoxin-like proteins (FLPs)	(Grossmann et al., 2008)
Ycp4		Similar to flavodoxin-like proteins (FLPs)	(Deng et al., 2009; Grossmann et al., 2008)
Rgc1		F-BAR domain	(Krogan et al., 2006)
Aim3		Glutamine and proline rich	(Krogan et al., 2006)
Mrp8		Coiled-coil	(Collins et al., 2007; Ito et al., 2001; Yu et al., 2008)
Sap1		Coiled-coil	(Yu et al., 2008)
Yta6		Coiled-coil	(Ho et al., 2002)
Msc3			(Moreira et al., 2009; Yu et al., 2008)
Ymr086w			(Deng et al., 2009; Krogan et al., 2006)

2.3.1 Protein composition of MCC

MCC is the first membrane microdomain that was described as the microdomain with specific protein composition. In 2003, MCC was visualized by fluorescently-tagged arginine (Arg) permease **Can1** - Can1 localized to distinct and evenly distributed patches. (Malinska et al., 2003). Later, several other nutrient transporters like uracil (Ura) permease **Fur4** and tryptophan (Trp) permease **Tat2** were reported to be enriched in MCC (Grossmann et al., 2007; Malinska et al., 2004). Recently, also lysine (Lys) permease **Lyp1** and methionine (Met) permease **Mup1** were shown to localize to MCC/eisosomes (Collins et al., 2007; Moharir et al., 2018). While inherent *S. cerevisiae* energy-independent hexose permeases do not localize to MCC, the hexose/H^+ symporter ***Ck*Hup1** from the green alga *Chlorella kessleri* does when it is heterogeneously expressed in yeast *S. cerevisiae* (Grossmann et al., 2006). The sequence important for targeting of the nutrient transporters into MCC was not identified. However, recent study shows that transporter proteins with large cytoplasmic domains (such as Pma1) are excluded from MCC/eisosomes (Bianchi et al., 2018). The authors propose that the localizations of transporter proteins into microdomains depend on "a combination of slow lateral diffusion, steric exclusion, and conditional trapping in membrane compartments" (Bianchi et al., 2018).

The accumulation of nutrient transporters at MCC/eisosomes depends also on the availability of their specific substrates in the medium (Grossmann et al., 2008). Nutrient transporters accumulate in MCC foci when their respective substrates are not present in the media. In this situation, transporters are protected from the turnover. Upon the addition of their specific substrate, the transporters leave MCC/eisosomes, become more homogeneous in the plasma membrane and also become more accessible for endocytic machinery. This mechanism of regulation of transporter endocytosis seems to be identical for Can1 (Bianchi et al., 2018; Gournas et al., 2018, 2017; Grossmann et al., 2008), Fur4 (Grossmann et al., 2008; Moharir et al., 2018), Mup1 (Busto et al., 2018; Moharir et al., 2018) and Lyp1 (Bianchi et al., 2018).

It was shown that it is the transporter conformation that regulates the accumulation of Can1 at MCC/eisosomes (Gournas et al., 2018). When Can1 is in outward-facing open conformation (without arginine present), it accumulates at MCC/eisosomes. Upon arginine addition, Can1 becomes to transport arginine and changes its conformation into the inward-facing state (Gournas et al., 2017). This leads to the dissipation of Can1 into the surrounding membrane and to uncovering of N-terminal cytosolic tail of Can1 (Gournas et al., 2018, 2017). The accessible

N-terminal cytosolic tail of Can1 is then targeted by the α-arrestin Art1 and ubiquitin ligase Rsp5 and the subsequent ubiquitylation of the transporter results in the transporter endocytosis (Ghaddar et al., 2014; Gournas et al., 2018, 2017). Similar conformation change was observed also in methionine permease Mup1 upon methionine addition (Busto et al., 2018).

The Sur7-family of proteins consists of **Sur7** protein and its homologues – **Fmp45, Ynl194c** and **Pun1**. They are all transmembrane proteins with four transmembrane segments. Sur7 and its homologues Fmp45 and Ynl194c were described to colocalize in cortical patches already in 2002 (Young et al., 2002) and they were found to be a part of the MCC in 2004 (Malinska et al., 2004). Later on, Pun1 was also found to accumulate in MCC (Grossmann et al., 2008).
Sur7 is one of the most stable proteins in the plasma membrane (Thayer et al., 2014) and is considered to be the marker of MCC/eisosomes, because it stably associates with MCC/eisosomes. However, upon the deletion of Sur7, MCC/eisosome structure seems to be preserved (Alvarez et al., 2008; Grossmann et al., 2008; Stradalova et al., 2009). These cells also have some alterations in the sphingolipid composition of the plasma membrane (Young et al., 2002).
Ynl194c and Fmp45 protein expression levels in growing cultures are not detectable by fluorescence microscopy, but upon overexpression, they partly colocalize with Sur7-marked MCC (Young et al., 2002).

Another family of proteins that localize to MCC is the Nce102-family of proteins consisting of **Nce102** and its homologue **Fhn1** (Grossmann et al., 2008). These are also transmembrane proteins and both accumulate in MCC (Loibl et al., 2010). In aerobically-grown cells, Fhn1 expression level is significantly lower than that of Nce102, suggesting that the expression level of these two proteins may be determined by specific growth conditions (Gasch et al., 2000; Loibl et al., 2010). For example, Fhn1 expression is slightly enhanced in late stationary phase (Gasch et al., 2000).
Nce102 is essential for the MCC/eisosome stabilization. Cells lacking Nce102 exhibit decrease in number of MCC/eisosome patches (Fröhlich et al., 2009). The residual MCC/eisosomes do not form furrows; instead, they appear as flat, smooth areas in the plasma membrane, suggesting that besides Pil1 and Lsp1, also Nce102 is necessary for the invagination formation (Stradalova et al., 2009). Moreover, arginine permease Can1 becomes more homogeneously distributed in these cells (Grossmann et al., 2008). This phenotype can be rescued by the Fhn1 overexpression (probably because endogenous levels of Fhn1 are too low) suggesting functional conservation

between Nce102 and Fhn1 (Loibl et al., 2010). Importantly, the C-terminal six amino acids of Nce102 are strictly conserved and truncated version of Nce102 can neither localize to MCC nor attract Can1 into them (Loibl et al., 2010).
Importantly, the localization of Nce102 changes with sphingolipid levels in the plasma membrane and Nce102 was suggested to play a role in sphingolipid homeostasis (Berchtold et al., 2012; Fröhlich et al., 2009); see also chapter 2.6.3).

2.3.2 Lipid composition of MCC

MCC domains have a specific lipid composition. It was shown that sterol-binding dye filipin colocalizes with Sur7 and Can1 proteins, showing that MCC membrane is enriched in sterols (Grossmann et al., 2007). Consistently with this, the localization and trafficking of nutrient transporters to the plasma membrane is dependent on ergosterol biosynthesis (Malinska et al., 2003; Pineau et al., 2008; Umebayashi and Nakano, 2003). In the case of Can1, also phosphatidylethanolamine (PE) and sphingolipids are required (Malinska et al., 2003; Opekarová et al., 2002). Additionally, core eisosomal protein Pil1 binds preferentially to $PI(4,5)P_2$-enriched membranes *in vitro*, and attracts $PI(4,5)P_2$-specific phosphatase Inp51 to the eisosome *in vivo*, leading to the suggestion that MCC is also enriched in $PI(4,5)P_2$ (Frohlich et al., 2014; Kabeche et al., 2015b, 2014; Karotki et al., 2011; Olivera-Couto et al., 2011).

2.3.3 Protein composition of eisosomes

Core eisosomal **Pil1** and **Lsp1** proteins contain banana-shaped BAR-domain in the central part of the protein as seen from their molecular structure reconstruction (Olivera-Couto et al., 2011; Ziółkowska et al., 2011). The BAR domains bind to the membranes and force them to adopt curved conformation (Mim and Unger, 2012; Nishimura et al., 2018). *In vitro* experiments showed that purified recombinant Pil1 and Lsp1 proteins form filamentary structures and are able to tubulate liposomes, especially the membranes enriched in $PI(4,5)P_2$ (Karotki et al., 2011; Olivera-Couto et al., 2011). *In vivo*, these proteins are also able to form tubular structures when expressed in COS-7 cells (Olivera-Couto et al., 2011). In *S. cerevisiae*, Pil1 and Lsp1 help to curve the membrane of MCC into the characteristic furrow-like invaginations (Stradalova et al., 2009). Positively charged patch of amino acids on the Pil1 concave surface is important for normal Pil1 localization and function (Olivera-Couto et al., 2011; Ziółkowska et al., 2011).

The number and size of eisosomes is determined by the level of Pil1 protein (Moreira et al., 2009). Additionally, the phosphorylation status of Pil1 defines the degree of eisosome assembly/disassembly ((Luo et al., 2008; Walther et al., 2007; Zhang et al., 2004); see also chapter 5.4.3).
Importantly, Pil1 is indispensable for MCC/eisosome formation. In the plasma membrane of cells lacking Pil1, no furrows can be observed (Stradalova et al., 2009). Instead, the structure collapses into big aggregates called eisosome remnants where Lsp1 accumulates (Walther et al., 2006). Plasma membrane transporters are homogeneous in the plasma membrane of these cells and Sur7 is still partly patchy, but the number and distinctness of the patches is significantly lower (Grossmann et al., 2008; Stradalova et al., 2012). This is in contrast to cells lacking Lsp1 that exhibit normal MCC/eisosome organization (Walther et al., 2006). Therefore, it can be assumed that Pil1 plays a main structural role of eisosomes and Lsp1 has only additional or modulatory function.

Another stable component of eisosomes is **Seg1**. Seg1 is important for eisosome formation and architecture (Moreira et al., 2012). Seg1 binds the membrane through its polybasic C-terminus. Presumably, it forms a platform where other eisosomal proteins can assemble (Moreira et al., 2012). Specifically, Seg1 is important for efficient incorporation of Pil1 into eisosomes as cells lacking Seg1 exhibited lower number of eisosomes and higher cytoplasmic pool of Pil1. Using mass spectrometry, Seg1 was shown to interact directly with Pil1 as well as with other eisosome components: Lsp1, Eis1 and Ygr130c (Moreira et al., 2012).
Seg1 affects also the shape of eisosomes (Moreira et al., 2012). In cells lacking Seg1, deeper, irregularly-shaped furrows are formed. In cells overexpressing Seg1, long, rod-shaped eisosomes that contain also other eisosomal proteins occur (Moreira et al., 2012).

Pkh1 and **Pkh2** are essential, evolutionarily conserved serine/threonine protein kinases and homologues of mammalian phosphoinositide-dependent protein kinase-1 (PDK1) (Casamayor et al., 1999). They are master regulators of AGC-family of protein kinases. They regulate conserved protein kinases Ypk1/2, Sch9 and Pkc1 (Roelants et al., 2004; Voordeckers et al., 2011). By modulating the activity of these kinases, Pkh1 and Pkh2 are involved in processes such as sphingolipid homeostasis, endocytosis, cell growth, stress response and cell wall integrity (deHart et al., 2002; Friant et al., 2001; Inagaki et al., 1999; Ke Liu et al., 2005; Luo et al., 2008; Niles et al., 2014; Roelants et al., 2002; Voordeckers et al., 2011).

The Pkh1/2 activity was shown to be regulated by the sphingolipid precursors, long chain bases (LCBs; (K. Liu et al., 2005; Ke Liu et al., 2005)). Pkh1 and Pkh2 were found to localize to the MCC/eisosomes in logarithmic cells, but they have also a significant cytoplasmic pool in these cells, suggesting they are important for many other activities (Roelants et al., 2002; Walther et al., 2007). Pkh2 possesses a phosphoinositide-binding PH domain (pleckstrin homology domain) that was hypothesized to be involved in eisosome targeting (Olivera-Couto et al., 2015).

Slm1 and **Slm2** are essential proteins known to have a role in actin cytoskeleton organization, sphingolipids homeostasis and cell growth (Audhya et al., 2004; Tabuchi et al., 2006). Slm1 and Slm2 possess PH domains that are important for their plasma membrane recruitment and PI(4,5)P_2 binding (Fadri et al., 2005; Yu et al., 2004). For their interaction with eisosomes, they need also their F-BAR domains (Olivera-Couto et al., 2011).

Xrn1 is an evolutionarily conserved 5′-3′ exoribonuclease that is responsible for the majority of cytoplasmic mRNA degradation in *S. cerevisiae* cells (Haimovich et al., 2013; Nagarajan et al., 2013). Xrn1 was shown to be localized to cytoplasm or to cytosolic ribonucleoprotein assemblies called processing bodies (P-bodies), where it was accumulated together with mRNAs and other components of mRNA decay machinery (Hu et al., 2009; Parker and Sheth, 2007). Importantly, in 2015, Xrn1 was also shown to be sequestered at MCC/eisosomes specifically in post-diauxic cells, e.g. the cells with chronic lack of glucose (Grousl et al., 2015).

Genome-wide screens identified other known MCC/eisosomal proteins. Visual analysis of the yeast GFP-tagged protein database identified Eis1, Mdg1, Ygr130c, Pst2, Rfs1 and Ycp4 as MCC/eisosomal proteins (Grossmann et al., 2008). Rgc1, Aim3, Mrp8, Sap1, Yta6, Msc3, Ymr086e were identified using affinity chromatography/mass spectrometry or yeast two-hybrid system (Collins et al., 2007; Deng et al., 2009; Ho et al., 2002; Ito et al., 2001; Krogan et al., 2006; Yu et al., 2008). However, little is known about these proteins and their role in either the MCC/eisosome structure or function.

Eis1 was shown to play a role in eisosome assembly as cells lacking Eis1 have larger cytoplasmic pool of Pil1 and Lsp1 than wild type cells (Aguilar et al., 2010).

2.4 Assembly and dynamics of MCC/eisosomes

2.4.1 Assembly of MCC/eisosomes *de novo*

MCC/eisosomes are formed *de novo* in growing buds (Moreira et al., 2009; Young et al., 2002). They form in buds larger than a certain size, start to appear at the bud neck and their formation proceeds in a polar manner from the bud neck to the bud tip (Moreira et al., 2009).

As the level of Pil1 protein determines the number and size of MCC/eisosomes, the proper number and length of emerging eisosomes is ensured by the cell cycle-regulated expression of Pil1 protein (Moreira et al., 2009). In dividing cells (G2/M phase), when new membrane and new eisosomes are being formed in the daughter cell, the expression of Pil1 protein is higher than in non-dividing cells (G1 phase). These results were confirmed both at the level of Pil1 protein fluorescence and mRNA level (Moreira et al., 2009).

Possibly, Seg1 is the first protein that appears at the site of the future MCC/eisosome and recruits other MCC/eisosomal proteins, especially Pil1 and Lsp1, but possibly also Nce102, that further shape and stabilize the microdomain structure (Moreira et al., 2012).

2.4.2 Dynamics of MCC/eisosomes

MCC/eisosomes were regarded as one of the most stable microdomains in yeast cells. In mature cells, MCC/eisosomes are distributed randomly with a certain constant density (Moreira et al., 2009). MCC/eisosomes were reported not to change their number, size, orientation or distribution as long as for 30 minutes of the time-course of experiments (Malinska et al., 2003; Walther et al., 2006; Young et al., 2002).

Using more advanced fluorescence microscopy techniques, however, it was shown that MCC/eisosomes are dynamic at the molecular level. In 2015, Olivera-Couto and co-workers used fluorescence fluctuation analytical methods to show that eisosomes can actively exchange core Pil1/Lsp1 heterodimers with the cytoplasm, where the heterodimers can diffuse freely (Olivera-Couto et al., 2015). In 2017, Lacy and co-workers employed Single-molecule Recovery After Photobleaching (SRAP) method to show that eisosomes exist in a dynamic steady state (Lacy et al., 2017). While the core of the eisosome is stable, there is a continuous and fast exchange of Pil1 molecules at the eisosome ends. Therefore, the authors proposed that

the eisosome can be perceived as a membrane bound filament in a dynamic equilibrium (Lacy et al., 2017).

2.4.3 Regulation of eisosome assembly by Pil1 phosphorylation

The phosphorylation status of Pil1 protein determines the ability of Pil1 to assemble eisosomes (Luo et al., 2008; Walther et al., 2007). This way, the Pil1 phosphorylation provides an efficient and adaptive system for modulating the eisosome molecular function.

In 2004, Pil1 and Lsp1 were shown to be phosphorylated by Pkh1/Pkh2 kinases *in vitro* (Zhang et al., 2004). Later on, two studies showed that Pil1 is phosphorylated in a Pkh1/2-dependent manner *in vivo* and this affects the eisosome ability to assemble (Luo et al., 2008; Walther et al., 2007). However, the results of the two studies were inconsistent. Walther and co-workers showed that decreased Pil1 phosphorylation facilitates eisosome assembly, whereas Luo and co-workers observed that decreased Pil1 phosphorylation induced eisosome disassembly. These contradictory results can be explained in part by possible different roles of individual identified phosphorylated residues, different growth or nutrient conditions or other undetermined factors. Importantly, Pil1 is also phosphorylated by Slt2 (mitogen-activated protein (MAP) kinase) (Mascaraque et al., 2013). Therefore, the influence of other kinases on Pil1 phosphorylation cannot be excluded. For the reversible Pil1 phosphorylation and regulation, also Pil1 dephosphorylating enzyme must exist, however, such an enzyme was not identified yet.

Pil1 phosphorylation by Pkh1/2 and MCC/eisosome assembly are controlled by sphingolipid levels. It was shown that Pkh1/2 activity is regulated by LCBs, the precursors of sphingolipids (K. Liu et al., 2005; Ke Liu et al., 2005). Moreover, cells lacking Lcb1 (component of serine palmytoyltransferase (SPT), the first enzyme in the sphingolipid biosynthesis pathway) or cells treated with myriocin (inhibitor of SPT) (e.g. the cells with low sphingolipid levels) disassembled eisosomes (Luo et al., 2008; Walther et al., 2007). Myriocin treatment also resulted in Nce102 dissipation from MCC/eisosomes and conversely, high sphingolipid content attracted Nce102 into MCC/eisosomes (Fröhlich et al., 2009). It was therefore hypothesized that when Nce102 is localized to MCC/eisosomes, it mediates Pkh1/2 inhibition, Pil1 is dephosphorylated and MCC/eisosomes remain assembled. Upon sphingolipid depletion, Nce102 leaves MCC/eisosomes, relieving Pkh1/2 activity that results in Pil1 phosphorylation and MCC/eisosome disassembly (Fröhlich et al., 2009).

Presumably, also Pkh1/2-dependent Ypk1/2 protein kinases are a part of Pkh1-dependent Pil1 phosphorylation cascade. In cells lacking Ypk1/2, eisosomes were disrupted as well (Luo et al., 2008). Ypk1/2 kinases are activated in response to low sphingolipid levels and in turn activate sphingolipid biosynthesis, starting with the production of LCBs (Roelants et al., 2011; Sun et al., 2012). LCBs were shown to directly inhibit Pil1 phosphorylation by Pkh2 kinase *in vitro* (Zhang et al., 2004). This might represent an important feedback loop in which the production of LCBs via Ypk1/2 would inhibit Pil1 phosphorylation and lead to the MCC/eisosome re-assembly upon the conditions with restoring sphingolipid levels.
In contrast to Pil1, Lsp1 phosphorylation by Ypk1/2 is activated by LCBs *in vitro* (Zhang et al., 2004). This suggests the possible opposite role of Lsp1 in sphingolipid signaling.

2.5 Conservation of MCC/eisosomes among fungi

The characteristic furrow-like invaginations formed in the yeast plasma membrane were first observed more than 50 years ago, when Moor and Mühlethaler employed freeze-etching method and electron microscopy to visualize plasma membrane of yeast *S. cerevisiae* (Moor and Mühlethaler, 1963). Since then, similar plasma membrane invaginations were found also in other yeast species (Barug and de Groot, 1985; Takeo, 1984) as well as in bacteria (Sleytr et al., 1976), fungi (Büdel and Rhiel, 1987; Lee et al., 2015; Svoboda and Trujillo-Gonzales, 1990), lichens (Lee et al., 2015), algae (Clarke and Leeson, 1985; Lee et al., 2015) and plants (Southworth et al., 1997). This shows that plasma membrane invaginations are widely evolutionary conserved and suggests their functional significance.
Additionally, the core protein components of eisosomes exhibit a high degree of sequence similarity between yeast species. *S. cerevisiae* Pil1 and Lsp1 proteins have their homologues in *S. pombe* (Kabeche et al., 2011), *Candida albicans* (*C. albicans)* (Wang et al., 2016), *Ashbya gossypii* (*A. gossypii*) (Seger et al., 2011), *Aspergillus nidulans* (*A. nidulans*) (Vangelatos et al., 2010) and *Beauveria bassiana* (*B. bassiana*) (Zhang et al., 2017) and all these proteins share their core BAR-domain structure (Olivera-Couto et al., 2011; Ziółkowska et al., 2011). MCC-accumulated transmembrane Sur7 and Nce102 proteins have their sequence homologues in *S. pombe* (Kabeche et al., 2011), *C. albicans* (Alvarez et al., 2008; Douglas et al., 2013; Wang et al., 2016) and *A. nidulans* (Athanasopoulos et al., 2015, 2013; Vangelatos et al., 2010).
Algal eisosomes adopt lineage-specific topologies (Lee et al., 2015). Usually, there are fine striations on the concave surface of the invaginations, similarly to invaginations in *S. cerevisiae*.

No homologues of fungal MCC/eisosomal conserved genes have been found in algae. However, Lee et al., identified two families of predicted BAR domains (they termed it Green-BAR and Red-BAR) that could organize algal eisosomes similarly to the fungal Pil1/Lsp1 (Lee et al., 2015).

The high degree of sequence similarity between these homologues suggests that the functions of these proteins are also conserved. Indeed, *S. cerevisiae* Pil1 protein can form eisosomes in the plasma membrane of *pil1Δpil2Δ S. pombe* cells and conversely, *S. pombe Sp*Pil1 protein is able to form eisosomes in *pil1Δ S. cerevisiae* cells (Kabeche et al., 2011). Similarly, *S. pombe Sp*Fhn1 is able to substitute for Nce102 function in recruiting Can1 into MCC/eisosomes in *nce102Δ* cells (Loibl et al., 2010).

It is therefore interesting, that in some species, some proteins gained or lost the certain ability comparing to their homologues. In *C. albicans*, the deletion of *Ca*Sur7 protein results in much more pronounced phenotypes than in other fungal species (Bernardo and Lee, 2010; Douglas et al., 2012; Douglas and Konopka, 2016; Wang et al., 2016, 2011), suggesting more prominent role of *C. albicans Ca*Sur7 protein in *C. albicans* physiology comparing to *S. cerevisiae*. In contrast, *S. pombe Sp*Sur7 protein does not even localize to MCC/eisosomes in *S. pombe* (Kabeche et al., 2011).

2.5.1 MCC/eisosomes in *Schizosaccharomyces pombe*

S. cerevisiae and *S. pombe* diverged approximately 420 to 330 million years ago and they differ from each other as they each differ from animals (Sipiczki, 2000). *S. pombe* forms rod-shaped cells and divides by fission.

S. pombe MCC/eisosomes (Fig. 5) are much longer than *S. cerevisiae* MCC/eisosomes - they can extend up to 1-2 μm and they exhibit filament-like morphology (comparing to 200-300nm MCC/eisosomes in *S. cerevisiae*) (Kabeche et al., 2011) (compare Fig. 5B and Fig. 5C). However, these two microdomains share many similarities (Fig. 5A). Similarly to *S. cerevisiae* MCC/eisosomes, *S. pombe* MCC/eisosomes in non-dividing cells are stable structures that do not grow or shrink and are immobile. They do not depend on the actin, microtubules or the cell wall (Kabeche et al., 2011). *S. pombe* MCC/eisosomes also avoid areas of growing membranes – they are located in the middle of the cells, not at the growing tips (in *S. cerevisiae*, MCC/eisosomes are not formed in small growing buds or shmoos). When the *S. pombe* cell is about to divide, *S. pombe* MCC/eisosomes can slowly assemble or break and they move away

from the zone of cell division and migrate into the central parts of the daughter cells (Kabeche et al., 2011).

The core of *S. pombe* MCC/eisosomes is formed by ***Sp*Pil1** protein, the homologue of *S. cerevisiae* Pil1 protein (Fig. 5C). The purified recombinant *Sp*Pil1 is able to form filaments in bacterial cells or *in vitro* (Kabeche et al., 2011). The overexpressed *Sp*Pil1 forms even longer filaments than in the wild type (Kabeche et al., 2011). Notably, *Sp*Pil1 may become phosphorylated at several sites, including Thr230 and Thr233, suggesting possible conserved regulation of Pil1 filaments via phosphorylation (Wilson-Grady et al., 2008).

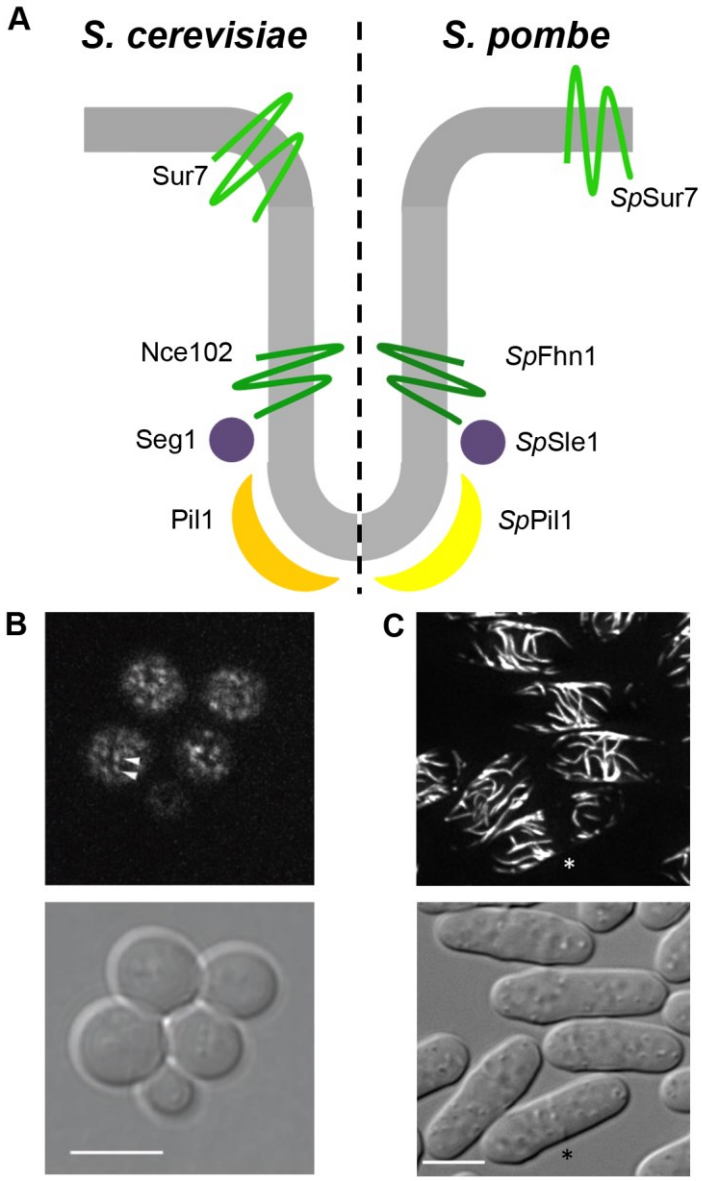

Figure 5. Comparison between *S. cerevisiae* and *S. pombe* MCC/eisosomes.

The model of *S. cerevisiae* (left panel) and *S. pombe* (right panel) MCC/eisosomes with the localizations of homologous proteins depicted (A).

Confocal fluorescence image of GFP-tagged Can1 protein in *S. cerevisiae* cells together with DIC image (B). Bar:5 μm. Maximum intensity projection of mCherry-tagged *Sp*Pil1 protein expressed in *S. pombe* cells together with DIC image (C). Bar: 5 μm.
The figures are adapted from (Kabeche et al., 2011; Malinska et al., 2003).

Moreover, *Sp*Pil1-related protein ***Sp*Pil2** was identified in *S. pombe* (Kabeche et al., 2011). In contrast to *Sp*Pil1, that forms MCC/eisosomes in both vegetative and mating cells, *Sp*Pil2 is expressed only after mating. In mating cells, *Sp*Pil1 localizes to the microdomains in the membrane of the ascus, whereas *Sp*Pil2 localizes to microdomains in the spore membranes (Kabeche et al., 2011).

Another important component of *S. pombe* MCC/eisosomes is ***Sp*Fhn1** that colocalizes with *Sp*Pil1 (Kabeche et al., 2011). It is the only orthologue of Nce102 in *S. pombe*. The localization of *Sp*Pil1 and *Sp*Fhn1 is interdependent. In cells lacking *Sp*Pil1, *Sp*Fhn1 localized to growing tips of the cells. In cells lacking *Sp*Fhn1, *Sp*Pil1 formed less and shorter filaments (Kabeche et al., 2011).

Also, ***Sp*Sle1** protein is the component of *S. pombe* MCC/eisosomes (Moreira et al., 2012). *Sp*Sle1 stands for "Seg1-Like Eisosome protein 1", although *Sp*Sle1 and Seg1 are not sequential homologues. *Sp*Sle1 is a large coiled-coil protein that colocalizes with *Sp*Pil1 filaments in the middle of the cell and also localizes to growing cell tips. The polybasic C-terminal domain is important for plasma membrane recruitment of *Sp*Sle1; the N-terminal region is important for MCC/eisosome targeting (Moreira et al., 2012). Similarly to the situation in *S. cerevisiae*, in *S. pombe* cells lacking *Sp*Sle1, *Sp*Pil1 filaments disassembled. Therefore, Seg1 in *S. cerevisiae* and *Sp*Sle1 in *S. pombe* are considered to be functional homologues (Moreira et al., 2012).

The other orthologues of *S. cerevisiae* MCC/eisosome components do not localize to *S. pombe* MCC/eisosomes. ***Sp*Sur7** and ***Sp*Slm1** proteins are localized to the growing tips of the cell (Kabeche et al., 2011).

Particularly interesting is the fact, that both Pil1 and *Sp*Pil1 form filaments, however, *Sp*Pil1 filaments in *S. pombe* are significantly longer than Pil1 filaments in *S. cerevisiae*. When Pil1 was expressed in *pil1Δpil2Δ S. pombe* cells, Pil1 formed long filaments as well. On the other hand, *Sp*Pil1 expressed in *pil1Δ S. cerevisiae* cells formed puncta of the size of normal *S. cerevisiae* MCC/eisosomes and colocalized with Lsp1 (Kabeche et al., 2011). Therefore, it was concluded, that the length of MCC/eisosomes is not determined by the intrinsic property of the proteins, but it is rather the consequence of the cellular environment (Kabeche et al.,

2011). We followed up on this study and compared the characteristics of the homologous proteins – Pil1 and *Sp*Pil1, Seg1 and *Sp*Sle1, Nce102 and *Sp*Fhn1 – in the *S. cerevisiae* plasma membrane, as will be described in the Results section (section 5.3).

2.5.2 MCC/eisosomes in *Candida albicans*

C. albicans is relatively closely related to *S. cerevisiae*. Normally, *C. albicans* is a commensal organism that lives on the human skin and in the gastrointestinal tract. However, it can enter a bloodstream (for example during surgical procedures), invade organs and tissues, switch its growth from budding to hyphal growth and cause lethal infections. Therefore, studying MCC/eisosomes in *C. albicans* represents an opportunity to better understand the role of plasma membrane in *C. albicans* infection and its survival in the host. This can lead to advanced therapeutic approaches of candidiasis and also to invention of novel antifungal drugs.

Morphologically, MCC/eisosomes of *C. albicans* are quite similar to the MCC/eisosomes of *S. cerevisiae*. They attract *Ca*Sur7, *Ca*Fmp45, *Ca*Lsp1, *Ca*Pil1, *Ca*Slm1 and *Ca*Seg1 and can be visualized as stable punctuate patches in the plasma membrane (Alvarez et al., 2008; Bernardo and Lee, 2010; Reijnst et al., 2011; Wang et al., 2011).

In contrast to *S. cerevisiae*, ***Ca*Sur7** has a more prominent role in *C. albicans* physiology and its deletion causes strong morphological defects, including long invaginations of the cell wall into the cell cytosol (Alvarez et al., 2008; Bernardo and Lee, 2010; Wang et al., 2011). Interestingly , in *C. albicans*, it is the *Ca*Sur7 localization that is dependent on sphingolipid synthesis (Alvarez et al., 2008).

***Ca*Pil1** and ***Ca*Lsp1** are necessary for proper MCC/eisosome formation and, similarly to the deletion of *Ca*Sur7, their deletion causes morphogenetic defects and inward cell wall invaginations (Wang et al., 2016). Outstandingly, $PI(4,5)P_2$ was accumulated at these invaginations (Wang et al., 2016). However, the sensitivity to different stresses was different in Ca*pil1Δ*Ca*lsp1Δ* and Ca*sur7Δ* cells, pointing to the overlapping, but diverse functions of these proteins (Wang et al., 2016).

***Ca*Nce102** is not enriched in MCC/eisosomes in logarithmic cells, but becomes associated with them in stationary cells (Douglas et al., 2013). The deletion of *Ca*Nce102 causes disruption of MCC/eisosomes and the defect in invasive hyphal growth into low concentration agar (Douglas et al., 2013).

Similarly to *S. cerevisiae*, ***Ca*Pkh2** and ***Ca*Pkh3** are regulated by lipids and play a role in regulating MCC/eisosome assembly (Pastor-Flores et al., 2016; Wang et al., 2016).

2.5.3 MCC/eisosomes in other fungi

MCC/eisosomes were investigated also in filamentous fungi *A. gossypii* and *A. nidulans* and in *B. bassiana*, the fungal insect pathogen. Homologues of MCC/eisosomal proteins were found in all these fungi species and they formed very stable puncta at the plasma membrane of cells.
In *B. bassiana*, ***Bb*Pil1A** and ***Bb*Pil1B** were found to colocalize in puncta at the periphery of hyphal cells (Zhang et al., 2017). Similarly, *A. gossypii* ***Ag*Pil1** and ***Ag*Lsp1** colocalized in punctuate structures in the subapical region of hyphal cells (Seger et al., 2011). Moreover, ***Ag*Seg1** was identified in *A. gossypii* and denominated after "stabilizer of eisosome" (Seger et al., 2011). *Ag*Seg1 was shown to play a role in MCC/eisosome stability, similarly to Seg1 in *S. cerevisiae* (Seger et al., 2011).
In *A. nidulans*, ***An*PilA**, ***An*PilB, *An*SurG** and ***An*Nce102** proteins were identified and found to form puncta in the conidiospores (spores of asexual cell cycle) and ascospores (spores of sexual cell cycle), but not in the hyphae (Athanasopoulos et al., 2015, 2013; Vangelatos et al., 2010). Similarly to Nce102 in *S. cerevisiae*, ***An*Nce102** was found to regulate eisosome density in *A. nidulans* (Athanasopoulos et al., 2015).

2.6 MCC/eisosome function in stress response

It is believed that MCC/eisosomes are signaling hubs where many proteins involved in stress response accumulate. Moreover, they are probably able to integrate signals from extracellular conditions and initiate many stress responses. They are involved in responses to lipid imbalance, osmotic stress, oxidative stress, changes in the plasma membrane potential and nutrient starvation conditions, as will be discussed further.

2.6.1 MCC/eisosomal proteins under stress conditions

The expression levels of MCC/eisosomal proteins depend largely on environmental conditions. The mRNA expression levels of Pil1 and Nce102 proteins were induced by various stress conditions (Gasch et al., 2001, 2000; Suzuki et al., 2003) and the deletion of Pil1 protein caused

many stress-related phenotypes (Kabeche et al., 2015b; Qian et al., 2012; Yoshikawa et al., 2009; Zhang et al., 2004).

The expression of Sur7 and Ynl194c proteins was induced by glycerol and by oleic acid (Jung et al., 2013). Additionally, the expression of Ynl194c and Fmp45 was induced by high salt (Young et al., 2002). The deletion of Sur7 caused defects in osmotic stress response and sporulation (Yoshikawa et al., 2009; Young et al., 2002). The deletion of Fmp45 affected cell survival in stationary phase (Martinez et al., 2004). Moreover, Pun1 expression was higher under the conditions of metal ion stress and nitrogen stress and the deletion of Pun1 caused increased metal ion sensitivity, nitrogen stress and cell wall stress (Hosiner et al., 2011; Xu et al., 2010).

Fhn1 protein has low expression in aerobic conditions, but its expression increases in anaerobic conditions (Stradalova, unpublished data). Moreover, its expression is also higher in late stationary phase of yeast cultures (Gasch et al., 2000). Under these conditions, we also observed higher expression of Nce102 protein and, interestingly, also Nce102 partial re-localization from the plasma membranes into the cell interior (our unpublished data). We will focus on this phenomenon in the Results section (section 5.2).

2.6.2 MCC/eisosomes and Pkh1/2-regulated stress signaling pathways

MCC/eisosomes accumulate Pkh1/2 kinases that are able to regulate Ypk1/2 kinases, Sch9 kinase and Pkc1 kinase (Roelants et al., 2004; Voordeckers et al., 2011; Walther et al., 2007). This way, MCC/eisosomes are involved in processes such as membrane stress, cell wall stress, actin localization, nutrient signaling, aging and longevity (Deprez et al., 2018; Dickson et al., 2006; Heinisch et al., 1999; Roelants et al., 2017; Swinnen et al., 2014, 2013).

Pkh1/2 targets - Ypk1/2, Sch9 and Pkc1 kinases - are dual-activated kinases of AGC family that require phosphorylation by Pkh1/2 kinases for their full activation together with the activation by additional co-activating protein (Fig. 6) (Arencibia et al., 2013). Ypk1/2 kinases have to be additionally phosphorylated by TORC2 complex (Kamada et al., 2005; Roelants et al., 2002), Sch9 has to be phosphorylated by TORC1 complex (Urban et al., 2007; Voordeckers et al., 2011) and Pkc1 needs to be activated by Rho1-GTP protein (Inagaki et al., 1999; Kamada et al., 1996).

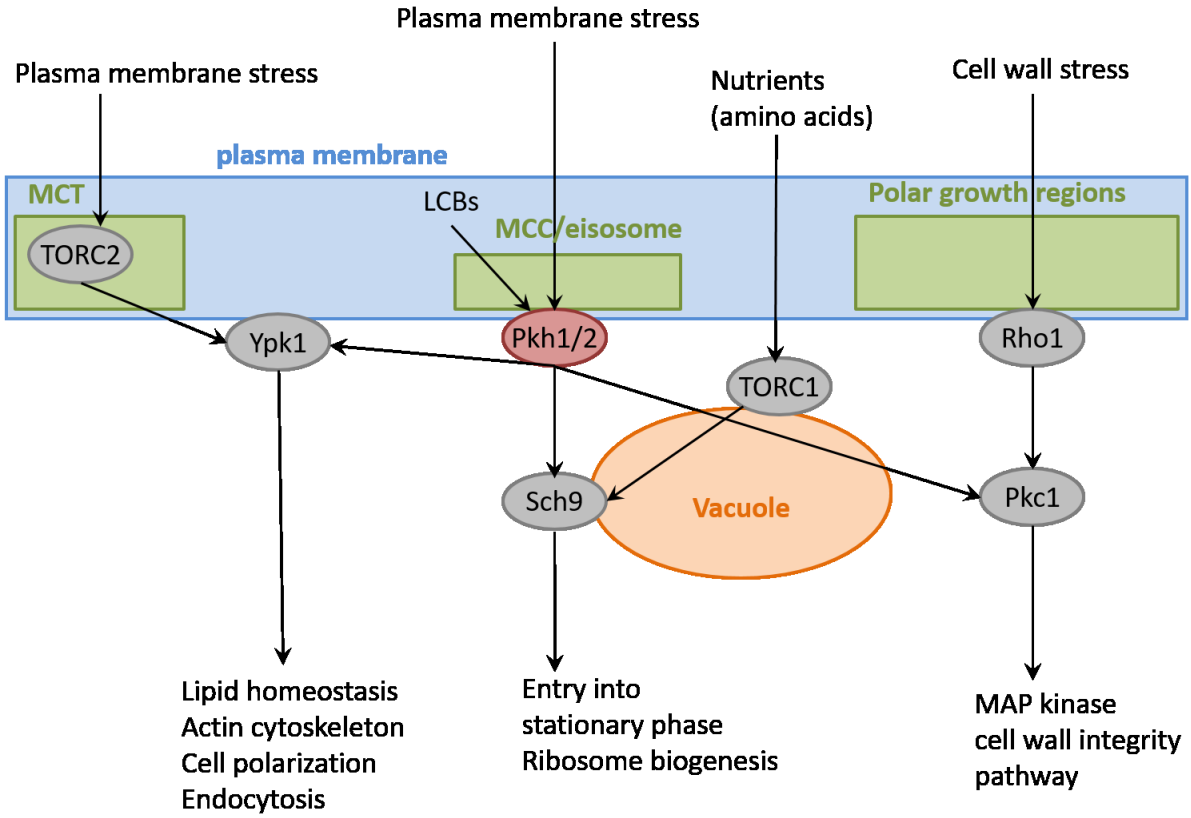

Figure 6. Scheme of Pkh1/2 signaling network.

Pkh1/2 kinases are in the center of stress signaling. Their substrates include Ypk1/2, Sch9 and Pkc1. Ypk1/2 is dually activated by Pkh1/2 and TORC2 (localized to the plasma membrane), Sch9 is dually activated by Pkh1/2 and TORC1 (localized to the vacuolar membrane) and Pkc1 is dually activated by Pkh1/2 and Rho1 (probably in the cytoplasm). Corresponding stress signals and signaling outputs are depicted.

Interestingly, neither the targets of Pkh1/2 kinases nor the co-activation proteins of these targets, accumulate at MCC/eisosomes together with Pkh1/2 kinases (Fig. 6). Ypk1/2 kinases are homogeneously dispersed throughout the plasma membrane in non-stressed conditions (Niles and Powers, 2012; Roelants et al., 2002; Sun et al., 2012) and in stress conditions, they are attracted to MCT for phosphorylation by TORC2 complex (Berchtold and Walther, 2009). Sch9 kinase localizes to the vacuolar membrane as well as their upstream activator, TORC1 (Sturgill et al., 2008; Urban et al., 2007). And Pkc1 and Rho1 are accumulated at the growing areas of the plasma membrane (Denis and Cyert, 2005; Levin, 2005). Therefore, either Pkh1/2 kinases or their targets (or both Pkh1/2 kinases and their targets) must change their localization in order to interact.

It was shown that MCC/eisosomes disintegrate in response to stress (Fröhlich et al., 2009; Kabeche et al., 2015b). Malinsky and Opekarová proposed that Pkh1/2 kinases are inhibited

when accumulated at MCC/eisosomes and in response to stress, as MCC/eisosomes disintegrate, Pkh1/2 kinases are released into the cytoplasm. The increased cytosolic pool of Pkh1/2 kinases then might phosphorylate their target kinases that are localized to different cell compartments and evoke appropriate stress response (Malinsky and Opekarová, 2016).

2.6.3 MCC/eisosomes and sphingolipid homeostasis

MCC/eisosomes play a role in regulating sphingolipid homeostasis in the plasma membrane. Sphingolipids are a wide family of lipids with sphingoid base backbone and play many vital functions such as roles in membrane integrity upon stresses, signaling, endocytosis and protein trafficking (Cowart and Obeid, 2007). Therefore, their levels have to be tightly regulated (Breslow, 2013; Dickson et al., 2006; Stancevic and Kolesnick, 2010). The first step in the synthesis of sphingolipids is catalyzed by the complex called serine palmitoyl transferase, (SPT) (Hanada, 2003). The activity of SPT is regulated by Orm1/2 proteins that, under normal conditions, inhibit SPT activity (Breslow et al., 2010). Upon sphingolipid depletion, the phosphorylation of Orm1/2 proteins occurs and this blocks their inhibitory activity on SPT (Breslow et al., 2010). It was shown that Pkh1/2-dependent Ypk1/2 kinases are able to phosphorylate Orm1/2 proteins and thereby relieve sphingolipid biosynthesis (Roelants et al., 2011; Sun et al., 2012).

MCC/eisosomes were shown to play a role in the process of sphingolipid homeostasis maintenance (Fig. 7) (Berchtold et al., 2012; Fröhlich et al., 2009). Upon decreased sphingolipid levels in the plasma membrane (caused for example by the drug myriocin), MCC/eisosomes partly disassemble – Nce102 protein and Slm1/2 proteins leave this compartment and initiate a pathway that leads to the recovery of sphingolipid biosynthesis.
Nce102 becomes homogeneous in the plasma membrane in these conditions and its dissociation from MCC/eisosomes leads to the activation of Pkh1/2 kinases, although the exact mechanism of Pkh1/2 activation is not clear (Fröhlich et al., 2009). Active Pkh1/2 kinases can subsequently phosphorylate Pil1 and this leads to even higher MCC/eisosome disassembly. Moreover, Pkh1/2 directly phosphorylate Ypk1/2 kinases (Breslow et al., 2010; Luo et al., 2008; Walther et al., 2007; Zhang et al., 2004).
Under the same conditions, Slm1/2 proteins re-localize from MCC/eisosomes to the MCT compartment, where they can associate with TORC2 complex (Berchtold et al., 2012). Here,

Slm1/2 recruit Ypk1/2 kinases to the plasma membrane, where Ypk1/2 can be phosphorylated by TORC2.

The dual phosphorylation of Ypk1/2 kinases at both Pkh1/2-dependent and TORC2-dependent phosphorylation sites leads to the full Ypk1/2 activity (Niles et al., 2012; Niles and Powers, 2012). Ypk1/2 kinases then phosphorylate Orm1/2 proteins, preventing them from negatively regulating SPT complex, resulting in increased sphingolipid production (Breslow et al., 2010; Han et al., 2010; Roelants et al., 2011; Sun et al., 2012).

The increased levels of LCBs, the first intermediates in the complex sphingolipid production, probably in turn induce the re-assembly of eisosomes, as Pil1 phosphorylation by Pkh1/2 kinases was shown to be inhibited by LCBs (Zhang et al., 2004). Therefore, upon sphingolipid biosynthesis restoration, MCC/eisosomes might be re-assembled to be able to sense plasma membrane stress signals again.

Moreover, MCC/eisosomes might potentially regulate sphingolipid biosynthesis via Pkh1/2-regulated kinases Sch9 and Pkc1, and all these processes are probably interconnected and redundant (reviewed in (Malinsky and Opekarová, 2016); (Aguilar et al., 2010; Swinnen et al., 2014)).

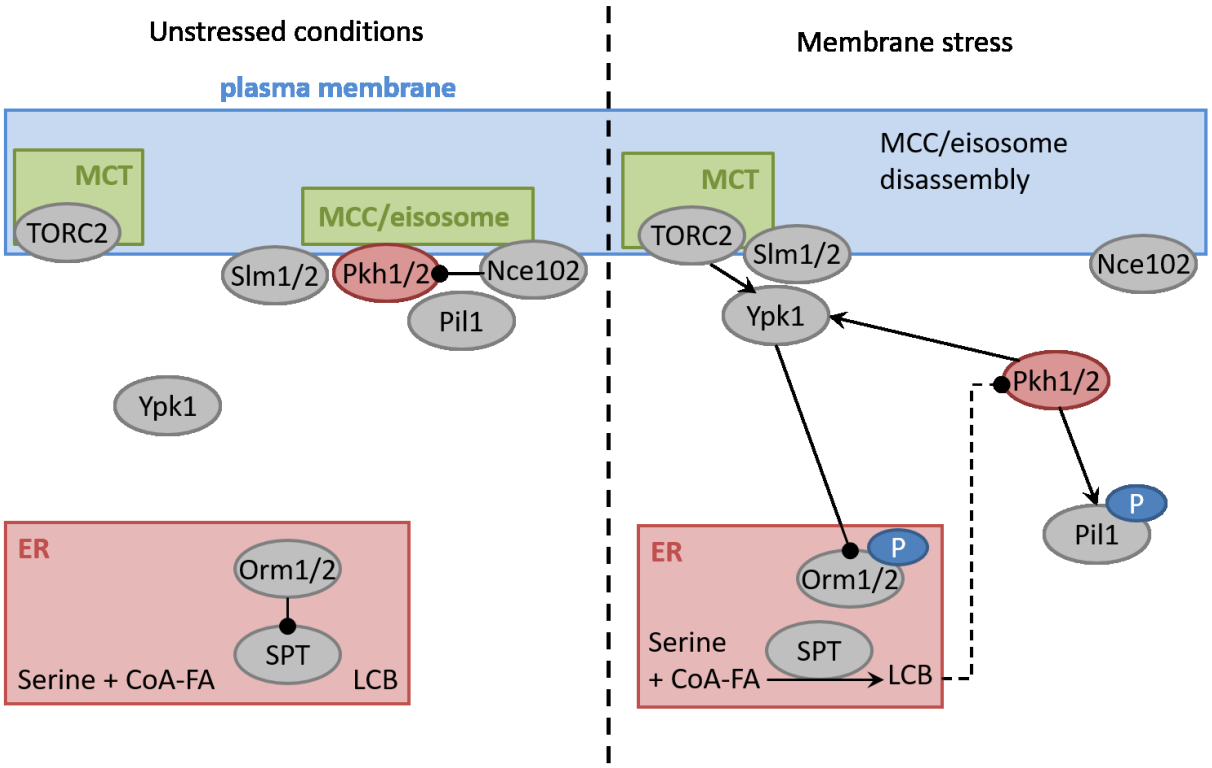

Figure 7. MCC/eisosome-regulated sphingolipid stress signaling.

In the basal conditions, Pkh1/2 kinases are accumulated at MCC/eisosomes together with Nce102 and Slm1/2 proteins. Nce102 is involved in the inhibition of Pkh1/2 activity. Ypk1/2 kinases are inactive in the cytoplasm and Orm1/2 proteins block the activity of SPT.
Upon plasma membrane stress conditions (low sphingolipids), Nce102 becomes homogeneous in the plasma membrane, allowing Pkh1/2 kinases to become active. Pkh1/2 kinases phosphorylate Pil1, which leads to the MCC/eisosome disassembly. Pkh1/2 kinases also phosphorylate Ypk1/2 kinases. These are attracted to MCT via re-localized Slm1/2 proteins and can be phosphorylated by active TORC2 complex. Activated Ypk1/2 inhibit Orm1/2 proteins, thereby relieving SPT activity and mediating sphingolipid production.

Taken together, upon low sphingolipid levels in the plasma membrane, MCC/eisosomes partly disassemble. Dissociation of Nce102 protein from MCC/eisosomes enables activation of Pkh1/2 kinases. Re-localization of Slm1/2 proteins into MCT results in Ypk1/2 attraction to the plasma membrane. Thus, Ypk1/2 kinases may be phosphorylated by both Pkh1/2 kinases and TORC2 complex, resulting in full Ypk1/2 activation. Activated Ypk1/2 then phosphorylate and inactivate Orm1/2 proteins. This leads to the relieving of SPT activity and activation of sphingolipid biosynthesis to compensate for the lack of sphingolipids. This subsequently results in the re-assembly of eisosomes into their basal, stress-signal sensing mode.
Importantly, the disassembly of eisosomes was observed also upon the mechanical stress in the plasma membrane (Berchtold et al., 2012) and Pil1 protein was shown to be phosphorylated by Pkc1-activated MAP kinase Slt2 upon stimulated cell wall-integrity pathway (Mascaraque et al., 2013). Moreover, sphingolipid levels were shown to change under the heat shock (Jenkins et al., 1997; Skrzypek et al., 1999). This suggests that membrane stress can be somehow reflected in the sphingolipid content (or availability). Upon membrane stress, MCC/eisosomes could sense this lipid misbalance and disassemble. This would lead to the activation of sphingolipid biosynthesis, which would in turn result in the strengthening of the plasma membrane and eisosome re-assembly.

The molecular mechanism by which Nce102 protein could sense sphingolipid content is currently unknown. MCC/eisosomes were shown to be enriched in sterols, but there is no evidence that sphingolipids are accumulated at MCC/eisosomes (Grossmann et al., 2007; Malinska et al., 2004, 2003; Malinsky and Opekarová, 2016). Moreover, nutrient transporters whose activity depends on sphingolipids, such as Pma1 and Gap1, avoid MCC/eisosomes (Lauwers et al., 2007; Malinska et al., 2004). However, it was shown that in the plasma membrane also sphingolipid-rich microdomains exist (Aresta-Branco et al., 2011; Vecer et al.,

2014). Malinsky and Opekarová proposed that sterols accumulated at MCC/eisosomes might in some conditions compensate for the imbalance in these sphingolipid-rich microdomains and Nce102 could sense sphingolipids indirectly, i.e. through the association of Nce102 with sterols (Malinsky and Opekarová, 2016).

As noted above, the Slm1/2 re-localization from MCC/eisosomes to MCT compartment was observed also during membrane stretching (Berchtold et al., 2012). Notably, the plasma membrane tension affects TORC2 signaling in both directions. The increased plasma membrane tension activates TORC2 via re-localization of Slm1/2 proteins as described above. The reduced plasma membrane tension leads to the formation of PI(4,5)P2-rich invaginated plasma membrane microdomains that sequester TORC2 complex to inactivate it (Riggi et al., 2019).

Importantly, also *A. nidulans* MCC/eisosomes seem to regulate sphingolipid homeostasis. It was shown that *An*Nce102, *An*PilA and *An*YpkA play a role in sphingolipid synthesis (Athanasopoulos et al., 2015). Moreover, similarly to the situation in *S. cerevisiae*, upon treatment of ascospore germlings with myriocin, *An*PilA foci were less abundant and their localization was altered (Athanasopoulos et al., 2013). This suggests that the interdependence between MCC/eisosomes and sphingolipids is widely conserved.

2.6.4 MCC/eisosomes and phosphoinositide homeostasis

MCC/eisosomes also play a role in regulating the phosphatidylinositol(4,5)bisphosphate ($PI(4,5)P_2$) levels in the plasma membrane. $PI(4,5)P_2$ is essential phospholipid that is enriched in the plasma membrane, where it can regulate endocytosis and actin cytoskeleton (Odorizzi et al., 2000). $PI(4,5)P_2$ is synthesized from phosphatidylinositol(4)phosphate (PI4P) by the PI4P kinase, Mss4 (Desrivières et al., 1998) and it is degraded by synaptojanin-like phosphatases Inp51, Inp52 and Inp53 to phosphatidylinositol (PI) (Stolz et al., 1998).
Interestingly, MCC/eisosome Pil1 and Lsp1 proteins are recruited to the plasma membrane by their interaction with $PI(4,5)P_2$ (Kabeche et al., 2014, 2011; Karotki et al., 2011; Olivera-Couto et al., 2011). Also, Slm1/2 proteins bind to the plasma membrane through interaction of their PH domains with $PI(4,5)P_2$ (Fadri et al., 2005). Moreover, MCC/eisosome assembly require $PI(4,5)P_2$ dynamics and in *S. pombe syj1Δ* strain, MCC/eisosome structure collapses (Kabeche

et al., 2014). Therefore, PI(4,5)P_2 is necessary for the functional organization of MCC/eisosome microdomains.

In *S. cerevisiae*, PI(4,5)P_2 phosphatase Inp51 (also called Sjl1) accumulates at MCC/eisosomes (Frohlich et al., 2014). Pil1 protein specifically recruited Inp51, but not homologous phosphatases Inp52 and Inp53, to the plasma membrane (Frohlich et al., 2014; Murphy et al., 2011). Pil1 was necessary for PI(4,5)P_2 phosphatase function and in the cells lacking Pil1, the levels of total as well as available PI(4,5)P_2 increased (Frohlich et al., 2014). The functional significance is documented by the observation that similarly to synaptojanin triple knockout *inp51Δinp52Δinp53Δ*, also *pil1Δinp52Δinp53Δ* cells were unviable. As mentioned previously, upon low sphingolipid levels, MCC/eisosomes partially disassemble (Berchtold et al., 2012; Fröhlich et al., 2009; Kabeche et al., 2014). It was suggested that this could lead also to the detachment of Inp51 from the plasma membrane and therefore also to the loss of the Inp51 phosphatase activity (Malinsky and Opekarová, 2016). This would cause the stabilization of PI(4,5)P_2 levels in the plasma membrane in the case of low sphingolipids (Malinsky and Opekarová, 2016).

The concept of MCC/eisosomes regulating the degradation of PI(4,5)P_2 was proposed also in *S. pombe*. Here, the genetic interactions between MCC/eisosome proteins *Sp*Pil1 and *Sp*Sle1 and Inp51 phosphatase orthologue *Sp*Syj1 was identified (Kabeche et al., 2014). Also, previously uncharacterized protein *Sp*Tax4 was identified as *Sp*Syj1 ligand (Kabeche et al., 2014). The authors proposed that these proteins act in linear pathway to regulate cellular PI(4,5)P_2 levels. Interestingly, in contrast to *S. cerevisiae*, Inp51 orthologue *Sp*Syj1 do not associate with *S. pombe* MCC/eisosomes. However, the deletions of all these proteins (*Sp*Pil1, *Sp*Sle1, *Sp*Syj1 and *Sp*Tax4) suppressed the growth defects of TORC2-deficient strain. Similarly, in *S. cerevisiae*, the deletion of Inp51-Tax4/Irs4 proteins restored the growth of TORC2 mutants (Morales-Johansson et al., 2004). Therefore, the authors proposed that PI(4,5)P_2 regulation via *Sp*Pil1-*Sp*Sle1-*Sp*Syj1-*Sp*Tax4 pathway intersects with TORC2-dependent signal transduction pathway (Kabeche et al., 2014).

2.6.5 MCC/eisosomes and osmotic stress

MCC/eisosomes stabilize plasma membrane integrity upon hypoosmotic stress (Kabeche et al., 2015a). Under hypoosmotic conditions, cells surface area extends and the membrane of

MCC/eisosome invaginations is used to support this expansion. In the protoplasts under hypoosmotic conditions, MCC/eisosomes disassembled and the invaginations in the plasma membrane flattened. The protoplasts from cells lacking MCC/eisosomes were unable to expand the cell surface and consequently lysed. Therefore, MCC/eisosomes can provide the membrane needed under hypoosmotic stress, similarly to caveolae in mammalian cells (Sinha et al., 2011).

MCC/eisosomes also maintain integrity of the plasma membrane during hyperosmotic conditions and dehydration (Dupont et al., 2010). In response to dehydration, MCC/eisosome invaginations extended into the cytoplasm in the form of large pleats of plasma membrane. These extended invaginations stabilized the plasma membrane and prevented the plasma membrane internalization that would otherwise lead to the cell death.
A different situation was observed in *S. pombe*. Here, upon hyperosmotic conditions, $P(4,5)P_2$ cortical clusters formed (Kabeche et al., 2015b). These clusters accumulated phosphatidylinositol-4-phosphate 5-kinase *Sp*Its3 and GTPase *Sp*Rho2 that activates MAP kinase *Sp*Pmk1 and subsequently cell wall integrity pathway. It is interesting that in this case, MCC/eisosomes were shown to negatively regulate the $PI(4,5)P_2$ clusters formation and also CWI pathway (Kabeche et al., 2015b).

2.6.6 MCC/eisosomes and oxidative stress

S. cerevisiae MCC/eisosomes accumulate also Pst2, Rfs1 and Ycp4 proteins (Grossmann, 2008). Their homologues in *C. albicans*, *Ca*Pst1, *Ca*Pst2, *Ca*Pst3 and *Ca*Ycp4 were recently shown to be important for protection during oxidative stress (Li et al., 2015).
All these proteins belong to the family of flavodoxin-like proteins (FLPs), that are enzymes with NAD(P)H:quinone oxidoreductase activity. These enzymes reduce ubiquinone so it could act as antioxidant to prevent the plasma membrane damage. It was shown that also *Ca*Pst1, *Ca*Pst2, *Ca*Pst3 and *Ca*Ycp4 proteins have these antioxidant abilities (Foderaro et al., 2017; Li et al., 2015). Quadruple mutant *pst1Δpst2Δpst3Δycp4Δ* was more sensitive to variety of oxidation conditions, especially those causing lipid peroxidation. Moreover, the mutant exhibited diminished virulence in mouse model of *C. albicans* kidney infection, which is presumably caused by the decreased ability of cells to survive oxidative attacks of host immune system (Li et al., 2015).

Of note, *S. cerevisiae* cells were shown to adapt to exposure to hydrogen peroxide by rapid biophysical changes in the permeability and anisotropy of the plasma membrane and by changes in plasma membrane lipid profiles (Folmer et al., 2008; Pedroso et al., 2009). As MCC/eisosomes are involved in the organization of the plasma membrane, it may be hypothesized that these microdomains could play roles also in these processes of oxidative stress response.

2.6.7 MCC/eisosomes and chronic glucose starvation

MCC/eisosomes accumulate Xrn1 exoribonuclease specifically in post-diauxic phase of yeast cell culture growth, e.g. under the conditions of chronic glucose depletion (Grousl et al., 2015). In logarithmic and diauxic phase cells, Xrn1 was observed to be localized diffusely in cytoplasm and accumulated in cytosolic ribonucleoprotein assemblies called processing bodies (P-bodies), respectively (Grousl et al., 2015). P-bodies are assemblies that are formed either after gradually incoming environmental stresses (such as nutrient starvation) or by acute environmental stresses (such as heat shock) (Decker and Parker, 2012). In P-bodies, Xrn1 was accumulated together with mRNAs and other components of mRNA decay machinery (Parker and Sheth, 2007). Grousl and co-workers showed that in post-diauxic cells, Xrn1 was spatially sequestered at MCC/eisosomes from the rest of the mRNA decay machinery. Moreover, this sequestration was reversible as the addition of the fermentable carbon source (e.g. glucose) caused Xrn1 redistribution back to cytoplasm.

Interestingly, the addition of glucose to cells grown on non-fermentable carbon source (e.g. lactate) causes process called “glucose-induced mRNA decay”, where a substantial portion of mRNAs encoding respiration genes is degraded (Yin et al., 1996). This ensures the shift of metabolism from aerobic respiration to anaerobic fermentation and adaption to changed environmental conditions.

The change in Xrn1 localization coupled to the environmental conditions might have important functional consequences regarding Xrn1 activity and we will address this question in the Results section (section 5.1).

2.6.8 MCC/eisosomes and acute nitrogen starvation

MCC/eisosomes reorganize upon acute nutrient starvation and this has functional consequences for nutrients transporters that localize to MCC/eisosomes (Gournas et al., 2018; Moharir et al., 2018). As mentioned previously, MCC/eisosomes act as storage compartments for nutrient transporters and when the substrate is not present, MCC/eisosomes protect the transporters from their endocytosis and subsequent degradation (Bianchi et al., 2018; Busto et al., 2018; Gournas et al., 2018, 2017; Grossmann et al., 2008; Moharir et al., 2018).

Upon acute nitrogen starvation conditions (medium only with proline as a nitrogen source), MCC/eisosomes increased in number and size (as marked by Pil1 fluorescence) (Gournas et al., 2018). This process was dependent on Lsp1 protein. The authors suggested that upon acute nitrogen starvation conditions, MCC/eisosome microdomain enlarges so it could attract higher number of transporters and subsequently protect them from bulk endocytosis that takes place upon starvation conditions. This way, the transporters would be still available, if the nutrients in the medium increased and this would lead to the more rapid recovery from stress conditions.

MCC/eisosome restructuring upon nitrogen starvation (medium completely without amino acids) was observed also in the study by Moharir and co-authors. However, the functional consequences of the MCC/eisosome restructuring proposed by these authors were different. In this case, MCC/eisosomes (marked by Nce102 protein) aggregated into fewer, but larger and/or elongated MCC/eisosomes. Under this reorganization, MCC/eisosomes were not able to accumulate nutrient transporters and the transporters were targeted for endocytosis and degradation. The authors proposed that this happens to prevent the loss of the nutrients from the cell cytoplasm as nutrient transporters can act in both directions (e.g. in the absence of nutrients in the medium, transporters could transport nutrients from the cell interior to the medium). The process of MCC/eisosome disintegration and subsequent degradation of transporters would therefore result in stabilization of cell integrity under starvation conditions. In the case of nutrients re-supply, the general amino acid permease Gap1 (that is not down-regulated upon nitrogen starvation) would detect amino acids in the medium and transport them to cell to recover from starvation (Moharir et al., 2018).

2.6.9 MCC/eisosomes and plasma membrane potential

The plasma membrane potential enables cells to transport nutrients throughout the plasma membrane and in fact, it reflects the cellular physiology.
Upon the depolarization of the plasma membrane, MCC/eisosomes partially disassembled – while Pil1 and Sur7 proteins remained accumulated at patches, Slm1 formed fewer but larger clusters and Nce102, together with nutrient transporters (HUP1, Can1, Fur4, Mup1), became diffuse in the plasma membrane (Grossmann et al., 2007; Moharir et al., 2018). The dissipation of nutrient transporters was reversible and upon membrane potential repolarization, nutrient transporters re-accumulated at MCC. Moreover, as under the acute nitrogen starvation conditions, the down-regulation of nutrient transporters occurred even in the absence of amino acids. The authors suggested that similarly to the previous situation, transporters have to be removed from the plasma membrane so the cell would not lose nutrients. The down-regulation of transporters on the plasma membrane would also lead to reduced proton flux through the membrane and to proton gradient stabilization.

It is also interesting, that all the transporters that localize to MCC/eisosomes are proton symporters for nutrients (i.e. they transport protons into the cell together with nutrients). On the other hand, plasma membrane H^+ ATPase Pma1 that pumps protons out of the cell is excluded from MCC/eisosomes. Therefore, MCC/eisosomes might organize proton flux through the plasma membrane – by spatially separating the inwards and outwards proton flux (Malinsky and Opekarová, 2016). Moreover, MCC/eisosomes were shown to limit the amount of transporters on the plasma membrane (Moharir et al., 2018). By this, MCC/eisosomes might regulate the balance of the proton flux from nutrient transporters and proton flux from Pma1. This way, MCC/eisosomes could maintain proton gradient, and subsequently membrane potential, through the plasma membrane.

2.6.10 MCC/eisosomes in cellular morphogenesis and virulence

In *S. cerevisiae*, cells lacking MCC/eisosomes do not exhibit strong morphogenetic defects. Only in cells lacking Sur7 and its homologues, Fmp45 and Ynl194c, some slight defects in sporulation could be observed (Young et al., 2002). *Aspergillus fumigatus* (*A. fumigatus*) *Afu*Nce102 was also shown to play a role in sporulation (Khalaj et al., 2012). Interestingly, in

filamentous fungus *A. gossypii*, the mRNA expression of MCC/eisosomal proteins was ten-fold higher in spores than in hyphae, pointing to the possible function of MCC/eisosomes in spore physiology (Seger et al., 2011). Douglas and Konopka propose that MCC/eisosomes might promote resistance to stresses in spores, such as dehydration (Douglas and Konopka, 2014).

Regarding pseudohyphal growth of *S. cerevisiae*, the deletion of the Sur7 homologue, Pun1, abolished the pseudohyphal growth (Xu et al., 2010). Similarly, *C. albicans* cells lacking *Ca*Sur7 or *Ca*Nce102 proteins exhibited defects in filamentation and formed aberrant hyphae (Bernardo and Lee, 2010, Douglas, 2013). In *A. gossypii*, the deletion of *Ag*Pil1 caused defects in polarized growth and formation of abnormally shaped hyphal tips (Seger et al., 2011). Therefore, MCC/eisosomes might also play some role in pseudohyphal/hyphal growth of these yeast species. In contrast, in another filamentous fungus, *A. nidulans*, the deletion of MCC/eisosomal proteins did not lead to any obvious growth phenotypes (Athanasopoulos et al., 2015; Vangelatos et al., 2010).

In contrast to *S. cerevisiae*, the deletion of MCC/eisosomal proteins in *C. albicans* causes strong morphogenetic defects. First of all, *C. albicans* cells lacking Sur7 protein exhibited mislocalized septins and actin (Alvarez et al., 2008). This resulted in misshapen buds, aberrant hyphae and defects in septation and endocytosis (Alvarez et al., 2008; Bernardo and Lee, 2010; Wang et al., 2011). It also probably lead to the formation of long, tube-like invaginations of cell wall into the cell interior (Alvarez et al., 2008). Moreover, cells lacking Sur7 protein produced weaker cell walls with decreased levels of β-glucan (Wang et al., 2011). All these phenotypes probably lead to the increased sensitivity of *sur7Δ* cells to cell wall-disturbing reagents and to a variety of stresses, including a growth in high temperature and exposure to copper (Alvarez et al., 2008; Bernardo and Lee, 2010; Douglas and Konopka, 2019). Especially the sensitivity to copper is tightly connected to the pathogenic potential of the yeast because immune system of the host uses copper to attack microbial pathogens (Douglas and Konopka, 2019). Moreover, the *sur7Δ* cells exhibited defective biofilm formation and defective invasive growth into the tissues (Bernardo and Lee, 2010; Douglas et al., 2012). Therefore, it is not surprising that *sur7Δ* cells exhibited diminished virulence in both *in vitro* macrophage model of virulence and *in vivo* mouse model of infection (Bernardo and Lee, 2010; Douglas et al., 2012).
Also the deletion of Nce102 in *C. albicans* caused actin mislocalization, abnormal hyphae formation and reduced invasive hyphal growth (Douglas et al., 2013). Similarly to *sur7Δ* cells, also cells lacking Nce102 displayed diminished virulence in *in vivo* mouse model of *C. albicans*

(Douglas et al., 2013). Similar, but slightly different phenotypes were observed also in cells lacking Pil1 and Lsp1 proteins (Wang et al., 2016). *pil1Δlsp1Δ* cells exhibited defects in actin organization and hyphal growth, but the morphology of cell wall invaginations was slightly different from *sur7Δ* cells and *pil1Δlsp1Δ* cells were also susceptible to different stresses (Wang et al., 2016). This suggests that Sur7 and Pil1/Lsp1 proteins perform overlapping, but somewhat divergent functions. In contrast, the deletion of Slm2, Pkh2 or Pkh3 did not lead to similar cell wall and morphogenetic defects, but it revealed the role of Pkh2 and Pkh3 in regulating furrow morphology (Wang et al., 2016).

Notably, also MCC/eisosomal proteins *Bb*Pil1A and *Bb*Pil1B of *B. bassiana* played a role in virulence of this fungal insect pathogen (Zhang et al., 2017). Pil1A and Pil1B were shown to play a role in autophagy, cell wall integrity and various stress responses. The cells lacking either *Bb*Pil1A and *Bb*Pil1B or both exhibited diminished pathogenicity due to decreased ability to penetrate host cuticle and due to defective morphogenesis in the host (Zhang et al., 2017).

Importantly, all these phenotypic defects might be connected to the lipid imbalance in the plasma membrane. As MCC/eisosomes are dysfunctional in these strains, this may lead to the inability of cells to properly regulate their lipid composition in response to the various stresses that infecting cells encounter during the infection of the host. For example, that *C. albicans* cells in the human host have to resist stresses such as higher temperatures, oxidation, nitrosylation and antimicrobial peptides (Brown et al., 2009; Dantas et al., 2015; O'Meara et al., 2017). Additionally, copper is a part of the innate immunity response and it binds to phosphatidylserine and phosphatidylethanolamine in the plasma membrane and causes membrane permeabilization and damage (Besold et al., 2016; García-Santamarina and Thiele, 2015; Hodgkinson and Petris, 2012). Interestingly, *C. albicans sur7Δ* and *pil1Δlsp1Δ* strains show increased sensitivity to copper, most likely due to the excessive exposure of phosphatidylserine in the outer leaflet of the plasma membrane (Douglas and Konopka, 2019). This suggests that the decreased virulence of MCC/eisosomal mutant strains may be closely connected to the defect in plasma membrane lipid regulation and organization and it may reflect the inability of cells to cope with the stress conditions in hosts.

3. Research aims

Role of MCC/eisosomes in regulation of mRNA decay during chronic glucose depletion

Aim 1.1: Investigate the functional significance of Xrn1 re-localization to MCC/eisosomes under the conditions of chronic glucose depletion.
Aim 1.2: Determine the role that MCC/eisosomes play in this process.

Investigation of Nce102 intracellular localization and its functional significance during chronic glucose depletion

Aim 2.1: Characterize the intracellular localization of Nce102 under the conditions of chronic glucose depletion.
Aim 2.2: Determine the functional significance of partial Nce102 re-localization from the plasma membrane into the cell interior.

Compatibility of *S. cerevisiae* and *S. pombe* MCC/eisosomal proteins

Aim 3.1: Investigate the compatibility of *S. pombe* and *S. cerevisiae* MCC/eisosomal proteins – Pil1 vs. *Sp*Pil1; Seg1 vs. *Sp*Sle1, Nce102 vs. SpFhn1. Compare their characteristics regarding MCC/eisosome assembly.
Aim 3.2: Reconstitute *S. pombe* MCC/eisosome microdomain in *S. cerevisiae*.

4. Material and Methods

4.1 Yeast strains

Table 2. Yeast strains used in the study.

Strain	Genotype	Source
BY4741	*MATa his3Δ1 leu2Δ0 met15Δ0 ura3Δ0*	Euroscarf
BY4742	*MATα his3Δ1 leu2Δ0 lys2Δ0 ura3Δ0*	Euroscarf
fab1Δ	BY4742; *fab1::KanMX4*	Euroscarf
fhn1Δ	BY4742; *fhn1::KanMX4*	Euroscarf
nem1Δ	BY4742; *nem1::KanMX4*	Euroscarf
vps4Δ	BY4742; *vps4::KanMX4*	Euroscarf
Y063 (*pil1Δ*)	BY4741; *pil1::KanMX4*	Euroscarf
Y090 (*nce102Δ*)	BY4742; *nce102::KanMX4*	Euroscarf
Y091 (*pil1Δ*)	BY4742; *pil1::KanMX4*	Euroscarf
Y112 (*pil1Δnce102*)	*MATα pil1::KanMX4 nce102::KanMX4*	Lab collection
Y123	BY4742; *Sur7::mRFP::LEU2 (YIp128)*	This study
Y124	BY4742; *Pil1::mRFP::LEU2 (YIp128)*	This study
Y143	BY4742; *Pma1::GFP::URA3 (YIp211)*	Lab collection
Y157	Y091; *Sur7::GFP::URA3 (YIp211)*	Lab collection
Y159	Y090; *Sur7::mCherry::URA3 (YIp211)*	Lab collection
Y176	BY4742; *Sur7::mCherry::URA3 (YIp211)*	Lab collection
Y193	BY4742; *Sur7::GFP::URA3 (YIp211)*	Lab collection
Y207	Y318; *Pil1::mRFP::LEU2 (YIp128)*	Lab collection
Y223	Y123 + pVT100U-*Sp*Sle1-GFP	This study
Y224	Y124 + pVT100U-*Sp*Sle1-GFP	This study
Y225	BY4742; *Hxt1::GFP::LEU2 (YIp128)*	Lab collection
Y234	Y207 + pVT100U-*Sp*Sle1-GFP	This study
Y240	BY4742; *Nce102::GFP::URA3 (YIp211)*	Lab collection
Y249	BY4742; *Pil1::GFP::URA3 (YIp211)*	Lab collection
Y307	BY4742; *Sur7::GFP::URA3 (YIp211)* + YCp111-Pil1PROM-SpPil1-mRFP	This study
Y315	Y157 + YCp111-Pil1PROM-SpPil1-mRFP	This study
Y318 (*seg1Δ*)	BY4742; *seg1::KanMX4*	Euroscarf
Y328	Y176 + pVT100L-SpFhn1-GFP	This study

Y330	Y159 + pVT100L-SpFhn1-GFP	This study
Y334	BY4742 + YCp111-Pil1PROM-SpPil1-mRFP + YCp33-Seg1PROM-SpSle1-GFP	This study
Y335	Y091+ YCp111-Pil1PROM-SpPil1-mRFP + YCp33-Seg1PROM-SpSle1-GFP	This study
Y337	Y091; *Sur7::CFP::SpHIS5 (pKT101)* + YCp111-Pil1PROM-SpPil1-mRFP + YCp33-Seg1PROM-SpSle1-GFP	This study
Y341	Y124 + YCp33-Seg1PROM-SpSle1-GFP	This study
Y342	Y207 + YCp33-Seg1PROM-SpSle1-GFP	This study
Y363	Y091; *Sur7::CFP::SpHIS5 (pKT101) Seg1::GFP::LEU2 (YIp128)* + YCp33-Pil1PROM-SpPil1-mRFP	This study
Y366	Y091; YCp111-Pil1PROM-SpPil1-mRFP + YCp33-Seg1PROM-SpSle1-STOP + pVT100L-SpFhn1-GFP	This study
Y368	Y112; YCp111-Pil1PROM-SpPil1-mRFP + YCp33-Seg1PROM-SpSle1-STOP + pVT100L-SpFhn1-GFP	This study
Y369	BY4742; YCp111-Pil1PROM-SpPil1-mRFP + YCp33-Seg1PROM-SpSle1-STOP + pVT100L-SpFhn1-GFP	This study
Y373	Y063 *Seg1::GFP::LEU2 (YIp128)*	This study
Y374	Y318; *Pil1::mRFP::URA3 (YIp211)*	This study
Y382	Y091; *Seg1::GFP::SpHIS5 (pKT128)* + YCp111-Pil1PROM-SpPil1-mRFP + YCp33-Seg1PROM-SpSle1-STOP	This study
Y407	Y091 x Y410; *MATα pil1::KanMX4 XRN1::GFP::HIS3MX6*	(Grousl et al., 2015)
Y410	BY4741; *XRN1::GFP::HIS3MX6*	(Grousl et al., 2015)
Y425	Y437 + YCp111-Pil1PROM-SpPil1-mRFP + YCp33-Seg1PROM-SpSle1-GFP	This study
Y427	Y437; *Sur7::GFP::URA3 (YIp211)* + YCp111-Pil1PROM-SpPil1-mRFP	This study
Y437 (*pil1Δseg1Δ*)	Y373 x Y374; *MATα pil1::KanMX4 seg1::KanMX4*	This study
Y441	Y437 + YCp111-Pil1PROM-SpPil1-mRFP + YCp33-Seg1PROM-Seg1-GFP	This study
Y501	Y410; *Pil1::mRFP::URA3 (YIp211)*	This study
Y566	Y410 + pCM189-*MFα2*, URA3	This study
Y568	Y410 + pCM189, URA3	This study
Y583	Y407 + pCM189-*MFα2*, URA3	This study
Y815 (*nce102Δfhn1Δ*)	*his3Δ1 leu2Δ0 lys2Δ0 met15Δ0 ura3Δ0*; nce*102::KanMX4 fhn1::KanMX4*	Lab collection
Y819 (*ski7Δ*)	BY4741; *ski7::KanMX4*	Euroscarf

Y839	Y819; *XRN1::GFP::SpHIS5* (pKT128)	This study
Y841	Y839 + pCM189-*MFα2*, URA3	This study
Y970	Y090; *Sur7-Nce102::GFP::URA3* (PCR cassette from YIp211-Nce102-GFP plasmid)	Lab collection
Y1009	*vps4Δ*; *Nce102::GFP::URA3 (YIp211)*	This study
Y1010	*fab1Δ*; *Nce102::GFP::URA3 (YIp211)*	This study
Y1011	*nem1Δ*; *Nce102::GFP::URA3 (YIp211)*	This study
Y1016	BY4742; *Nce102(438)::GFP::URA3 (YIp211)*	This study
Y1044	BY4742; *Vph1::mCherry::clonNAT (pFA6a-mCherry)*	This study
Y1057	Y240; *Vph1::mCherry::clonNAT (pFA6a-mCherry)*	This study
Y1079	Y090; *Vph1::mCherry::clonNAT (pFA6a-mCherry)*	This study
Y1080	Y091; Nce102::GFP::*URA3 (YIp211)*	This study
Y1083	Y970; *Vph1::mCherry::clonNAT (pFA6a-mCherry)*	This study
Y1089	Y815; *Vph1::mCherry::clonNAT (pFA6a-mCherry)*	This study
Y1099	*fhn1Δ*; Vph1::mCherry::clonNAT *(pFA6a-mCherry)*	This study
Y1115	BY4742; *Erg6::GFP::LEU2 (YIp128)*	This study
Y1123	*fhn1Δ*; *Erg6::GFP::LEU2 (YIp128)*	This study
Y1124	Y090; *Erg6::GFP::LEU2 (YIp128)*	This study
Y1137	Y815; *Erg6::GFP::LEU2 (YIp128)*	This study

4.2 Plasmids

Table 3. Plasmids used in the study.

Plasmid name	Type	Promoter	ORF	Selection marker	Source
Integrative plasmids					
YIp128-Erg6-GFP	Integrative	-	Erg6-GFP	LEU2	This study
YIp128-Hxt1-GFP	Integrative	-	Hxt1-GFP	LEU2	Lab collection
YIp128-Pil1-mRFP	Integrative	-	Pil1-mRFP	LEU2	Lab collection
YIp128-Seg1-GFP	Integrative	-	Seg1-GFP	LEU2	This study
YIp128-Sur7-mRFP	Integrative	-	Sur7-mRFP	LEU2	Lab collection
YIp211-Nce102-GFP	Integrative	-	Nce102-GFP	URA3	Lab collection

YIp211-Nce102(438)-GFP	Integrative	-	Nce102(438)-GFP	URA3	Lab collection
YIp211-Pil1-GFP	Integrative	-	Pil1-GFP	URA3	Lab collection
YIp211-Pil1-mRFP	Integrative	-	Pil1-mRFP	URA3	Lab collection
YIp211-Pma1-GFP	Integrative	-	Pma1-GFP	URA3	Lab collection
YIp211-Sur7-GFP	Integrative	-	Sur7-GFP	URA3	(Grossmann et al., 2007)
YIp211-Sur7-mCherry	Integrative	-	Sur7-mCherry	URA3	Lab collection
Multicopy plasmids					
pVT100L-SpFhn1-GFP	Multicopy (2µ)	ADH1	SpFhn1-GFP	LEU2	This study
pVT100U-*Sp*Pil1-mRFP	Multicopy (2µ)	ADH1	*Sp*Pil1-GFP	URA3	This study
pVT100U-*Sp*Sle1-GFP	Multicopy (2µ)	ADH1	*Sp*Sle1-GFP	URA3	This study
Centromeric plasmids					
YCplac33-PIL1PROM-*Sp*Pil1-mRFP	Centromeric	PIL1	*Sp*Pil1-mRFP	URA3	This study
YCplac111-PIL1PROM-*Sp*Pil1-mRFP	Centromeric	PIL1	*Sp*Pil1-mRFP	LEU2	This study
YCplac33-SEG1PROM-Seg1-GFP	Centromeric	SEG1	Seg1-GFP	URA3	This study
YCplac33-SEG1PROM-*Sp*Sle1-GFP	Centromeric	SEG1	*Sp*Sle1-GFP	URA3	This study
YCplac33-SEG1PROM-*Sp*Sle1-STOP	Centromeric	SEG1	*Sp*Sle1	URA3	This study
Tetracycline-regulated plasmids					
pCM189	Centromeric	tetO7	-	URA3	Euroscarf
pCM189-MFα2	Centromeric	tetO7	*MFα2*	URA3	This study
Plasmids for genomic tagging					
pFA6a-mCherry	pFA6a	-	mCherry	clonNAT	Lab collection
pKT101	pFA6a	-	yECFP	*Sp*HIS5	Euroscarf
pKT128	pFA6a	-	yEGFP	*Sp*HIS5	Euroscarf

4.3 Primers

Table 4. Primers used in the study.

Primer name	Sequence	Purpose
Preparation of integrative plasmids		
Erg6-HindIII-F	5′-ATCGAAGCTTTATGAGTGAAACAGAATTGAG-3′	Erg6 cloning into YIp128-GFP vector
Erg6-BamHI-R	5′-TATAGGATCCTTGAGTTGCTTCTTGGGAAG-3′	Erg6 cloning into YIp128-GFP vector
Seg1_YIp_Xho_F	5′-ATCGCTCGAGATGTTTAGAAGAAGAAC-3′	Seg1 cloning into YIp128-GFP vector
Seg1_YIp_BamH_R	5′-AGCTGGATCCTTTCTTTCTACCAAAG-3′	Seg1 cloning into YIp128-GFP vector
Preparation of multicopy plasmids		
POMBE_NCE_FW	5′-CCCAAAGCTTAT GGTTGGAATCAG-3′	*Sp*Fhn1 cloning into pVT100L-GFP
POMBE_NCE_FW	5′-AAAAGGATCCAACGGCAGACATGAC-3′	*Sp*Fhn1 cloning into pVT100L-GFP
Sle1-pVT_Xho_F	5′-CATACTCGAGATGAGCCATGCTTC-3′	*Sp*Sle1 cloning into pVT100U-GFP
Sle1-pVT_Xba_R	5′-CCGGTCTAGAGAAACGCATTTTAAAAAATTTC-3′	*Sp*Sle1 cloning into pVT100U-GFP
SpPil1_pVT_Hind_F	5′-CATATCTAGAAGCAACCTGGACGG-3′	*Sp*Pil1 cloning into pVT100U-mRFP
SpPil1_pVT_Xba_R	5′-CCTATCTAGATTAAGCAACCTGGACG-3′	*Sp*Pil1 cloning into pVT100U-mRFP
Preparation of centromeric plasmids		
Pil1-PROM_Hind_F	5′-ACGCAAGCTTCCACTGATTCAGAGTTC-3′	*PIL1* promoter cloning into YCp111 plasmid
Pil1-PROM_SalI_R2	5′-CGACGTCGACACTATATACTTGATGCTG-3′	*PIL1* promoter cloning into YCp111 plasmid
SpPil1_YCp_Sal_F	5′-ATAGGTCGACATGATGAACCGTGC-3′	Cloning of *Sp*Pil1 into YCp111-Pil1PROM plasmid

SpPil1-mRFP_YCp_EcoRI_R	5′-ATTCGAATTCTTAGGCGCCGGTGG-3′	Cloning of *Sp*Pil1 into YCp111-Pil1PROM plasmid
Seg1_PROM_Hind_F	5′-GCTCAAGCTTTAACAAGGGGCATAAG-3′	*SEG1* promoter cloning into YCp111 plasmid
Seg1_PROM_SalI_R	5′-GACAGTCGACTTTTAGGAACGAACGG-3′	*SEG1* promoter cloning into YCp111 plasmid
Seg1_YCp_Sal_F	5′-CTCGGTCGACATGTTTAGAAGAAGAAC-3′	Cloning of Seg1 into YCp33-SEG1PROM plasmid
Seg-Sle-GFP_YCp_Sac_R	5′-GACCGAGCTCTTATTTGTA-CAATTCATCC-3′	Cloning of Seg1 into YCp33-SEG1PROM plasmid
Tetracycline-regulated plasmids		
MFα2_pCM_BamH_F	5′-TGATCTGCAGTCAGTACATTGGTTGGCC-3′	Cloning of *MFα2* into pCM189
MFα2_pCM_Pst_R	5′-GACAGAATTCGGAAATAGGTCTTTGACAG-3′	Cloning of *MFα2* into pCM189
Genomic tagging		
Kem1_gnmtg_F	5′-AGTCACAAAGCAATGCTGCTGACCGTGATAATAAAAAAGACGAATCTACTCGGATCGGTGACGGTGCTGG-3′	Genomic tagging of Xrn1
Kem1_gnmtg_R	5′-GGTCTCAGATATACTATTAAAGTAACCTCGAATATACTTCGTTTTTAGTCGTATGCATCGATGAATTCGAGCTCG-3′	Genomic tagging of Xrn1
Kem1-gnmtg-ctrl-F	5′-ACAGCACAGCAATGGTTCAA-3′	Verification of Xrn1 genomic tagging
Kem1-gnmtg-ctrl-R	5′-CTATGCGGAAAGCTTTGTGT-3′	Verification of Xrn1 genomic tagging
Seg1_gnmtg_F	5′-TTTCGGCAAAAAACTGAAAAAAATCTTTGGTAGAAAGAAACGGATCGGTGACGGTGCTGG-3′	Genomic tagging of Seg1
Seg1_gnmtg_R	5′-ATGGAAGCCATCGTTCAGAAGTTGAACGAGCACGAAAAAGCATCGATGAATTCGAGCTCG-3′	Genomic tagging of Seg1
SEG1_CTRgnm_F	5′-AGCTGCCAGTGAAGCTGAAC-3′	Verification of Seg1 genomic tagging

SEG1_CTRgnm_R	5′-ATCGCCATTGATTGCAGTGG-3′	Verification of Seg1 genomic tagging
Sur7-gnmtg_F	5′-TATAAGAAAATCACACGAGCGCCCGGACGATGTCTCTGTTCGGATCGGTGACGGTGCTGG-3′	Genomic tagging of Sur7
Sur7-gnmtg_R	5′-GGGTATAAATATATATTACAAAGCGGAAAACTTGCGCCATCATCGATGAATTCGAGCTCG-3′	Genomic tagging of Sur7
SUR7_CTRgnm_F	5′-CTGACCCAATATTGACTGCC-3′	Verification of Sur7 genomic tagging
SUR7_CTRgnm_R	5′-AGTGCGCCGGTAAATGAAG-3′	Verification of Sur7 genomic tagging
Vph1-pFA6amCherryNat-F	5′-GGAAGTCGCTGTTGCTAGTGCAAGCTCTTCCGCTTCAAGCCGTACGCTGCAGGTCGAC-3′	Genomic tagging of Vph1
Vph1-pFA6amCherryNat-R	5′-AAGGCAAATGATGGTCACTGGTGGATTGGATTGCAAGTCTAACCATCGATGAATTCGAGCTCG-3′	Genomic tagging of Vph1
Primers for qPCR analysis		
RT_MFα2_for3	5′-TGGATACTTGGATTTCGGAGG-3′	qPCR detection of *MFα2*
RT_MFα2_rev3	5′-CCGCCTCAGCAATAGTGGT-3′	qPCR detection of *MFα2*
RT_ACT1_for	5′-ACCGCTGCTCAATCTTCTTC-3′	qPCR detection of *ACT1*
RT_ACT1_rev	5′-GGTCAATACCGGCAGATTCC-3′	qPCR detection of *ACT1*
RT_IPP1_for	5′-ATGAAGGTGAGACCGATTGG-3′	qPCR detection of *IPP1*
RT_IPP1_rev	5′-CTGGCTTACCATCTGGGATT-3′	qPCR detection of *IPP1*

4.4 Yeast cultivation

Yeast cells cultivation and growth conditions

For yeast maintenance, yeast cells were grown on complete rich medium (YPD) agar plates (2% peptone, 1% yeast extract, 2% glucose, 2% agar) or selective agar plates (0,67% Difco yeast nitrogen base without amino acids, 2% glucose, and amino acids as required, 2% agar) according to the selection marker of the strain. Cells were kept in + 4°C for short time periods. Otherwise, cells were resuspended in 20% glycerol, freezed in liquid nitrogen and stored in - 80°C as stock cultures.

For liquid culturing, yeast cells were grown either in YPD (2% peptone, 1% yeast extract, 2% glucose) (mostly for pre-culturing of cells before yeast transformation, chromosomal DNA

isolation, etc.) or in synthetic medium (for actual experiments) (0,67% Difco yeast nitrogen base without amino acids, 2% glucose, and amino acids as required).

For fluorescence microscopy of Xrn1-GFP and determination of *MFα2* (mating factor α 2) mRNA level, yeast cells were cultured as follows: Cells were grown in the synthetic medium (ON, 30°C, on a shaker) and next day, cells were inoculated into the fresh synthetic medium (to OD_{600} 0.2) and grown into the required phase (at 30°C, on a shaker). The growth of the culture as well as the localization of the Xrn1-GFP signal at confocal microscope was monitored. The required phases we defined as previously (Grousl et al., 2015). In fast-growing exponential cells, Xrn1-GFP was homogeneously distributed in the cytoplasm and all the strains reached this phase after 4h incubation. Diauxic cells were characterized by the slowing of the cell culture growth and these cells exhibited Xrn1-GFP accumulated in P-bodies. Wild type strain (Y410) reached this phase after 24h after inoculation. In post-diauxic cells, the concentration of the glucose in the medium dropped below 0.05% (500 mg/l) as was always determined by standard test stripes (GlukoPhan, ErbaLachema, Czech Republic). In these cells, Xrn1-GFP was associated with eisosomes and wild type cells (Y410) reached this phase after 30h of growth.

Cultures of wild type cells expressing empty plasmid pCM189 (Y568) or plasmid pCM189-*MFα2* (Y566) reached these Xrn1-GFP fluorescence patterns faster than the wild type strain. Xrn1-GFP was accumulated in P-bodies already after 18h of incubation and Xrn1-GFP associated with eisosomes after 24h of incubation. In contrast, *ski7Δ* strain bearing pCM189-*MFα2* vector (Y841) required 28h and 33h of growth to reach phases of Xrn1-GFP accumulated in P-bodies, or of Xrn1-GFP association with eisosomes, respectively. *pil1Δ* strain expressing pCM189-MFα2 vector (Y583) exhausted glucose under the limit already after 24h incubation. However, these cells had still Xrn1-GFP accumulated in P-bodies (Grousl et al., 2015). Because of the absence of eisosomes in these cells, we were not able to observe cortical localization of Xrn1-GFP even after prolonged times of culture growth (up to 54 hours).

For fluorescence microscopy of Nce102-GFP localizations, yeast cells were grown in the synthetic medium (ON, 30°C, on a shaker) and next day, cells were inoculated into the fresh synthetic medium (to OD_{600} 0.2) and grown into the required phase (at 30°C, on a shaker). Nce102-GFP localizations were monitored after 7h (logarithmic phase), 24h, 48h, 72h, 96h, 120h, 144h and 196h, as indicated in the Results section. At the indicated time points, aliquots for cell lysate preparation were withdrawn from the growing cultures.

For FM4-64 staining, FM4-64 dye (N-(3-triethylammoniumpropyl)-4-(6-(4-(diethylamino) phenyl) hexatrienyl) pyridinium dibromide) (ThermoFisher Scientific, Waltham, MA, USA)

was added to the freshly inoculated yeast culture (final concentration 10 μM) and incubated with cells for the whole time of their incubation. Prior to imaging, cells were washed twice with distilled H_2O.

For fluorescence microscopy in experiments of *S. pombe* proteins expression in *S. cerevisiae*, yeast cells were first grown in synthetic medium (ON, 30°C, on a shaker) and next day, cells were inoculated into the fresh synthetic medium (to OD_{600} 0.2) and grown into the mid-log phase (OD_{600} 0.8 – 1.0) at + 30°C on a shaker.

4.5 Expression of fluorescently-tagged proteins

Basic molecular biology methods

For polymerase chain reaction (PCR), Q5 Hot Start DNA polymerase (New England Biolabs, Ipswich, MA, USA) or Phusion Hot Start DNA polymerase (ThermoFisher Scientific, Waltham, MA, USA) were used. For colony PCR, DreamTaq DNA polymerase (ThermoFisher Scientific, Waltham, MA, USA) was used. dNTP mix (10mM each) (ThermoFisher Scientific, Waltham, MA, USA) was used in PCR reactions.

DNA electrophoresis was performed in 1% agarose gel in TAE buffer (40mM Tris-Cl, 20mM glacial acetic acid, 1mM EDTA (pH 8.0)). Samples were mixed with DNA gel loading dye (6x) (ThermoFisher Scientific, Waltham, MA, USA) and GeneRuler DNA ladder (1kb) (ThermoFisher Scientific, Waltham, MA, USA) was used as a marker.

All restriction enzymes used were FastDigest variants (ThermoFisher Scientific, Waltham, MA, USA). For ligation, T4 DNA ligase (ThermoFisher Scientific, Waltham, MA, USA) was used.

Plasmid preparation

- Integrative plasmids for *S. cerevisiae* proteins expression

YIp128-Erg6-GFP: The ERG6 gene was PCR-amplified from *S. cerevisiae* genomic DNA using **Erg6-HindIII-F** and **Erg6-BamHI-R** primers. The PCR fragment was digested with HindIII and BamHI restriction enzymes and ligated into YIp128-GFP plasmid. Before yeast transformation, the plasmid was linearized with ApaI restriction enzyme.

YIp128-Seg1-GFP: The SEG1 gene was PCR-amplified from *S. cerevisiae* genomic DNA using **Seg1_YIp_Xho_F** and **Seg1_YIp_BamH_R** primers. The PCR fragment was digested with XhoI and BamHI restriction enzymes and ligated into YIp128-GFP plasmid. Before yeast transformation, the plasmid was linearized with NheI restriction enzyme.

- Multicopy plasmids for expression of proteins in *S. cerevisiae*

pVT100L-*Sp*Fhn1-GFP: The *Sp*Fhn1 gene was PCR-amplified from *S. pombe* genomic DNA using **Pombe_NCE_FW** and **Pombe_NCE_RV** primers. The PCR fragment was digested with HindIII and BamHI restriction enzymes and ligated into pVT100L-GFP plasmid.

pVT100U-*Sp*Pil1-mRFP: The *Sp*Sle1 gene was PCR-amplified from *S. pombe* genomic DNA using **SpPil1_pVT_Hind_F** and **SpPil1_pVT_Xba_R** primers. The PCR fragment was digested with HindIII and XbaI restriction enzymes and ligated into pVT100U-mRFP plasmid.

pVT100U-*Sp*Sle1-GFP: The *Sp*SLE1 gene was PCR-amplified from *S. pombe* genomic DNA using **Sle1-pVT_Xho_F** and **Sle1-pVT_Xba_R** primers. The PCR fragment was digested with XhoI and XbaI restriction enzymes and ligated into pVT100U-GFP plasmid.

- Centromeric plasmids for expression of proteins in *S. cerevisiae*

YCplac111-PIL1PROM-*Sp*Pil1-mRFP: First, the promoter region (800bp) of *PIL1* gene was amplified from the *S. cerevisiae* genomic DNA using **Pil1-PROM_Hind_F** and **Pil1-PROM_SalI_R2** primers. The *PIL1* promoter region was than ligated into YCplac111 plasmid using HindIII and SalI restriction sites. The *SpPIL1-mRFP* gene was amplified from pVT100U-*Sp*Pil1-mRFP plasmid using **SpPil1_YCp_Sal_F** and **SpPil1-mRFP_YCp_EcoRI_R** plasmids. The *Sp*Pil1-mRFP fragment was then ligated into YCplac111-PIL1PROM plasmid using SalI and EcoRI restriction sites. As this plasmid did not contain terminator sequence, PIL1PROM-SpPil1 sequence was cut out from this plasmid using HindIII and XbaI restriction enzymes and ligated into YCplac111-mRFP.

YCplac33-PIL1PROM-*Sp*Pil1-mRFP: This plasmid was prepared in the same way as YCplac111-PIL1PROM-*Sp*Pil1-mRFP. The only difference was that the YCplac33 plasmid was used as a backbone.

YCplac33-SEG1PROM-*Sp*Sle1-GFP: First, the promoter region (617bp) of *SEG1* gene was amplified from the *S. cerevisiae* genomic DNA using **Seg1_PROM_Hind_F** and **Seg1_PROM_SalI_R** primers. The *SEG1* promoter region was than ligated into YCplac33 plasmid using HindIII and SalI restriction sites. The *SpSLE1-GFP* gene was cut out from pVT100U-*Sp*Sle1-GFP plasmid together with *ADH1* terminator sequence using XhoI and SacI restriction sites and ligated into YCp33-Seg1-PROM plasmid.

YCplac33-SEG1PROM-Seg1-GFP: The Seg1-GFP sequence was amplified from Yip128-Seg1-GFP plasmid using **Seg1_YCp_Sal_F** and **Seg-Sle-GFP_YCp_Sac_R** primers. The fragment was then ligated into YCp33-Seg1PROM plasmid using SalI and SacI restriction sites. The resulting plasmid did not contain transcription terminator, therefore, the GFP sequence was

replaced by GFP-ADH1 terminator sequence cut out from pVT100U-GFP plasmid using BamHI and SacI restriction sites.

YCplac33-SEG1PROM-*Sp*Sle1-STOP: From the YCplac33-SEG1PROM-*Sp*Sle1-GFP plasmid, the GFP sequence was cut out using XbaI and BssHII restriction enzymes. The ends of the fragment were blunted by MungBean nuclease and ligated together.

- Tetracycline-regulated plasmids

pCM189-*MFα2*: For *MFα2* mRNA expression in *S. cerevisiae* cells, tetracycline-repressible centromeric expression vector pCM189 was used. *MFα2* gene was amplified by PCR from *S. cerevisiae* chromosomal DNA using **MFα2_pCM_BamH_F** and **MFα2_pCM_Pst_R** primers. PCR fragment was digested with BamHI and PstI restriction enzymes and ligated into the similarly digested pCM189 vector. Empty pCM189 vector was used as a control for determining the endogenous *MFα2* mRNA expression level.

Plasmid maintenance and bacteria cultivation

All plasmids used were amplified and stored in the *Escherichia coli* XL1-blue cells. Plasmids were transformed into competent bacteria using the heat shock method. After transformation, the transformants bearing a plasmid were selected using ampicillin resistance.

For bacteria maintenance, bacteria cells were grown on LBa agar plates (1% tryptone, 0.5% yeast extract, 1% NaCl, 50µg/ml ampicillin, 1.5% agar) and kept in + 4°C for short time periods. Otherwise, cells were resuspended in 20% glycerol, freezed in liquid nitrogen and stored in - 80°C as stock cultures. For plasmid isolation, bacteria bearing plasmids were cultivated in LBa medium (1% tryptone, 0.5% yeast extract, 1% NaCl, 50µg/ml ampicillin) at 37°C overnight. Plasmids were isolated using miniprep kits (QIAprep Spin Miniprep Kit (Qiagen, Hilden, Germany) and FastPlasmid Mini Kit (5PRIME, Hamburg, Germany)).

Yeast transformation

Plasmids or PCR fragments were transformed into yeast cells using LiAc method. Briefly, cells were grown in YPD medium from OD_{600} 0.5 to OD_{600} 1, two times washed with 0.1M LiAc, and then incubated with transfection mixture (240 µl 50% PEG, 36 µl 1M LiAc, 50 µl ssDNA, plasmid DNA) for 30 min at + 30°C at a shaker and subsequently, incubated 20 min at + 42°C. For non-integrative plasmids, cells were then washed with H_2O and plated on a selective plate according to the plasmid selection marker. For integrative plasmids transformation, cells were additionally incubated for 3 h in YPD medium at + 30°C on a shaker and afterwards plated on a selective plate.

Genomic tagging of *S. cerevisiae* proteins

To visualize some *S. cerevisiae* proteins, the method of genomic tagging was employed – the sequence of fluorescent protein was inserted after the target gene directly into chromosomal DNA. The cassette bearing fluorescent protein and selection marker was amplified by PCR from specialized plasmids using primers with specific ends homologous to the end of the target gene. PCR-amplified cassette was transformed directly into yeast cells and transformants were selected using selection marker. Finally, they were verified using colony PCR on chromosomal DNA testing for the presence of the cassette after the target gene.

- Genomic GFP-tagging of **Seg1** protein

To genomically express GFP-tagged Seg1 protein, the cassette bearing GFP and histidine (*Sp*HIS5) selection was amplified from pKT128 plasmid (EUROSCARF, Scientific Research and Development GmbH, Germany) using primers **Seg1_gnmtg_F** and **Seg1_gnmtg_R**. For colony PCR verification, plasmids **SEG1_CTRgnm_F** and **SEG1_CTRgnm_R** were used.

- Genomic CFP-tagging of **Sur7** protein

To genomically express CFP-tagged Sur7 protein, the cassette bearing CFP and histidine (*Sp*HIS5) selection was amplified from pKT101 plasmid (EUROSCARF, Scientific Research and Development GmbH, Germany) using primers **Sur7-gnmtg_F** and **Sur7-gnmtg_R**. For colony PCR verification, plasmids **SUR7_CTRgnm_F** and **SUR7_CTRgnm_R** were used.

- Genomic GFP-tagging of **Vph1** protein

To visualize Vph1, the cassette bearing mCherry and nourseothricin (clonNAT) selection was amplified from pFA6a-mCherry plasmid (laboratory collection) using primers **Vph1-pFA6amCherryNat-F** and **Vph1-pFA6amCherryNat-R**.

- Genomic GFP-tagging of **Xrn1** protein

To visualize Xrn1, the cassette bearing yEGFP and histidine (*Sp*HIS5) selection was amplified from pKT128 plasmid (EUROSCARF, Scientific Research and Development GmbH, Germany) using primers **Kem1_gnmtg_F** and **Kem1_gnmtg_R**. For colony PCR verification, plasmids **Kem1-gnmtg-ctrl-F** and **Kem1-gnmtg-ctrl-R** were used.

Preparation of *pil1Δseg1Δ* double deletion strain

ON grown cells *pil1Δ*(MATa)-Seg1::GFP::LEU2 (Y373) and *seg1Δ*(MATα)-Pil1::mRFP::URA3 (Y374) were incubated together in liquid YPD medium (ratio of liquid cultures 1:1) in + 30°C, ON to allow them for mate. Subsequently, they were let to sporulate at

Fowell agar plates (1% yeast extract, 0.5% glucose, 10% potassium acetate, 2% agar) and tetrades weakened by Zymolyase 20T (Seikagaku, Japan) were dissected on YPD plates using MSM 400 dissection microscope (Singer Instruments, Roadwater, Watchet, UK). Double deletants were pre-screened at the confocal microscope (non-fluorescent colonies were chosen) and the deletions were next verified by the colony PCR.

4.6 mRNA and protein analyses

RNA isolation from yeast cells

Yeast cultures expressing pCM189 or pCM189-*MFα2* vectors were grown into the desired state as described in part 4.4. When needed, glucose (final concentration 2%) or cycloheximide (CHX, final concentration 10 μg/ml) (Sigma-Aldrich, Saint-Louis, MO, USA) were added to the cultures 10 min before the experiment. Then, the cultures were divided into two subcultures – one was supplemented with doxycycline (2μg/ml final concentration) (Sigma-Aldrich, Saint-Louis, MO, USA) to stop the translation of *MFα2* mRNA and monitor the activity of Xrn1 and the second was supplemented with the same amount of distilled H_20 and served as a control sample with equilibrium level of *MFα2* mRNA. Aliquots were withdrawn from the both cultures at time points 0 min (before the addition of doxycycline or water) and 15, 30 and 60 min after the addition of doxycycline or water. Samples were briefly centrifuged and frozen in liquid nitrogen.

Total RNA isolation was performed from the all the samples from one experiment at once using the GeneJET RNA purification kit (ThermoFisher Scientific, Waltham, MA, USA) according to the protocol provided. Contaminant DNA was digested with RapidOut DNA removal kit (ThermoFisher Scientific, Waltham, MA, USA).

qPCR (quantitative PCR) analysis

From the total RNA isolates, cDNA was synthesized using Oligo$(dT)_{18}$ Primer and Random Hexamer Primer (both from ThermoFisher Scientific, Waltham, MA, USA) and Revert Aid Reverse Transcriptase (ThermoFisher Scientific, Waltham, MA, USA). To prevent RNA degradation, RiboLock RNase Inhibitor (ThermoFisher Scientific, Waltham, MA, USA) was added to the reaction.

cDNA was used as a template in the qPCR reaction for the quantification of the *MFα2* transcript abundance. The *MFα2* sequence was amplified using primers **RT_MFα2_for3** and

RT_MFα2_rev3 and Maxima SYBR Green qPCR Master Mix (ThermoFisher Scientific, Waltham, MA, USA) in the 7900HT Fast Real-Time PCR System (Applied Biosystems, Foster City, CA, USA). The correct products were verified by melting curve analysis. The *MFα2* data were normalized to the control genes – *ACT1* (primers **RT_ACT1_for** and **RT_ACT1_rev**) and *IPP1* (primers **RT_IPP1_for** and **RT_IPP1_rev**), whose mRNA levels at time point 0 min were set as 1. Statistical significance was determined from three independent experiments by the one-way ANOVA test in SigmaPlot 12.5 software (Systat Software Inc., San Jose, CA, USA).

Preparation of cell lysates

Method 1 - The cultures were grown into the desired phase or treated as needed. 8 OD_{600} of cells was withdrawn from the culture, centrifuged, resuspended in distilled H20 and precipitated by the 100% TCA (final concentration 6 %) for 10 min. Precipitates were two-times washed in cold acetone (500 µl) and resuspended in urea buffer (100 µl) (25mM Tris-Cl at pH 6.8, 6M urea, 1% SDS). Next, glass beads (0.43-0.57mm (Glass Sphere s.r.o., Jablonec nad Nisou, Czech Republic)) were added to the samples and samples were homogenized in a BeadBug Microtube Homogenizer (Benchmark Scientific, Edison, NJ, USA). Finally, samples were heated at 95°C for 5 min, centrifuged to dispose of the glass beads and diluted into the 2x SDS sample buffer (125mM Tris-Cl at pH6.8, 20% glycerol, 2% SDS, 0.02% bromphenol blue, 200mM DTT).

Method 2 - The cultures were grown into the desired phase or treated as needed. 25 ml of cells was withdrawn from the culture, centrifuged, washed twice in TNE buffer and resuspended in 500 µl of TNE buffer (50mM Tris-HCl at pH 7.4, 150mM NaCl, 5mM EDTA) with protease and phosphatase inhibitors (cOmplete Mini protease inhibitor cocktail tablets (Roche Diagnostics GmbH, Mannheim, Germany) – 1 pill per 10ml TNE buffer, leupeptin – final concentration 1 µg/ml, pepstatin – final concentration 1 µg/ml, PMSF (phenylmethylsulfonyl fluoride) – final concentration 1 mM, ABA (benzamidine) – final concentration 1mM). Glass beads (0.43-0.57mm (Glass Sphere s.r.o., Jablonec nad Nisou, Czech Republic)) were added to the samples and samples were homogenized in a BeadBug Microtube Homogenizer (Benchmark Scientific, Edison, NJ, USA). The protein concentration in cell homogenates was determined using Pierce BCA Protein Assay Kit (ThermoFisher Scientific, Waltham, MA, USA) and samples were diluted to the same protein concentration. Finally, 5x SDS sample buffer (62.5mM Tris-Cl at pH6.8, 5% glycerol, 2% SDS, 5% 2-mercaptoethanol, 0.019% bromphenol blue) was added and samples were heated at + 95°C for 5 min.

Protein electrophoresis and Western blot analysis

Proteins samples were separated in the polyacrylamide gel (percentage according to the molecular weight of the protein of interest, run at approximately 15 mA/gel in stacking gel and 20 mA/gel in separating gel) in the running buffer (25mM Tris-Cl pH 8,8, 0.192M glycine, 0.1% SDS). PageRuler Plus pre-stained protein ladder (ThermoFisher Scientific, Waltham, MA, USA) was used as a marker. Proteins were transferred onto the PVDF membrane (Pall Corporation, New York, USA or Merck, Darmstadt, Germany) in a wet Western blot (360 mA, 30 min) in blotting buffer (20mM Tris-Cl, 150mM glycine, 20% methanol, 0.02% SDS). Membranes were washed briefly in TBST buffer (50mM Tris-Cl at pH 7.4, 0.15M NaCl, 0.05% Tween 20), blocked in 5% milk in TBST buffer (2 h, room temperature (RT)) and incubated with the primary antibody (4°C, overnight (ON)). Next day, membranes were washed three times in TBST buffer and incubated with secondary antibody (1 h, RT) or directly developed, depending on the type of primary antibody. The HRP-signal was visualized using SuperSignal West Femto Maximum Sensitivity Substrates (ThermoFisher Scientific, Waltham, MA, USA) or Radiance Plus highest sensitivity chemiluminescent HRP substrates (Azure Biosystems, Bublic, CA, USA) in the c400 Imaging System (Azure Biosystems, Bublic, CA, USA). Signals were analyzed in Adobe Photoshop CS3 software (Adobe Systems Inc., San Jose, CA, USA). The statistical significance was determined from three independent experiments by the one-way ANOVA test in SigmaPlot 12.5 software (Systat Software Inc., San Jose, CA, USA).

List of primary antibodies

- HRP-conjugated anti-GFP antibody (Santa Cruz Biotechnology, Dallas, TX USA) – dilution 1000x in 1% milk in TBST
- Rat monoclonal anti-tubulin 1 antibody (Abcam, Cambridge, UK) – dilution 1000x in 1% milk in TBST (ab6160 and ab6161)
- Rabbit polyclonal anti-dsRed antibody (Takara Bio, Kusatsu, Shiga, Japan) – dilution 1000x-3000x in 5% milk in TBST

List of secondary antibodies

- HRP-conjugated anti-rat secondary antibody (Jackson ImmunoResearch, West Grove, PA, USA) – dilution 10 000x in 1% milk in TBST

- HRP-conjugated anti-rabbit secondary antibody (Jackson ImmunoResearch, West Grove, PA, USA) – dilution 10 000x in 5% milk in TBST

4.7 Fluorescence microscopy

The aliquot of living cells was withdrawn from the growing culture, cells were concentrated by brief centrifugation, loaded onto the standard No. 1.5 coverslip and immobilized by a thin layer of agarose (1%) diluted either in 50mM phosphate buffer (pH 6,3; (77.5 ml 0.2M KH2PO4, 22.5 ml 0.2M K2HPO4 / 400 ml distilled H2O)) (for the experiments of *S. pombe* proteins expression in *S. cerevisiae*) or in the conditioned medium (in experiments for determining the Xrn1 localization as Xrn1 localization in cells was largely dependent on the nutrition status of the medium). Samples were observed under the LSM510-META laser scanning confocal microscope (Zeiss, Oberkochen, Germany) or an FV1200MPE laser scanning confocal microscope (Olympus, Tokyo, Japan). In LSM510-META confocal microscope a 100x PlanApochromat oil-immersion objective (NA=1.4) was used. In FV1200MPE confocal microscope a 100x UPlanSApo oil-immersion objective (NA=1.4) was used. Fluorescence signal of GFP was excited by 488nm line of an Ar laser and was detected using a 500-545nm emission filter. Fluorescence signal of mRFP was excited by 561nm line of solid state laser and detected using a 575-615 emission filter. Fluorescence signal of CFP was excited by 458nm line of an Ar laser and detected using a 475-525 emission filter. Fluorescence signal of FM4-64 was excited by 488nm line of Ar laser and was detected using 634-734nm emission filter. Images were analyzed in Adobe Photoshop CS3 software (Adobe Systems Inc., San Jose, CA, USA) or ImageJ software (Schneider et al., 2012).

5. Results

5.1 Role of MCC/eisosomes in regulation of mRNA decay during chronic glucose depletion

Bulk mRNA degradation occurs through two distinct pathways, either in 5′-3′ or 3′-5′direction (Łabno et al., 2016). The 3′-5′ mRNA degradation is mediated by a complex of cytoplasmic proteins called exosome (Araki et al., 2001). The 5′-3′ mRNA degradation is executed by Xrn1 exoribonuclease enzyme (Haimovich et al., 2013; Nagarajan et al., 2013).

Xrn1 is widely evolutionarily conserved from yeast to mammals and in yeast, Xrn1 is responsible for the degradation of the majority of mRNA. Grousl and coworkers found that the localization of Xrn1 depends on the availability of glucose in the medium (Grousl et al., 2015). In exponential cells with a fermentative metabolism (supplemented with enough glucose in the medium), Xrn1 is homogeneously dispersed throughout the cytoplasm. In the cells undergoing a so-called diauxic shift, i.e. the adaptation to the exhaustion of the glucose as the carbon source, during which cells switch from the anaerobic to aerobic metabolism (diauxic cells), Xrn1 accumulates in processing bodies (P-bodies). P-bodies are cytoplasmic ribonucleoprotein particles implicated in either mRNA decay or translational inhibition (Parker and Sheth, 2007). Finally, in post-diauxic cells (with the chronic lack of glucose in the medium and with the aerobic metabolism), Xrn1 is re-localized to the MCC/eisosomes. This happens in contrast to other components of mRNA 5′-3′ decay pathway that stay accumulated in P-bodies (Grousl et al., 2015). We aimed to investigate the functional significance of Xrn1 accumulation at MCC/eisosomes in post-diauxic cells.

5.1.1 *MFα2* mRNA is degraded through Xrn1-mediated 5′-3′ degradation pathway

To investigate the functional significance of Xrn1 re-localization, we first aimed to establish a reliable method for determining the enzymatic activity of Xrn1. Mating factor mRNAs were previously reported to be degraded by Xrn1 and, due to their short life-time, they were shown to be suitable for monitoring of Xrn1 activity (Hsu and Stevens, 1993; Solinger et al., 1999). To assess its exoribonuclease activity, we monitored the amount of the reporter mRNA, mRNA

for mating factor α 2 (*MFα2*). We cloned the sequence for *MFα2* under the doxycycline-repressible promoter in the centromeric expression vector (pCM189). In cells possessing this plasmid growing in the synthetic medium without doxycycline, the *MFα2* mRNA was produced from the expression vector. Upon the addition of doxycycline into the medium, the transcription of *MFα2* mRNA was stopped and the definite amount of *MFα2* mRNA could be then degraded by Xrn1. We measured the amount of *MFα2* mRNA before the addition of doxycycline (time point 0 min) and after doxycycline treatment in certain time points (15 min, 30 min, 60 min). At these time points, the total mRNA was isolated from yeast cultures and the amount of *MFα2* mRNA was determined using quantitative PCR (qPCR) method. This way, we were able to monitor the potential decrease in *MFα2* mRNA level that we used as a measure of overall mRNA decay.

To test our method, the plasmid carrying doxycycline-repressible *MFα2* gene was transformed into wild type cells with genomically GFP-tagged Xrn1 protein (Xrn1-GFP). In logarithmically growing yeast cell cultures, a substantial decrease in *MFα2* mRNA level, indicating *MFα2* mRNA degradation was observed already after 30 minutes after doxycycline treatment (Fig. 8A). It is important to note, that the *MFα2* mRNA expression from the expression vector was much higher than the expression of the endogenous *MFα2* mRNA (monitored in cells with the empty vector) (Fig. 8H). Therefore, the endogenous *MFα2* mRNA expression levels did not interfere with our system for monitoring the Xrn1 activity.

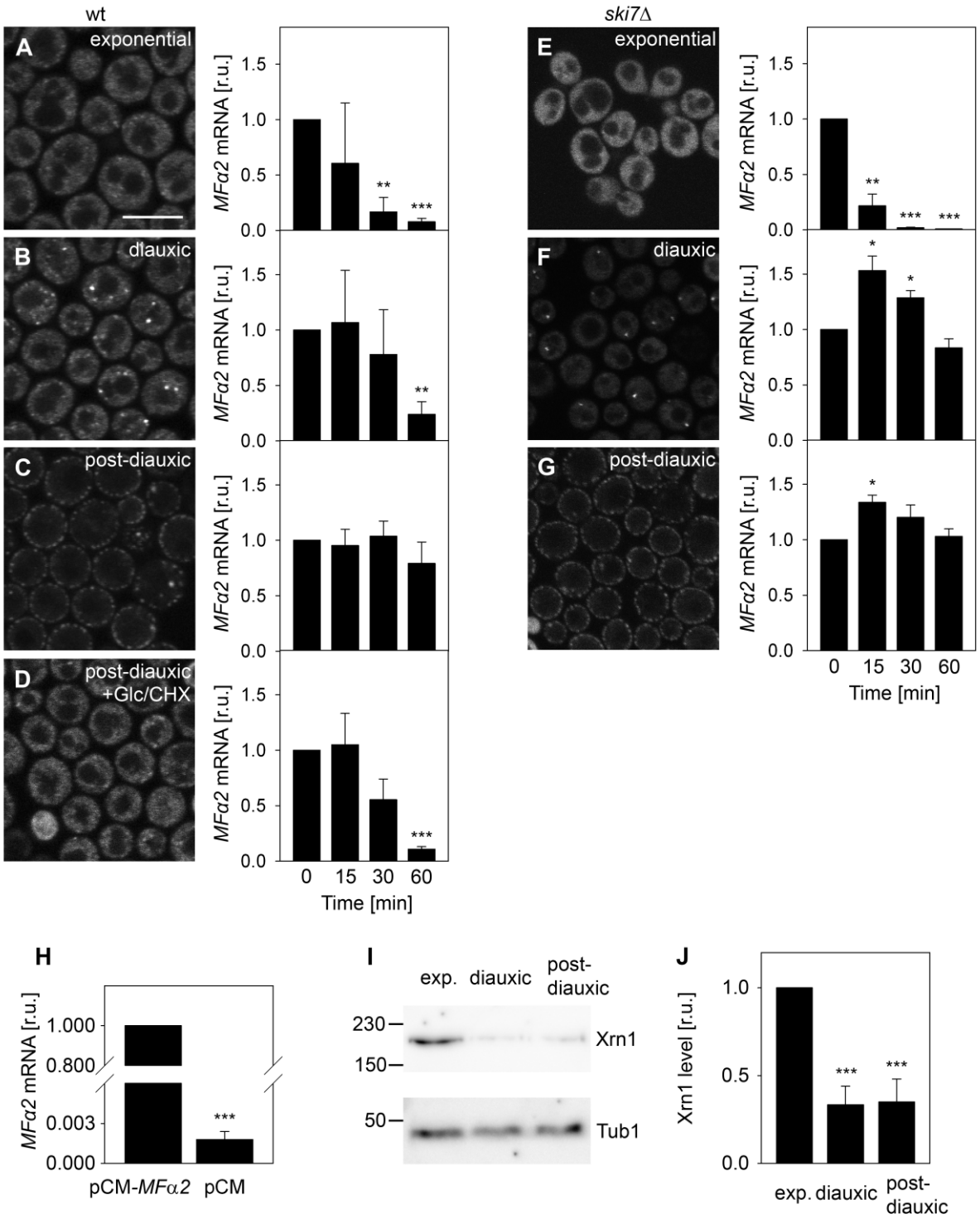

Figure 8. Xrn1 exoribonuclease activity correlates with Xrn1 localization in cells.

Xrn1-GFP localization and activity was monitored in wild type (Y566; A, B, C, D) and *ski7Δ* (Y841; E, F, G) cells. Logarithmic (row 1), diauxic (row 2) and post-diauxic (row 3) phase cells were analyzed. To wild-type post-diauxic cells, also glucose (final concentration 2 %) and cycloheximide (10 µg/ml) were added (D). Xrn1-GFP localizations in these cells are presented on transversal sections in left columns. Corresponding *MFα2* mRNA decays are presented in right columns. The levels of *MFα2* mRNA were measured using qPCR at the indicated

time points (0, 15, 30, 60 min) after the addition of doxycycline to the cultures. *ACT1* and *IPP1* genes were used as internal normalization controls. Quantification of three independent experiments is shown. The data were normalized to the mRNA levels at the time point 0min. The bars represent S.E.M. The asterisks show statistical significance of one-way ANOVA test (* = p<0,1, ** = p<0.01, *** = p<0.001). Bar: 5 μm. The levels of *MFα2* mRNA in wild type cells expressing *MFα2* mRNA from plasmid (pCM189-*MFα2*; Y566) or expressing *MFα2* mRNA only from endogenous *MFα2* gene (bearing empty pCM189 plasmid; Y568) are shown (H). *ACT1* and *IPP1* genes were used as internal normalization controls. Quantification of four replications of three independent experiments is shown. The bars represent S.E.M. The asterisks show statistical significance of one-way ANOVA test (*** = p<0.001). Bar: 5 μm. Xrn1-GFP protein levels were determined by Western blot analysis in wild type logarithmic, diauxic and post-diauxic cells. Tubulin was used as a loading control. Representative immunoblots (A) and their quantifications (B) are presented. The data were normalized to the Xrn1 protein level in logarithmic cells. The bars represent standard deviations. The asterisks show statistical significance of one-way ANOVA test (*** = p<0.001). The figure is adapted from (Vaškovičová et al., 2017).

To exclude the possibility that the *MFα2* mRNA decay was executed by the competing 3′-5′ degradation pathway mediated by exosome, the *MFα2* mRNA decay was monitored also in cells lacking Ski7 protein. Ski7 is a multi-domain adaptor protein connecting exosome to the SKI complex and is critical for exosome function. In cells lacking Ski7 protein (*ski7Δ*), the 3′-5′ mRNA decay pathway is completely inactivated and mRNA decay can proceed only via 5′-3′ Xrn1-dependent pathway (Araki et al., 2001).

The plasmid carrying doxycycline repressible *MFα2* gene was transformed into *ski7Δ* cells with genomically GFP-tagged Xrn1 protein (Xrn1-GFP) and *MFα2* mRNA decay was measured in logarithmically growing cells. Importantly, MFα2 mRNA decay could be still clearly observed (Fig. 8E). This means that the *MFα2* mRNA degradation proceeds even in the absence of 3′-5′ decay pathway and is indeed mediated by Xrn1-regulated 5′-3′ decay pathway.

To sum up, *MFα2* mRNA is a specific substrate for Xrn1 exoribonuclease and can be used as a reporter mRNA for determining the exoribonuclease activity of Xrn1.

5.1.2 The intensity of mRNA decay correlates with the Xrn1 localization

As the Xrn1 localization changes during the progression of the growth of the yeast cell culture and the availability of the glucose in the medium (Grousl et al., 2015), we asked whether the change in Xrn1 localization could reflect changes in Xrn1 activity and mRNA decay regulation.

To monitor the Xrn1 activity in the cell cultures with different Xrn1 localizations, the wild type cells with Xrn1-GFP expressing *MFα2* expression vector were used. These cells were grown into the stages where Xrn1-GFP was distributed homogeneously in the cytoplasm (exponential cells), accumulated in P-bodies (diauxic shift cells) or associated with eisosomes (post-diauxic cells). We checked the Xrn1 localization pattern using confocal microscopy. We added doxycycline to these cell cultures to stop the *MFα2* mRNA transcription and withdrew samples of cells at time points 0, 15, 30 and 60 minutes after doxycycline addition. The total mRNA was isolated from these samples and the level of *MFα2* mRNA was determined by the quantitative PCR (qPCR) using *MFα2* specific primers.

In exponentially growing cells, where Xrn1 localized homogeneously in the cytoplasm, the immediate and fast mRNA decay was observed (Fig. 8A). The approximate half-life of *MFα2* mRNA in these cells was 10.6 ± 2.0 minutes. This value is in agreement with the previously published half-lives of *MFα2* mRNA (Decker and Parker, 1993). In contrast, in control exponential cells where no doxycycline was added, the level of *MFα2* mRNA stayed unchanged (not shown).

In diauxic-shift cells, where Xrn1 was accumulated in P-bodies, the *MFα2* mRNA decay was significantly slower than in the cells with Xrn1 dispersed in cytoplasm (Fig. 8B). The approximate half-life of *MFα2* mRNA in these cells was 32.3 ± 5.1 minutes.

Importantly, in the post-diauxic cells, where Xrn1 was associated with eisosomes, no significant *MFα2* mRNA decay was detected during the time course of the experiment (Fig. 8C). We calculated that the *MFα2* mRNA half-life was more than 100 minutes.

Notably, the relationship between Xrn1 localization and *MFα2* mRNA degradation was also preserved in logarithmic, diauxic and post-diauxic *ski7Δ* cells that have inactive 3′-5′ mRNA decay pathway (Fig. 8E, F, G). This clearly shows that the 3′-5′ mRNA decay pathway is not involved in this mRNA decay regulation.

Together, our data show that mRNA decay intensity correlates with the Xrn1 localization. In cells with cytoplasmic Xrn1 and Xrn1 accumulated in P-bodies, mRNA decay proceeded. In cells where Xrn1 associated with eisosomes, mRNA decay ceased.

5.1.3 mRNA decay attenuation in post-diauxic cells is caused by Xrn1 sequestration at eisosomes

Two different aspects can contribute to the cessation of Xrn1 activity in post-diauxia: the reduced amount of the enzyme or the down-regulation of its exoribonuclease activity. We aimed to distinguish between these two possibilities.

First, we compared the Xrn1 protein levels in exponential, diauxic and post-diauxic shift cells. Western blot analysis showed that in diauxic cells, the Xrn1 protein level was approximately three-fold lower than in exponential cells (Fig. 8I, J). In post-diauxic cells, the Xrn1 protein level was approximately the same as in diauxic shift cells (Fig. 8I, J).

The decrease in protein abundance in diauxic cells comparing to the logarithmic cells may be the reason for the decreased rate of *MFα2* mRNA decay in diauxic shift cells comparing to the logarithmic cells. However, in post-diauxic cells, the decay of *MFα2* mRNA was completely attenuated, but the level of the Xrn1 protein was still the same when compared to the diauxic shift cells. Therefore, the attenuation of the mRNA decay in post-diauxic cells (where Xrn1 is associated with eisosomes) cannot be ascribed to the decreased Xrn1 protein level. Thus, the reason for mRNA decay attenuation in post-diauxic cells is probably the decreased Xrn1 enzymatic activity.

Next, we asked, whether it is the specific binding to eisosomes in post-diauxic cells that leads to the Xrn1 inactivation. For this purpose, we used cells lacking Pil1 protein which do not form MCC/eisosomes (*pil1Δ*) (Walther et al., 2006). In a post-diauxic phase culture we confirmed that Xrn1 is not associated with the plasma membrane in these cells, rather, it remains accumulated at P-bodies ((Grousl et al., 2015), Fig 9A). Importantly, the Xrn1 activity was retained in *pil1Δ* post-diauxic cells (Fig. 9A). The *MFα2* mRNA half-life was calculated to be 35.0±0.3 min, the value comparable to the *MFα2* mRNA half-life in diauxic phase wild type cells when Xrn1 was localized to P-bodies. Of note, the Xrn1 protein level was the same in wild type and *pil1Δ* post-diauxic cells, showing that it is not the increased Xrn1 protein abundance, but rather its inability to sequester at the plasma membrane in the absence of eisosomes, that causes the higher *MFα2* mRNA degradation in post-diauxic pil1Δ cells (Fig. 10A, B).

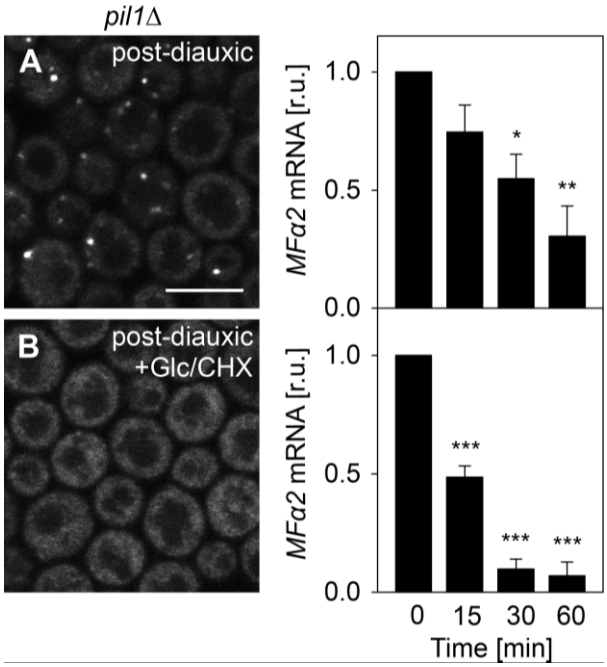

Figure 9. Xrn1 exoribonuclease activity is preserved in post-diauxic *pil1Δ* cells.

Post-diauxic *pil1Δ* cells expressing Xrn1-GFP (Y583) are shown before (A) and after (B) the addition of glucose and cycloheximide. Xrn1-GFP localizations in these cells on transversal sections are displayed in left column and corresponding *MFα2* mRNA decays are displayed in right column. As described in Fig. 8, *MFα2* mRNA levels were measured by qPCR at the indicated time points (0, 15, 30, 60 min) after the addition of doxycycline to the culture. The data were normalized to the mRNA levels at the time point 0min. Quantification of three independent experiments is shown. *ACT1* and *IPP1* genes were used as internal normalization controls. The bars represent S.E.M. The asterisks show statistical significance of one-way ANOVA test (** = $p<0.01$, *** = $p<0.001$). Bar: 5 μm. The figure is adapted from (Vaškovičová et al., 2017).

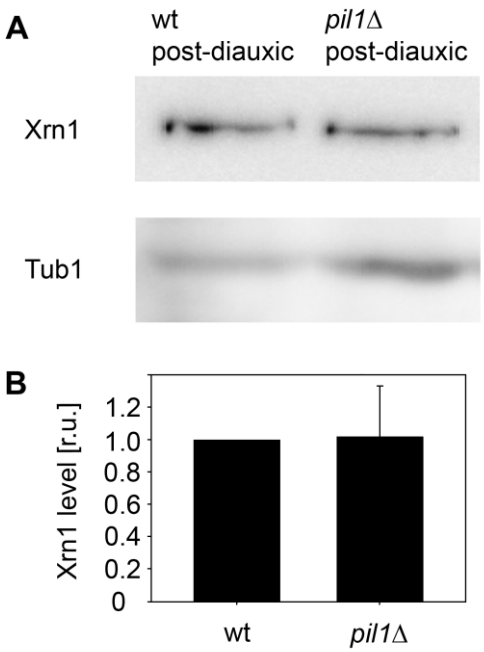

Figure 10. Xrn1 protein levels are the same in wild type and *pil1Δ* post-diauxic cells.
Xrn1-GFP protein levels were determined by Western blot analysis in wild type (Y566) and *pil1Δ* (Y583) post-diauxic cells. Tubulin was used as a loading control. Representative immunoblots (A) and their quantifications (B) from two independent experiments are presented. The data were normalized to the Xrn1 protein level in wild type cells. The figure is adapted from (Vaškovičová et al., 2017).

5.1.4 Attenuation of Xrn1 activity in post-diauxic cells is reversible

Xrn1 is sequestered at MCC/eisosomes in post-diauxic cells, e.g. the cells that exhausted glucose in the medium and adapted to the aerobic metabolism. Under these conditions, Xrn1 is not active. We were interested whether this Xrn1 sequestration leads to subsequent Xrn1 degradation, because the enzyme is no longer needed, or, conversely, whether the Xrn1 inactivation is only temporal and Xrn1 could be activated in case it is necessary. The addition of glucose to the post-diauxic cells causes shift from respiration back to the fermentation metabolism, together with the re-localization of Xrn1 from eisosomes back to the cytoplasm (Grousl et al., 2015). We investigated the Xrn1 activity under these conditions.

The wild type cells possessing Xrn1-GFP and expressing *MFα2* mRNA were grown into post-diauxic state, glucose was added to the medium to induce the Xrn1 re-localization and *MFα2* mRNA decay was measured in these conditions. Importantly, also cycloheximide (CHX) was added to the culture to block the possible de novo synthesis of the Xrn1 protein. The level of

Xrn1 protein stayed the same after glucose and CHX addition, as measured by the Western blot analysis (Fig. 11A, B). The addition of CHX alone did not change the association of the Xrn1 with eisosomes (Fig. 12, second column). In contrast, treatment of the cells with glucose (or glucose with CHX) resulted in rapid (in less than 10 minutes) Xrn1 re-localization from eisosomes to cytoplasm (Fig. 8D, 12). Additionally, this change in Xrn1 localization was accompanied with the restoration of the *MFα2* mRNA decay (Fig. 8D; half-life 21.5 ± 6.7 min). Our data show that the Xrn1 enzyme remains functional in post-diauxic cells and its activity can be restored when glucose is added.

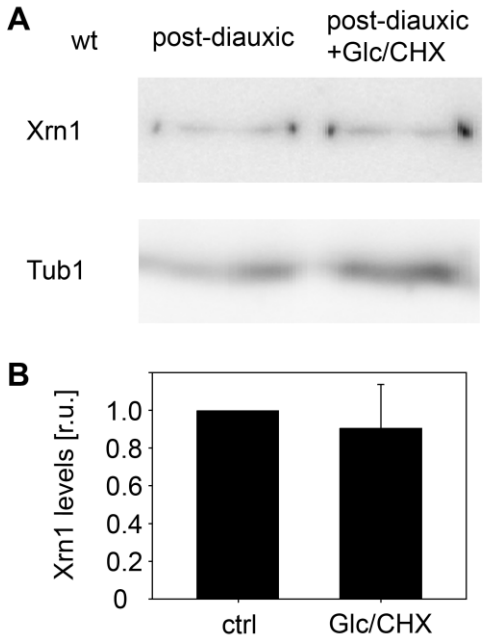

Figure 11. Xrn1 protein levels are the same before and after glucose and cycloheximide addition in wild type post-diauxic cells.

Xrn1-GFP protein levels were determined by Western blot analysis in wild type (Y566) post-diauxic cells before and after the addition of glucose and cycloheximide. Tubulin was used as a loading control. Representative immunoblots (A) and their quantifications (B) from three independent experiments are presented. The data were normalized to the Xrn1 protein level in wild type cells. The figure is adapted from (Vaškovičová et al., 2017).

It is important to note that the integrity of eisosomes was not affected in our experiments. We used the cells with GFP-tagged Xrn1 and mRFP-tagged Pil1 to investigate eisosome integrity upon glucose addition and/or CHX treatment. We observed that although glucose addition caused the Xrn1 release into cytoplasm, Pil1 localization was not affected, showing that

MCC/eisosomes remained intact. The situation was the same upon glucose and CHX treatment (Fig. 12). The addition of CHX alone did not change the Pil1 or Xrn1 localizations (Fig. 12). Therefore, it was not the disassembly of eisosomes that led to the Xrn1 release into the cytoplasm, rather, some unidentified signal might have caused specific Xrn1 dissociation from eisosomes.

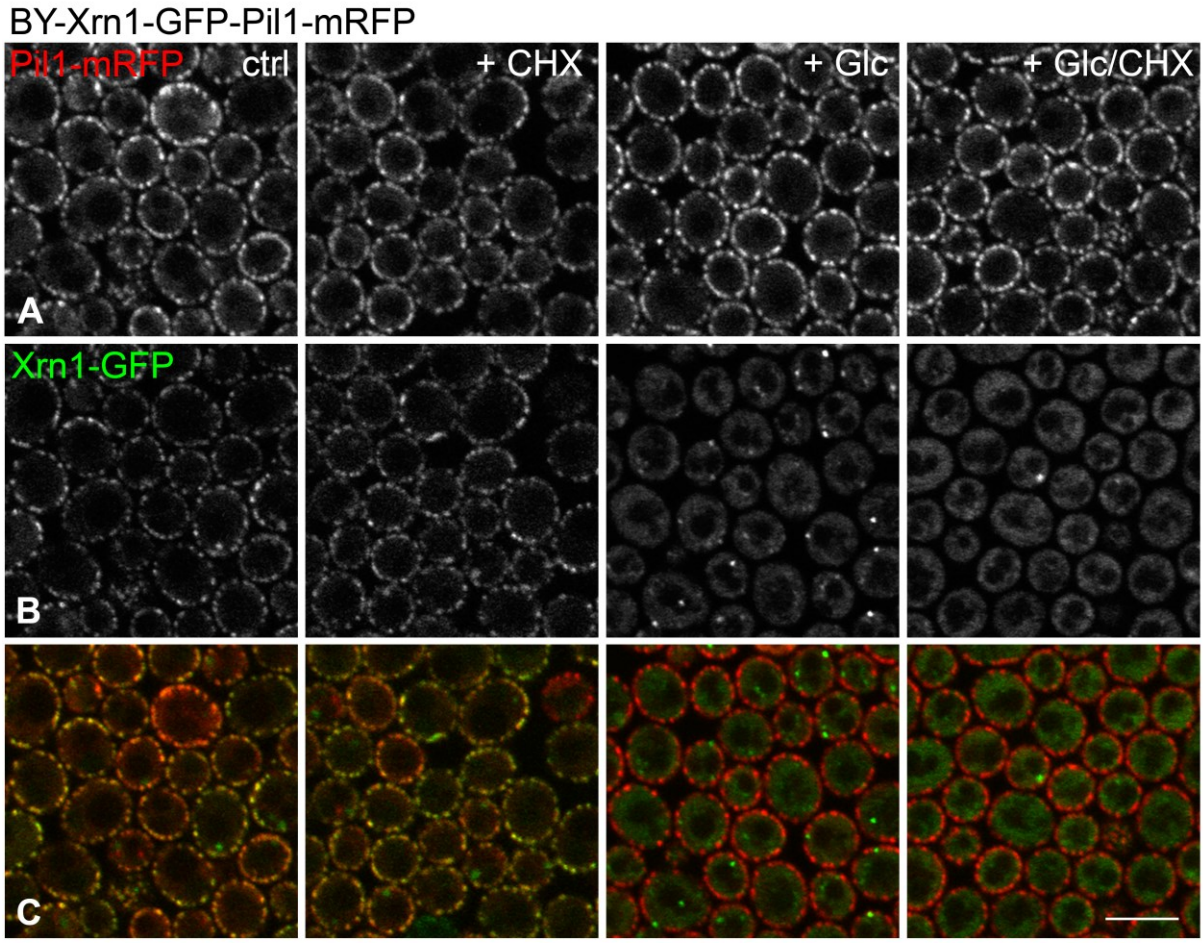

Figure 12. The change in Xrn1 localization upon glucose and cycloheximide addition in wild type post-diauxic cells is not caused by MCC/eisosome disassembly.

Pil1-mRFP (A) and Xrn1-GFP (B) localizations were monitored in wild type (Y501) post-diauxic cells before (column 1) and after the addition of cycloheximide (column 2), glucose (column 3) or glucose together with cycloheximide (column 4). Representative Pil1-mRFP (A) and Xrn1-GFP (B) localizations and their co-localizations (C) on transversal sections are displayed. Bar: 5 μm. The figure is adapted from (Vaškovičová et al., 2017).

Next, also the *pil1Δ* cells were grown into the post-diauxic phase and treated with glucose and CHX. We observed the rapid re-localization of Xrn1 from P-bodies into the cytoplasm in these cells, the same effect as in wild type cells (Fig. 9B). Moreover, similarly to wild type cells, the Xrn1 re-localization from P-bodies to cytoplasm led to restoration of Xrn1 activity in this strain (Fig. 9A, B). Again, the half-life of *MFα2* mRNA was 10.6±2.3 min, the half-life comparable to the half-life in wild type exponential cells. Therefore, even though there is no Xrn1 attenuation in post-diauxic *pil1Δ* cells, the glucose-regulated Xrn1 translocation signaling is still preserved in this strain.

In summary, we showed that the Xrn1-mediated mRNA decay is ceased in post-diauxic cells by the sequestration of the Xrn1 enzyme at the eisosomes, which prevents its association with the rest of the mRNA decay machinery accumulated at P-bodies. Upon the supplementation of glucose to these cells, however, Xrn1 is re-localized back to the cytoplasm and its enzymatic activity is restored.

Together, in this section we showed that:

- *MFα2* mRNA reporter is suitable for monitoring the Xrn1 activity in *S. cerevisiae* cells
- The intensity of mRNA decay correlates with the Xrn1 localization
- Xrn1 sequestered at eisosomes is inactive and does not degrade mRNA
- Xrn1 sequestered at eisosomes retains its functionality and upon glucose supplementation, Xrn1 re-localizes back to cytoplasm and becomes active again
- In the absence of MCC/eisosomes, the attenuation of Xrn1 activity in post-diauxic cells does not take place

5.2 Investigation of Nce102 intracellular localization and functional significance under chronic glucose depletion

5.2.1 Nce102 localizes to vacuolar membrane in stationary phase yeast cells

To investigate the Nce102 localization in detail, Nce102 was genomically-tagged with GFP using integrative plasmid. Nce102 localization was observed in different time points after the inoculation of cells into the fresh medium.

In logarithmically growing wild type cells, Nce102-GFP localized to the plasma membrane and was significantly accumulated in bright patches representing MCC/eisosomes (Fig. 13). After 24 h of cultivation, in addition to the plasma membrane pool of Nce102-GFP, a small portion of Nce102-GFP could be observed inside cells. After 48 h of cultivation and in later time points, Nce102-GFP still remained largely associated with MCC/eisosomes at the plasma membrane, but a substantial amount of Nce102-GFP localized also to the cell interior (Fig. 13). In the cell cytoplasm, Nce102-GFP localized to the surface of large, round-shaped organelles. This is in strong contrast to Sur7-GFP and Pil1-GFP proteins that do not localize to any cytoplasmic organelles even after 144 h of cultivation (Sur7 and Pil1 were both tagged using integrative plasmid) (Fig. 13).

To identify the large round-shaped organelles into which Nce102-GFP localized in stationary cells, we stained the cells with FM4-64 dye (N-(3-triethylammoniumpropyl)-4-(6-(4-(diethylamino) phenyl) hexatrienyl) pyridinium dibromide). FM4-64 dye stains the plasma membrane and as the plasma membrane is being endocytosed, FM4-64 stains the membrane intermediates of the endocytic pathway. After prolonged incubation times, FM4-64 accumulates in the vacuolar membrane (Vida and Emr, 1995). The co-localization of Nce102-GFP and FM4-64 clearly showed that after 24 h of cultivation and later, Nce102 accumulated in the vacuolar membrane (Fig. 14). This experiment suggests that a notable portion of Nce102 protein re-localizes from the plasma membrane to vacuolar membrane in stationary cells.

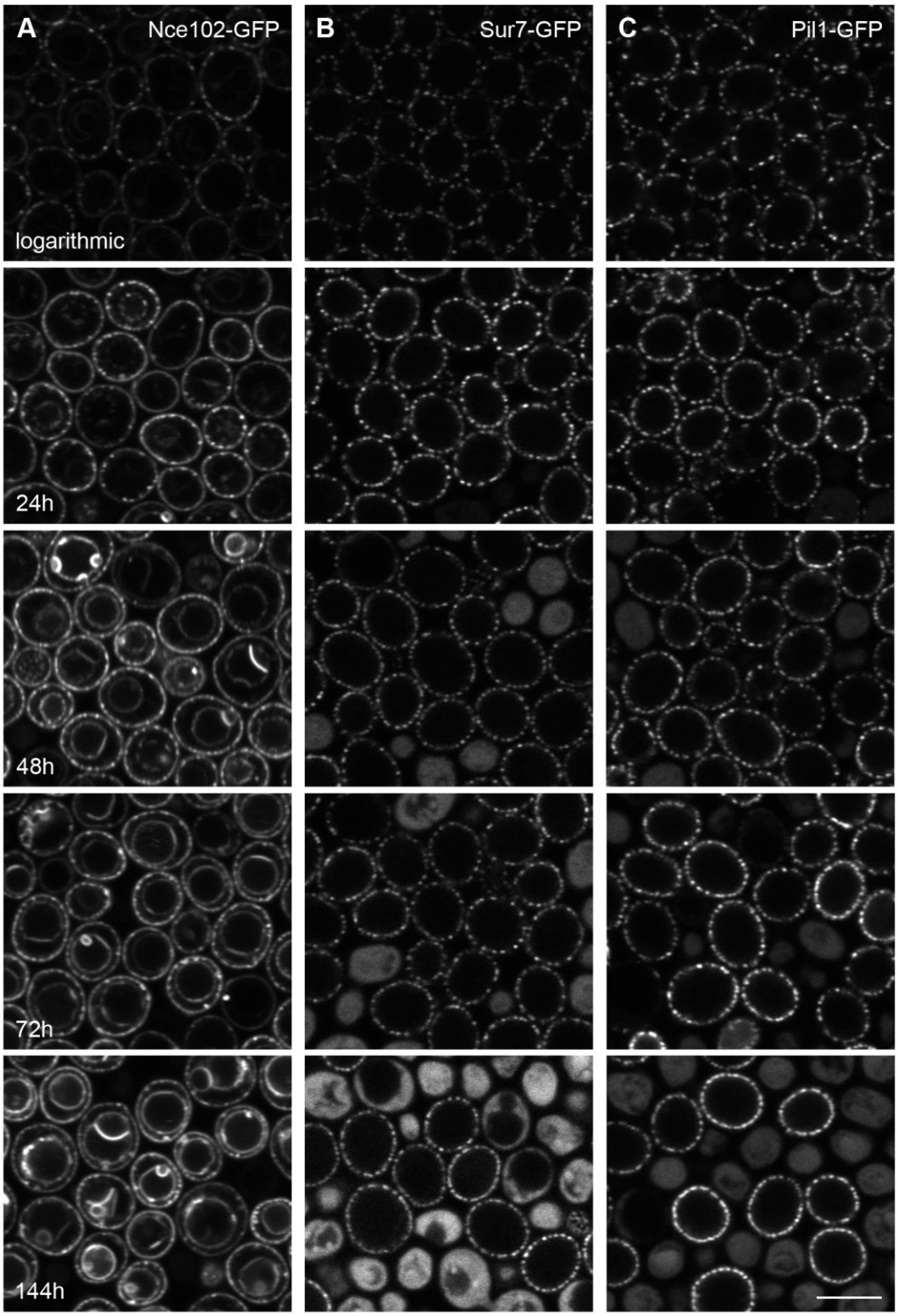

Figure 13. Nce102 is internalized to internal membranes in cells with chronic lack of glucose.

Nce102-GFP (Y240; A), Sur7-GFP (Y123; B) and Pil1-GFP (Y124; C) localizations were monitored in wild type cells after 7 h (logarithmic), 24 h, 48 h, 72 h and 144 h after inoculation into fresh medium. Representative transversal sections are presented. All time points were scanned using the same settings. Because of the increase in Nce102-GFP expression, the intensity of the laser was lowered after 72h of incubation. Bar: 5 μm.

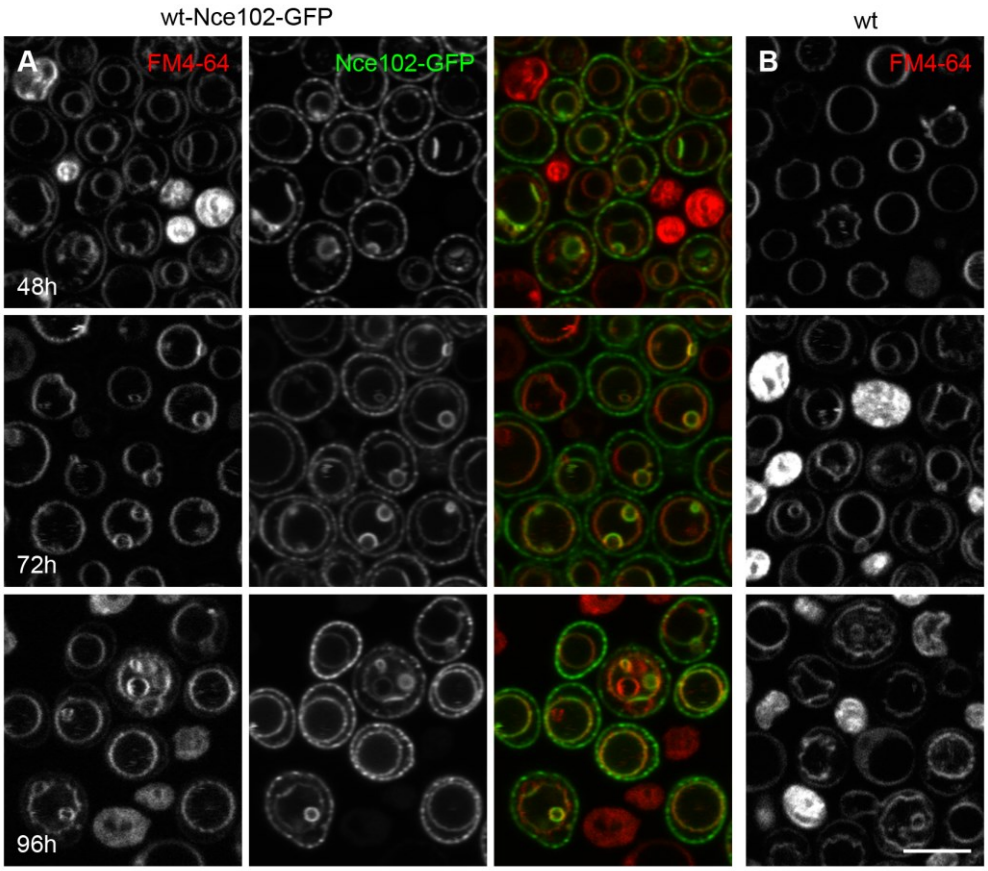

Figure 14. Nce102 re-localizes to vacuole in cells with chronic lack of glucose.

Vacuolar membranes stained by FM4-64 together with Nce102-GFP signal were monitored in wild type cells expressing Nce102-GFP (Y240; A, left panel) after 48 h, 72 h and 96 h after inoculation into fresh medium. Vacuoles were visualized also in wild type cells without any tag (B, right panel) under the same conditions. Please note that the cells with internal vacuolar circles were selected for presentation. All strains and all time points were scanned using the same settings. Representative transversal sections are presented. Bar: 5 μm.

Next, we asked whether the Nce102-GFP protein re-localization from plasma membrane to vacuoles proceeds via classical endocytic pathway, i.e. via endocytosis of the plasma membrane and subsequent vesicular transport. It was shown previously that endocytosis takes place in the plasma membrane outside of MCC/eisosomes (Stradalova et al., 2012). Moreover, transmembrane proteins that are accumulated at MCC/eisosomes can be endocytosed from the plasma membrane and internalized into the vacuole only after they leave MCC compartment (Busto et al., 2018; Gournas et al., 2018; Grossmann et al., 2008; Moharir et al., 2018). To test whether Nce102 outside MCC/eisosomes is more prone to internalization, we used mutants where Nce102 is not associated with MCC/eisosomes. First, in *pil1Δ* strain that lacks MCC/eisosomes, Nce102 is more homogeneously dispersed in the plasma membrane when

compared to the wild type strain (Fröhlich et al., 2009). Second, the shortened version of Nce102, Nce102(438), is homogeneously dispersed in the plasma membrane even in the presence of MCC/eisosomes (Loibl et al., 2010). Importantly, the Nce102-GFP re-localization from plasma membrane to vacuoles did not take place earlier in these strains (Fig. 15). However, Nce102(438)-GFP protein was significantly enriched in vacuolar membranes already after 24 h of cultivation. Moreover, the amount of Nce102-GFP localizing to vacuolar membranes after 48 h of incubation was significantly higher in both these strains when compared to the wild type strain. In these strains, also larger cytoplasmic or vacuole-associated aggregates of Nce102-GFP protein could be observed. Notably, when Nce102 protein was fused to Sur7 protein, it stayed trapped in MCC/eisosomes and no Sur7-Nce102-GFP re-localization from plasma membrane to vacuoles could be observed (Fig. 15).

Therefore, it is possible that Nce102 protein might be endocytosed from the plasma membrane outside of MCC/eisosomes and transferred via endocytic pathway to the vacuolar membrane.

Additionally, also bright Nce102-GFP circles in vacuolar lumen could be observed in yeast cultures after prolonged cultivation times in wild type strain as well as in *pil1Δ* and Nce102(438)-GFP strains (Fig. 14, Fig. 15). In the two latter strains, Nce102-GFP (or Nce102(438)-GFP) circles were even more abundant. These circles were also stained with FM4-64 dye and were either static and associated with the vacuolar membrane or mobile in the vacuolar lumen (Fig. 14). However, they were not abundant to this extent when wild type cells without GFP-tagged Nce102 protein were stained using FM4-64 (Fig. 14). This suggests that Nce102-GFP circles in vacuolar lumen are a physiological phenomenon, however, they are unnaturally stabilized by GFP-tagging of Nce102 protein.

The transmembrane proteins in the plasma membrane are being endocytosed to be subsequently degraded in the vacuole. The degradation of fluorescently-tagged nutrient transporters such as Pma1, Hxt1, Can1, Mup1 and Fur4 can be observed by diffuse fluorescence signal in the vacuole (the first step in tagged protein degradation is presumably the cutting of the fluorescent protein into the vacuolar lumen) (Busto et al., 2018; Gournas et al., 2018; Moharir et al., 2018)). Consistently, we observed diffuse GFP vacuolar signal already after 24h after inoculation in wild type strain where either Pma1 or Hxt1 were tagged using integrative plasmids (Fig. 16). Importantly, Nce102-GFP in our strains accumulated in the vacuolar membrane and no diffuse signal in the vacuolar lumen could be observed. Together with the localization of Nce102 into the membranous circles inside vacuolar lumen, these results might suggest a functional significance of Nce102 accumulation in the vacuolar membrane upon conditions of chronic glucose depletion.

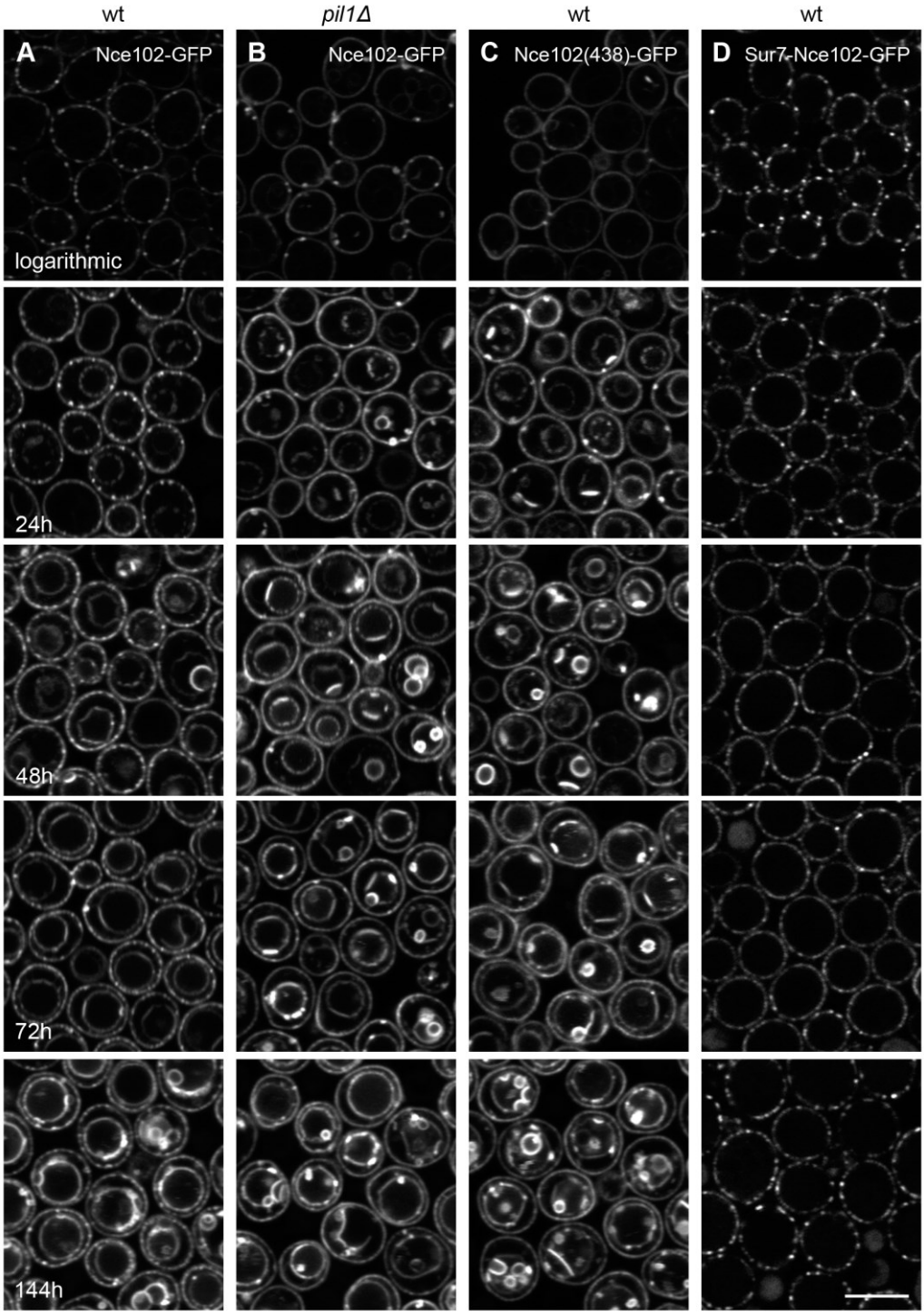

Figure 15. Nce102 re-localization to internal membranes is affected in *pil1Δ* strain and strains with mutated Nce102 protein.

Nce102-GFP localizations were monitored in wild type cells (Y240; A) and *pil1*Δ cells (Y1080; B) after 7 h, 24 h, 48 h, 72 h and 144 h after inoculation into fresh medium. Representative transversal sections are presented. Under the same conditions, also patterns of Nce102(438)-GFP (Y1016; C) and Sur7-Nce102-GFP (Y970; D) proteins in wild type cells were monitored. All strains (except wild type strain expressing fusion Sur7-Nce102-GFP protein) were scanned using the same settings. The intensity of the laser was lowered after 72 h of incubation because the increase in Nce102-GFP expression. Bar: 5 μm.

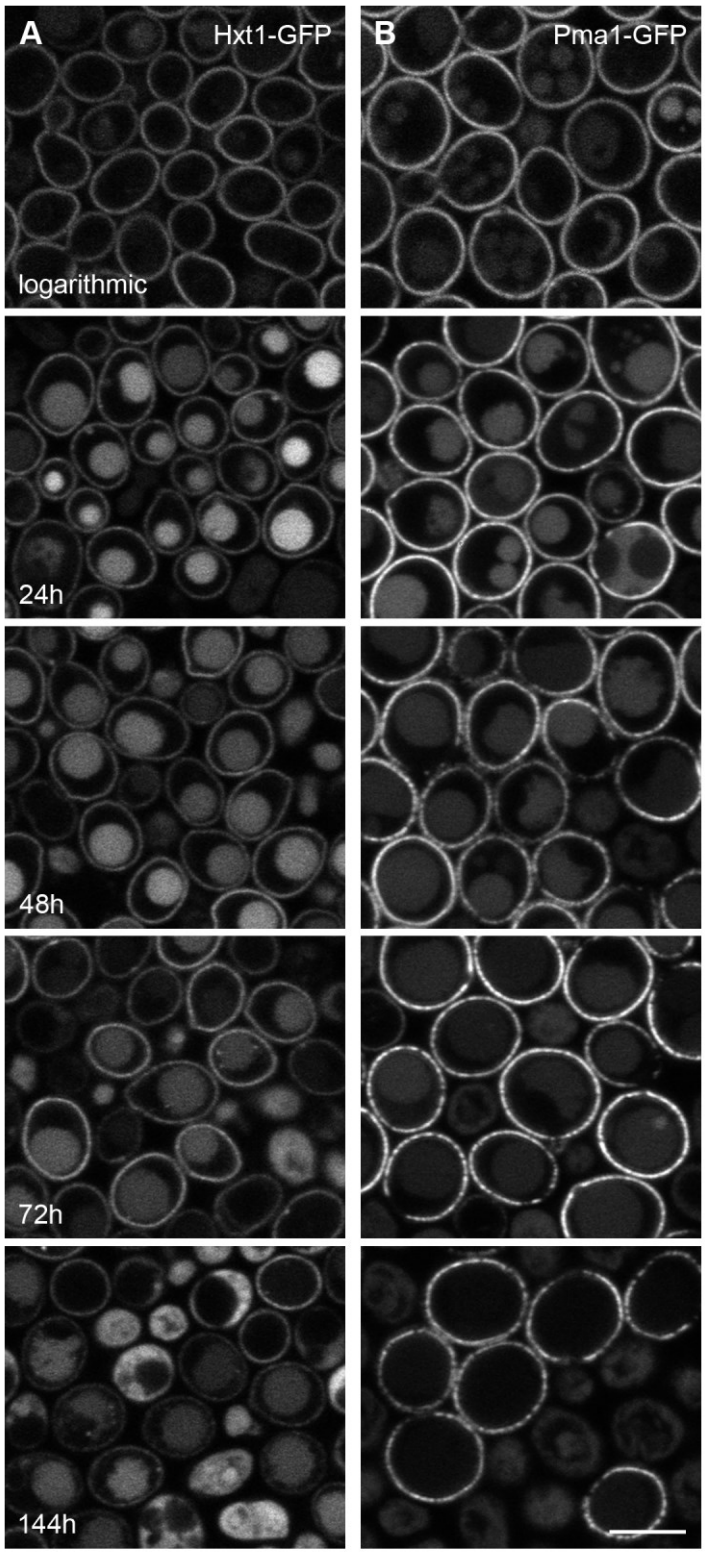

Figure 16. In contrast to Nce102, Hxt1 and Pma1 plasma membrane transporters do not re-localize to vacuolar membrane under chronic glucose depletion.

Hxt1-GFP (Y225; A) and Pma1-GFP (Y143; B) localizations were monitored in wild type cells after 7 h (logarithmic), 24 h, 48 h, 72 h and 144 h after inoculation into fresh medium. Representative transversal sections are presented. Bar: 5 μm.

5.2.2 Nce102 localizes to sterol-enriched vacuolar microdomains

Detailed observation of Nce102-GFP localization on vacuolar membrane revealed that Nce102-GFP was not always distributed homogeneously in the vacuolar membrane. In approximately 60% of cells, Nce102-GFP concentrated in specific microdomains. The percentage of cells with microdomains did not significantly change in time (microdomains were observed in 55% cases of 24h cells, 65% of cases of 48h cells and 55% of cases of 72h cells). These microdomains varied from small dot-like puncta to big microdomains covering large area of the vacuolar membrane (Fig. 13, Fig 15). It is interesting that the pattern of Nce102 in vacuolar microdomains developed in time (Fig. 13, Fig. 15). First, Nce102-GFP localized to small, evenly-distributed dot-like microdomains that were dispersed throughout the whole vacuolar surface (24 h and 48 h of incubation). Later on, Nce102-GFP was found in a few larger microdomains (in this case, vacuole often looked like a polyhedron) (48 h of incubation and more).

The Nce102 patterns on vacuolar membrane reminded us the vacuolar membrane microdomains described by Toulmay and Prinz in 2013 (Toulmay and Prinz, 2013). Toulmay and Prinz showed that proteins in vacuolar membrane segregate into one or the other of the two stable lipid microdomains (Toulmay and Prinz, 2013). One of these two microdomains is liquid-ordered, sterol-enriched (it can be stained with filipin) and contains Ivy1 and Gtr2 proteins. The other microdomain is liquid-disordered (preferentially stained with FM4-64) and accumulates Vph1 protein. These two microdomains are complementary to each other and exhibit quasi-symmetrical patterns, similar to our Nce102 vacuolar microdomain patterns. The authors suggested that small dot-like microdomains fuse to form large coalesced vacuolar microdomains. Moreover, they observed the formation of these microdomains in stationary phase cells (Toulmay and Prinz, 2013). Therefore, we asked whether Nce102 also segregates into one of the two lipid vacuolar membrane microdomains.

First, we observed that some Nce102 vacuolar microdomains are excluded from FM4-64 microdomains (Fig. 17). Interestingly, Nce102 often localized to highly curved invaginations of the vacuolar membrane.

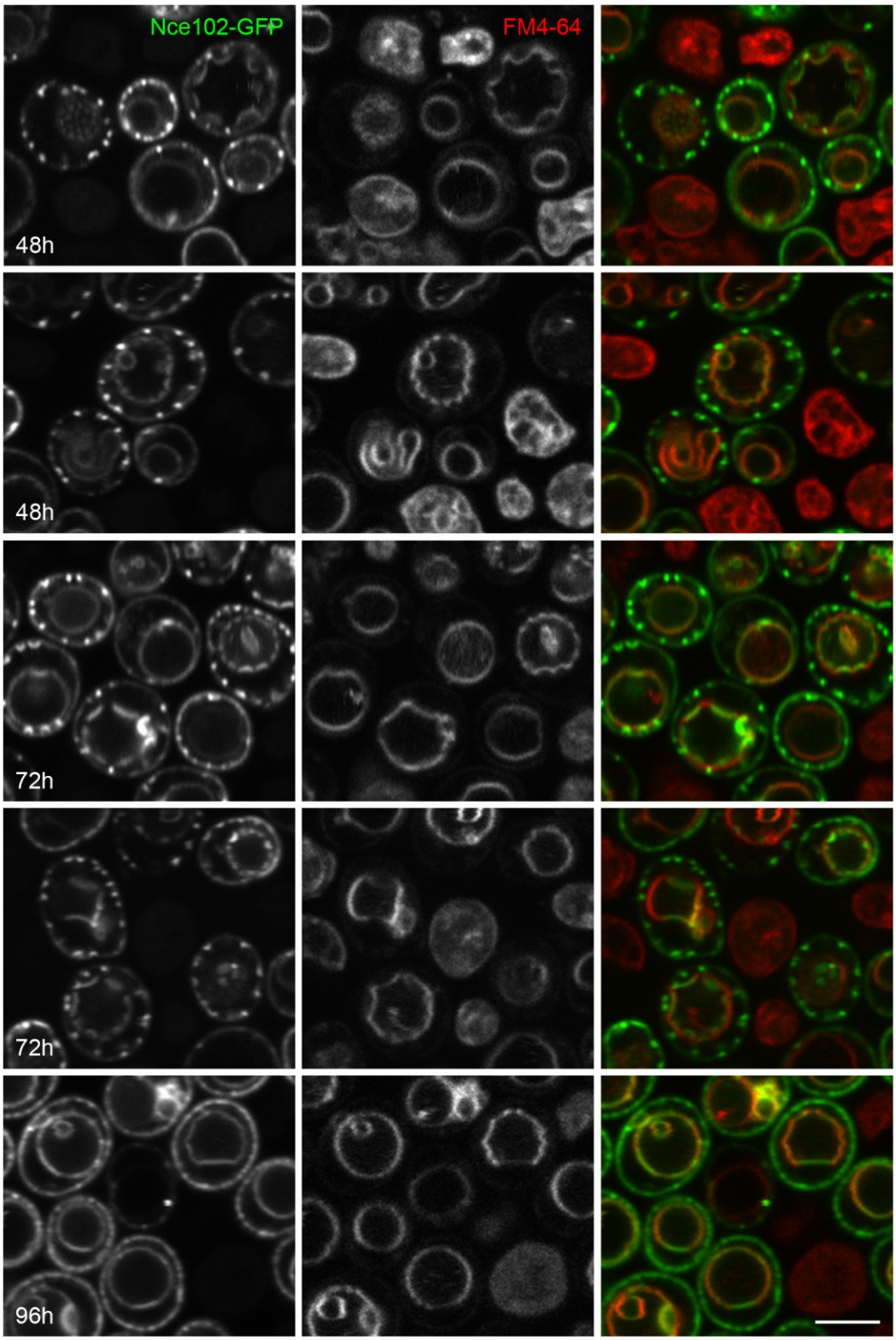

Figure 17. Nce102 is excluded from FM4-64-enriched vacuolar microdomains.

Vacuolar membranes stained by FM4-64 together with Nce102-GFP signal were monitored in wild type cells expressing Nce102-GFP (Y240) after 48 h, 72 h and 96 h after inoculation into fresh medium. The cells with vacuolar domains were selected for the presentation. The images were adjusted to improve the microdomain visualization. Bar: 5 μm.

Next, we tagged Vph1 protein with mCherry (using genomic tagging method) and analyzed their patterns with respect to Nce102-GFP distribution. Similarly to Nce102-GFP, after 24 h, 48 h and 72 h of cultivation, Vph1-mCherry formed dot-like puncta on vacuolar membrane. After 72 h, also larger coalesced vacuolar microdomains of Vph1-mCherry started to appear. Importantly, Vph1-mCherry microdomains and Nce102-GFP microdomains excluded from each other (Fig. 18). This was visible on small dot-like microdomains as well as on large coalesced microdomains. Often, Nce102-GFP was found on the faces of polyhedron and Vph1-mCherry on its edges.

As Nce102 microdomains were mutually exclusive with both FM4-64-stained and Vph1-rich microdomains, we concluded that Nce102 accumulates in the other vacuolar microdomain, the previously described sterol-enriched vacuolar microdomain.

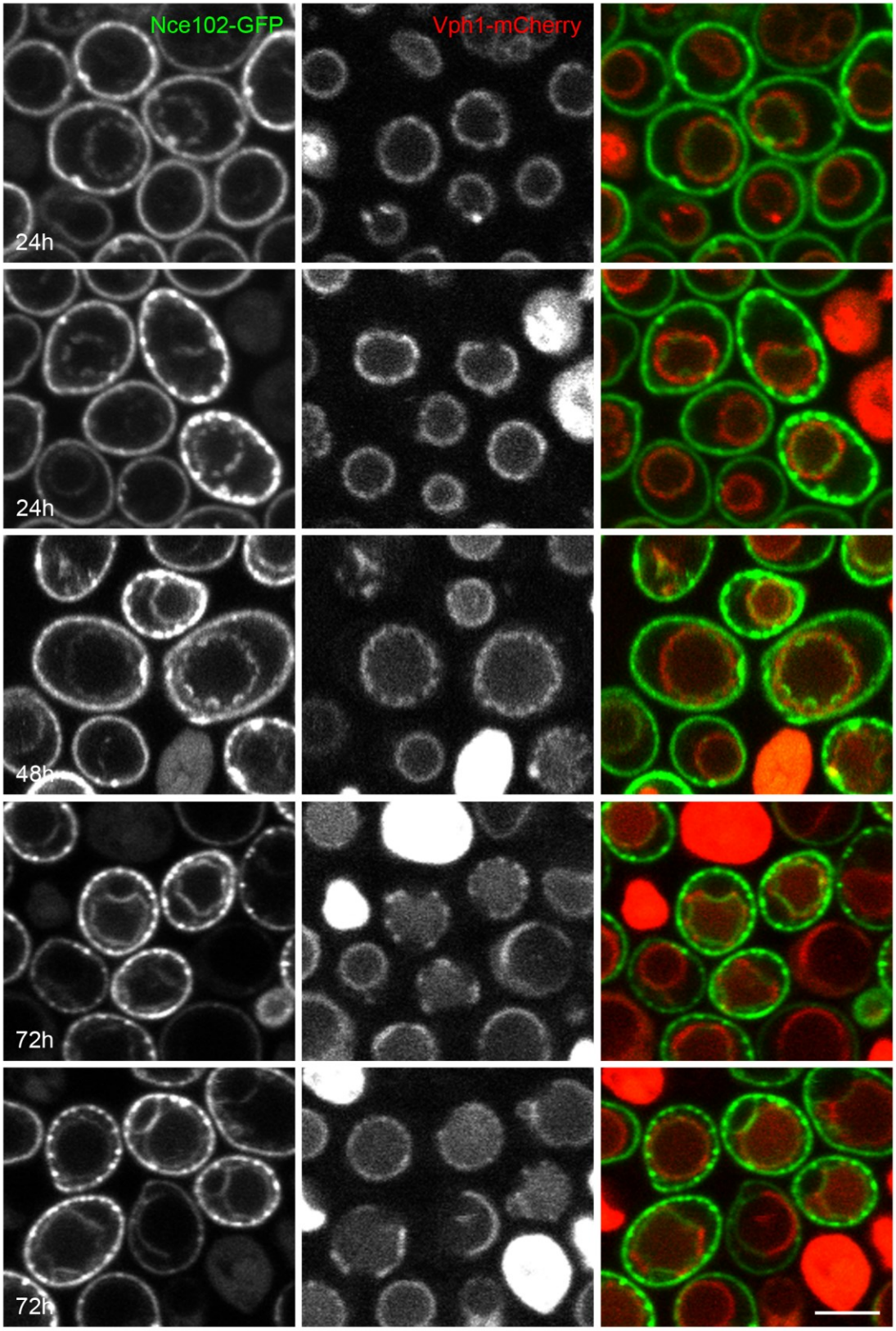

Figure 18. Nce102 is excluded from Vph1-enriched vacuolar microdomains.

Nce102-GFP and Vph1-mCherry localizations were monitored in wild type cells (Y1057) after 24 h, 48 h and 72 h after inoculation into fresh medium. The cells with vacuolar domains were selected for the presentation. The images were adjusted to improve the microdomain visualization. Bar: 5 μm.

5.2.3 Nce102 vacuolar localization depends on vacuolar physiology

As Nce102 localizes to sterol-enriched vacuolar microdomains, we next asked whether Nce102 vacuolar re-localization depends on vacuolar domain formation. Yeast strains *vps4Δ*, *fab1Δ* and *nem1Δ* were previously shown not to form Vph1-enriched vacuolar microdomains (Toulmay and Prinz, 2013). It is important to note here that both *vps4Δ* and *fab1Δ* strains have altered general vacuolar protein sorting and homeostasis. Vps4 is an ATPase involved in multivesicular body protein sorting (Babst et al., 1998, 1997; Zahn et al., 2001). *S*train lacking Vps4 protein has relatively normal vacuoles, however, it has enlarged pre-vacuolar organelle called "class E compartment" possessing markers of both late-Golgi and vacuole (Raymond et al., 1992). Fab1 is a vacuolar membrane lipid kinase that synthesize phosphatidylinositol(3,5)bisphosphate (Cooke et al., 1998; Yamamoto et al., 1995). This lipid is important for vacuolar identity, integrity, morphology, acidification, membrane recycling, protein sorting and autophagy (Gary et al., 1998; Jin et al., 2014; Odorizzi et al., 1998; Yamamoto et al., 1995). In contrast, Nem1 is a protein phosphatase involved in nuclear envelope organization and *nem1Δ* strain has problems with mitophagy, ER-phagy and pexophagy that seem to be more specialized processes (Siniossoglou et al., 1998; Xu and Okamoto, 2018). We investigated the localization of Nce102-GFP in these strains.

Nce102-GFP neither formed vacuolar microdomains nor did it re-localize from plasma membrane to vacuoles in *vps4Δ* strain, even after prolonged cultivation times (Fig. 19). At later time points, the accumulation of Nce102-GFP in class E compartment could be observed in some cells (Fig. 19). In *fab1Δ* strain, Nce102-GFP did not re-localized to vacuolar membrane in majority of cells. When Nce102-GFP localized to vacuolar membrane, it was only very weakly and it was distributed homogeneously (Fig. 19). In contrast, Nce102-GFP was able to re-localize to vacuolar membrane in *nem1Δ* cells. It distributed either homogeneously or occasionally accumulated in large coalesced microdomains (Fig. 19).

The specific phenotype of the deletion strain regarding vacuolar physiology may be the reason why Nce102-GFP did not re-localize to vacuoles in *vps4Δ* strain, re-localized to vacuoles very weakly in *fab1Δ* strain and re-localized to vacuoles and possibly also some domains in *nem1Δ* strain. The changes in Nce102-GFP localization to vacuole and vacuolar microdomains in *vps4Δ*, *fab1Δ* and *nem1Δ* strains may reflect overall alteration in vacuolar physiology, and probably altered vacuolar lipid composition, of these strains. It is probable that this physiological alteration of vacuoles consequently affects also the ability of these cells to form

vacuolar microdomains and attract Nce102 into them. The existence of vacuolar microdomains is not a pre-requisite for Nce102 re-localization from plasma membrane to vacuolar membrane.

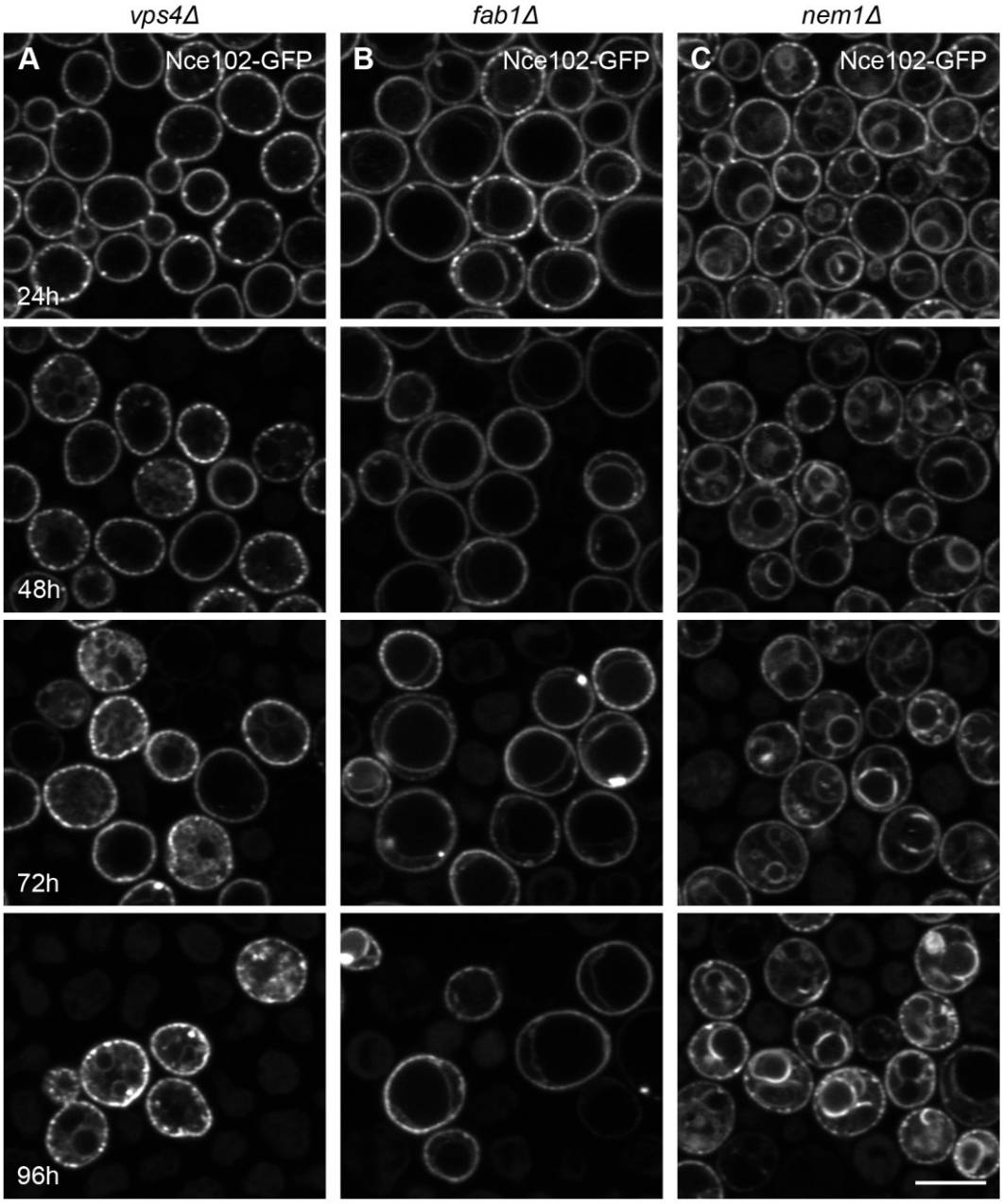

Figure 19. The localization of Nce102 into vacuolar microdomains depends on vacuolar physiology.
Nce102-GFP localizations were observed in *vps4Δ* (Y1009; A), *fab1Δ* (Y1010; B) and *nem1Δ* (Y1011; C) strains. Cells were observed after 24 h, 48 h, 72 h and 96 h after inoculation into fresh medium. All strains and all time points were scanned using the same settings. Representative transversal sections are presented. Bar: 5 μm.

5.2.4 Nce102 may be involved in vacuolar fusion and protein degradation

As Nce102 localizes to sterol-rich vacuolar microdomains, we tested whether Nce102 is necessary for vacuolar domain formation. For this purpose, we expressed Vph1-mCherry protein as a vacuolar domain marker in *nce102Δ* strain. Moreover, in *S. cerevisiae* genome, Nce102 has its structural homologue, Fhn1. Fhn1 expression is in our conditions strikingly lower than that of Nce102 and we were not able to detect its signal when Fhn1-GFP was expressed from its native promoter (not shown; (Loibl et al., 2010)). Fhn1 has still unclear physiological role in yeast cells and we asked whether it could play similar role at vacuoles as Nce102. To test this, we expressed Vph1-mCherry also in *fhn1Δ* and *nce102Δfhn1Δ* strains.

As mentioned above, in wild type cells during cultivation, Vph1-mCherry was first homogeneously distributed throughout the vacuolar membrane and after 24 h of cultivation, it continually adopted dot-like microdomain pattern. Later on (72 h of cultivation and more), also coalesced microdomains marked with Vph1-mCherry were formed in these cells (Fig. 20 – part 1). Similar vacuolar microdomain formation was observed also in *nce102Δ* cells (Fig. 20 – part 1). After 24 h of cultivation, small dot-like microdomains of Vph1-mCherry started to appear in these cells, consistently with the onset of vacuolar domain formation in wild type strain. After 72 h of cultivation, also large, coalesced microdomains could be observed. Similarly, also in *fhn1Δ* and *nce102Δfhn1Δ* strains both types of vacuolar microdomains can be formed (Fig. 20 - part 2). Therefore, we conclude that neither Nce102 nor Fhn1 is necessary for formation of vacuolar microdomains.

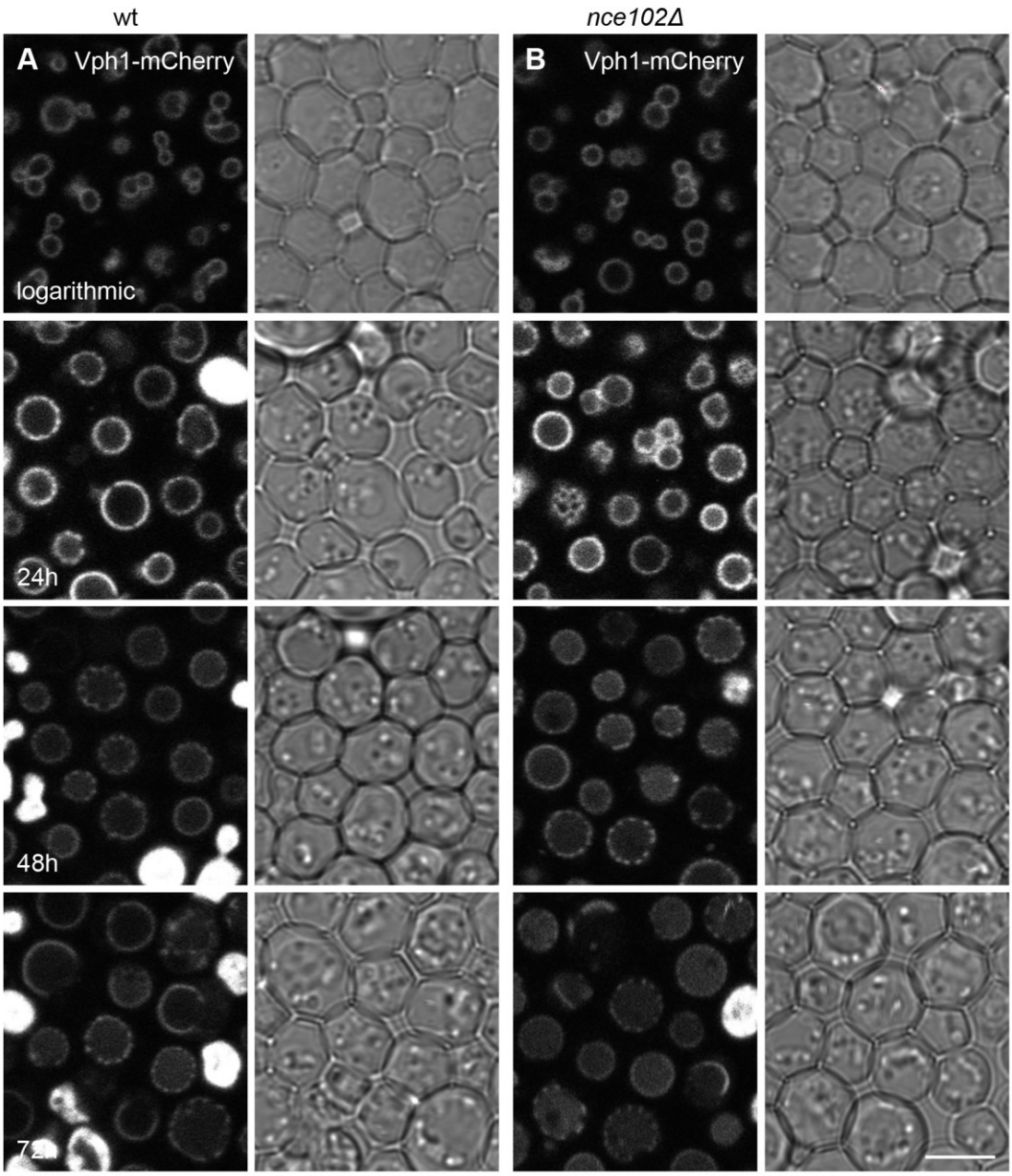

Figure 20 – part 1. Nce102 and Fhn1 are not necessary for vacuolar microdomain formation.

Vph1-mCherry localizations were observed in wild type (Y1044, A), *nce102Δ* (Y1079; B) *fhn1Δ* (Y1099; C), *nce102Δfhn1Δ* (Y1089; D) strains and wild type strain expressing fusion Sur7-Nce102-GFP protein (Y1083; E). Cells were observed after 7 h (logarithmic), 24 h, 72 h, 96 h and 144 h after inoculation into fresh medium. Representative transversal sections with corresponding wide field images are presented. Bar: 5 μm.

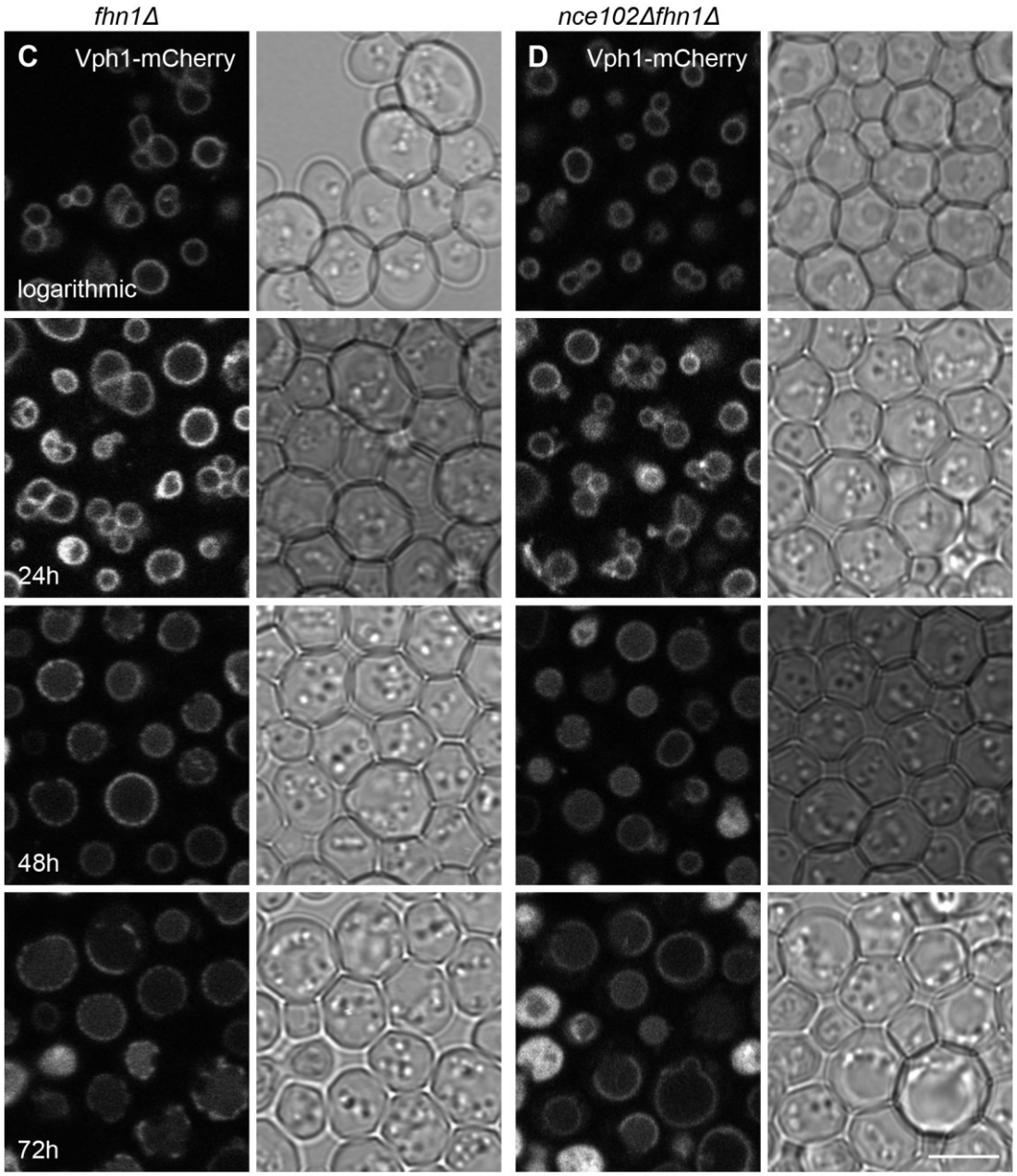

Figure 20 – part 2. Nce102 and Fhn1 are not necessary for vacuolar microdomain formation.

Vph1-mCherry localizations were observed in wild type (Y1044, A), *nce102Δ* (Y1079; B) *fhn1Δ* (Y1099; C), *nce102Δfhn1Δ* (Y1089; D) strains and wild type strain expressing fusion Sur7-Nce102-GFP protein (Y1083; E). Cells were observed after 7 h (logarithmic), 24 h, 72 h, 96 h and 144 h after inoculation into fresh medium. Representative transversal sections with corresponding wide field images are presented. Bar: 5 µm.

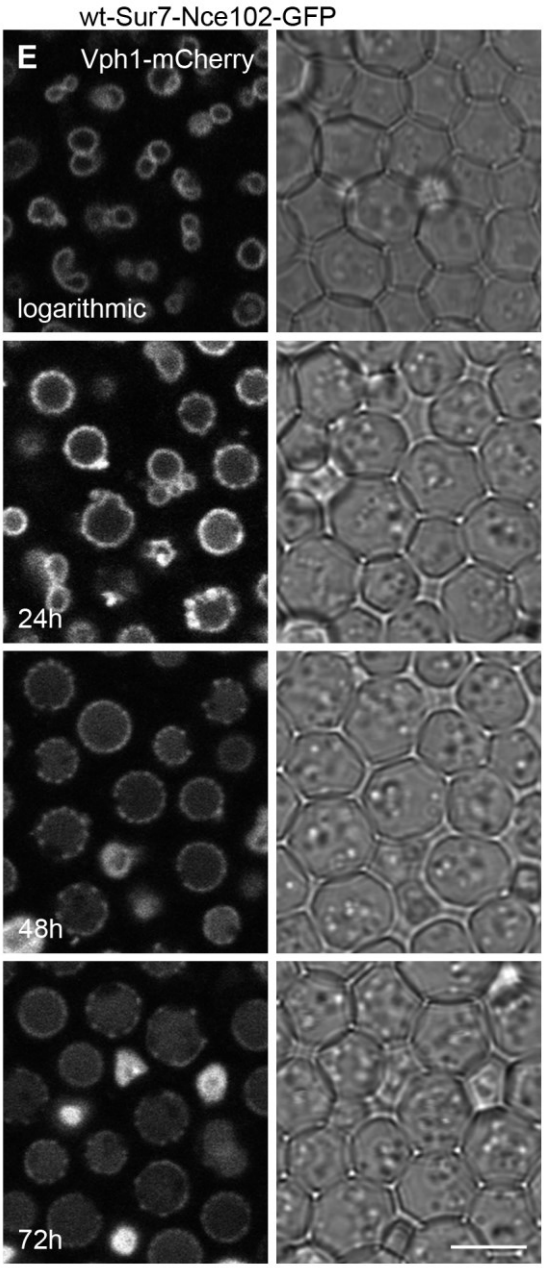

Figure 20 – part 3. Nce102 and Fhn1 are not necessary for vacuolar microdomain formation.
Vph1-mCherry localizations were observed in wild type (Y1044, A), *nce102Δ* (Y1079; B) *fhn1Δ* (Y1099; C), *nce102Δfhn1Δ* (Y1089; D) strains and wild type strain expressing fusion Sur7-Nce102-GFP protein (Y1083; E). Cells were observed after 7 h (logarithmic), 24 h, 72 h, 96 h and 144 h after inoculation into fresh medium. Representative transversal sections with corresponding wide field images are presented. Bar: 5 μm.

However, we noticed two distinct vacuole-related phenotypes of *nce102Δ*, *fhn1Δ* and *nce102Δfhn1Δ* strains when compared to the wild type strain.

The first phenotype was connected to the vacuolar fusion. It is known that logarithmic cell possesses many small vacuoles that later in the stationary phase fuse into one big vacuole (Li

and Kane, 2009). Consistently, logarithmic wild type cells expressing Vph1-mCherry possessed many small vacuoles. After 24 h of cultivation, one big vacuole could be observed in all wild type cells (Fig. 20 – part 1, quantification in Fig. 21). In the *nce102Δ* strain, however, there was small, but still a significant portion of cells that possessed more than one vacuole after 24 h of cultivation (Fig. 20 – part 1, quantification in Fig. 21). After 48h of cultivation, also *nce102Δ* cells came to the state when all the cells contained only one big vacuole (Fig. 20 – part 1). This indicates that *nce102Δ* strain exhibited slightly delayed vacuolar fusion. Interestingly, *fhn1Δ* and *nce102Δfhn1Δ* strains exhibited even more profound phenotypes (Fig. 20 – part 2, quantification in Fig. 21).

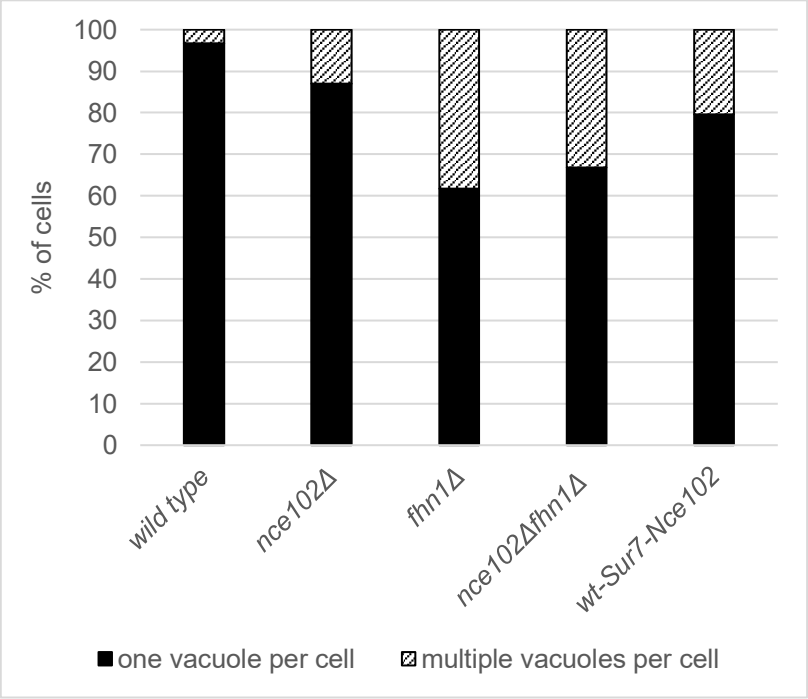

Figure 21. Vacuolar fusion is delayed in strains with the deletion of Nce102 and/or Fhn1 proteins and in the strain with the defect in Nce102 translocation to vacuolar membrane.

The number of vacuoles per cell was determined in wild type (Y1044), *nce102Δ* (Y1079), *fhn1Δ* (Y1099), *nce102Δfhn1Δ* (Y1089) strains and wild type strain expressing fusion Sur7-Nce102-GFP protein (Y1083). Cells were analyzed after 24 hours after inoculation into fresh medium. The percentage of cells with one vacuole and percentage of cells with multiple vacuoles is depicted. The data were obtained from one representative experiment. For each strain, at least 800 cells was counted.

The second phenotype of the mutant strains was related to the Vph1-mCherry protein degradation. After 48 h of cultivation and more, we noticed a substantial pool of diffuse mCherry signal in the vacuolar lumen of *nce102Δ*, *fhn1Δ* and *nce102Δfhn1Δ* cells that was not

present in wild type cells (Fig. 20 – part 1 and 2, quantification in Fig. 22). As stated previously, the diffuse fluorescence signal in the vacuolar lumen indicates the degradation of the fluorescently-tagged protein. This suggests that in *nce102Δ*, *fhn1Δ* and *nce102Δfhn1Δ* strains, vacuolar membrane protein Vph1 may be more prone to degradation than in wild type cells.

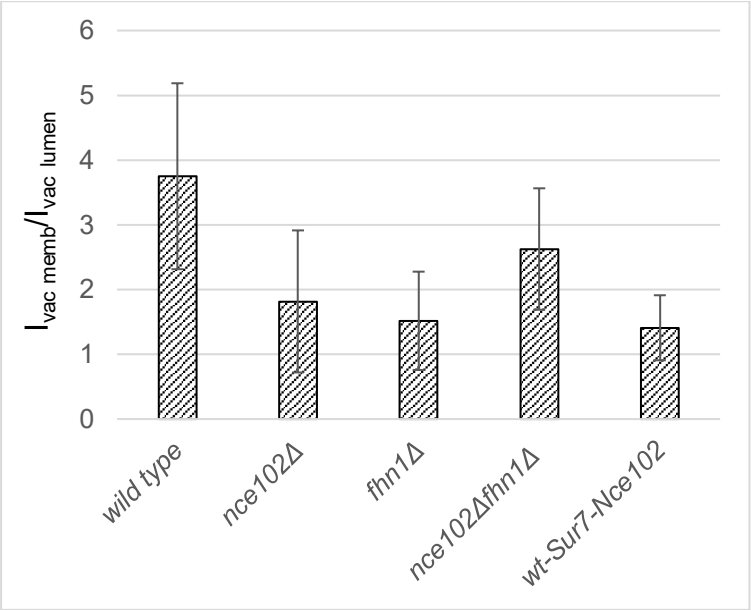

Figure 22. Vph1 is internalized to vacuolar lumen in strains that lack Nce102 and/or Fhn1 proteins and in the strain with the defect in Nce102 translocation to vacuolar membrane.

The ratio between intensity of Vph1-mCherry vacuolar membrane signal and intensity of Vph1-mCherry signal in vacuolar lumen was determined in wild type (Y1044), *nce102Δ* (Y1079), *fhn1Δ* (Y1099), *nce102Δfhn1Δ* (Y1089) strains and wild type strain expressing fusion Sur7-Nce102-GFP protein (Y1083). Cells were analyzed after 72 hours after inoculation into fresh medium. The data were obtained from one representative experiment. For each strain, at least 150 cells was counted. Error bars represent standard deviation.

Together, these results indicate that both Nce102 and Fhn1 proteins might be involved in vacuolar fusion and Vph1 vacuolar protein degradation. Importantly, similar results were obtained when Nce102 was fused to Sur7 protein and did not re-localize to vacuoles in stationary cells (Fig. 20 - part 3, quantification in Fig. 21 and 22). As these cells have similar phenotype to mutant cells regarding vacuolar phenotypes, this suggests that it is the function of Nce102 on vacuole that might affect the vacuolar fusion and Vph1-mCherry degradation.

5.2.5 Nce102 and Fhn1 might play a role in lipid droplets degradation

We showed that in stationary cells, Nce102 localizes to sterol-rich vacuolar microdomains and together with Fhn1 affects vacuolar fusion and possibly vacuolar protein degradation. Sterol-rich microdomains were previously shown to be sites where the stationary phase microautophagy of lipid droplets (so-called lipophagy) occurs (Wang et al., 2014). Therefore, we asked whether Nce102 and Fhn1 proteins play a role in this process.

To visualize lipid droplets, Erg6 was tagged with GFP (using integrative vector) in our strains. Erg6 is an enzyme involved in ergosterol biosynthesis and is widely used as a marker of lipid droplets (Leber et al., 1994; van Zutphen et al., 2014; Wang et al., 2014). Wang and co-workers showed that as cells enter the stationary phase, lipid droplets marked by Erg6-mCherry are engulfed by vacuolar membrane and subsequently digested (Wang et al., 2014).

First, we monitored the lipid droplet patterns in our strains. In logarithmic wild type cells, lipid droplets marked with Erg6-GFP were small patches in cytoplasm (Fig. 23). As the culture got older, lipid droplets grew in size and intensity with the peak in 72h cultures. After 120 h of cultivation and more, lipid droplets again became dimmer. However, we did not observe any engulfment of lipid droplets by the vacuole or increased GFP signal in vacuolar lumen in wild type strain. Moreover, *nce102Δfhn1Δ* strain did not seem to differ significantly from wild type strain (Fig. 23).

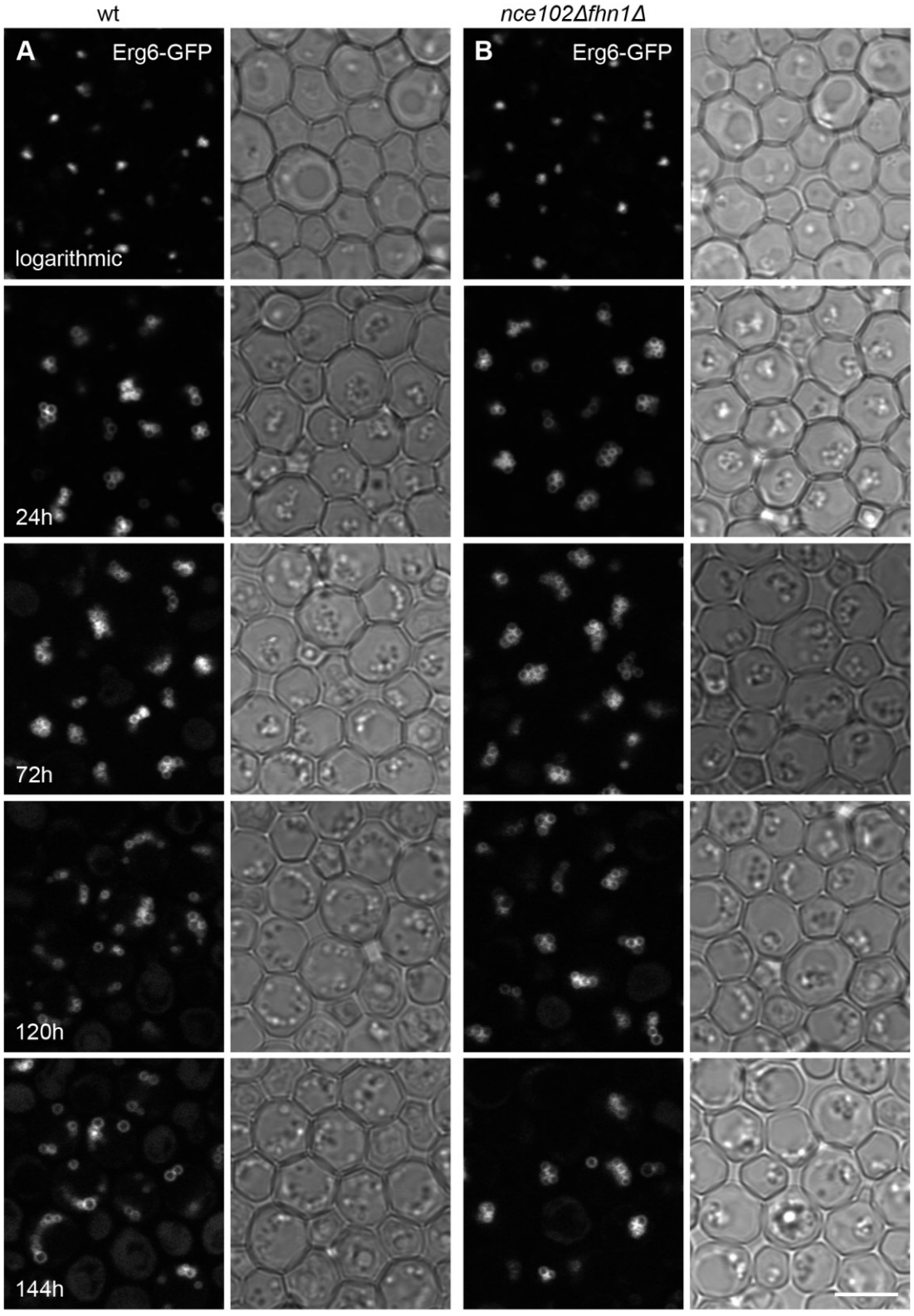

Figure 23. Pattern of lipid droplets marked by Erg6-GFP is similar in wild type and *nce120Δfhn1Δ* strains. Lipid droplets were visualized by tagging Erg6 protein with GFP in wild type (Y1115; A) and *nce102Δfhn1Δ* (Y1137; B) strain. Patterns of lipid droplets were observed after 7 h (logarithmic), 24 h, 72 h, 120 h and 144 h after inoculation into fresh medium. Representative transversal sections with corresponding wide field images are presented. All strains and all time points were scanned using the same settings. Bar: 5 μm.

Another way how to measure the degradation of lipid droplets is monitoring the degradation of lipid droplets marker protein (Seo et al., 2017; Shpilka et al., 2015; van Zutphen et al., 2014; Wang et al., 2014). As noted above, the first step of tagged protein degradation is the cleavage of the fluorescent protein from the native protein. Therefore, by monitoring the amount of free GFP protein that was cleaved from Erg6-GFP, we should be able to measure the extent of lipid droplets degradation. The measuring of cleaved tagged protein is usually done using Western blot analysis (van Zutphen et al., 2014; Wang et al., 2014).

We first wanted to verify that we can monitor free GFP in wild type strain after Erg6-GFP degradation. To reach this aim, we employed the analysis of Erg6-GFP degradation after nitrogen starvation (Numrich et al., 2015; Tsuji et al., 2017; van Zutphen et al., 2014). The cells were grown into logarithmic phase and then incubated the cells in medium without nitrogen for 5 hours. In logarithmic cells, lipid droplets marked with Erg6-GFP were small and after nitrogen starvation, they became slightly larger and dimmer (Fig. 24). Notably, we did not observe any lipid droplets engulfment by vacuoles or any diffuse GFP signal in vacuolar lumen. Similar Erg6-GFP fluorescence patterns were observed also in *nce120Δ*, *fhn1Δ* and *nce102Δfhn1Δ* strains (Fig. 24 and not shown). However, using Western blot analysis, we were able to observe small band (approximately 27kDa) that was not apparent in logarithmic cells and appeared after nitrogen starvation in wild type cells (Fig. 25). We assume that this fragment is free GFP and points to the Erg6-GFP degradation (and lipophagy) after nitrogen starvation. This validates the Western blot analysis to be suitable for monitoring of Erg6-GFP degradation as a method to monitor lipid droplets degradation.

Importantly, the 27kDa band appeared in wild type, as well as *nce120Δ*, *fhn1Δ* and *nce102Δfhn1Δ* strains (Fig. 25). This suggests that neither Nce102 nor Fhn1 (nor both) are necessary for lipophagy after nitrogen starvation. This result is not surprising, however, because after nitrogen starvation in logarithmic cells, Nce102 protein does not re-localize to vacuolar membrane from the plasma membrane (Fig. 26). As Nce102 does not localize to vacuolar membrane under nitrogen starvation, it is probable that it does not play a function under these conditions.

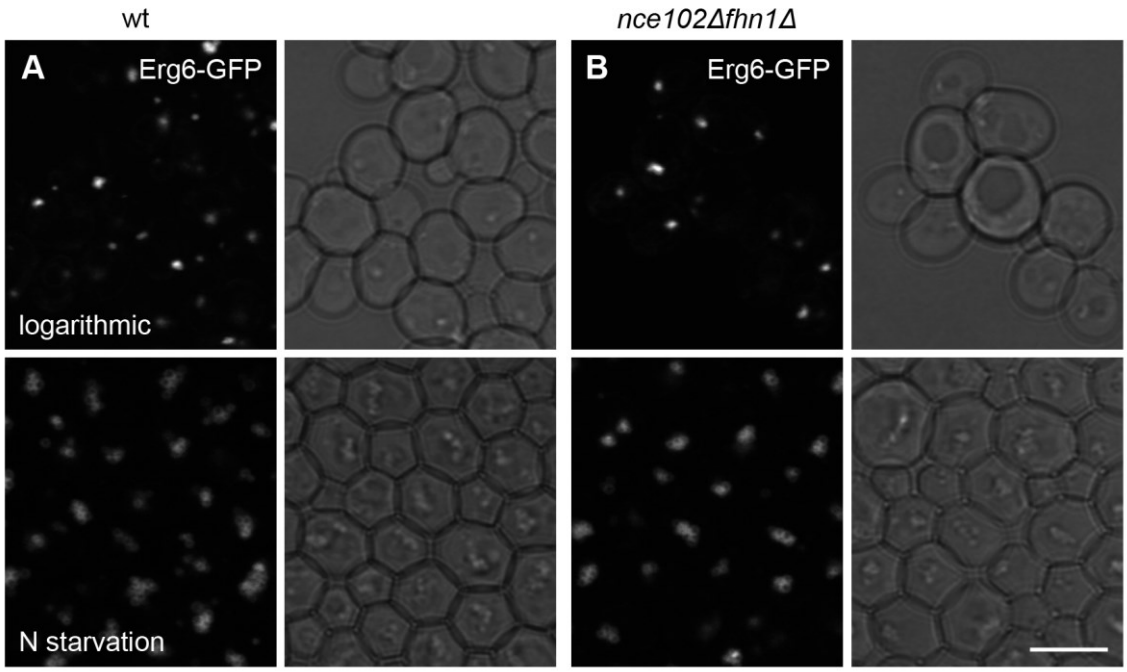

Figure 24. Lipid droplets morphology changes after nitrogen starvation similarly in wild type and *nce102Δfhn1Δ* strains.

Lipid droplets were visualized by tagging Erg6 protein with GFP in wild type (Y1115; A) and *nce102Δfhn1Δ* (Y1137; B) strain. Patterns of lipid droplets were observed in logarithmic phase (left column) and after 5 h of nitrogen starvation (right column). Representative transversal sections with corresponding wide field images are presented. Bar: 5 μm.

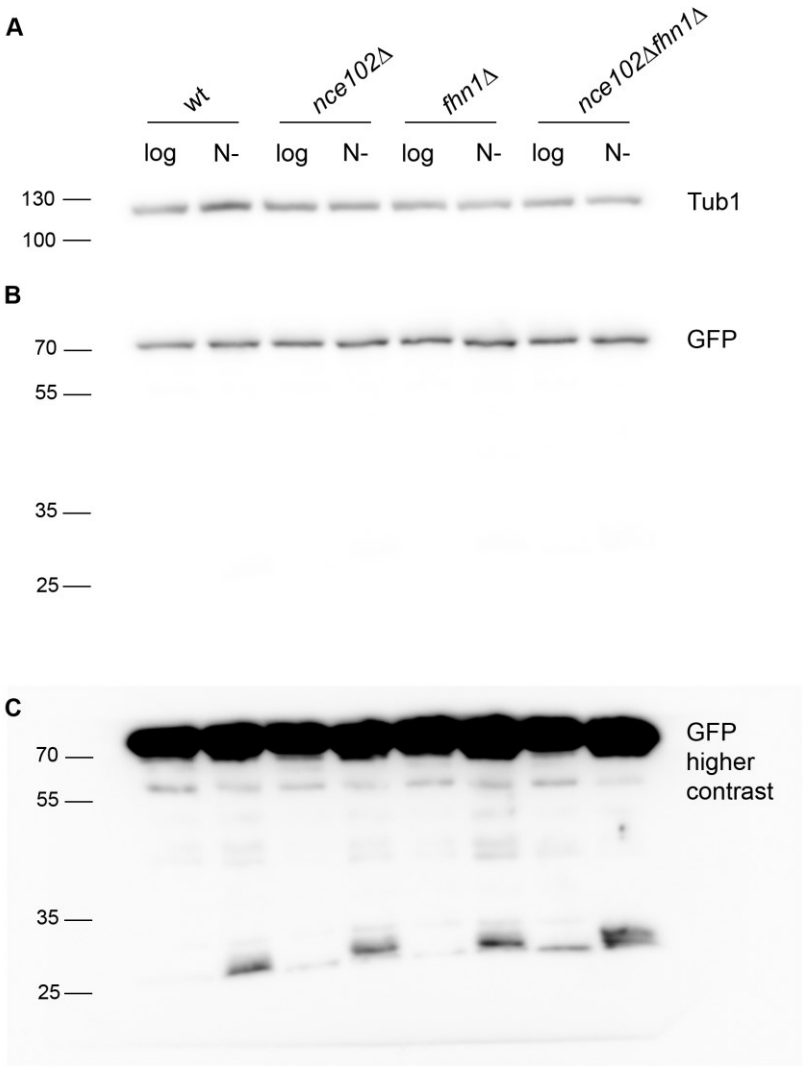

Figure 25. Erg6-GFP is degraded after nitrogen starvation in wild type, *nce120Δ*, *fhn1Δ* and *nce102Δfhn1Δ* strains.

Erg6-GFP protein and free GFP protein fragment levels were determined by Western blot analysis in wild type (Y1115), *nce102Δ* (Y1124), *fhn1Δ* (Y1123) and *nce102Δfhn1Δ* (Y1137) strains in logarithmic cells and after 5h of nitrogen starvation. Tubulin was used as a loading control (A). Representative raw immunoblot is presented in (B), the immunoblot with higher contrast to better visualize lower bands is presented in (C).

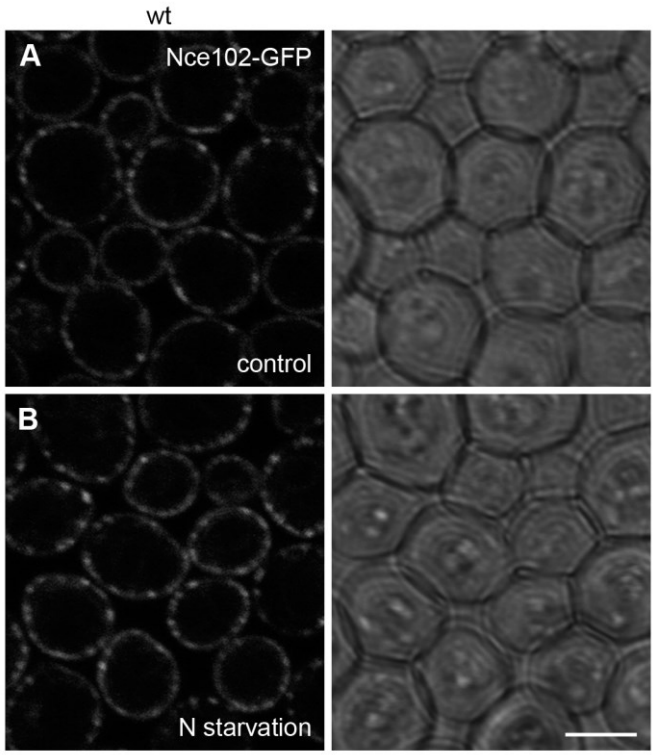

Figure 26. Nce102 does not re-localize to vacuolar membrane after nitrogen starvation.
Nce102-GFP pattern was monitored in logarithmic wild type cells (Y240; A) and wild type cells after 5 h of nitrogen starvation (B). Representative transversal sections with corresponding wide field images are presented. Bar: 5 μm.

Next, we got back to the question whether Nce102 and Fhn1 could play a role in stationary phase lipophagy. We monitored the Erg6-GFP degradation using Western blotting analysis in our strains in 24h and 144h cultures (Fig. 27). After 24 h of cultivation, in all strains, intact Erg6-GFP could be observed and no free GFP band was present. After 144 h of cultivation, according to our expectations, in wild type strain, the free GFP band appeared, corresponding to the stationary phase Erg6-GFP degradation. This band was present also in *nce102Δ* and *fhn1Δ* strains. However, no free GFP could be observed *in nce102Δfhn1Δ* strain, suggesting that in *nce102Δfhn1Δ* cells, the Erg6-GFP degradation and stationary phase lipophagy is compromised (Fig. 27). Taken together, these data suggest that Nce102 and Fhn1 proteins might play a role in stationary phase lipophagy.

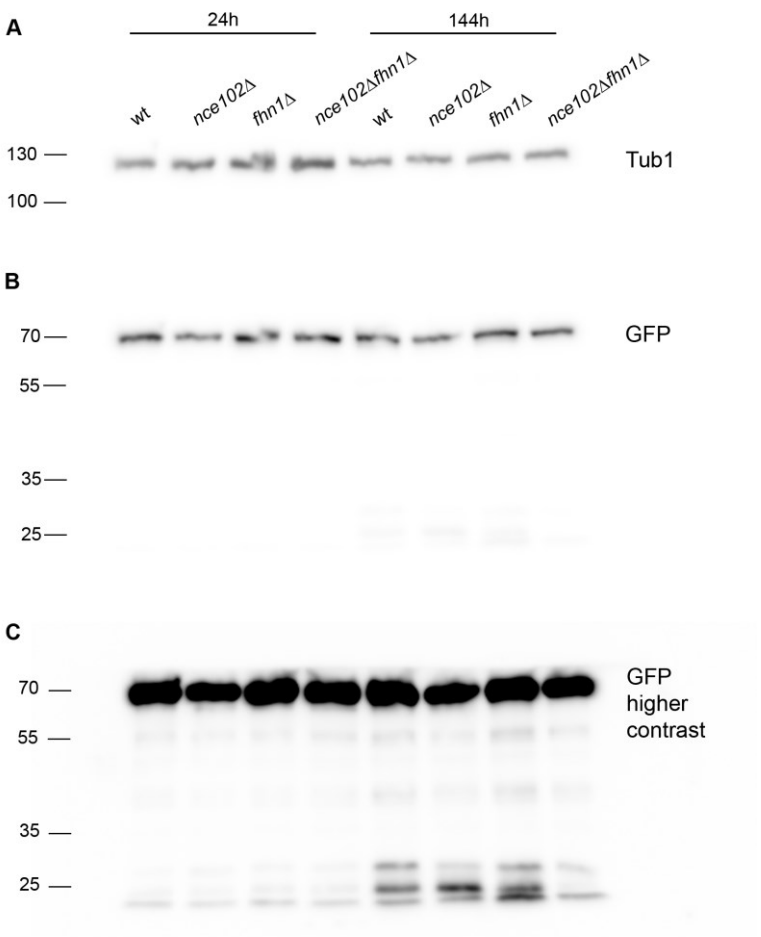

Figure 27. Nce102 and Fhn1 proteins might act together to regulate stationary phase lipophagy.
Erg6-GFP protein and free GFP protein fragment levels were determined by Western blot analysis in wild type (Y1115), *nce102Δ* (Y1124), *fhn1Δ* (Y1123) and *nce102Δfhn1Δ* (Y1137) strains in cells after 24h and 144h of incubation with fresh medium. Tubulin was used as a loading control (A). Representative raw immunoblot is presented in (B), the immunoblot with higher contrast to better visualize lower bands is presented in (C).

Together, in this section we showed that:

- Nce102 translocates from plasma membrane to vacuolar membrane in stationary phase cells
- Nce102 localizes to sterol-enriched vacuolar membrane microdomains
- Nce102 localization to vacuolar membrane depends on the vacuolar membrane physiology
- Nce102 or its homologue Fhn1 are not necessary for formation of vacuolar microdomains
- Nce102 and Fhn1 play a role in vacuolar fusion
- Nce102 and Fhn1 do not play a role in lipophagy after nitrogen starvation
- Nce102 and Fhn1 might play a role in the degradation of vacuolar ATPase subunit and in the stationary-phase lipophagy

5.3 Compatibility of *S. cerevisiae* and *S. pombe* MCC/eisosomal proteins

Kabeche and co-workers compared the compatibility of S. *cerevisiae* Pil1 and *S. pombe Sp*Pil1 protein with respect to the morphology of the eisosomes (Kabeche et al., 2011). They found that *Sp*Pil1 expressed in *pil1Δ S. cerevisiae* cells is able to form dot-like patches in the *S. cerevisiae* plasma membrane that colocalized with Lsp1 patches. Conversely, Pil1 expressed in *pil1Δpil2Δ S. pombe* cells formed elongated filaments associated with the plasma membrane (Kabeche et al., 2011). Based on these results, Kabeche and co-workers concluded that "differences in the cellular environment, not the respective proteins, underlie the distinct appearance of Pil1 in budding yeast versus fission yeast" and that "the budding yeast plasma membrane restricts elongation of cortical Pil1 filaments" (Kabeche et al., 2011).

However, a few studies have already shown that also in *S. cerevisiae*, elongated MCC/eisosomes can form. For example, mutants lacking *MAK3* gene or *YPR050C* open reading frame ("dubious open reading frame, unlikely to encode a functional protein" (Fisk et al., 2006), that overlaps significantly with *MAK3* locus) exhibited elongated MCC/eisosomes visible using fluorescence as well as electron microscopy (Malinsky et al., 2010; Stradalova et al., 2009). Additionally, also cells overexpressing Seg1 produced elongated MCC/eisosomes (Moreira et al., 2012).

We aimed to investigate whether the MCC/eisosome morphology is determined by the plasma membrane composition (as Kabeche and co-workers suggest) or whether it is determined by the protein composition of MCC/eisosome. Moreover, we examined the compatibility of *S. pombe* and *S. cerevisiae* MCC/eisosomal proteins - Pil1 vs. *Sp*Pil1, Seg1 vs. *Sp*Sle1 and Nce102 vs. *Sp*Fhn1. We wanted to compare their characteristics regarding MCC/eisosome assembly in *S. cerevisiae* cells.

5.3.1 *S. pombe Sp*Pil1 protein can substitute for *S. cerevisiae* Pil1 protein function

To investigate the compatibility of *S. pombe Sp*Pil1 protein with Pil1 eisosomes, we expressed *Sp*Pil1 in *S. cerevisiae* cells. We cloned *Sp*Pil1-mRFP into a centromeric expression vector possessing *S. cerevisiae PIL1* promoter. We expressed *Sp*Pil1-mRFP in wild type cells

possessing genomically tagged Sur7-GFP, the marker of endogenous *S. cerevisiae* MCC/eisosomes.

We observed that most of the *Sp*Pil1-mRFP signal was distributed homogeneously in the cytoplasm (Fig. 28A, D). In some cells, also large elongated *Sp*Pil1-mRFP cytosolic aggregates could be observed (arrowheads in Fig. 28A, D). Importantly, a small fraction of *Sp*Pil1-mRFP was also associated with the plasma membrane and accumulated specifically in blurred patches that colocalized with Sur7-GFP marked MCC/eisosomes (Fig. 28A, D). These results show that *S. pombe* protein *Sp*Pil1 is partly able to incorporate into Pil1 eisosomes in *S. cerevisiae*.

Next, we asked whether this is due to its ability to interact with *S. cerevisiae* plasma membrane or because of its interactions with endogenous *S. cerevisiae* Pil1 protein. To test this, we expressed *Sp*Pil1 in *pil1Δ* cells, the cells that contain no endogenous Pil1 protein, the potential interacting partner of *Sp*Pil1. As mentioned previously, *S. cerevisiae* cells lacking Pil1 protein do not form MCC/eisosomes. While wild type cells contain clearly distinguishable evenly distributed MCC/eisosomes marked by Sur7 (Malinska et al., 2003), in *pil1Δ* cells, Sur7 protein becomes more dispersed in the plasma membrane and accumulates in eisosome remnants (Grossmann et al., 2007; Stradalova et al., 2012; Walther et al., 2006).

When *Sp*Pil1-mRFP was expressed in *S. cerevisiae pil1Δ* cells, its association with *S. cerevisiae* plasma membrane improved remarkably comparing to the situation in wild type cells (Fig. 28B, E). Furthermore, the defect in MCC/eisosome formation characteristic for *pil1Δ* strain was rescued significantly in these cells (compare Fig. 28C, F with Fig. 28B, E). Sur7-GFP pattern was more similar to the wild type pattern of MCC/eisosomes: Sur7-GFP formed increased number of more distinct patches and these patches clearly colocalized with patches formed by *Sp*Pil1-mRFP protein (compare Fig. 28C, F with Fig. 28B, E).

We concluded that when *S. pombe Sp*Pil1 is expressed in the wild type *S. cerevisiae* cells, it competes with the endogenous Pil1 protein in the eisosome organization. Therefore, it incorporates weakly into Pil1 eisosomes. In contrast, in the absence of the endogenous Pil1 protein, *Sp*Pil1 forms eisosomes in the *S. cerevisiae* plasma membrane rather effectively. This result shows that *Sp*Pil1 is functional in *S. cerevisiae* cells and is able to interact with *S. cerevisiae* plasma membrane. Moreover, *Sp*Pil1-organized eisosomes are recognized by inherent Sur7 protein. Therefore, *S. pombe Sp*Pil1 protein is able to take over the function of endogenous Pil1 protein in *S. cerevisiae*, when the endogenous Pil1 protein is missing.

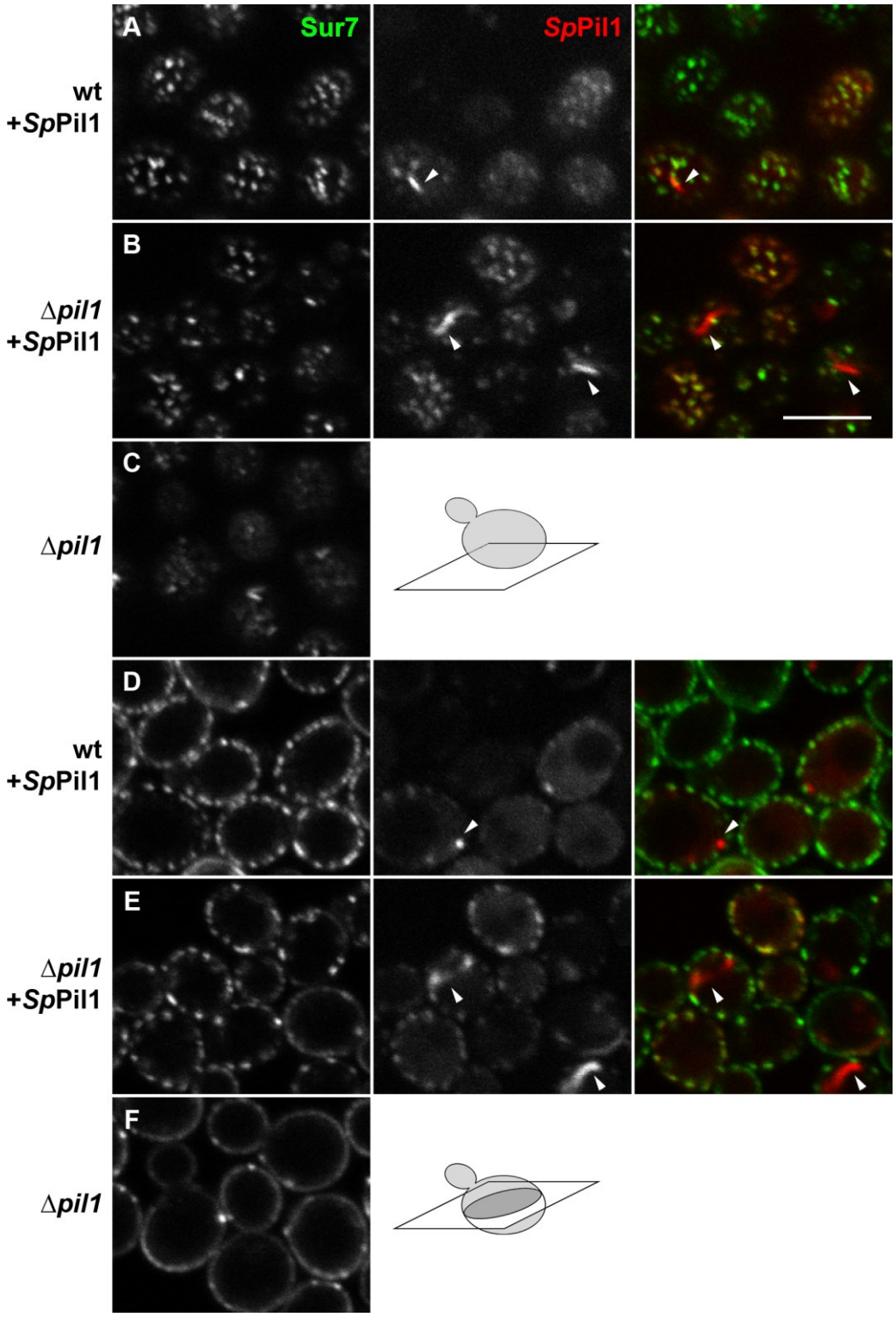

Figure 28. *S. pombe Sp*Pil1 is able to substitute for *S. cerevisiae* Pil1 function in *S. cerevisiae* cells.
*Sp*Pil1-mRFP (middle column, red in right column) was expressed in *S. cerevisiae* wild type (Y307; A, D) and *pil1Δ* (Y315; B, E) strains in which Sur7-GFP (left column, green in right column) was used as a marker of *S. cerevisiae* MCC/eisosomes. Co-localizations are shown in right column (*Sp*Pil1-mRFP in red, Sur7-GFP in green). *pil1Δ* cells expressing only Sur7-GFP were used to visualize the *pil1Δ* phenotype (Y157; C, F). Representative tangential (A, B, C) and transversal (D, E, F) sections are presented. Large cytoplasmic aggregates of *Sp*Pil1 are marked with arrowheads. Bar: 5 μm. The figure was used in (Vaskovicova et al., 2015).

5.3.2 *S. pombe* protein *Sp*Sle1 forms specific microdomains in the *S. cerevisiae* plasma membrane

S. cerevisiae Pil1 and *S. pombe* *Sp*Pil1 are sequence homologues with a high degree of similarity (Vangelatos et al., 2010). In contrast, *S. cerevisiae* Seg1 and its functional equivalent in *S. pombe*, *Sp*Sle1, are not sequentially related (Moreira et al., 2012). We asked whether also the *S. pombe* eisosome stabilizer *Sp*Sle1 is compatible with eisosomes of *S. cerevisiae*.

To answer this question, we cloned *S. pombe* *Sp*Sle1-GFP protein into a multicopy expression vector. In this plasmid, *Sp*Sle1 was under the control of constitutive promoter and was highly overexpressed. We examined the localization of *Sp*Sle1-GFP in wild type *S. cerevisiae* cells expressing genomically tagged Pil1 or Sur7, the markers of *S. cerevisiae* MCC/eisosomes.

In these cells, *Sp*Sle1-GFP protein was highly associated with the plasma membrane and clearly accumulated in numerous bright evenly distributed patches resembling the pattern of MCC/eisosomes (Fig. 29). However, these patches did not colocalize with endogenous MCC/eisosomes marked by Pil1-mRFP or Sur7-mRFP (Fig 29).

This *Sp*Sle1 pattern was not caused by *Sp*Sle1 overexpression, as the expression of *Sp*Sle1-GFP from the centromeric plasmid under the control of endogenous SEG1 promoter yielded the same conclusion. Because of the lower protein level, the number and intensity of *Sp*Sle1-GFP patches were significantly reduced, but still, these plasma membrane patches did not correspond to the *S. cerevisiae* MCC/eisosomes (Fig. 30). Importantly, this pattern of *Sp*Sle1-GFP was preserved even when the protein was expressed in *S. cerevisiae* cells lacking endogenous Seg1 protein (Fig. 30). This indicates that there is no competition between Seg1 and *Sp*Sle1 proteins in associating with MCC/eisosomes.

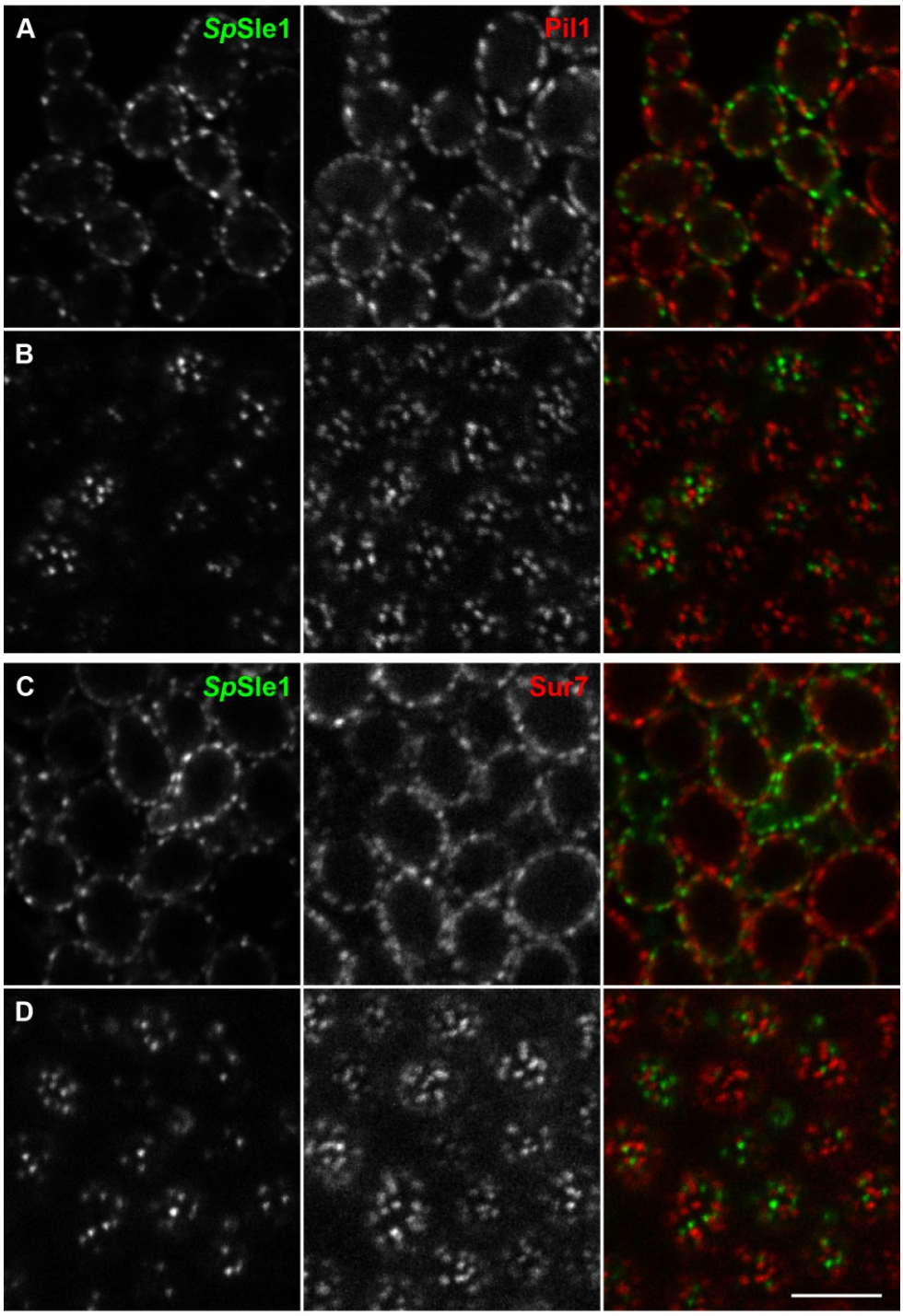

Figure 29. *S. pombe Sp*Sle1 forms microdomains in the plasma membrane of *S. cerevisiae* that are different from endogenous MCC/eisosomes.

*Sp*Sle1-GFP (left column (A-D), green in right column (A-D)) was expressed from multicopy plasmid in *S. cerevisiae* wild type cells in which Pil1-mRFP (Y224; A and B of middle column, red in right column (A, B)) or Sur7-mRFP (Y223; C and D of middle column, red in right column (C, D)) were used as markers of *S. cerevisiae* MCC/eisosomes. Co-localizations are shown in right column (A-D) (*Sp*Sle1-GFP in green, Pil1-mRFP/Sur7-mRFP in red). Representative tangential (B, D) and transversal (A, C) sections are presented. Bar: 5 µm. The figure was partly adapted from (Vaskovicova et al., 2015).

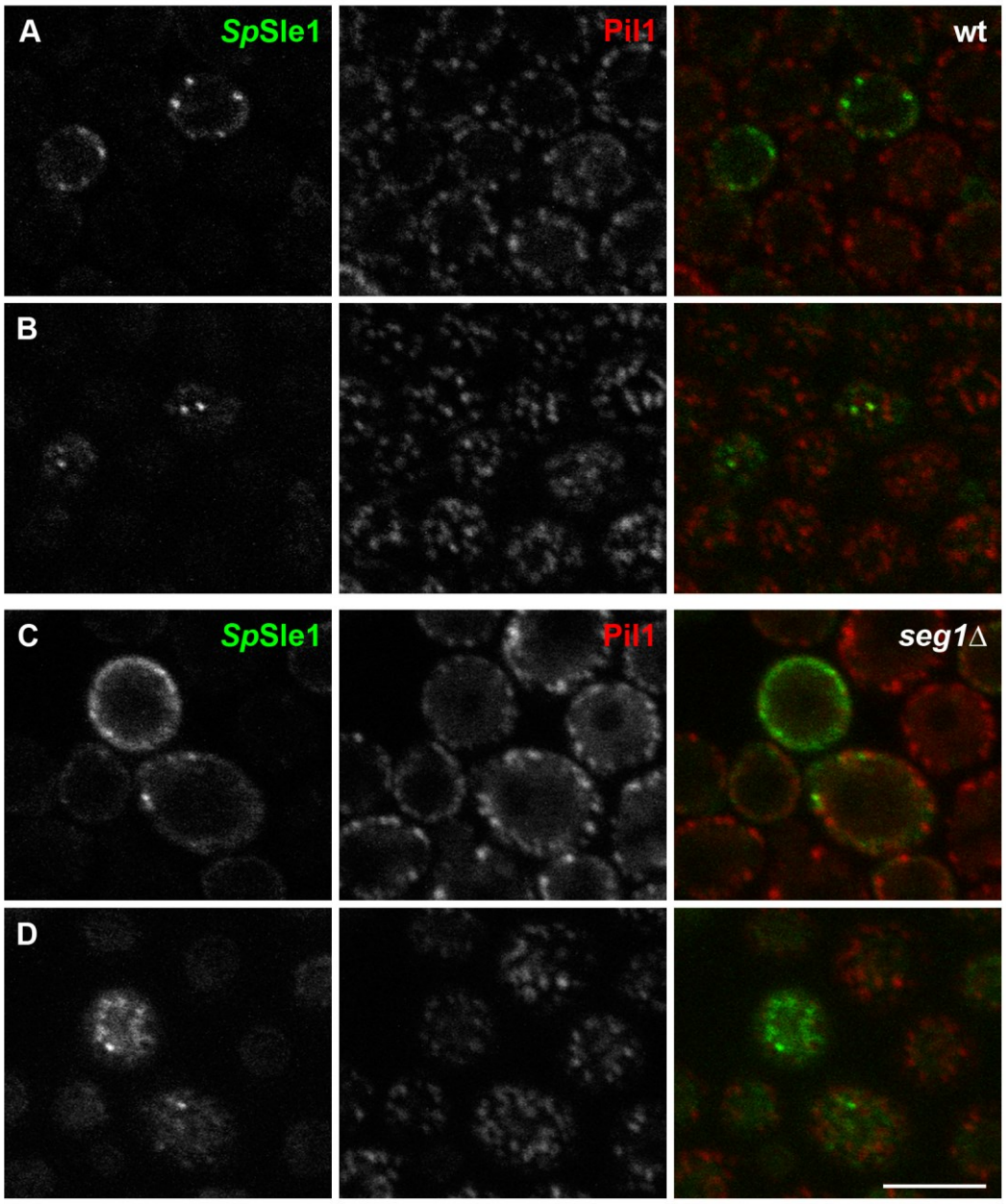

Figure 30. *S. pombe Sp*Sle1 forms distinct microdomains both in wild type and in *seg1Δ* strain.
*Sp*Sle1-GFP (left column (A-D), green in right column (A-D)) was expressed from centromeric plasmid under *SEG1* promoter in *S. cerevisiae* wild type (Y341) and *seg1Δ* (Y342) cells in which Pil1-mRFP (A-D of middle column, red in right column (A-D)) were used as markers of *S. cerevisiae* MCC/eisosomes. Co-localizations are shown in right column (A-D) (*Sp*Sle1-GFP in green, Pil1-mRFP in red). The contrast was adjusted as needed to improve the visibility of the signal. Representative tangential (B, D) and transversal (A, C) sections are presented. Bar: 5 μm.

These results suggest that when expressed in *S. cerevisiae* cells, *Sp*Sle1 is capable of association with the plasma membrane, but it cannot interact with *S. cerevisiae* MCC/eisosome

components, not even in the absence of its possible competitor, Seg1. Instead, *Sp*Sle1 forms its own, novel microdomains in the plasma membrane of *S. cerevisiae*.

To investigate whether *Sp*Sle1 is able to take over Seg1 function in Seg1 absence, similarly to *Sp*Pil1 compensating for Pil1 function in *pil1Δ* cells, the ability of *Sp*Sle1 to rescue the *seg1Δ* phenotype was tested. In *seg1Δ* cells, Pil1-mRFP protein level in cytoplasm is significantly higher than in wild type cells suggesting eisosome disassembly and the role of Seg1 protein in eisosome stabilization (Moreira et al., 2012). From fluorescence microscopy images, we quantified the fraction of Pil1 protein associating with the plasma membrane in wild type strain, *seg1Δ* strain and *seg1Δ* strain expressing *Sp*Sle1 protein. We expressed this value as a ratio of the mean fluorescence intensities measured in the plasma membrane and in the cytoplasm. In *seg1Δ* cells, this ratio dropped almost three-fold compared to wild type cells, consistently with previously published results (Fig. 31). Importantly, the *seg1Δ* phenotype was not rescued by the overexpression of *Sp*Sle1-GFP from a multicopy plasmid (Fig. 31). This suggests that *Sp*Sle1 is not able to substitute for Seg1 function in *seg1Δ* cells.

Together, our results indicate that *Sp*Sle1 neither incorporates into MCC/eisosomes of *S. cerevisiae* nor is able to substitute for Seg1 function. Particularly, *Sp*Sle1 cannot stabilize Pil1 eisosomes in the absence of Seg1.

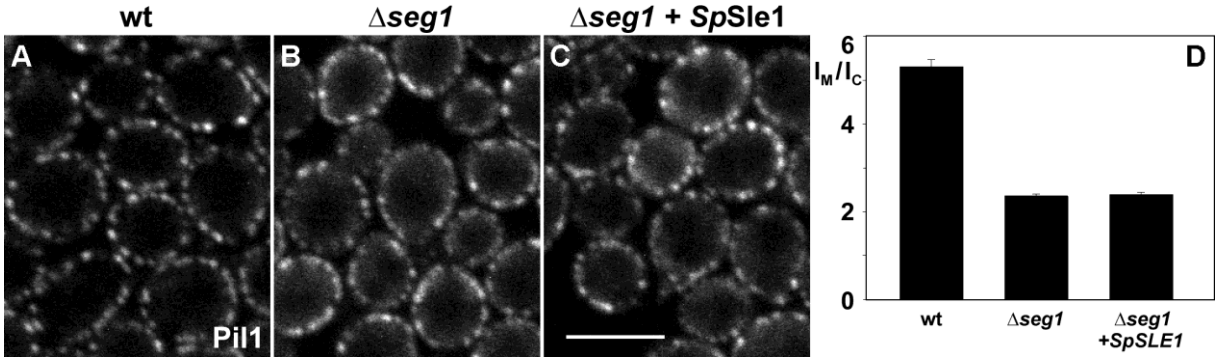

Figure 31. *S. pombe Sp*Sle1 is not able to rescue the *seg1Δ* phenotype of *S. cerevisiae*.

Pil1-mRFP pattern was monitored in wild type strain (Y124; A), *seg1Δ* strain (Y207; B) and *seg1Δ* strain expressing *Sp*Sle1 protein (Y234; C). Representative transversal sections are presented. Bar: 5μm. The ratio of the mean fluorescence intensities of Pil1-mRFP measured in the plasma membrane (I_M) and in the cytoplasm (I_C) was calculated in these strains (D). Standard errors are depicted in the graph. The figure was used in (Vaskovicova et al., 2015).

5.3.3 *S. pombe Sp*Sle1 protein keeps its functionality at the plasma membrane of *S. cerevisiae*

In principle, there are two possible reasons why *Sp*Sle1 could fail to associate with *S. cerevisiae* eisosomes. Either it is incompatible with *S. cerevisiae* Pil1 protein, or it does not function properly when expressed in *S. cerevisiae*.

To test which of these two takes place in our system, we co-expressed *Sp*Sle1-GFP with its natural interaction partner, *Sp*Pil1-mRFP, in *S. cerevisiae* cells. We quantified the plasma membrane-associated *Sp*Pil1-mRFP fractions both in the presence and in the absence of *Sp*Sle1-GFP-expressing centromeric plasmid. Again, the ratio between the mean fluorescence intensities measured at the plasma membrane and in cytoplasm was calculated.

We observed that upon co-expression of *Sp*Pil1-mRFP and *Sp*Sle1-GFP (both from centromeric plasmids), the plasma membrane-association of *Sp*Pil1 increased significantly compared to the cells where *Sp*Pil1 was expressed alone (Fig. 32). This result was the same for both wild type and *pil1Δ* cells (Fig. 32). Remarkably, the co-expression of *Sp*Pil1-mRFP and *Sp*Sle1-GFP proteins in *pil1Δ* cells of *S. cerevisiae* resulted in *Sp*Pil1 eisosomes of filamentous shape, the morphology that resembled filamentous eisosomes of *S. pombe* (Fig. 32D).

These results suggest that *Sp*Sle1 is functional in *S. cerevisiae* cells, but recognizes only *Sp*Pil1, and not Pil1, as an interaction partner. Moreover, *S. pombe Sp*Sle1 is effective in recruiting *S. pombe Sp*Pil1 protein to the plasma membrane of *S. cerevisiae* cells and the co-expression of these proteins results in the formation of *S. pombe*-like filamentous eisosomes.

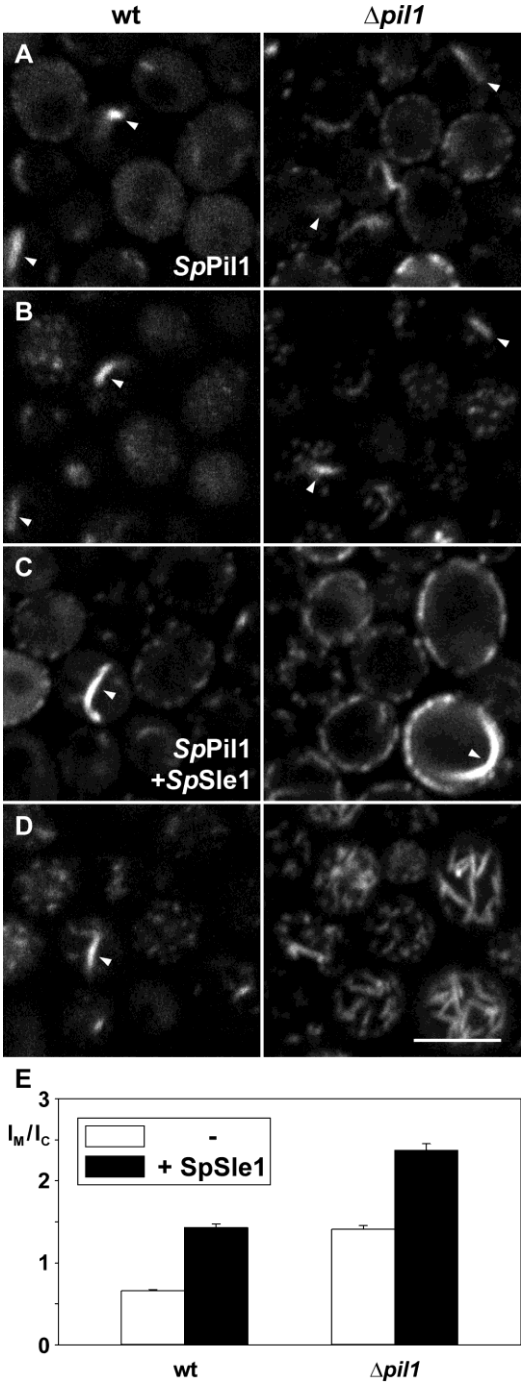

Figure 32. *Sp*Sle1 recruits *Sp*Pil1 to the plasma membrane in *S. cerevisiae*.

*Sp*Pil1 patterns were monitored in wild type (left column) and *pil1Δ* (right column) *S. cerevisiae* cells both in the absence (A, B, empty bars in E) and in the presence (C, D, full bars in E) of *Sp*Sle1 protein. Following strains were used: wild type strain expressing *Sp*Pil1-mCherry and Sur7-GFP (Y307), wild type strain expressing *Sp*Pil1-mCherry and *Sp*Sle1-GFP (Y334), *pil1Δ* strain expressing *Sp*Pil1-mCherry and Sur7-GFP (Y315), *pil1Δ* strain expressing *Sp*Pil1-mCherry and *Sp*Sle1-GFP (Y335). Representative transversal (A, C) and tangential (B, D) sections are presented. Large cytoplasmic aggregates of *Sp*Pil1 are marked with arrowheads. Bar: 5 μm. The association of *Sp*Pil1mRFP with the plasma membrane in these strains was calculated as the ratio of the mean fluorescence intensities of *Sp*Pil1-mRFP measured in the plasma membrane (I_M) and in the cytoplasm (I_C). Standard errors are depicted in the graph. The figure was used in (Vaskovicova et al., 2015).

5.3.4 Seg1 and *Sp*Sle1 cooperate in stabilization of *Sp*Pil1 eisosomes in the plasma membrane of *S. cerevisiae*

As described above, we found that *Sp*Sle1 does not accept Pil1 as an interaction partner. We next tested the opposite - whether the inherent eisosome stabilizer of *S. cerevisiae*, Seg1, can stabilize eisosomes composed of *Sp*Pil1.

As a measure of *Sp*Pil1 eisosome stability, the length of *Sp*Pil1 eisosomes was used. In each analyzed cell, we estimated the mean eisosome length and subsequently, we divided the analyzed cells into three groups – cells with eisosomes shorter than 0.5 µm (dot-like pattern, standard *S. cerevisiae* eisosomes), cells with eisosome length between 0.5-1 µm (elongated eisosomes) and cells with eisosomes longer than 1 µm (filamentous pattern, *S. pombe*-like eisosomes) (Fig. 33A). This way, we were able to quantify the stability of *Sp*Pil1-mRFP eisosomes in strains expressing different amounts of Seg1 and *Sp*Sle1 proteins.

Cells expressing *Sp*Pil1-mRFP in the *pil1Δseg1Δ* background contained no eisosome stabilizer and the vast majority of cells (approximately 90 %) exhibited dot-like *Sp*Pil1 eisosome pattern; the rest of the cells exhibited elongated eisosomes (Fig. 33B, row 1). The same *Sp*Pil1 eisosome pattern could be observed in cells possessing a chromosomal copy of *SEG1* gene (*pil1Δ* cells expressing *Sp*Pil1-mRFP; Fig. 33B, row 2). When Seg1 was expressed from a centromeric plasmid in *pil1Δseg1Δ*, however, the fraction of the cells with dot-like eisosome pattern dropped to 60 % and the fraction of cells with elongated eisosomes increased to 30 % (Fig. 33B, row 3). This might be due to the potentially higher Seg1 protein expression level from plasmid and it suggests that also Seg1 protein can stabilize *Sp*Pil1 eisosomes. Importantly, when *Sp*Sle1 was expressed in *pil1Δseg1Δ* cells from the same centromeric plasmid, the fraction of cells with punctuate *Sp*Pil1 eisosomes dropped to 40 % and the fraction of cells exhibiting filamentous *Sp*Pil1 eisosomes increased from almost none to more than 20 % (Fig. 33B, row 4), indicating that *Sp*Sle1 might be a more effective *Sp*Pil1 stabilizer compared to Seg1. However, without the determined protein levels of Seg1 and *Sp*Sle1 we cannot confirm this conclusion directly. In cells co-expressing chromosomal Seg1 protein and *Sp*Sle1 from centromeric plasmid, less than 30 % of cells exhibited punctuate *Sp*Pil1 eisosomes and almost 30 % of cells exhibited filamentous *Sp*Pil1 eisosomes (Fig. 33B, row 5). This additive effect suggested a cooperation of both Seg1 and *Sp*Sle1 in the stabilization of *Sp*Pil1 eisosome.

Together, these results indicate that both Seg1 and *Sp*Sle1 proteins can stabilize *Sp*Pil1 eisosomes. The stabilization effect of these proteins is positively correlated with the overall

amount of the stabilizer proteins and *Sp*Sle1 might possibly stabilize *Sp*Pil1 eisosomes more effectively than Seg1. Interestingly, both proteins can co-operate in *Sp*Pil1 stabilization.

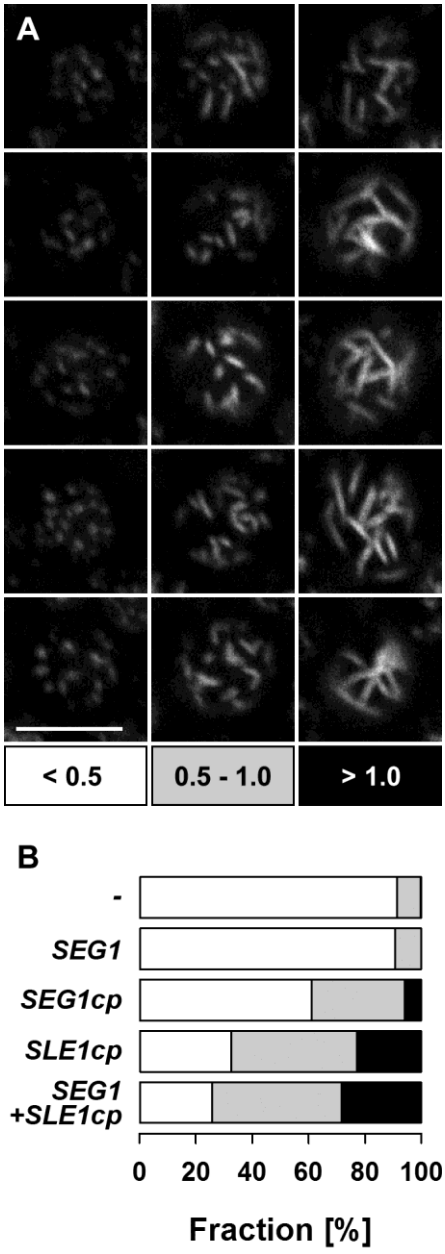

Figure 33. *Sp*Pil1 eisosomes can be stabilized by both *Sp*Sle1 and Seg1.

Quantitative analysis of *Sp*Pil1 eisosome length was performed in strains with different amounts of *Sp*Sle1 or Seg1 stabilizer proteins. In each culture, cells were divided into three groups based on the average *Sp*Pil1 eisosome length (A): (i) cells with eisosomes shorter than 0.5 µm (normal, dot-like eisosomes, resembling *S. cerevisiae* eisosomes) (A, left column), (ii) cells with eisosomes from 0.5 µm to 1.0 µm (A, middle column) and (iii) cells with eisosomes longer than 1.0 µm (long, filamentous eisosomes, resembling *S. pombe* eisosomes) (A, right column). The cells were analyzed from tangential sections and more than 300 cells were counted in each strain. The relative abundance of each group was plotted into the graph for each strain (B).We analyzed following strains:

pil1Δseg1Δ strain (possessing no eisosome stabilizer) (Y427), *pil1Δ* strain (possessing one genomic copy of *SEG1* gene) (Y315), *pil1Δseg1Δ* strain expressing either *SEG1* (*SEG1cp*) (Y441) or *Sp*Sle1 gene (*SLE1cp*) (Y425) from centromeric plasmid, *pil1Δ* strain expressing *SEG1* from genomic copy and *Sp*Sle1 from centromeric plasmid (*SEG1* + *SLE1cp*) (Y335). All these strains also expressed *Sp*Pil1-mRFP from centromeric plasmid. Bar: 5 μm. The figure was used in (Vaskovicova et al., 2015).

5.3.5 *S. pombe Sp*Fhn1 protein is attracted to *Sp*Pil1-*Sp*Sle1 eisosomes in the plasma membrane of *S. cerevisiae*

Next, we asked whether *Sp*Pil1-*Sp*Sle1 eisosomes formed in the plasma membrane of *S. cerevisiae* are able to attract also *S. pombe* MCC proteins. To reach this aim, we cloned fluorescently tagged *Sp*Fhn1 protein, the homologue of Nce102 protein, into the multicopy expression vector and observed its localization in *S. cerevisiae* cells.

In wild type cells, *Sp*Fhn1-GFP was homogeneously dispersed in the plasma membrane with no preferential localization to MCC as judged from the co-localization with Sur7-mRFP protein (Fig. 34A, B). Additionally, *Sp*Fhn1-GFP was found in the intracellular structures, perhaps the endoplasmic reticulum, possibly because of the high protein levels caused by *Sp*Fhn1-GFP overexpression from the plasmid. In cells lacking endogenous Nce102 protein, however, *Sp*Fhn1-GFP partially accumulated also in patches that co-localized with Sur7-marked MCC (Fig. 34C, D). This indicated that in the absence of Nce102, *Sp*Fhn1 was able to interact with *S. cerevisiae* MCC. It is in agreement with the previous data of Loibl and co-workers that showed that *Sp*Fhn1 localizes to MCC in the absence of endogenous Nce102 and is able to substitute for Nce102 function in attracting Can1 protein into MCC (Loibl et al., 2010). Our results further suggest the competition between *S. pombe Sp*Fhn1 and *S. cerevisiae* Nce102, where Nce102 has significantly higher affinity for *S. cerevisiae* MCC/eisosomes than *Sp*Fhn1 (Fig. 34).

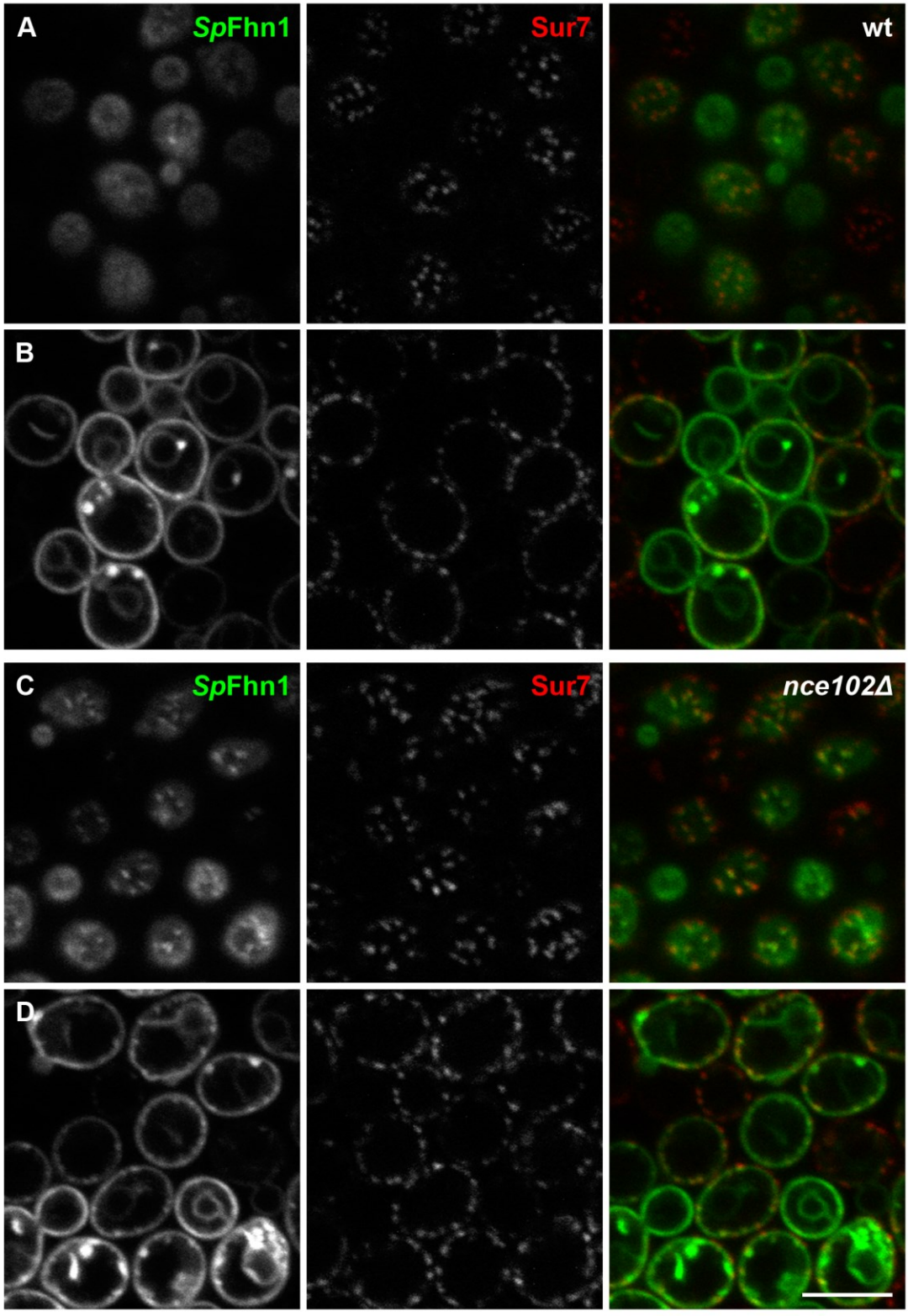

Figure 34. In the absence of Nce102, *Sp*Fhn1 is partly able to incorporate into *S. cerevisiae* MCC/eisosomes. *Sp*Fhn1-GFP (left column, green in right column) was expressed in *S. cerevisiae* wild type (Y328; A, B) and *nce102Δ* (Y330; C, D) strains in which Sur7-mRFP (middle column, red in right column) was used as a marker of *S. cerevisiae* MCC/eisosomes. Co-localizations are shown in right column (*Sp*Fhn1-GFP in green, Sur7-mRFP in red). Representative tangential (A, C) and transversal (B, D) sections are presented. Bar: 5 μm.

Similarly, *Sp*Fhn1 was not able to interact with *Sp*Pil1-*Sp*Sle1 eisosomes, when these were formed either in wild type or in *pil1Δ S. cerevisiae* cells (Fig. 35A, B, C, D). However, in the absence of Nce102 (in *pil1Δnce102Δ* strain), *Sp*Fhn1 strongly associated with elongated *Sp*Pil1-*Sp*Sle1 eisosomes (Fig. 35E, F). This is in agreement with the hypothesis that Nce102 is a competitor of *Sp*Fhn1. However, it is interesting that *S. cerevisiae* Nce102 is more efficient at associating with *S. pombe Sp*Pil1-*Sp*Sle1 proteins than *S. pombe Sp*Fhn1.

We conclude that *S. pombe Sp*Fhn1 protein is able to associate with both *S. cerevisiae* and *S. pombe* MCC/eisosomes, but only in the absence of its competitor, the homologues protein Nce102. Surprisingly, Nce102 is more effective than *Sp*Fhn1 in associating with both sets of MCC/eisosomal proteins.

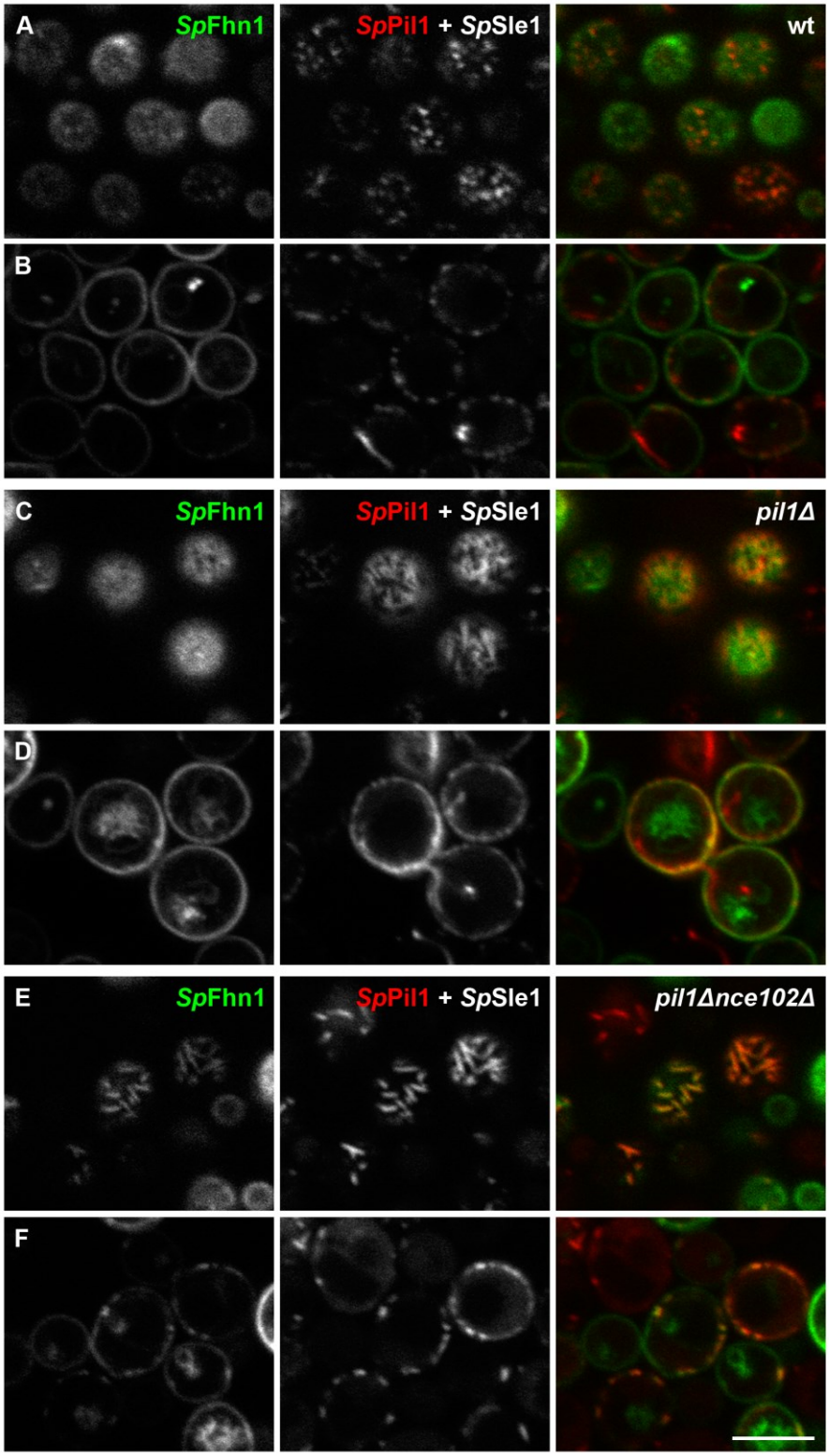

Figure 35. *Sp*Fhn1 incorporates into the *Sp*Pil1-*Sp*Sle1 eisosomes only in the absence of *S. cerevisiae* Nce102. *Sp*Fhn1-GFP (left column, green in right column) was expressed in *S. cerevisiae* wild type (Y369; A, B), *pil1Δ* (Y366; C, D) and *pil1Δnce102Δ* (Y368; E, F) strains. These cells also co-expressed *Sp*Pil1-mRFP protein (middle column) and untagged *Sp*Sle1 protein. Co-localizations of *Sp*Fhn1-GFP and *Sp*Pil1-mRFP are shown in right column (*Sp*Fhn1-GFP in green, *Sp*Pil1-mRFP in red). Representative tangential (A, C. E) and transversal (B, D, F) sections are presented. Bar: 5 μm.

5.3.6 The coalescence of Seg1 and *Sp*Sle1 microdomains in the plasma membrane of *S. cerevisiae*

The comparison between wild type and *pil1Δ S. cerevisiae* cells expressing *S. pombe* MCC/eisosomal proteins revealed one more remarkable phenomenon.

As shown above, when *Sp*Sle1 was expressed in wild type *S. cerevisiae* cells (cells possessing endogenous *S. cerevisiae* Pil1 protein), it formed microdomains distinct from *S. cerevisiae* MCC/eisosomes (Fig. 29). In contrast, when *Sp*Sle1 was co-expressed with *Sp*Pil1 in *pil1Δ* cells (cells lacking *S. cerevisiae* Pil1 protein), *Sp*Sle1 was attracted to *Sp*Pil1-formed eisosomes (Fig. 36). Moreover, also *S. cerevisiae* Seg1 and Sur7 proteins were associated with *Sp*Pil1 eisosomes in these cells (Fig. 36). This means that in the absence of Pil1, *S. pombe Sp*Sle1 and *Sp*Pil1 and *S. cerevisiae* Seg1 and Sur7 coalesced into one specific microdomain in the plasma membrane of *S. cerevisiae*. Notably, the cells where *Sp*Pil1-mRFP expression was low still reminded of *pil1Δ* phenotype. In this case, Seg1 and Sur7 localized to eisosome remnants, consistently with the *pil1Δ* phenotype (asterisks in Fig. 36). Importantly, also *Sp*Sle1 localized to the eisosome remnants in these cells (asterisks in Fig. 36). Again, this suggested the coalescence of *Sp*Sle1 and Seg1 and Sur7 microdomains in the absence of Pil1 protein.

Our data suggest that *S. pombe Sp*Sle1 is compatible only with its native interaction partner, *Sp*Pil1. In contrast, *S. cerevisiae* Seg1 is able to interact with Pil1 homologues across species – with both *S. cerevisiae* Pil1 and *S. pombe Sp*Pil1. Moreover, in the presence of *S. cerevisiae* Pil1, *Sp*Sle1 and Seg1 microdomains are distinct from each other. In the absence of *S. cerevisiae* Pil1, *Sp*Sle1 and Seg1 microdomains coalesce into one specialized microdomain. This indicates that the absence of *S. cerevisiae* Pil1 (not the presence of *S. pombe Sp*Pil1) causes the merging of *Sp*Sle1 and Seg1 microdomains.

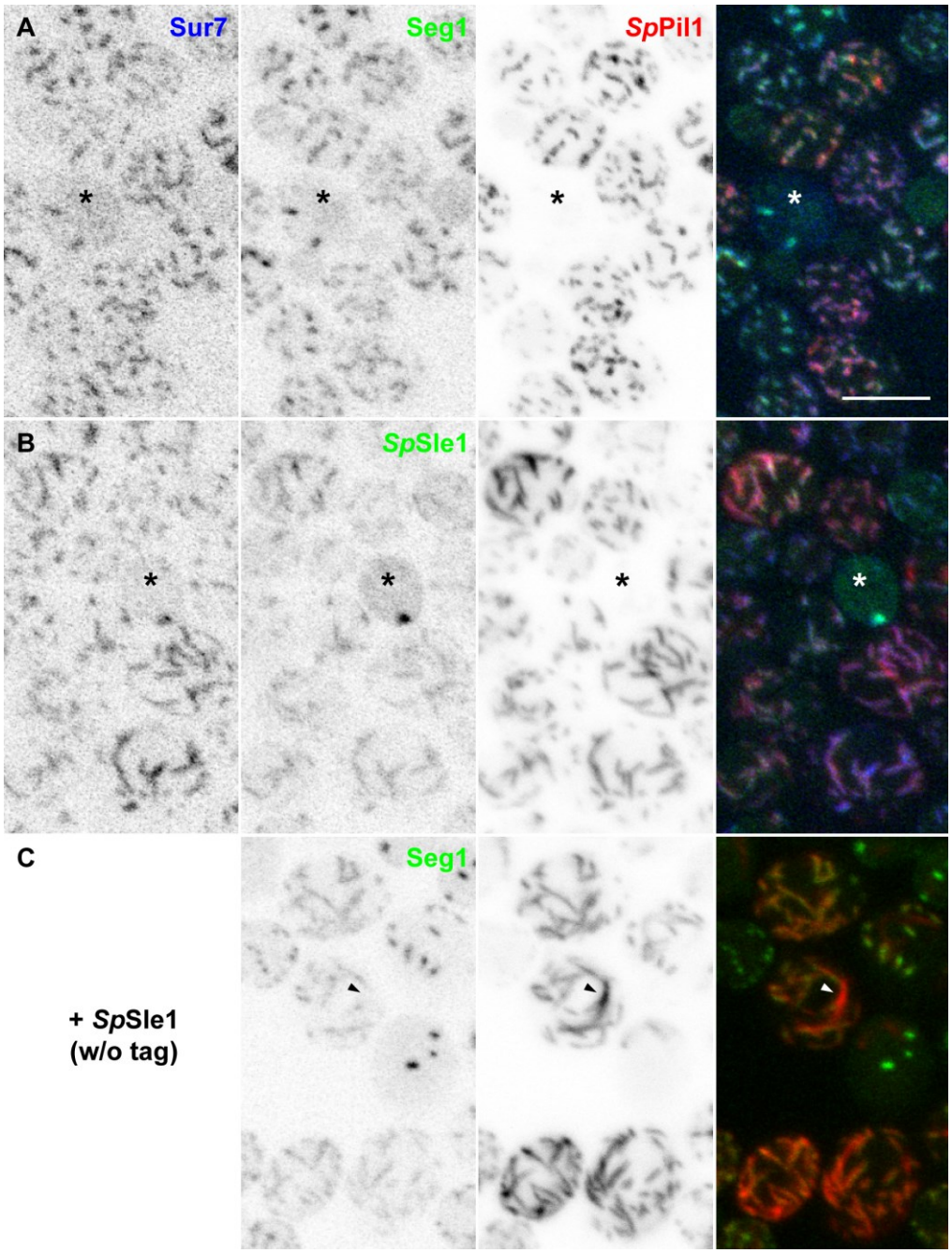

Figure 36. *S. cerevisiae* and *S. pombe* MCC/eisosomes coalesce in the absence of Pil1.

Fluorescence patterns of SpPil1, Sur7, Seg1 and SpSle1 proteins in the absence of Pil1 were investigated. The following cells were analyzed: *pil1Δ* strain expressing *Sp*Pil1-mRFP, Sur7-CFP and Seg1-GFP (Y363, A), *pil1Δ* strain expressing *Sp*Pil1-mRFP, Sur7-CFP and *Sp*Sle1-GFP (Y337, B) and *pil1Δ* strain expressing *Sp*Pil1-mRFP, Seg1-GFP and untagged *Sp*Sle1 (Y382, C). Please note that in cells with low SpPil1 expression (marked by asterisks), eisosome remnants accumulating Sur7-CFP, Seg1-GFP and *Sp*Sle1-GFP can be observed. Moreover, in some cells, also SpPil1 cytoplasmic aggregates were present (marked by arrowheads). Presented figures are superpositions of five consecutive confocal sections (470nm spacing). Gaussian filter (FWHM = 0.3px) was applied to reduce the noise in blue and green channels. Individual fluorescence channels are shown in inverse contrast to increase the visibility of low fluorescence intensities. Bar: 5 μm. The figure was used in (Vaskovicova et al., 2015).

Together, in this section we showed that:

- *S. pombe Sp*Pil1 incorporates into *S. cerevisiae* MCC/eisosomes and is a competitor of endogenous *S. cerevisiae* Pil1
- In the absence of *S. cerevisiae* MCC/eisosomes, *S. pombe Sp*Pil1 forms eisosomes in the plasma membrane of *S. cerevisiae* and is able to substitute for *S. cerevisiae* Pil1 function
- *Sp*Pil1 eisosomes attract *S. cerevisiae* MCC/eisosome proteins
- *S. pombe Sp*Sle1 forms its own microdomains in the plasma membrane of *S. cerevisiae* and cannot substitute for *S. cerevisiae* Seg1 function
- Both *S. pombe Sp*Sle1 and *S. cerevisiae* Seg1 proteins are able to stabilize *Sp*Pil1 eisosomes in the plasma membrane of *S. cerevisiae*, *Sp*Sle1 being more effective
- *S. pombe Sp*Fhn1 associates with both *S. cerevisiae* and *Sp*Pil1-*Sp*Sle1 eisosomes
- *S. cerevisiae* Nce102 is a competitor of *S. pombe Sp*Fhn1 and it is more effective than *Sp*Fhn1 in binding both *S. cerevisiae* and *S. pombe* eisosomes
- Seg1 and *Sp*Sle1 microdomains coalesce in the absence of *S. cerevisiae* Pil1 protein

6. Discussion

6.1 Changes in MCC/eisosomes under the conditions of chronic glucose depletion

During life, yeast cells encounter with the vast variety of environmental stresses – such as low and high temperatures, dehydration, osmotic stress, oxidative stress, exposure to toxic substances and, maybe most frequently, lack of nutrients. Yeast plasma membrane microdomains, MCC/eisosomes, were shown to play a central role as signaling hubs at the plasma membrane that sense, integrate and communicate signals under stress conditions, in particular in the response to lipid imbalance in the plasma membrane, osmotic stress, oxidative stress, changes in plasma membrane potential and acute nitrogen starvation (Berchtold et al., 2012; Dupont et al., 2010; Fröhlich et al., 2009; Gournas et al., 2018; Grossmann et al., 2007; Kabeche et al., 2015a; Li et al., 2015; Moharir et al., 2018). It is interesting that various yeast species employ different strategies to cope with the stresses. However, these yeast species possess MCC/eisosomes that are in principle very similar, highlighting the role that MCC/eisosomes play in stress perception, modulation of plasma membrane structure and regulation of stress response.

In response to altered conditions, the composition of MCC/eisosomes changes. For example, under myriocin treatment (which causes the decrease in sphingolipid levels), Nce102 and Slm1/2 proteins leave MCC/eisosomes (Berchtold et al., 2012; Fröhlich et al., 2009). Nce102 becomes homogeneously dispersed in the plasma membrane (Fröhlich et al., 2009), while Slm1/2 proteins accumulate in another compartment, MCT (Berchtold et al., 2012). Slm1/2 re-localization from MCC/eisosomes to MCT also occurs upon mechanical stress (Berchtold et al., 2012). Nce102 and MCC-specific transporters dissipate in the plasma membrane also upon plasma membrane depolarization (Grossmann et al., 2007; Moharir et al., 2018). Moreover, nutrient transporters change their association with MCC/eisosomes based on the nutrient availability in the medium (Bianchi et al., 2018; Busto et al., 2018; Gournas et al., 2018; Grossmann et al., 2008; Moharir et al., 2018).

In this study, we investigated the changes in localization of two proteins in response to specific conditions of chronic glucose depletion. First, Xrn1 exoribonuclease re-localizes from cytoplasm and P-bodies to MCC/eisosomes under these conditions (Grousl et al., 2015). We

observed that the change in Xrn1 localization is accompanied by the change in its enzymatic activity. Second, we observed the partial re-localization of Nce102 from MCC/eisosomes to vacuolar membrane microdomains under these conditions. We hypothesize that Nce102, together with its homologue Fhn1, might play a role in vacuolar fusion and lipid droplets degradation. The re-localization of both Xrn1 and Nce102 proteins might be important for cell survival upon chronic glucose depletion as will be discussed below.

6.2 Xrn1 attenuation under the conditions of chronic lack of glucose

It was previously shown that under the conditions of chronic glucose depletion, Xrn1 exoribonuclease re-localizes from cytoplasm and P-bodies to MCC/eisosomes (Grousl et al., 2015). Interestingly, in cytoplasm and in P-bodies, Xrn1 is accompanied by its co-factors, such as the decapping enzyme Dcp2 and helicase Dhh1, that together cooperate in mRNA degradation (Parker and Sheth, 2007). In contrast, Xrn1 accumulated at MCC/eisosomes is spatially separated from these cofactors that stay localized to cytoplasm and P-bodies under chronic glucose depletion (Grousl et al., 2015). Therefore, we had hypothesized that the change in the Xrn1 localization could be connected to the changes in Xrn1 enzymatic activity.

Indeed, we have shown that when Xrn1 is localized to cytoplasm and P-bodies (logarithmic and diauxic cells), mRNA degradation of our reporter mRNA proceeds (Fig. 8). In contrast, when Xrn1 is accumulated at MCC/eisosomes (post-diauxic cells), the degradation of our reporter mRNA ceases (Fig. 8). This regulation of mRNA degradation is independent on 3′-5′ mRNA degradation pathway (Fig. 8), confirming that our reporter mRNA is degraded via Xrn1-mediated 5′-3′ degradation pathway. The Xrn1 protein levels are unchanged in diauxic and post-diauxic cells, but the Xrn1 protein localization significantly changes (Fig. 8). Therefore, we show that the Xrn1 enzymatic activity changes with the Xrn1 localization.

As Xrn1 is the major mRNA degradation enzyme in yeast (Haimovich et al., 2013; Nagarajan et al., 2013), we hypothesize that the cessation of Xrn1 enzymatic activity under the conditions of chronic glucose depletion might be important for preserving important mRNA molecules in case they would be again necessary. Cells in the conditions of chronic glucose depletion do not have the energy supply from exterior and the biosynthesis of new mRNAs is energetically demanding. If the extracellular conditions became more favorable, the cells could readily use the preserved mRNA molecules without the need to synthesize new ones. This would help them

to recover from the stress faster and more effectively. The sequestration of Xrn1 at MCC/eisosomes is stable in time, while the association of Xrn1 with P-bodies is dynamic as shown by FRAP experiments (Vaškovičová et al., 2017). This may reflect the dynamic mRNA metabolism of cells in diauxic phase and relatively stable preservation of mRNA molecules in cells in post-diauxic phase. This way, the post-diauxic cells would protect their mRNAs for the situation with more favorable conditions.

The physiological significance of this phenomenon is underlined by the fact that yeast colony, the structure in which yeast cells are usually found in nature, is also stratified regarding the Xrn1 pattern (Vaškovičová et al., 2017). While Xrn1 was localized to cytoplasm in the most upper layer of the colony and was accumulated in P-bodies in the deeper layers of the colony, it associated with MCC/eisosomes in the central part of the colony. Consistently with our results, the upper part of the colony is composed of fermenting cells, while the lower part of the colony contains respiring cells (Čáp et al., 2015).

Importantly, this regulation of Xrn1 activity is perturbed in cells lacking Pil1 protein (Fig. 9). In these cells, Xrn1 cannot be sequestered at MCC/eisosomes in post-diauxic cells and remains active all the time. We propose that this might result in disturbed cellular physiology. Consistently with our results, *pil1Δ* mutant strain exhibits decreased competitive fitness and decreased resistance to certain chemicals and stresses (Kabeche et al., 2015b; Qian et al., 2012; Yoshikawa et al., 2009; Zhang et al., 2004).

The molecular mechanism of Xrn1 shuttling between cytoplasm/P-bodies and MCC/eisosomes was not revealed yet. We hypothesize that some posttranslational modification of Xrn1 protein, such as phosphorylation, might be involved in this process. It was shown that Xrn1 is phosphorylated in a Snf1-dependent manner (Snf1 is a yeast homologue of mammalian adenosine monophosphate-activated protein kinase (AMPK)) (Braun et al., 2014). Interestingly, the addition of glucose to starved cells causes so-called “glucose-induced mRNA decay” (Braun et al., 2016; Prieto et al., 2000; Scheffler et al., 1998; Yin et al., 1996). In this process, the degradation of mRNAs encoding respiratory enzymes takes place in order to change the metabolism from aerobic to fermentation. This is consistent with our observation that upon glucose addition to post-diauxic cells, Xrn1 rapidly re-localizes back to the cytoplasm and becomes active again (Fig. 8). It is interesting that impairment of Snf1-depedent phosphorylation of Xrn1 reduced the glucose-induced mRNA decay, showing that the Xrn1 phosphorylation is involved in the Xrn1 activity regulation (Braun et al., 2014). It remains to be tested whether Xrn1 phosphorylation is also involved in Xrn1 activity attenuation at MCC/eisosomes. Moreover, it was shown that Pkh1/2-Pkc1 pathway is required for P-body

formation and mRNA deadenylation occurring during the stress response (Luo et al., 2011). This might indicate that eisosome-associated Pkh1/2 kinases or their targets might regulate Xrn1 phosphorylation.

We propose a novel, fast and cost-effective mechanism of mRNA decay regulation via Xrn1 enzyme localization that prevents the unwanted mRNA decay in cells with the chronic lack of glucose. In these cells, Xrn1 is sequestered at MCC/eisosomes and this prevents Xrn1 interaction with its cofactors and results in cessation of Xrn1 activity. Upon glucose addition, however, Xrn1 rapidly re-localizes back to cytoplasm, its activity is restored and Xrn1 may act in the process of glucose-induced mRNA decay, which causes fast adaptation of yeast metabolism from aerobic respiration to anaerobic fermentation. The regulation of enzymatic activity via enzyme localization may be very useful mechanism in general.

6.3 Functional relevance of Nce102-like proteins in chronic lack of glucose

In contrast to Xrn1, which translocates to MCC/eisosomes under the conditions of chronic lack of glucose, we observed that Nce102 protein partly leaves this compartment under the same conditions. This is consistent with the overall stress-induced plasticity of MCC/eisosomes reported earlier. As noted above, upon plasma membrane stress signals, MCC/eisosomes disassemble and Slm1/2 proteins and Pkh1/2 kinases leave MCC/eisosomes to activate stress-response signaling pathways (Berchtold et al., 2012; Kabeche et al., 2014; Luo et al., 2008; Walther et al., 2007). Also Nce102 has been shown to re-localize from MCC/eisosomes to the surrounding membrane when sphingolipid synthesis was inhibited (Fröhlich et al., 2009). Here, we show that in the conditions of chronic lack of glucose, Nce102 re-localizes to internal membranes (Fig. 13).

Importantly, Nce102 translocates to vacuolar membrane, where it is stably integrated and not degraded (Fig. 14). This is in contrast to other plasma membrane proteins, such as Pma1 or Hxt1, that are being degraded in the vacuole (Fig. 16). We hypothesize that Nce102 might play a specific role on vacuolar membranes that is needed in these conditions.

Nce102 localizes specifically to sterol-enriched vacuolar microdomains (Fig. 17 and Fig. 18). This is not surprising, because also MCC/eisosomes are thought to be enriched in sterols (Grossmann et al., 2007). It seems that Nce102 protein strongly prefers sterol-rich environment and it is likely that this environment facilitates the proper Nce102 conformation and function.

Similarly, sterols are important for localization and trafficking of some MCC-specific nutrient transporters (Malinska et al., 2003; Pineau et al., 2008; Umebayashi and Nakano, 2003). Nce102 is considered to be a protein with four transmembrane segments, but also a conformation with two middle segments positioned parallel to the membrane was proposed (Loibl et al., 2010). It is imaginable that Nce102 might change the conformation based on the membrane composition and only in the membranes with high sterol content, its conformation is functional.

It was previously hypothesized, that Nce102 can sense sphingolipid levels in the plasma membrane (Fröhlich et al., 2009). Because Nce102 prefers high sterol content in the membrane, we propose that Nce102 could sense the sterol content in the membranes. This would be consistent with the idea that upon sphingolipid depletion, sphingolipid-enriched, gel-like microdomains are dissolved in the plasma membrane and the excess of sphingolipids in the membrane is compensated by their association with sterols (Malinsky and Opekarová, 2016). This way, Nce102 could sense sterols directly and sphingolipids indirectly, i.e. through the association with sphingolipid-free sterols (Malinsky and Opekarová, 2016).

Generally, vacuolar membranes are considered to be a sterol-poor environment (Zinser et al., 1993; Zinser and Daum, 1995), but recent data suggest that the sterol content in vacuoles rises in the conditions of glucose depletion (Toulmay and Prinz, 2013). If Nce102 directly associates with sterols, this may be the reason for Nce102 translocation from plasma membrane to vacuoles under these conditions.

We also investigated the Nce102 re-localization in strains that do not form vacuolar microdomains (Toulmay and Prinz, 2013). We found that Nce102 does not translocate to vacuoles in *vps4Δ* strain, it translocates to some vacuoles, but remains homogeneous in *fab1Δ* strain and localizes to vacuolar microdomains in *nem1Δ* strain (Fig. 19). Importantly, all these strains exhibit specifically altered vacuolar physiology (Babst et al., 1998, 1997; Cooke et al., 1998; Gary et al., 1998; Jin et al., 2014; Odorizzi et al., 1998; Raymond et al., 1992; Siniossoglou et al., 1998; Xu and Okamoto, 2018; Yamamoto et al., 1995; Zahn et al., 2001). We propose that these complex physiological changes influence the ability of vacuoles to form microdomains, maybe partially through changed lipid composition. These changes also affect the re-localization of Nce102 from the plasma membrane to vacuolar membrane and its ability to accumulate in specific lipid domains. For example, Fab1 is a lipid kinase synthesizing phosphatidylinositol(3,5)bisphosphate (Cooke et al., 1998; Yamamoto et al., 1995) and in *fab1Δ* strain, Nce102 is homogeneously dispersed in the vacuolar membrane (Fig. 19).

Therefore, maybe not only sterols, but also misbalance of other lipids might influence Nce102 re-localization to the vacuolar microdomains.

We hypothesized that also Nce102 homologue, Fhn1, might be associated with the vacuolar membrane, similarly to Nce102. However, we were not able to visualize Fhn1-GFP protein when it was expressed upon native promoter because of its low expression level. We did not overexpress Fhn1 as it may influence the Fhn1 localization as well as function. However, the previously published data show that Fhn1 expression is increased in late stationary phase (Gasch et al., 2000). This would fit to the idea that Fhn1 is specifically needed upon chronic lack of glucose and that Fhn1 might play a role on vacuolar membrane.

We have shown that Nce102 and Fhn1 proteins are not important for vacuolar microdomain formation (Fig. 20). On the other hand, we found that both these proteins are involved in vacuolar fusion that occurs at the onset of the stationary phase (Fig. 21). Moreover, these proteins seem to negatively regulate Vph1 protein degradation (Fig. 22). The exact molecular mechanism by which Nce102 and Fhn1 mediate these actions and the specific physiological significance of their role in these processes remain to be elucidated. Notably, the fusion Sur7-Nce102 protein, which is stably associated with the plasma membrane, has the same vacuolar phenotypes as strain lacking Nce102 protein (Fig. 20, 21, 22). This suggests that these vacuolar phenotypes are not consequence of the complete lack of Nce102 in cells, but, rather, they reflect the lack of Nce102 in the vacuolar membrane. This is another indication that Nce102 has a significant role on vacuolar membrane.

Nce102 is accumulated in sterol-enriched vacuolar microdomains (Fig. 17, 18), into which also Ivy1 protein localizes (Toulmay and Prinz, 2013). Ivy1 is an inverse (I)-BAR protein and was described as an effector of Ypt7 GTPase (GTPase involved in the fusion of the vesicles with the vacuolar membrane) and regulator of Gtr-dependent TORC1 signaling (Numrich et al., 2015; Varlakhanova et al., 2018). Ivy1 was implicated in vacuolar morphology, fusion, sorting and homeostasis (Numrich et al., 2015). Ivy1 overexpression leads to the vacuolar fragmentation, the phenotype similar to the lack of Nce102 protein (Numrich et al., 2015). This suggests that Nce102 and Ivy1 proteins may be together involved in the vacuolar fusion process and that their levels need to be balanced to ensure proper vacuolar morphology. Moreover, it is tempting to hypothesize that via Ivy1, Nce102 could be involved in TORC1 regulation. Ivy1 also localizes to sites of negative curvature on vacuoles (Numrich et al., 2015). This is interesting because Nce102 at MCC/eisosomes also localizes to highly curved membranes. This may be the second reason for preferential localization of Nce102 into these vacuolar microdomains. Importantly, *nce102Δ* cells do not have invaginated MCC/eisosomes

(Stradalova et al., 2009), suggesting that Nce102 shapes MCC membrane into invaginations. It is possible that Nce102 could play the same role at the vacuolar membrane and induce the formation of vacuolar invaginations as well.

Vacuolar microdomains play an important role in lipid droplets degradation in the stationary phase, so-called stationary phase lipophagy (Tsuji et al., 2017; Tsuji and Fujimoto, 2018; Wang et al., 2014). This mechanism is considered a microautophagy mechanism and it was shown that also conversely, lipophagy is needed for vacuolar microdomains maintenance (Wang et al., 2014). Importantly, lipid droplets interact specifically with the liquid-ordered, sterol-enriched vacuolar microdomains (Tsuji et al., 2017; Tsuji and Fujimoto, 2018).

Our results indicate that Nce102 together with Fhn1 may also be involved in stationary phase lipophagy. Our results indicate that upon prolonged lack of glucose, lipid droplets are not degraded as efficiently in *nce102Δfhn1Δ* strain as in the wild type strain. We observed the degradation of Erg6-GFP protein upon chronic glucose depletion on Western blot in wild type strain, but not in the *nce102Δfhn1Δ* strain (Fig. 27). This result suggests that in strain lacking both Nce102 and Fhn1, the stationary phase lipophagy is, at least partly, dysfunctional. Ivy1 was shown to be also present at sites of microautophagy (Numrich et al., 2015) and this further strengthens the hypothesis that sterol-enriched vacuolar microdomains and the proteins therein are important for stationary phase lipophagy.

In contrast to vacuolar fusion and Vph1 protein degradation, single deletion mutants do exhibit defect in stationary phase lipophagy – Erg6-GFP protein is degraded similarly to wild type cells (Fig. 27). This indicates that the two proteins might be exchangeable in facilitating this process - when either of these two proteins is missing, the second protein can take over the first protein´s function. If both these proteins are not present, the stationary phase lipid droplets degradation could not proceed effectively.

Under the conditions of nitrogen starvation, both wild type and *nce102Δfhn1Δ* strain were equally able to proceed with lipid droplet degradation (Fig. 25). This is not surprising, however, because Nce102 does not re-localize to vacuolar membrane upon nitrogen starvation and cannot therefore mediate any vacuolar-connected functions. Moreover, this suggests that lipophagy under the conditions of nitrogen starvation and lipophagy under the conditions of chronic lack of glucose might be two slightly different processes. It is generally thought that general lipophagy apparatus is composed of the same set of proteins (Tsuji et al., 2017; van Zutphen et al., 2014). Our data indicate that some proteins may be specific for one or the other process, including Nce102 and Fhn1 being specific for stationary phase lipophagy.

Although our data are only preliminary and need to be verified, the idea that Nce102 and Fhn1 proteins might play a role in stationary phase lipophagy is truly compelling. As stationary phase lipophagy is thought to supply stationary phase cells with sterols (Wang, 2014), it would be interesting to assess the lipid profiles of vacuoles in wild type and *nce102Δfhn1Δ* strains in logarithmic and in stationary phase and determine the surviving of the mutant strain under challenging conditions. Our results would describe a novel function that MCC/eisosomal proteins play under the conditions of chronic glucose depletion.

6.4 Conservation of pathways involved in the glucose response

As noted above, all yeast species have to deal with the multiple stresses that the cells encounter in the cell environment. Is it possible that these diverse cells use the same MCC/eisosomes? This hypothesis is highly plausible because many components of MCC/eisosomes and proteins interacting with MCC/eisosomes are conserved in evolution.

For example, Pkh1/2 kinases and their substrate kinases (Ypk1/2, Sch9, and Pkc1) as well as their stress signaling pathways are preserved in *S. cerevisiae*, *S. pombe*, *C. albicans* and *A. nidulans*, but also in plants, mammals and humans (Arencibia et al., 2013; Athanasopoulos et al., 2015; Garcia et al., 2012; Leroux et al., 2018; Luo et al., 2008; Nakashima et al., 2012; Pastor-Flores et al., 2016). Regarding glucose metabolism, Pkh1 homologue in *S. pombe*, *Sp*Ksg1, and its effector, *Sp*Psk1, were shown to play a role in response to glucose starvation (Nakashima et al., 2012; Saitoh et al., 2015). Also in mammals and humans, AGC kinases are involved in glucose response (Pearce et al., 2010; Standaert et al., 1999). Especially Akt and protein kinase C (PKC) kinases are involved in glucose uptake and storage, glycogen synthesis, blood glucose levels and insulin signaling (Engin, 2017; Pearce et al., 2010). The deregulation of these pathways leads to the insulin resistance, type 2 diabetes and obesity (Engin, 2017; Pearce et al., 2010). Nce102 and its role in Pkh1/2 signaling and sphingolipid regulation seem to be also conserved. Similarly to *S. cerevisiae*, *An*Nce102 was shown to regulate sphingolipid synthesis and be a part of *An*YpkA (homologue of Ypk1) signaling in *A. nidulans* (Athanasopoulos et al., 2015; Fröhlich et al., 2009; García-Marqués et al., 2016).

Xrn1 exoribonuclease is also evolutionarily conserved (Haimovich et al., 2013; Nagarajan et al., 2013) and we propose that some aspects of mRNA decay regulation described in this study may be evolutionarily conserved as well. The dependence of mRNA degradation process on the membrane association was previously shown in bacteria. In *Escherichia coli*, the

endoribonuclease RNase E was shown to bind the inner bacterial plasma membrane (Khemici et al., 2008). This resulted in better endoribonuclease stabilization and in increased affinity of the RNase to its substrate (Laalami et al., 2014; Murashko et al., 2012). In *Staphylococcus aureus*, the ribonuclease RNase Y is permanently associated with the plasma membrane via its N-terminal transmembrane domain and this prevents its promiscuous activity (Khemici et al., 2015; Redder, 2016). This is consistent with our idea of spatial separation of Xrn1 from the rest of mRNA decay machinery when Xrn1 translocates to the MCC/eisosomes.

Additionally, signal-dependent regulation of Xrn1 localization was observed in mouse and rat hippocampal neurons (Luchelli et al., 2015; Thomas and Boccaccio, 2016). In the dendrites of these cells, rodent homologue of Xrn1 was found to be accumulated at the post-synaptic XRN1 bodies (SX-bodies). Similarly to the situation in yeast, where Xrn1 accumulated at MCC/eisosomes in post-diauxic cells with chronic lack of glucose and down-regulated proteosynthetic activity, also SX-bodies increased in number and size upon *N*-methyl-D-aspartate (NMDA) stimulation, e.g. when the proteosynthesis was globally attenuated (Luchelli et al., 2015). Moreover, in yeast, the sequestered Xrn1 became soluble after addition of fermentative sugar source to the post-diauxic cells. Similarly, SX-bodies dissolved in response to activation of metabotropic glutamate receptors (Luchelli et al., 2015). This signify that certain aspects of Xrn1 regulation that we describe in this study may be relevant also for higher eukaryotes.

6.5 Compatibility of *S. cerevisiae* and *S. pombe* MCC/eisosomal proteins

To validate the conservation of MCC/eisosomal proteins in MCC/eisosome assembly, we have also investigated the relationship between *S. cerevisiae* and *S. pombe* homologues – Pil1 vs. *Sp*Pil1, Seg1 vs. *Sp*Sle1 and Nce102 vs. *Sp*Fhn1 - in the plasma membrane of *S. cerevisiae*.

When expressed in wild type *S. cerevisiae* cells, *S. pombe Sp*Pil1 is able to weakly incorporate into *S. cerevisiae* MCC/eisosomes (Fig. 28). It is therefore compatible with *S. cerevisiae* MCC/eisosomes. Moreover, in the absence of endogenous Pil1, *Sp*Pil1 form patches in the plasma membrane and attract *S. cerevisiae* MCC/eisosomal proteins into these patches (Fig. 28). This shows that *S. pombe Sp*Pil1 and *S. cerevisiae* Pil1 proteins are competitors and *S. pombe Sp*Pil1 can substitute for *S. cerevisiae* Pil1 function in the *S. cerevisiae* plasma membrane. These results are consistent with the results of the previous study of Kabeche and

co-workers (Kabeche et al., 2011) that observed formation of *Sp*Pil1 patches in *S. cerevisiae* plasma membrane upon the same conditions.

In contrast, *S. pombe Sp*Sle1 protein does not incorporate into *S. cerevisiae* MCC/eisosomes and cannot substitute for *S. cerevisiae* Seg1 function (Fig. 29, 30, 31). This might be explained by the fact that Seg1 and *Sp*Sle1 were identified only as functional homologues in *S. pombe*, not sequential homologues (Moreira et al., 2012), and the structure of *Sp*Sle1 is not compatible with *S. cerevisiae* MCC/eisosomal proteins.

*Sp*Sle1 is able to stabilize *Sp*Pil1 patches in *S. cerevisiae* and upon co-expression, both proteins form elongated, filamentous, *S. pombe*-like eisosomes (Fig. 32, 33). This is inconsistent with the idea of Kabeche and co-workers that suggested that it is the plasma membrane composition that restricts the elongation of *Sp*Pil1 eisosomes in *S. cerevisiae* plasma membrane (Kabeche et al., 2011). We show, on the contrary, that it is the protein composition of *S. pombe* eisosomes in *S. cerevisiae* (and possibly also in *S. pombe*) that determines the eisosome morphology. Moreover, it is not true that *S. cerevisiae* plasma membrane would restrict the MCC/eisosome length, as previously suggested (Kabeche et al., 2011). Also *S. cerevisiae* cells are able to form elongated eisosomes composed of *S. cerevisiae* proteins. Elongated *S. cerevisiae* MCC/eisosomes were observed in cells lacking Mak3 N-terminal acetyltransferase (Stradalova et al., 2009) or in cells overexpressing Seg1 protein (Moreira et al., 2012). The latter observation is consistent with our observation that the abundance of eisosome stabilizers is the limiting factor for eisosome length (Fig. 33).

Importantly, both Seg1 and *Sp*Sle1 proteins are able to stabilize *Sp*Pil1 patches in the *S. cerevisiae* plasma membrane, but *Sp*Sle1 seems to be more effective stabilizer than Seg1 (Fig. 33). Therefore, elongated, filamentous eisosomes of *S. pombe* can be a result of more effective eisosome stabilization via *Sp*Sle1. The punctuate *S. cerevisiae* Pil1 eisosomes would be a result of less stable stabilization of Pil1 eisosomes via Seg1 protein.

It is also interesting that *Sp*Pil1 eisosomes are stabilized by both Seg1 and *Sp*Sle1 proteins, while Pil1 eisosomes are stabilized by Seg1, but not *Sp*Sle1 (Fig. 33, 31). This is probably not due to the difference between Pil1 and *Sp*Pil1 proteins as these are very similar in sequence (Kabeche et al., 2011). Rather, this would be the difference between Seg1 and *Sp*Sle1 proteins. This difference – and Pil1-*Sp*Sle1 incompatibility - may result from the above-mentioned fact that Seg1 and *Sp*Sle1 are only functional, not sequential, homologues in *S. pombe* (Moreira et al., 2012). *Sp*Sle1 protein might possess different structure or contain a domain that prevents specific interaction with Pil1 protein. This would be consistent with the fact that upon expression of *Sp*Sle1 in wild type *S. cerevisiae* cells, *Sp*Sle1 localizes to membrane

microdomains, that are different from *S. cerevisiae* MCC/eisosomes (Fig. 29, 30). Importantly, in the absence of endogenous Pil1, *Sp*Pil1-*Sp*Sle1 eisosomes merge with *S. cerevisiae* eisosomes (Fig. 36). Therefore, it is probable that *S. pombe* and *S. cerevisiae* eisosomes reside in the same or similar lipid/protein environment, and the incompatibility of *Sp*Sle1 with Pil1 protein causes the separation of the two microdomains.

Our results also show that *S. pombe Sp*Fhn1 protein is able to incorporate into both *S. cerevisiae* and *S. pombe* MCC/eisosomes, but only in the absence of its homologue, *S. cerevisiae* Nce102 (Fig. 34, 35). This means that *Sp*Fhn1 and Nce102 proteins are competitors, similarly to *Sp*Pil1 and Pil1 proteins. Nce102 appears to be more effective in binding to *S. cerevisiae* MCC/eisosomes than *Sp*Fhn1, analogically to the situation of Pil1 and *Sp*Pil1 proteins when expressed in *S. cerevisiae*.

It is very interesting that *S. cerevisiae* Nce102 is more effective than *Sp*Fhn1 in binding not only to *S. cerevisiae* eisosomes (its native interactors), but also to ("foreign") *S. pombe* eisosomes (Fig. 34, 35). This could mean that Nce102 has higher affinity for MCC/eisosomal proteins in general. While the sequences of Nce102 and *Sp*Fhn1 are very similar at the N-terminus and in the middle part of the proteins, these sequences differ more significantly in the last third of the proteins (Loibl et al., 2010). The very C-terminus is again well conserved (Loibl et al., 2010). It was shown that the C-terminus of Nce102 is needed for proper association of Nce102 with MCC/eisosomes (Loibl et al., 2010). We propose that the not-so-well conserved region of Nce102 could be more efficient interactor with MCC/eisosomes than the corresponding part of *Sp*Fhn1 protein. Seg1 and *Sp*Sle1 differ significantly in their sequence and structure, while Pil1 and *Sp*Pil1 are very similar (Kabeche et al., 2011; Moreira et al., 2012). Therefore, if the Nce102/*Sp*Fhn1 were bound directly to MCC/eisosomal proteins, it would be more probable that they would interact with Pil1/*Sp*Pil1 proteins and not with Seg1/*Sp*Sle1 proteins. We can also speculate that general lower efficiency of *Sp*Fhn1 association with *S. pombe* eisosomes might affect the efficiency of *Sp*Fhn1 function in *S. pombe* MCC/eisosomes, but this remains to be tested.

Importantly, it was also shown that when expressed in *pil1Δ S. cerevisiae* cells, *Sp*Pil1 is able to form shallow invaginations of the plasma membrane and upon co-expression of *Sp*Pil1 and *Sp*Sle1 proteins, these invaginations are even more pronounced (Vaskovicova et al., 2015). This means that *Sp*Pil1-*Sp*Sle1 assemblies are also able to bend the *S. cerevisiae* plasma membrane and it suggests that not only the composition of *S. pombe* eisosomes in *S. cerevisiae* plasma membrane was preserved, but also their ultrastructure.

This structural conservation of MCC/eisosomes subsequently raises the question whether transferred *S. pombe* eisosomes in the plasma membrane of *S. cerevisiae* preserve also their function in stress response. As many other proteins of MCC/eisosomes are widely evolutionarily conserved, together with general conservation of stress signaling pathways, this hypothesis seems to be highly plausible. For example, the *pil1Δseg1Δnce102Δ* cells expressing *S. pombe Sp*Pil1, *Sp*Sle1 and *Sp*Fhn1 proteins could be used for such a study. *pil1Δ* cells exhibit many stress-related phenotypes (Kabeche et al., 2015b; Qian et al., 2012; Yoshikawa et al., 2009; Zhang et al., 2004) and the expression of *S. pombe* MCC/eisosomes in these cells could be used to determine whether this expression would complement these phenotypes. Alternatively, the expression of *S. cerevisiae* MCC/eisosomes in *S. pombe* (or any other yeast species) could be tested for the *pil1Δ* phenotype compensation. Interestingly, *C. albicans* MCC/eisosomal mutants exhibit diminished filamentous growth and decrease in virulence (Douglas and Konopka, 2016). It would be interesting to test whether the expression of *S. cerevisiae* MCC/eisosomes in these cells would restore the ability of *C. albicans* cells to be effectively virulent. If this were true, it would emphasize the significance of MCC/eisosomes as potential targets for anti-fungal therapies.

7. Conclusions

Role of MCC/eisosomes in regulation of mRNA decay during chronic glucose depletion

Aim 1.1: Investigate the functional significance of Xrn1 re-localization to MCC/eisosomes under the conditions of chronic glucose depletion.

The Xrn1 activity is determined by the Xrn1 localization. When Xrn1 is localized to cytoplasm and P-bodies, it is active. When Xrn1 is sequestered at MCC/eisosomes, it is not active. Significantly, Xrn1 is sequestered at MCC/eisosomes specifically under the conditions of the chronic lack of glucose. This might reflect the need of the cell to attenuate mRNA metabolism under these conditions and protect mRNA substrates that could be utilized later, when the conditions are more favorable.

The addition of glucose to the cells results in rapid Xrn1 translocation back to cytoplasm and the restoration of Xrn1 activity. Therefore, the regulation of the enzyme activity via the enzyme localization might represent a fast and adaptable mechanism of regulating the enzymatic activity.

Aim 1.2: Determine the role that MCC/eisosomes play in this process.

In cells lacking MCC/eisosomes, the attenuation of Xrn1 activity under chronic glucose depletion does not take place. Instead, Xrn1 is still active and degrades mRNA. We hypothesize that this may lead to the non-economic management with mRNA substrates in the mutant strain and potentially contribute to its decreased fitness.

Investigation of Nce102 intracellular localization and its functional significance during chronic glucose depletion

Aim 2.1: Characterize the intracellular localization of Nce102 under the conditions of chronic glucose depletion.

Under the conditions of chronic glucose depletion, Nce102 partly re-localizes from the plasma membrane to the cell interior. Nce102 translocates to the vacuolar membrane and interestingly,

it accumulates at the specific sterol-rich vacuolar microdomains. The Nce102 re-localization depends on vacuolar physiology.

Aim 2.2: Determine the functional significance of partial Nce102 re-localization from the plasma membrane into the cell interior.

Nce102 is not necessary for the formation of vacuolar microdomains as cells without Nce102 are still able to form these microdomains. However, Nce102, together with its homologue, Fhn1, seems to play a role in the vacuolar fusion that occurs at the onset of the stationary phase. Moreover, Nce102 and Fhn1 might also be involved in the degradation of vacuolar ATPase subunit Vph1 and in the degradation of lipid droplet protein Erg6. This indicates that Nce102, and possibly also Fhn1, are re-localized to vacuolar microdomains under the conditions of chronic lack of glucose to facilitate the degradation of specific structures, potentially for supplementing the cell with more nutrients. However, more experiments need to be performed to confirm this hypothesis.

Compatibility of *S. cerevisiae* and *S. pombe* MCC/eisosomal proteins

Aim 3.1: Investigate the compatibility of *S. pombe* and *S. cerevisiae* MCC/eisosomal proteins – Pil1 vs. *Sp*Pil1; Seg1 vs. *Sp*Sle1, Nce102 vs. SpFhn1. Compare their characteristics regarding MCC/eisosome assembly.

*S. pombe Sp*Pil1 protein is compatible with *S. cerevisiae* MCC/eisosomes as it is partly able to incorporate into them. However, it is a competitor of *S. cerevisiae* Pil1 protein and in the absence of Pil1, *Sp*Pil1 is able to substitute for Pil1 function and organize *S. cerevisiae* MCC/eisosomes. *S. pombe Sp*Sle1 protein is not able to incorporate into *S. cerevisiae* MCC/eisosomes and cannot substitute for Seg1 function in organizing *S. cerevisiae* MCC/eisosomes. However, it can incorporate into *Sp*Pil1 microdomains formed in the *S. cerevisiae* plasma membrane, where it stabilizes these structures. Interestingly, also Seg1 protein stabilizes *Sp*Pil1 microdomains, but *Sp*Sle1 is more efficient. *S. pombe Sp*Fhn1 protein is able to incorporate into both *S. cerevisiae* and *Sp*Pil1-*Sp*Sle1 microdomains, but only in the absence of its competitor, Nce102 protein. Nce102 therefore seems to be more effective than *Sp*Fhn1 at binding both sets of MCC/eisosomal proteins.

Aim 3.2: Reconstitute *S. pombe* MCC/eisosome microdomain in *S. cerevisiae*.

We successfully transferred *S. pombe* MCC/eisosome into the plasma membrane of *S. cerevisiae* – upon the co-expression of *Sp*Pil1, *Sp*Sle1 and *Sp*Fhn1 proteins in *S. cerevisiae*, these proteins co-assembled into filamentous *S. pombe*-like MCC/eisosomes. These structures were more prominent in the absence of endogenous Pil1 protein and in these conditions, also *S. cerevisiae* MCC/eisosome proteins were attracted to these microdomains.

8. References

Aguilar, P.S., Fröhlich, F., Rehman, M., Shales, M., Ulitsky, I., Olivera-Couto, A., Braberg, H., Shamir, R., Walter, P., Mann, M., Ejsing, C.S., Krogan, N.J., Walther, T.C., 2010. A plasma-membrane E-MAP reveals links of the eisosome with sphingolipid metabolism and endosomal trafficking. Nat. Struct. Mol. Biol. 17, 901–908. https://doi.org/10.1038/nsmb.1829.

Alberts, B., Johnson, A., Lewis, J., Morgan, D., Raff, M., Roberts, K., Walter, P., 2015a. Cell junctions and the Extracellular Matrix, in: Molecular Biology of the Cell. Garland Science, New York, p. 1048.

Alberts, B., Johnson, A., Lewis, J., Morgan, D., Raff, M., Roberts, K., Walter, P., 2015b. Membrane Transport of Small Molecules and the Electrical Properties of Membranes, in: Molecular Biology of the Cell. Garland Science, New York, p. 637.

Alberts, B., Johnson, A., Lewis, J., Raff, M., Roberts, K., Walter, P., 2008a. Membrane Transport of Small Molecules and the Electrical Properties of Membranes, in: Molecular Biology of the Cell. Garland Science, New York, pp. 651–694.

Alberts, B., Johnson, A., Lewis, J., Raff, M., Roberts, K., Walter, P., 2008b. Mechanisms of Cell Communication, in: Molecular Biology of the Cell. Garland Science, New York, pp. 879–964.

Alberts, B., Johnson, A., Lewis, J., Raff, M., Roberts, K., Walter, P., 2008c. Cell Junctions, Cell Adhesion, and the Extracellular Matrix, in: Molecular Biology of the Cell. Garland Science, New York, pp. 1148–1149.

Alvarez, F.J., Douglas, L.M., Rosebrock, A., Konopka, J.B., 2008. The Sur7 Protein Regulates Plasma Membrane Organization and Prevents Intracellular Cell Wall Growth in Candida albicans. Mol. Biol. Cell 19, 5214–5225. https://doi.org/10.1091/mbc.e08-05-0479.

Araki, Y., Takahashi, S., Kobayashi, T., Kajiho, H., Hoshino, S.I., Katada, T., 2001. Ski7p G protein interacts with the exosome and the ski complex for 3′-to-5′ mRNA decay in yeast. EMBO J. 20, 4684–4693. https://doi.org/10.1093/emboj/20.17.4684.

Arencibia, J.M., Pastor-Flores, D., Bauer, A.F., Schulze, J.O., Biondi, R.M., 2013. AGC protein kinases: from structural mechanism of regulation to allosteric drug development for the treatment of human diseases. Biochim. Biophys. Acta 1834, 1302–21. https://doi.org/10.1016/j.bbapap.2013.03.010.

Aresta-Branco, F., Cordeiro, A.M., Marinho, H.S., Cyrne, L., Antunes, F., de Almeida, R.F.M., 2011. Gel domains in the plasma membrane of Saccharomyces cerevisiae: highly ordered, ergosterol-free, and sphingolipid-enriched lipid rafts. J. Biol. Chem. 286, 5043–54. https://doi.org/10.1074/jbc.M110.154435.

Athanasopoulos, A., Boleti, H., Scazzocchio, C., Sophianopoulou, V., 2013. Eisosome distribution and localization in the meiotic progeny of Aspergillus nidulans. Fungal Genet. Biol. 53, 84–96. https://doi.org/10.1016/j.fgb.2013.01.002.

Athanasopoulos, A., Gournas, C., Amillis, S., Sophianopoulou, V., 2015. Characterization of AnNce102 and its role in eisosome stability and sphingolipid biosynthesis. Sci. Rep. 5, 15200. https://doi.org/10.1038/srep15200.

Audhya, A., Loewith, R., Parsons, A.B., Gao, L., Tabuchi, M., Zhou, H., Boone, C., Hall, M.N., Emr, S.D., 2004. Genome-wide lethality screen identifies new PI4,5P2 effectors that regulate the actin cytoskeleton. EMBO J. 23, 3747–3757. https://doi.org/10.1038/sj.emboj.7600384.

Babst, M., Sato, T.K., Banta, L.M., Emr, S.D., 1997. Endosomal transport function in yeast requires a novel AAA-type ATPase, Vps4p. EMBO J. 16, 1820–31. https://doi.org/10.1093/emboj/16.8.1820.

Babst, M., Wendland, B., Estepa, E.J., Emr, S.D., 1998. The Vps4p AAA ATPase regulates membrane association of a Vps protein complex required for normal endosome function. EMBO J. 17, 2982–93. https://doi.org/10.1093/emboj/17.11.2982.

Barug, D., de Groot, K., 1985. Effect of the imidazole derivative lombazole on the ultrastructure of Staphylococcus epidermidis and Candida albicans. Antimicrob. Agents Chemother. 28, 643–7. https://doi.org/10.1128/aac.28.5.643.

Berchtold, D., Piccolis, M., Chiaruttini, N., Riezman, I., Riezman, H., Roux, A., Walther, T.C., Loewith, R., 2012. Plasma membrane stress induces relocalization of Slm proteins and activation of TORC2 to promote sphingolipid synthesis. Nat. Cell Biol. 14, 542–547. https://doi.org/10.1038/ncb2480.

Berchtold, D., Walther, T.C., 2009. TORC2 Plasma Membrane Localization Is Essential for Cell Viability and Restricted to a Distinct Domain. Mol. Biol. Cell 20, 1565–1575. https://doi.org/10.1091/mbc.e08-10-1001

Bernardo, S.M., Lee, S.A., 2010. Candida albicans SUR7 contributes to secretion, biofilm formation, and macrophage killing. BMC Microbiol. 10, 133. https://doi.org/10.1186/1471-2180-10-133.

Besold, A.N., Culbertson, E.M., Culotta, V.C., 2016. The Yin and Yang of copper during infection. J. Biol. Inorg. Chem. 21, 137–44. https://doi.org/10.1007/s00775-016-1335-1.

Bharat, T.A.M., Hoffmann, P.C., Kukulski, W., 2018. Correlative Microscopy of Vitreous Sections Provides Insights into BAR-Domain Organization In Situ. Structure 26, 879-886.e3. https://doi.org/10.1016/j.str.2018.03.015.

Bianchi, F., Syga, Ł., Moiset, G., Spakman, D., Schavemaker, P.E., Punter, C.M., Seinen, A.-B., van Oijen, A.M., Robinson, A., Poolman, B., 2018. Steric exclusion and protein conformation determine the localization of plasma membrane transporters. Nat. Commun. 9, 501. https://doi.org/10.1038/s41467-018-02864-2.

Braun, K.A., Dombek, K.M., Young, E.T., 2016. Snf1-Dependent Transcription Confers Glucose-Induced Decay upon the mRNA Product. Mol. Cell. Biol. 36, 628–644. https://doi.org/10.1128/mcb.00436-15.

Braun, K.A., Vaga, S., Dombek, K.M., Fang, F., Palmisano, S., Aebersold, R., Young, E.T., 2014. Phosphoproteomic analysis identifies proteins involved in transcription-coupled mRNA decay as targets of Snf1 signaling. Sci. Signal. 7. https://doi.org/10.1126/scisignal.2005000.

Breslow, D.K., 2013. Sphingolipid homeostasis in the endoplasmic reticulum and beyond. Cold Spring Harb. Perspect. Biol. 5, a013326. https://doi.org/10.1101/cshperspect.a013326.

Breslow, D.K., Collins, S.R., Bodenmiller, B., Aebersold, R., Simons, K., Shevchenko, A., Ejsing, C.S., Weissman, J.S., 2010. Orm family proteins mediate sphingolipid homeostasis. Nature 463, 1048–53. https://doi.org/10.1038/nature08787.

Brown, A.J.P., Haynes, K., Quinn, J., 2009. Nitrosative and oxidative stress responses in fungal pathogenicity. Curr. Opin. Microbiol. 12, 384–91. https://doi.org/10.1016/j.mib.2009.06.007.

Büdel, B., Rhiel, E., 1987. Studies on the ultrastructure of some cyanolichen haustoria. Protoplasma 139, 145–152.

Busto, J. V, Elting, A., Haase, D., Spira, F., Kuhlman, J., Schäfer-Herte, M., Wedlich-Söldner, R., 2018. Lateral plasma membrane compartmentalization links protein function and turnover. EMBO J. 37, e99473. https://doi.org/10.15252/embj.201899473.

Čáp, M., Váchová, L., Palková, Z., 2015. Longevity of U cells of differentiated yeast colonies grown on respiratory medium depends on active glycolysis. Cell Cycle 14, 3488–3497. https://doi.org/10.1080/15384101.2015.1093706.

Casamayor, A., Torrance, P.D., Kobayashi, T., Thorner, J., Alessi, D.R., 1999. Functional counterparts of mammalian protein kinases PDK1 and SGK in budding yeast. Curr. Biol. 9, 186–197. https://doi.org/10.1016/S0960-9822(99)80088-8.

Clarke, K.J., Leeson, E.A., 1985. Plasmalemma structure in freezing tolerant unicellular algae. Protoplasma 129, 120–126. https://doi.org/10.1007/BF01279909.

Collins, S.R., Kemmeren, P., Zhao, X.-C., Greenblatt, J.F., Spencer, F., Holstege, F.C.P., Weissman, J.S., Krogan, N.J., 2007. Toward a comprehensive atlas of the physical interactome of Saccharomyces cerevisiae. Mol. Cell. Proteomics 6, 439–50. https://doi.org/10.1074/mcp.M600381-MCP200.

Cooke, F.T., Dove, S.K., McEwen, R.K., Painter, G., Holmes, A.B., Hall, M.N., Michell, R.H., Parker, P.J., 1998. The stress-activated phosphatidylinositol 3-phosphate 5-kinase Fab1p is essential for vacuole function in S. cerevisiae. Curr. Biol. 8, 1219–22. https://doi.org/10.1016/s0960-9822(07)00513-1.

Cowart, L.A., Obeid, L.M., 2007. Yeast sphingolipids: Recent developments in understanding biosynthesis, regulation, and function. Biochim. Biophys. Acta - Mol. Cell Biol. Lipids 1771, 421–31. https://doi.org/10.1016/j.bbalip.2006.08.005.

Dantas, A. da S., Day, A., Ikeh, M., Kos, I., Achan, B., Quinn, J., 2015. Oxidative stress responses in the human fungal pathogen, Candida albicans. Biomolecules 5, 142–65. https://doi.org/10.3390/biom5010142.

Decker, C.J., Parker, R., 2012. P-bodies and stress granules: Possible roles in the control of translation and mRNA degradation. Cold Spring Harb. Perspect. Biol. 4, a012286. https://doi.org/10.1101/cshperspect.a012286.

Decker, C.J., Parker, R., 1993. A turnover pathway for both stable and unstable mRNAs in yeast: Evidence for a requirement for deadenylation. Genes Dev. 7, 1632–1643. https://doi.org/10.1101/gad.7.8.1632.

deHart, A.K.A., Schnell, J.D., Allen, D.A., Hicke, L., 2002. The conserved Pkh-Ypk kinase cascade is required for endocytosis in yeast. J. Cell Biol. 156, 241–8. https://doi.org/10.1083/jcb.200107135.

Deng, C., Xiong, X., Krutchinsky, A.N., 2009. Unifying Fluorescence Microscopy and Mass Spectrometry for Studying Protein Complexes in Cells. Mol. Cell. Proteomics 8, 1413–1423. https://doi.org/10.1074/mcp.M800397-MCP200.

Denis, V., Cyert, M.S., 2005. Molecular analysis reveals localization of Saccharomyces cerevisiae protein kinase C to sites of polarized growth and Pkc1p targeting to the nucleus and mitotic spindle. Eukaryot. Cell 4, 36–45. https://doi.org/10.1128/EC.4.1.36-45.2005.

Deprez, M.-A., Eskes, E., Winderickx, J., Wilms, T., 2018. The TORC1-Sch9 pathway as a crucial mediator of chronological lifespan in the yeast Saccharomyces cerevisiae. FEMS Yeast Res. 18. https://doi.org/10.1093/femsyr/foy048.

Desrivières, S., Cooke, F.T., Parker, P.J., Hall, M.N., 1998. MSS4, a phosphatidylinositol-4-phosphate 5-kinase required for organization of the actin cytoskeleton in Saccharomyces cerevisiae. J. Biol. Chem. 273, 15787–93. https://doi.org/10.1074/jbc.273.25.15787.

Dickson, R.C., Sumanasekera, C., Lester, R.L., 2006. Functions and metabolism of sphingolipids in Saccharomyces cerevisiae. Prog. Lipid Res. 45, 447–65. https://doi.org/10.1016/j.plipres.2006.03.004.

Douglas, L.M., Konopka, J.B., 2019. Plasma membrane architecture protects Candida albicans from killing by

copper. PLoS Genet. 15, e1007911. https://doi.org/10.1371/journal.pgen.1007911.

Douglas, L.M., Konopka, J.B., 2016. Plasma membrane organization promotes virulence of the human fungal pathogen Candida albicans. J. Microbiol. 54, 178–91. https://doi.org/10.1007/s12275-016-5621-y.

Douglas, L.M., Konopka, J.B., 2014. Fungal Membrane Organization: The Eisosome Concept. Annu. Rev. Microbiol. 68, 377–393. https://doi.org/10.1146/annurev-micro-091313-103507.

Douglas, L.M., Wang, H.X., Keppler-Ross, S., Dean, N., Konopka, J.B., 2012. Sur7 promotes plasma membrane organization and is needed for resistance to stressful conditions and to the invasive growth and virulence of Candida albicans. MBio 3, 1–12. https://doi.org/10.1128/mBio.00254-11.

Douglas, L.M., Wang, H.X., Konopka, J.B., 2013. The MARVEL domain protein Nce102 regulates actin organization and invasive growth of Candida albicans. MBio 4, e00723-13. https://doi.org/10.1128/mBio.00723-13.

Dupont, S., Beney, L., Ritt, J.-F., Lherminier, J., Gervais, P., 2010. Lateral reorganization of plasma membrane is involved in the yeast resistance to severe dehydration. Biochim. Biophys. Acta 1798, 975–85. https://doi.org/10.1016/j.bbamem.2010.01.015.

Engin, A., 2017. Human protein kinases and obesity, in: Advances in Experimental Medicine and Biology. Springer New York LLC, pp. 111–134. https://doi.org/10.1007/978-3-319-48382-5_5.

Fadri, M., Daquinag, A., Wang, S., Xue, T., Kunz, J., 2005. The Pleckstrin Homology Domain Proteins Slm1 and Slm2 Are Required for Actin Cytoskeleton Organization in Yeast and Bind Phosphatidylinositol-4,5-Bisphosphate and TORC2. Mol. Biol. Cell 16, 1883–1900. https://doi.org/10.1091/mbc.e04-07-0564.

Fisk, D.G., Ball, C.A., Dolinski, K., Engel, S.R., Hong, E.L., Issel-Tarver, L., Schwartz, K., Sethuraman, A., Botstein, D., Cherry, J.M., Saccharomyces Genome Database Project, 2006. Saccharomyces cerevisiae S288C genome annotation: a working hypothesis. Yeast 23, 857–65. https://doi.org/10.1002/yea.1400.

Foderaro, J.E., Douglas, L.M., Konopka, J.B., 2017. MCC/Eisosomes Regulate Cell Wall Synthesis and Stress Responses in Fungi. J. fungi (Basel, Switzerland) 3. https://doi.org/10.3390/jof3040061.

Folmer, V., Pedroso, N., Matias, A.C., Lopes, S.C.D.N., Antunes, F., Cyrne, L., Marinho, H.S., 2008. H2O2 induces rapid biophysical and permeability changes in the plasma membrane of Saccharomyces cerevisiae. Biochim. Biophys. Acta 1778, 1141–7. https://doi.org/10.1016/j.bbamem.2007.12.008.

Friant, S., Lombardi, R., Schmelzle, T., Hall, M.N., Riezman, H., 2001. Sphingoid base signaling via Pkh kinases is required for endocytosis in yeast. EMBO J. 20, 6783–92. https://doi.org/10.1093/emboj/20.23.6783.

Frohlich, F., Christiano, R., Olson, D.K., Alcazar-Roman, A., DeCamilli, P., Walther, T.C., 2014. A role for eisosomes in maintenance of plasma membrane phosphoinositide levels. Mol. Biol. Cell 25, 2797–806. https://doi.org/10.1091/mbc.e13-11-0639.

Fröhlich, F., Moreira, K., Aguilar, P.S., Hubner, N.C., Mann, M., Walter, P., Walther, T.C., 2009. A genome-wide screen for genes affecting eisosomes reveals Nce102 function in sphingolipid signaling. J. Cell Biol. 185, 1227–1242. https://doi.org/10.1083/jcb.200811081.

García-Marqués, S., Randez-Gil, F., Dupont, S., Garre, E., Prieto, J.A., 2016. Sng1 associates with Nce102 to regulate the yeast Pkh-Ypk signalling module in response to sphingolipid status. Biochim. Biophys. Acta - Mol. Cell Res. 1863, 1319–1333. https://doi.org/10.1016/j.bbamcr.2016.03.025.

García-Santamarina, S., Thiele, D.J., 2015. Copper at the Fungal Pathogen-Host Axis. J. Biol. Chem. 290, 18945–53. https://doi.org/10.1074/jbc.R115.649129.

Garcia, A.V., Al-Yousif, M., Hirt, H., 2012. Role of AGC kinases in plant growth and stress responses. Cell. Mol. Life Sci. 69, 3259–67. https://doi.org/10.1007/s00018-012-1093-3.

Gary, J.D., Wurmser, A.E., Bonangelino, C.J., Weisman, L.S., Emr, S.D., 1998. Fab1p is essential for PtdIns(3)P 5-kinase activity and the maintenance of vacuolar size and membrane homeostasis. J. Cell Biol. 143, 65–79.

Gasch, A.P., Huang, M., Metzner, S., Botstein, D., Elledge, S.J., Brown, P.O., 2001. Genomic expression responses to DNA-damaging agents and the regulatory role of the yeast ATR homolog Mec1p. Mol. Biol. Cell 12, 2987–3003. https://doi.org/10.1091/mbc.12.10.2987.

Gasch, A.P., Spellman, P.T., Kao, C.M., Carmel-Harel, O., Eisen, M.B., Storz, G., Botstein, D., Brown, P.O., 2000. Genomic expression programs in the response of yeast cells to environmental changes. Mol. Biol. Cell 11, 4241–57. https://doi.org/10.1091/mbc.11.12.4241.

Ghaddar, K., Merhi, A., Saliba, E., Krammer, E.-M., Prévost, M., André, B., 2014. Substrate-induced ubiquitylation and endocytosis of yeast amino acid permeases. Mol. Cell. Biol. 34, 4447–63. https://doi.org/10.1128/MCB.00699-14.

Gournas, C., Gkionis, S., Carquin, M., Twyffels, L., Tyteca, D., André, B., 2018. Conformation-dependent partitioning of yeast nutrient transporters into starvation-protective membrane domains. Proc. Natl. Acad. Sci. U. S. A. 115, E3145–E3154. https://doi.org/10.1073/pnas.1719462115.

Gournas, C., Saliba, E., Krammer, E.-M., Barthelemy, C., Prévost, M., André, B., 2017. Transition of yeast Can1 transporter to the inward-facing state unveils an α-arrestin target sequence promoting its ubiquitylation and endocytosis. Mol. Biol. Cell 28, 2819–2832. https://doi.org/10.1091/mbc.E17-02-0104.

Gross, H., Kuebler, O., Bas, E., Moor, H., 1978. Decoration of specific sites on freeze-fractured membranes. J. Cell Biol. 79, 646–56. https://doi.org/10.1083/jcb.79.3.646.

Grossmann, G., Malinsky, J., Stahlschmidt, W., Loibl, M., Weig-Meckl, I., Frommer, W.B., Opekarová, M., Tanner, W., 2008. Plasma membrane microdomains regulate turnover of transport proteins in yeast. J. Cell Biol. 183, 1075–88. https://doi.org/10.1083/jcb.200806035.

Grossmann, G., Opekarová, M., Malinsky, J., Weig-Meckl, I., Tanner, W., 2007. Membrane potential governs lateral segregation of plasma membrane proteins and lipids in yeast. EMBO J. 26, 1–8. https://doi.org/10.1038/sj.emboj.7601466.

Grossmann, G., Opekarova, M., Novakova, L., Stolz, J., Tanner, W., 2006. Lipid raft-based membrane compartmentation of a plant transport protein expressed in Saccharomyces cerevisiae. Eukaryot. Cell 5, 945–953. https://doi.org/10.1128/EC.00206-05.

Grousl, T., Opekarová, M., Stradalova, V., Hasek, J., Malinsky, J., 2015. Evolutionarily conserved 5′-3′ exoribonuclease Xrn1 accumulates at plasma membrane-associated eisosomes in post-diauxic yeast. PLoS One 10, e0122770. https://doi.org/10.1371/journal.pone.0122770.

Guimarães, L.L., Toledo, M.S., Ferreira, F.A.S., Straus, A.H., Takahashi, H.K., 2014. Structural diversity and biological significance of glycosphingolipids in pathogenic and opportunistic fungi. Front. Cell. Infect. Microbiol. 4, 138. https://doi.org/10.3389/fcimb.2014.00138.

Haimovich, G., Medina, D.A., Causse, S.Z., Garber, M., Millán-Zambrano, G., Barkai, O., Chávez, S., Pérez-Ortín, J.E., Darzacq, X., Choder, M., 2013. Gene Expression Is Circular: Factors for mRNA Degradation Also Foster mRNA Synthesis. Cell 153, 1000–11. https://doi.org/10.1016/j.cell.2013.05.012.

Han, S., Lone, M.A., Schneiter, R., Chang, A., 2010. Orm1 and Orm2 are conserved endoplasmic reticulum

membrane proteins regulating lipid homeostasis and protein quality control. Proc. Natl. Acad. Sci. 107, 5851–6. https://doi.org/10.1073/pnas.0911617107.

Hanada, K., 2003. Serine palmitoyltransferase, a key enzyme of sphingolipid metabolism. Biochim. Biophys. Acta 1632, 16–30. https://doi.org/10.1016/s1388-1981(03)00059-3.

Heinisch, J.J., Lorberg, A., Schmitz, H.P., Jacoby, J.J., 1999. The protein kinase C-mediated MAP kinase pathway involved in the maintenance of cellular integrity in Saccharomyces cerevisiae. Mol. Microbiol. 32, 671–80. https://doi.org/10.1046/j.1365-2958.1999.01375.x.

Ho, Y., Gruhler, A., Heilbut, A., Bader, G.D., Moore, L., Adams, S.-L., Millar, A., Taylor, P., Bennett, K., Boutilier, K., Yang, L., Wolting, C., Donaldson, I., Schandorff, S., Shewnarane, J., Vo, M., Taggart, J., Goudreault, M., Muskat, B., Alfarano, C., Dewar, D., Lin, Z., Michalickova, K., Willems, A.R., Sassi, H., Nielsen, P.A., Rasmussen, K.J., Andersen, J.R., Johansen, L.E., Hansen, L.H., Jespersen, H., Podtelejnikov, A., Nielsen, E., Crawford, J., Poulsen, V., Sørensen, B.D., Matthiesen, J., Hendrickson, R.C., Gleeson, F., Pawson, T., Moran, M.F., Durocher, D., Mann, M., Hogue, C.W. V., Figeys, D., Tyers, M., 2002. Systematic identification of protein complexes in Saccharomyces cerevisiae by mass spectrometry. Nature 415, 180–183. https://doi.org/10.1038/415180a.

Hodgkinson, V., Petris, M.J., 2012. Copper homeostasis at the host-pathogen interface. J. Biol. Chem. 287, 13549–55. https://doi.org/10.1074/jbc.R111.316406.

Hosiner, D., Sponder, G., Graschopf, A., Reipert, S., Schweyen, R.J., Schüller, C., Aleschko, M., 2011. Pun1p is a metal ion-inducible, calcineurin/Crz1p-regulated plasma membrane protein required for cell wall integrity. Biochim. Biophys. Acta 1808, 1108–19. https://doi.org/10.1016/j.bbamem.2011.01.002.

Hsu, C.L., Stevens, A., 1993. Yeast cells lacking 5'-->3' exoribonuclease 1 contain mRNA species that are poly(A) deficient and partially lack the 5' cap structure. Mol. Cell. Biol. 13, 4826–4835. https://doi.org/10.1128/MCB.13.8.4826.

Hu, W., Sweet, T.J., Chamnongpol, S., Baker, K.E., Coller, J., 2009. Co-translational mRNA decay in Saccharomyces cerevisiae. Nature 461, 225–9. https://doi.org/10.1038/nature08265.

Inagaki, M., Schmelzle, T., Yamaguchi, K., Irie, K., Hall, M.N., Matsumoto, K., 1999. PDK1 homologs activate the Pkc1-mitogen-activated protein kinase pathway in yeast. Mol. Cell. Biol. 19, 8344–52. https://doi.org/10.1128/mcb.19.12.8344.

Ito, T., Chiba, T., Ozawa, R., Yoshida, M., Hattori, M., Sakaki, Y., 2001. A comprehensive two-hybrid analysis to explore the yeast protein interactome. Proc. Natl. Acad. Sci. 98, 4569–4574. https://doi.org/10.1073/pnas.061034498.

Jenkins, G.M., Richards, A., Wahl, T., Mao, C., Obeid, L., Hannun, Y., 1997. Involvement of yeast sphingolipids in the heat stress response of Saccharomyces cerevisiae. J. Biol. Chem. 272, 32566–32572. https://doi.org/10.1074/jbc.272.51.32566.

Jin, N., Mao, K., Jin, Y., Tevzadze, G., Kauffman, E.J., Park, S., Bridges, D., Loewith, R., Saltiel, A.R., Klionsky, D.J., Weisman, L.S., 2014. Roles for PI(3,5)P2 in nutrient sensing through TORC1. Mol. Biol. Cell 25, 1171–85. https://doi.org/10.1091/mbc.E14-01-0021.

Jung, S., Smith, J.J., von Haller, P.D., Dilworth, D.J., Sitko, K.A., Miller, L.R., Saleem, R.A., Goodlett, D.R., Aitchison, J.D., 2013. Global analysis of condition-specific subcellular protein distribution and abundance. Mol. Cell. Proteomics 12, 1421–35. https://doi.org/10.1074/mcp.O112.019166.

Kabeche, R., Baldissard, S., Hammond, J., Howard, L., Moseley, J.B., 2011. The filament-forming protein Pil1 assembles linear eisosomes in fission yeast. Mol. Biol. Cell 22, 4059–4067. https://doi.org/10.1091/mbc.E11-07-0605.

Kabeche, R., Howard, L., Moseley, J.B., 2015a. Eisosomes provide membrane reservoirs for rapid expansion of the yeast plasma membrane. J. Cell Sci. 128, 4057–62. https://doi.org/10.1242/jcs.176867.

Kabeche, R., Madrid, M., Cansado, J., Moseley, J.B., 2015b. Eisosomes regulate phosphatidylinositol 4,5-bisphosphate (PI(4,5)P2) cortical clusters and mitogen-activated protein (MAP) kinase signaling upon osmotic stress. J. Biol. Chem. 290, 25960–25973. https://doi.org/10.1074/jbc.M115.674192.

Kabeche, R., Roguev, A., Krogan, N.J., Moseley, J.B., 2014. A Pil1-Sle1-Syj1-Tax4 functional pathway links eisosomes with PI(4,5)P2 regulation. J. Cell Sci. 127, 1318–1326. https://doi.org/10.1242/jcs.143545.

Kamada, Y., Ohsumi, Y., Fujioka, Y., Suzuki, N.N., Inagaki, F., Wullschleger, S., Loewith, R., Hall, M.N., 2005. Tor2 directly phosphorylates the AGC kinase Ypk2 to regulate actin polarization. Mol. Cell. Biol. 25, 7239–48. https://doi.org/10.1128/MCB.25.16.7239-7248.2005.

Kamada, Y., Qadota, H., Python, C.P., Anraku, Y., Ohya, Y., Levin, D.E., 1996. Activation of yeast protein kinase C by Rho1 GTPase. J. Biol. Chem. 271, 9193–6. https://doi.org/10.1074/jbc.271.16.9193.

Karotki, L., Huiskonen, J.T., Stefan, C.J., Ziółkowska, N.E., Roth, R., Surma, M.A., Krogan, N.J., Emr, S.D., Heuser, J., Grünewald, K., Walther, T.C., 2011. Eisosome proteins assemble into a membrane scaffold. J. Cell Biol. 195, 889–902. https://doi.org/10.1083/jcb.201104040.

Karp, G., Iwasa, J., Marshall, W., 2016. The Structure and Function of the Plasma Membrane, in: Cell and Molecular Biology: Concepts and Experiments. Wiley..

Khalaj, V., Azizi, M., Enayati, S., Khorasanizadeh, D., Ardakani, E.M., 2012. NCE102 homologue in Aspergillus fumigatus is required for normal sporulation, not hyphal growth or pathogenesis. FEMS Microbiol. Lett. 329, 138–145. https://doi.org/10.1111/j.1574-6968.2012.02513.x.

Khemici, V., Poljak, L., Luisi, B.F., Carpousis, A.J., 2008. The RNase E of Escherichia coli is a membrane-binding protein. Mol. Microbiol. 70, 799–813. https://doi.org/10.1111/j.1365-2958.2008.06454.x.

Khemici, V., Prados, J., Linder, P., Redder, P., 2015. Decay-Initiating Endoribonucleolytic Cleavage by RNase Y Is Kept under Tight Control via Sequence Preference and Sub-cellular Localisation. PLoS Genet. 11, e1005577. https://doi.org/10.1371/journal.pgen.1005577.

Krogan, N.J., Cagney, G., Yu, H., Zhong, G., Guo, X., Ignatchenko, A., Li, J., Pu, S., Datta, N., Tikuisis, A.P., Punna, T., Peregrín-Alvarez, J.M., Shales, M., Zhang, X., Davey, M., Robinson, M.D., Paccanaro, A., Bray, J.E., Sheung, A., Beattie, B., Richards, D.P., Canadien, V., Lalev, A., Mena, F., Wong, P., Starostine, A., Canete, M.M., Vlasblom, J., Wu, S., Orsi, C., Collins, S.R., Chandran, S., Haw, R., Rilstone, J.J., Gandi, K., Thompson, N.J., Musso, G., St Onge, P., Ghanny, S., Lam, M.H.Y., Butland, G., Altaf-Ul, A.M., Kanaya, S., Shilatifard, A., O'Shea, E., Weissman, J.S., Ingles, C.J., Hughes, T.R., Parkinson, J., Gerstein, M., Wodak, S.J., Emili, A., Greenblatt, J.F., 2006. Global landscape of protein complexes in the yeast Saccharomyces cerevisiae. Nature 440, 637–643. https://doi.org/10.1038/nature04670.

Kukulski, W., Schorb, M., Kaksonen, M., Briggs, J.A.G., 2012. Plasma membrane reshaping during endocytosis is revealed by time-resolved electron tomography. Cell 150, 508–520. https://doi.org/10.1016/j.cell.2012.05.046.

Laalami, S., Zig, L., Putzer, H., 2014. Initiation of mRNA decay in bacteria. Cell. Mol. Life Sci. 71, 1799–828.

https://doi.org/10.1007/s00018-013-1472-4.

Łabno, A., Tomecki, R., Dziembowski, A., 2016. Cytoplasmic RNA decay pathways - Enzymes and mechanisms. Biochim. Biophys. Acta 1863, 3125–3147. https://doi.org/10.1016/j.bbamcr.2016.09.023.

Lacy, M.M., Baddeley, D., Berro, J., 2017. Single-molecule imaging of the BAR-domain protein Pil1p reveals filament-end dynamics. Mol. Biol. Cell 28, 2251–2259. https://doi.org/10.1091/mbc.E17-04-0238.

Lauwers, E., Grossmann, G., André, B., 2007. Evidence for coupled biogenesis of yeast Gap1 permease and sphingolipids: essential role in transport activity and normal control by ubiquitination. Mol. Biol. Cell 18, 3068–80. https://doi.org/10.1091/mbc.e07-03-0196.

Leber, R., Zinser, E., Paltauf, F., Daum, G., Zellnig, G., 1994. Characterization of lipid particles of the yeast,Saccharomyces cerevisiae. Yeast 10, 1421–1428. https://doi.org/10.1002/yea.320101105.

Lee, J.H., Heuser, J.E., Roth, R., Goodenough, U., 2015. Eisosome ultrastructure and evolution in fungi, microalgae, and lichens. Eukaryot. Cell 14, 1017–1042. https://doi.org/10.1128/EC.00106-15.

Leroux, A.E., Schulze, J.O., Biondi, R.M., 2018. AGC kinases, mechanisms of regulation and innovative drug development. Semin. Cancer Biol. https://doi.org/10.1016/j.semcancer.2017.05.011.

Levin, D.E., 2005. Cell Wall Integrity Signaling in Saccharomyces cerevisiae. Microbiol. Mol. Biol. Rev. 69, 262–91. https://doi.org/10.1128/mmbr.69.2.262-291.2005.

Li, L., Naseem, S., Sharma, S., Konopka, J.B., 2015. Flavodoxin-Like Proteins Protect Candida albicans from Oxidative Stress and Promote Virulence. PLoS Pathog. 11, e1005147. https://doi.org/10.1371/journal.ppat.1005147.

Li, S.C., Kane, P.M., 2009. The yeast lysosome-like vacuole: endpoint and crossroads. Biochim. Biophys. Acta 1793, 650–63. https://doi.org/10.1016/j.bbamcr.2008.08.003.

Liu, Ke, Zhang, X., Lester, R.L., Dickson, R.C., 2005. The Sphingoid Long Chain Base Phytosphingosine Activates AGC-type Protein Kinases in *Saccharomyces cerevisiae* Including Ypk1, Ypk2, and Sch9. J. Biol. Chem. 280, 22679–22687. https://doi.org/10.1074/jbc.M502972200.

Liu, K., Zhang, X., Sumanasekera, C., Lester, R.L., Dickson, R.C., 2005. Signalling functions for sphingolipid long-chain bases in Saccharomyces cerevisiae. Biochem. Soc. Trans. 33, 1170. https://doi.org/10.1042/BST20051170.

Lodish, H., Berk, A., Kaiser, C.A., Krieger, M., Scott, M.P., Bretscher, A., Ploegh, H., Matsudaira, P., 2008. Transport across Epithelia, in: Molecular Cell Biology. W. H. Freeman and Company, New York.

Loibl, M., Grossmann, G., Stradalova, V., Klingl, A., Rachel, R., Tanner, W., Malinsky, J., Opekarová, M., 2010. C terminus of Nce 102 determines the structure and function of microdomains in the Saccharomyces cerevisiae plasma membrane. Eukaryot. Cell 9, 1184–1192. https://doi.org/10.1128/EC.00006-10.

Luchelli, L., Thomas, M.G., Boccaccio, G.L., 2015. Synaptic control of mRNA translation by reversible assembly of XRN1 bodies. J. Cell Sci. 128, 1542–1554. https://doi.org/10.1242/jcs.163295.

Luo, G., Costanzo, M., Boone, C., Dickson, R.C., 2011. Nutrients and the Pkh1/2 and Pkc1 protein kinases control mRNA decay and P-body assembly in yeast. J. Biol. Chem. 286, 8759–70. https://doi.org/10.1074/jbc.M110.196030.

Luo, G., Gruhler, A., Liu, Y., Jensen, O.N., Dickson, R.C., 2008. The sphingolipid long-chain base-Pkh1/2-Ypk1/2 signaling pathway regulates eisosome assembly and turnover. J. Biol. Chem. 283, 10433–44. https://doi.org/10.1074/jbc.M709972200.

Malinska, K., Malinsky, J., Opekarova, M., Tanner, W., 2004. Distribution of Can1p into stable domains reflects lateral protein segregation within the plasma membrane of living S. cerevisiae cells. J. Cell Sci. 117, 6031–6041. https://doi.org/10.1242/jcs.01493.

Malinska, K., Malínský, J., Opekarová, M., Tanner, W., 2003. Visualization of Protein Compartmentation within the Plasma Membrane of Living Yeast Cells. Mol. Biol. Cell 14, 4427–4436. https://doi.org/10.1091/mbc.E03-04-0221.

Malinsky, J., Opekarová, M., 2016. New Insight Into the Roles of Membrane Microdomains in Physiological Activities of Fungal Cells. Int. Rev. Cell Mol. Biol. 325, 119–80. https://doi.org/10.1016/bs.ircmb.2016.02.005.

Malinsky, J., Opekarová, M., Tanner, W., 2010. The lateral compartmentation of the yeast plasma membrane. Yeast. https://doi.org/10.1002/yea.1772.

Martinez, M.J., Roy, S., Archuletta, A.B., Wentzell, P.D., Anna-Arriola, S.S., Rodriguez, A.L., Aragon, A.D., Quiñones, G.A., Allen, C., Werner-Washburne, M., 2004. Genomic analysis of stationary-phase and exit in Saccharomyces cerevisiae: gene expression and identification of novel essential genes. Mol. Biol. Cell 15, 5295–305. https://doi.org/10.1091/mbc.e03-11-0856.

Mascaraque, V., Hernáez, M.L., Jiménez-Sánchez, M., Hansen, R., Gil, C., Martín, H., Cid, V.J., Molina, M., 2013. Phosphoproteomic Analysis of Protein Kinase C Signaling in Saccharomyces cerevisiae Reveals Slt2 Mitogen-activated Protein Kinase (MAPK)-dependent Phosphorylation of Eisosome Core Components. Mol. Cell. Proteomics 12, 557–574. https://doi.org/10.1074/mcp.M112.020438.

Mim, C., Unger, V.M., 2012. Membrane curvature and its generation by BAR proteins. Trends Biochem. Sci. 37, 526–33. https://doi.org/10.1016/j.tibs.2012.09.001.

Moharir, A., Gay, L., Appadurai, D., Keener, J., Babst, M., 2018. Eisosomes are metabolically regulated storage compartments for APC-type nutrient transporters. Mol. Biol. Cell 29, 2113–2127. https://doi.org/10.1091/mbc.E17-11-0691.

Moor, H., Mühlethaler, K., 1963. Fine structure in frozen-etched yeast cells. J. Cell Biol. 17, 609–628. https://doi.org/10.1083/jcb.17.3.609.

Morales-Johansson, H., Jenoe, P., Cooke, F.T., Hall, M.N., 2004. Negative regulation of phosphatidylinositol 4,5-bisphosphate levels by the INP51-associated proteins TAX4 and IRS4. J. Biol. Chem. 279, 39604–10. https://doi.org/10.1074/jbc.M405589200.

Moreira, K.E., Schuck, S., Schrul, B., Fröhlich, F., Moseley, J.B., Walther, T.C., Walter, P., 2012. Seg 1 controls eisosome assembly and shape. J. Cell Biol. 198, 405–420. https://doi.org/10.1083/jcb.201202097.

Moreira, K.E., Walther, T.C., Aguilar, P.S., Walter, P., 2009. Pil1 Controls Eisosome Biogenesis. Mol. Biol. Cell 20, 809–818. https://doi.org/10.1091/mbc.e08-03-0313.

Murashko, O.N., Kaberdin, V.R., Lin-Chao, S., 2012. Membrane binding of Escherichia coli RNase E catalytic domain stabilizes protein structure and increases RNA substrate affinity. Proc. Natl. Acad. Sci. U. S. A. 109, 7019–7024. https://doi.org/10.1073/pnas.1120181109.

Murphy, E.R., Boxberger, J., Colvin, R., Lee, S.J., Zahn, G., Loor, F., Kim, K., 2011. Pil1, an eisosome organizer, plays an important role in the recruitment of synaptojanins and amphiphysins to facilitate receptor-mediated endocytosis in yeast. Eur. J. Cell Biol. 90, 825–833. https://doi.org/10.1016/j.ejcb.2011.06.006.

Nagarajan, V.K., Jones, C.I., Newbury, S.F., Green, P.J., 2013. XRN 5'→3' exoribonucleases: structure,

mechanisms and functions. Biochim. Biophys. Acta 1829, 590–603. https://doi.org/10.1016/j.bbagrm.2013.03.005.

Nakashima, A., Otsubo, Y., Yamashita, A., Sato, T., Yamamoto, M., Tamanoi, F., 2012. Psk1, an AGC kinase family member in fission yeast, is directly phosphorylated and controlled by TORC1 and functions as S6 kinase. J. Cell Sci. 125, 5840–5849. https://doi.org/10.1242/jcs.111146.

Niles, B.J., Joslin, A.C., Fresques, T., Powers, T., 2014. TOR Complex 2-Ypk1 Signaling Maintains Sphingolipid Homeostasis by Sensing and Regulating ROS Accumulation. Cell Rep. 6, 541–552. https://doi.org/10.1016/j.celrep.2013.12.040.

Niles, B.J., Mogri, H., Hill, A., Vlahakis, A., Powers, T., 2012. Plasma membrane recruitment and activation of the AGC kinase Ypk1 is mediated by target of rapamycin complex 2 (TORC2) and its effector proteins Slm1 and Slm2. Proc. Natl. Acad. Sci. U. S. A. 109, 1536–41. https://doi.org/10.1073/pnas.1117563109.

Niles, B.J., Powers, T., 2012. Plasma membrane proteins Slm1 and Slm2 mediate activation of the AGC kinase Ypk1 by TORC2 and sphingolipids in S. cerevisiae. Cell Cycle 11, 3745–9. https://doi.org/10.4161/cc.21752

Nishimura, T., Morone, N., Suetsugu, S., 2018. Membrane re-modelling by BAR domain superfamily proteins via molecular and non-molecular factors. Biochem. Soc. Trans. 46, 379–389. https://doi.org/10.1042/BST20170322.

Numrich, J., Péli-Gulli, M.-P., Arlt, H., Sardu, A., Griffith, J., Levine, T., Engelbrecht-Vandré, S., Reggiori, F., De Virgilio, C., Ungermann, C., 2015. The I-BAR protein Ivy1 is an effector of the Rab7 GTPase Ypt7 involved in vacuole membrane homeostasis. J. Cell Sci. 128, 2278–92. https://doi.org/10.1242/jcs.164905.

O'Meara, T.R., Robbins, N., Cowen, L.E., 2017. The Hsp90 Chaperone Network Modulates Candida Virulence Traits. Trends Microbiol. 25, 809–819. https://doi.org/10.1016/j.tim.2017.05.003.

Odorizzi, G., Babst, M., Emr, S.D., 2000. Phosphoinositide signaling and the regulation of membrane trafficking in yeast. Trends Biochem Sci 25, 229–35. https://doi.org/10.1016/s0968-0004(00)01543-7.

Odorizzi, G., Babst, M., Emr, S.D., 1998. Fab1p PtdIns(3)P 5-kinase function essential for protein sorting in the multivesicular body. Cell 95, 847–58. https://doi.org/10.1016/s0092-8674(00)81707-9.

Olivera-Couto, A., Grana, M., Harispe, L., Aguilar, P.S., 2011. The eisosome core is composed of BAR domain proteins. Mol. Biol. Cell 22, 2360–2372. https://doi.org/10.1091/mbc.E10-12-1021.

Olivera-Couto, A., Salzman, V., Mailhos, M., Digman, M.A., Gratton, E., Aguilar, P.S., 2015. Eisosomes are dynamic plasma membrane domains showing Pil1-Lsp1 heteroligomer binding equilibrium. Biophys. J. 108, 1633–1644. https://doi.org/10.1016/j.bpj.2015.02.011.

Opekarová, M., Robl, I., Tanner, W., 2002. Phosphatidyl ethanolamine is essential for targeting the arginine transporter Can1p to the plasma membrane of yeast. Biochim. Biophys. Acta - Biomembr. 1564, 9–13. https://doi.org/10.1016/S0005-2736(02)00455-8.

Parker, R., Sheth, U., 2007. P bodies and the control of mRNA translation and degradation. Mol. Cell 25, 635–46. https://doi.org/10.1016/j.molcel.2007.02.011.

Parton, R.G., 2018. Caveolae: Structure, Function, and Relationship to Disease. Annu. Rev. Cell Dev. Biol. 34, 111–136. https://doi.org/10.1146/annurev-cellbio-100617-062737.

Parton, R.G., 2001. Life without caveolae. Science (80-.). https://doi.org/10.1126/science.1065677.

Pastor-Flores, D., Schulze, J.O., Bahí, A., Süß, E., Casamayor, A., Biondi, R.M., 2016. Lipid regulators of Pkh2 in Candida albicans, the protein kinase ortholog of mammalian PDK1. Biochim. Biophys. Acta - Mol. Cell

Biol. Lipids 1861, 249–259. https://doi.org/10.1016/j.bbalip.2015.12.016.

Pearce, L.R., Komander, D., Alessi, D.R., 2010. The nuts and bolts of AGC protein kinases. Nat. Rev. Mol. Cell Biol. 11, 9–22. https://doi.org/10.1038/nrm2822.

Pedroso, N., Matias, A.C., Cyrne, L., Antunes, F., Borges, C., Malhó, R., de Almeida, R.F.M., Herrero, E., Marinho, H.S., 2009. Modulation of plasma membrane lipid profile and microdomains by H2O2 in Saccharomyces cerevisiae. Free Radic. Biol. Med. 46, 289–98. https://doi.org/10.1016/j.freeradbiomed.2008.10.039.

Pineau, L., Bonifait, L., Berjeaud, J.-M., Alimardani-Theuil, P., Bergès, T., Ferreira, T., 2008. A Lipid-mediated Quality Control Process in the Golgi Apparatus in Yeast. Mol. Biol. Cell 19, 807–821. https://doi.org/10.1091/mbc.e07-06-0600.

Prieto, S., De La Cruz, B.J., Scheffler, I.E., 2000. Glucose-regulated turnover of mRNA and the influence of poly(A) tail length on half-life. J. Biol. Chem. 275, 14155–14166. https://doi.org/10.1074/jbc.275.19.14155.

Qian, W., Ma, D., Xiao, C., Wang, Z., Zhang, J., 2012. The genomic landscape and evolutionary resolution of antagonistic pleiotropy in yeast. Cell Rep. 2, 1399–410. https://doi.org/10.1016/j.celrep.2012.09.017.

Raymond, C.K., Howald-Stevenson, I., Vater, C.A., Stevens, T.H., 1992. Morphological classification of the yeast vacuolar protein sorting mutants: evidence for a prevacuolar compartment in class E vps mutants. Mol. Biol. Cell 3, 1389–1402. https://doi.org/10.1091/mbc.3.12.1389.

Redder, P., 2016. How does sub-cellular localization affect the fate of bacterial mRNA? Curr. Genet. https://doi.org/10.1007/s00294-016-0587-1.

Reijnst, P., Walther, A., Wendland, J., 2011. Dual-colour fluorescence microscopy using yEmCherry-/GFP-tagging of eisosome components Pil1 and Lsp1 in Candida albicans. Yeast 28, 331–338. https://doi.org/10.1002/yea.1841.

Riggi, M., Bourgoint, C., Macchione, M., Matile, S., Loewith, R., Roux, A., 2019. TORC2 controls endocytosis through plasma membrane tension. J. Cell Biol. 218, 2265–2276. https://doi.org/10.1083/jcb.201901096.

Roelants, F.M., Breslow, D.K., Muir, A., Weissman, J.S., Thorner, J., 2011. Protein kinase Ypk1 phosphorylates regulatory proteins Orm1 and Orm2 to control sphingolipid homeostasis in Saccharomyces cerevisiae. Proc. Natl. Acad. Sci. U. S. A. 108, 19222–7. https://doi.org/10.1073/pnas.1116948108.

Roelants, F.M., Leskoske, K.L., Martinez Marshall, M.N., Locke, M.N., Thorner, J., 2017. The TORC2-Dependent Signaling Network in the Yeast Saccharomyces cerevisiae. Biomolecules 7. https://doi.org/10.3390/biom7030066.

Roelants, F.M., Torrance, P.D., Bezman, N., Thorner, J., 2002. Pkh1 and Pkh2 differentially phosphorylate and activate Ypk1 and Ykr2 and define protein kinase modules required for maintenance of cell wall integrity. Mol. Biol. Cell 13, 3005–28. https://doi.org/10.1091/mbc.e02-04-0201.

Roelants, F.M., Torrance, P.D., Thorner, J., 2004. Differential roles of PDK1- and PDK2-phosphorylation sites in the yeast AGC kinases Ypk1, Pkc1 and Sch9. Microbiology 150, 3289–304. https://doi.org/10.1099/mic.0.27286-0.

Saitoh, S., Mori, A., Uehara, L., Masuda, F., Soejima, S., Yanagida, M., 2015. Mechanisms of expression and translocation of major fission yeast glucose transporters regulated by CaMKK/phosphatases, nuclear shuttling, and TOR. Mol. Biol. Cell 26, 373–386. https://doi.org/10.1091/mbc.E14-11-1503.

Scheffler, I.E., De La Cruz, B.J., Prieto, S., 1998. Control of mRNA turnover as a mechanism of glucose repression

in Saccharomyces cerevisiae. Int. J. Biochem. Cell Biol. https://doi.org/10.1016/S1357-2725(98)00086-7.

Schneider, C.A., Rasband, W.S., Eliceiri, K.W., 2012. NIH Image to ImageJ: 25 years of image analysis. Nat. Methods. https://doi.org/10.1038/nmeth.2089.

Seger, S., Rischatsch, R., Philippsen, P., 2011. Formation and stability of eisosomes in the filamentous fungus Ashbya gossypii. J. Cell Sci. 124, 1629–1634. https://doi.org/10.1242/jcs.082487.

Seo, A.Y., Lau, P.-W., Feliciano, D., Sengupta, P., Gros, M.A. Le, Cinquin, B., Larabell, C.A., Lippincott-Schwartz, J., 2017. AMPK and vacuole-associated Atg14p orchestrate μ-lipophagy for energy production and long-term survival under glucose starvation. Elife 6. https://doi.org/10.7554/eLife.21690.

Shpilka, T., Welter, E., Borovsky, N., Amar, N., Mari, M., Reggiori, F., Elazar, Z., 2015. Lipid droplets and their component triglycerides and steryl esters regulate autophagosome biogenesis. EMBO J. 34, 2117–31. https://doi.org/10.15252/embj.201490315.

Sinha, B., Köster, D., Ruez, R., Gonnord, P., Bastiani, M., Abankwa, D., Stan, R. V., Butler-Browne, G., Vedie, B., Johannes, L., Morone, N., Parton, R.G., Raposo, G., Sens, P., Lamaze, C., Nassoy, P., 2011. Cells respond to mechanical stress by rapid disassembly of caveolae. Cell 144, 402–13. https://doi.org/10.1016/j.cell.2010.12.031.

Siniossoglou, S., Santos-Rosa, H., Rappsilber, J., Mann, M., Hurt, E., 1998. A novel complex of membrane proteins required for formation of a spherical nucleus. EMBO J. 17, 6449–6464. https://doi.org/10.1093/emboj/17.22.6449.

Sipiczki, M., 2000. Where does fission yeast sit on the tree of life? Genome Biol. 1, 1011.1-1011.4. https://doi.org/10.1186/gb-2000-1-2-reviews1011.

Skrzypek, M.S., Nagiec, M.M., Lester, R.L., Dickson, R.C., 1999. Analysis of phosphorylated sphingolipid long-chain bases reveals potential roles in heat stress and growth control in Saccharomyces. J. Bacteriol. 181, 1134–1140.

Sleytr, U., Silva, M., Kocur, M., Lewis, N., 1976. The fine structure of Micrococcus radiophilus and Micrococcus radioproteolyticus. Arch. Microbiol. 107, 313–20.

Solinger, J.A., Pascolini, D., Heyer, W.-D., 1999. Active-Site Mutations in the Xrn1p Exoribonuclease of Saccharomyces cerevisiae Reveal a Specific Role in Meiosis. Mol. Cell. Biol. 19, 5930–5942. https://doi.org/10.1128/MCB.19.9.5930.

Southworth, D., Strout, G., Russell, S.D., 1997. Freeze-fracture of sperm of Plumbago zeylanica L. in pollen and in vitro. Sex. Plant Reprod. 10, 217–226. https://doi.org/10.1007/s004970050090.

Spira, F., Mueller, N.S., Beck, G., Von Olshausen, P., Beig, J., Wedlich-Söldner, R., 2012. Patchwork organization of the yeast plasma membrane into numerous coexisting domains. Nat. Cell Biol. 14, 640–648. https://doi.org/10.1038/ncb2487.

Stancevic, B., Kolesnick, R., 2010. Ceramide-rich platforms in transmembrane signaling. FEBS Lett. 584, 1728–40. https://doi.org/10.1016/j.febslet.2010.02.026.

Standaert, M.L., Bandyopadhyay, G., Galloway, L., Soto, J., Ono, Y., Kikkawa, U., Farese, R. V., Leitges, M., 1999. Effects of knockout of the protein kinase C β gene on glucose transport and glucose homeostasis. Endocrinology 140, 4470–4477. https://doi.org/10.1210/endo.140.10.7073.

Stimpson, H.E.M., Toret, C.P., Cheng, A.T., Pauly, B.S., Drubin, D.G., 2009. Early-Arriving Syp1p and Ede1p Function in Endocytic Site Placement and Formation in Budding Yeast. Mol. Biol. Cell 20, 4640–4651.

https://doi.org/10.1091/mbc.E09-05-0429.

Stolz, L.E., Huynh, C. V, Thorner, J., York, J.D., 1998. Identification and characterization of an essential family of inositol polyphosphate 5-phosphatases (INP51, INP52 and INP53 gene products) in the yeast Saccharomyces cerevisiae. Genetics 148, 1715–29.

Stradalova, V., Blazikova, M., Grossmann, G., Opekarová, M., Tanner, W., Malinsky, J., 2012. Distribution of cortical endoplasmic reticulum determines positioning of endocytic events in yeast plasma membrane. PLoS One 7, e35132. https://doi.org/10.1371/journal.pone.0035132.

Stradalova, V., Stahlschmidt, W., Grossmann, G., Blazikova, M., Rachel, R., Tanner, W., Malinsky, J., 2009. Furrow-like invaginations of the yeast plasma membrane correspond to membrane compartment of Can1. J. Cell Sci. 122, 2887–2894. https://doi.org/10.1242/jcs.051227.

Sturgill, T.W., Cohen, A., Diefenbacher, M., Trautwein, M., Martin, D.E., Hall, M.N., 2008. TOR1 and TOR2 have distinct locations in live cells. Eukaryot. Cell 7, 1819–30. https://doi.org/10.1128/EC.00088-08.

Sun, Y., Miao, Y., Yamane, Y., Zhang, C., Shokat, K.M., Takematsu, H., Kozutsumi, Y., Drubin, D.G., 2012. Orm protein phosphoregulation mediates transient sphingolipid biosynthesis response to heat stress via the Pkh-Ypk and Cdc55-PP2A pathways. Mol. Biol. Cell 23, 2388–98. https://doi.org/10.1091/mbc.E12-03-0209.

Suzuki, C., Hori, Y., Kashiwagi, Y., 2003. Screening and characterization of transposon-insertion mutants in a pseudohyphal strain of Saccharomyces cerevisiae. Yeast 20, 407–15. https://doi.org/10.1002/yea.970

Svoboda, A., Trujillo-Gonzales, A., 1990. Sporothrix schenckii--a freeze-fracture study. J. Basic Microbiol. 30, 371–8.

Swinnen, E., Ghillebert, R., Wilms, T., Winderickx, J., 2014. Molecular mechanisms linking the evolutionary conserved TORC1-Sch9 nutrient signalling branch to lifespan regulation in Saccharomyces cerevisiae. FEMS Yeast Res. 14, 17–32. https://doi.org/10.1111/1567-1364.12097.

Swinnen, E., Wilms, T., Idkowiak-Baldys, J., Smets, B., De Snijder, P., Accardo, S., Ghillebert, R., Thevissen, K., Cammue, B., De Vos, D., Bielawski, J., Hannun, Y.A., Winderickx, J., 2013. The protein kinase Sch9 is a key regulator of sphingolipid metabolism in Saccharomyces cerevisiae. Mol. Biol. Cell 25, 196–211. https://doi.org/10.1091/mbc.e13-06-0340.

Tabuchi, M., Audhya, A., Parsons, A.B., Boone, C., Emr, S.D., 2006. The Phosphatidylinositol 4,5-Biphosphate and TORC2 Binding Proteins Slm1 and Slm2 Function in Sphingolipid Regulation. Mol. Cell. Biol. 26, 5861–5875. https://doi.org/10.1128/MCB.02403-05.

Takeo, K., 1984. Lack of invaginations of the plasma membrane during budding and cell division of Saccharomyces cerevisiae and Schizosaccharomyces pombe. FEMS Microbiol. Lett. 22, 97–100.

Thayer, N.H., Leverich, C.K., Fitzgibbon, M.P., Nelson, Z.W., Henderson, K.A., Gafken, P.R., Hsu, J.J., Gottschling, D.E., 2014. Identification of long-lived proteins retained in cells undergoing repeated asymmetric divisions. Proc. Natl. Acad. Sci. U. S. A. 111, 14019–26. https://doi.org/10.1073/pnas.1416079111.

Thomas, M.G., Boccaccio, G.L., 2016. Novel mRNA-silencing bodies at the synapse: A never-ending story. Commun. Integr. Biol. 9, e1139251. https://doi.org/10.1080/19420889.2016.1139251.

Toulmay, A., Prinz, W.A., 2013. Direct imaging reveals stable, micrometer-scale lipid domains that segregate proteins in live cells. J. Cell Biol. 202, 35–44. https://doi.org/10.1083/jcb.201301039.

Tsuji, T., Fujimoto, M., Tatematsu, T., Cheng, J., Orii, M., Takatori, S., Fujimoto, T., 2017. Niemann-Pick type C proteins promote microautophagy by expanding raft-like membrane domains in the yeast vacuole. Elife 6. https://doi.org/10.7554/eLife.25960.

Tsuji, T., Fujimoto, T., 2018. Lipids and lipid domains of the yeast vacuole. Biochem. Soc. Trans. https://doi.org/10.1042/BST20180120.

Umebayashi, K., Nakano, A., 2003. Ergosterol is required for targeting of tryptophan permease to the yeast plasma membrane. J. Cell Biol. 161, 1117–1131. https://doi.org/10.1083/jcb.200303088.

Urban, J., Soulard, A., Huber, A., Lippman, S., Mukhopadhyay, D., Deloche, O., Wanke, V., Anrather, D., Ammerer, G., Riezman, H., Broach, J.R., De Virgilio, C., Hall, M.N., Loewith, R., 2007. Sch9 Is a Major Target of TORC1 in Saccharomyces cerevisiae. Mol. Cell 26, 663–74. https://doi.org/10.1016/j.molcel.2007.04.020.

van Zutphen, T., Todde, V., de Boer, R., Kreim, M., Hofbauer, H.F., Wolinski, H., Veenhuis, M., van der Klei, I.J., Kohlwein, S.D., 2014. Lipid droplet autophagy in the yeast Saccharomyces cerevisiae. Mol. Biol. Cell 25, 290–301. https://doi.org/10.1091/mbc.E13-08-0448.

Vangelatos, I., Roumelioti, K., Gournas, C., Suarez, T., Scazzocchio, C., Sophianopoulou, V., 2010. Eisosome organization in the filamentous ascomycete Aspergillus nidulans. Eukaryot. Cell 9, 1441–1454. https://doi.org/10.1128/EC.00087-10.

Varlakhanova, N. V., Tornabene, B.A., Ford, M.G.J., 2018. Ivy1 is a negative regulator of Gtr-dependent TORC1 activation. J. Cell Sci. 131. https://doi.org/10.1242/jcs.218305.

Vaškovičová, K., Awadová, T., Veselá, P., Balážová, M., Opekarová, M., Malinsky, J., 2017. mRNA decay is regulated via sequestration of the conserved 5′-3′ exoribonuclease Xrn1 at eisosome in yeast. Eur. J. Cell Biol. 96, 591–599. https://doi.org/10.1016/j.ejcb.2017.05.001.

Vaskovicova, K., Stradalova, V., Efenberk, A., Opekarova, M., Malinsky, J., 2015. Assembly of fission yeast eisosomes in the plasma membrane of budding yeast: Import of foreign membrane microdomains. Eur. J. Cell Biol. 94, 1–11. https://doi.org/10.1016/j.ejcb.2014.10.003.

Vecer, J., Vesela, P., Malinsky, J., Herman, P., 2014. Sphingolipid levels crucially modulate lateral microdomain organization of plasma membrane in living yeast. FEBS Lett. 588, 443–9. https://doi.org/10.1016/j.febslet.2013.11.038.

Vida, T.A., Emr, S.D., 1995. A new vital stain for visualizing vacuolar membrane dynamics and endocytosis in yeast. J. Cell Biol. 128, 779–92.

Voordeckers, K., Kimpe, M., Haesendonckx, S., Louwet, W., Versele, M., Thevelein, J.M., 2011. Yeast 3-phosphoinositide-dependent protein kinase-1 (PDK1) orthologs Pkh1-3 differentially regulate phosphorylation of protein kinase A (PKA) and the protein kinase B (PKB)/S6K ortholog Sch9. J. Biol. Chem. 286, 22017–27. https://doi.org/10.1074/jbc.M110.200071.

Walther, T.C., Aguilar, P.S., Fröhlich, F., Chu, F., Moreira, K., Burlingame, A.L., Walter, P., 2007. Pkh-kinases control eisosome assembly and organization. EMBO J. 26, 4946–4955. https://doi.org/10.1038/sj.emboj.7601933.

Walther, T.C., Brickner, J.H., Aguilar, P.S., Bernales, S., Pantoja, C., Walter, P., 2006. Eisosomes mark static sites of endocytosis. Nature 439, 998–1003. https://doi.org/10.1038/nature04472.

Wang, C.-W., 2014. Stationary phase lipophagy as a cellular mechanism to recycle sterols during quiescence.

Autophagy 10, 2075–6. https://doi.org/10.4161/auto.36137.

Wang, C.-W., Miao, Y.-H., Chang, Y.-S., 2014. A sterol-enriched vacuolar microdomain mediates stationary phase lipophagy in budding yeast. J. Cell Biol. 206, 357–366. https://doi.org/10.1083/jcb.201404115.

Wang, H.X., Douglas, L.M., Aimanianda, V., Latgé, J.P., Konopka, J.B., 2011. The Candida albicans Sur7 protein is needed for proper synthesis of the fibrillar component of the cell wall that confers strength. Eukaryot. Cell 10, 72–80. https://doi.org/10.1128/EC.00167-10.

Wang, H.X., Douglas, L.M., Vesela, P., Rachel, R., Malinsky, J., Konopka, J.B., 2016. Eisosomes promote the ability of Sur7 to regulate plasma membrane organization in Candida albicans. Mol. Biol. Cell 27, 1663–1675. https://doi.org/10.1091/mbc.E16-01-0065.

Wilson-Grady, J.T., Villen, J., Gygi, S.P., 2008. Phosphoproteome analysis of fission yeast. J. Proteome Res. 7, 1088–1097. https://doi.org/10.1021/pr7006335.

Xu, T., Shively, C.A., Jin, R., Eckwahl, M.J., Dobry, C.J., Song, Q., Kumar, A., 2010. A Profile of Differentially Abundant Proteins at the Yeast Cell Periphery during Pseudohyphal Growth. J. Biol. Chem. 285, 15476. https://doi.org/10.1074/JBC.M110.114926.

Xu, X., Okamoto, K., 2018. The Nem1-Spo7 protein phosphatase complex is required for efficient mitophagy in yeast. Biochem. Biophys. Res. Commun. 496, 51–57. https://doi.org/10.1016/j.bbrc.2017.12.163.

Yamamoto, A., DeWald, D.B., Boronenkov, I. V, Anderson, R.A., Emr, S.D., Koshland, D., 1995. Novel PI(4)P 5-kinase homologue, Fab1p, essential for normal vacuole function and morphology in yeast. Mol. Biol. Cell 6, 525–39. https://doi.org/10.1091/mbc.6.5.525.

Yin, Z., Smith, R.J., Brown, A.J., 1996. Multiple signalling pathways trigger the exquisite sensitivity of yeast gluconeogenic mRNAs to glucose. Mol. Microbiol. 20, 751–64. https://doi.org/10.1111/j.1365-2958.1996.tb02514.x.

Yoshikawa, K., Tanaka, T., Furusawa, C., Nagahisa, K., Hirasawa, T., Shimizu, H., 2009. Comprehensive phenotypic analysis for identification of genes affecting growth under ethanol stress in Saccharomyces cerevisiae. FEMS Yeast Res. 9, 32–44. https://doi.org/10.1111/j.1567-1364.2008.00456.x.

Young, M.E., Karpova, T.S., Brugger, B., Moschenross, D.M., Wang, G.K., Schneiter, R., Wieland, F.T., Cooper, J.A., 2002. The Sur7p Family Defines Novel Cortical Domains in Saccharomyces cerevisiae, Affects Sphingolipid Metabolism, and Is Involved in Sporulation. Mol. Cell. Biol. 22, 927–934. https://doi.org/10.1128/MCB.22.3.927-934.2002.

Yu, H., Braun, P., Yildirim, M.A., Lemmens, I., Venkatesan, K., Sahalie, J., Hirozane-Kishikawa, T., Gebreab, F., Li, N., Simonis, N., Hao, T., Rual, J.-F., Dricot, A., Vazquez, A., Murray, R.R., Simon, C., Tardivo, L., Tam, S., Svrzikapa, N., Fan, C., de Smet, A.-S., Motyl, A., Hudson, M.E., Park, J., Xin, X., Cusick, M.E., Moore, T., Boone, C., Snyder, M., Roth, F.P., Barabasi, A.-L., Tavernier, J., Hill, D.E., Vidal, M., 2008. High-Quality Binary Protein Interaction Map of the Yeast Interactome Network. Science (80-.). 322, 104–110. https://doi.org/10.1126/science.1158684.

Yu, J.W., Mendrola, J.M., Audhya, A., Singh, S., Keleti, D., DeWald, D.B., Murray, D., Emr, S.D., Lemmon, M.A., 2004. Genome-wide analysis of membrane targeting by S. cerevisiae pleckstrin homology domains. Mol. Cell 13, 677–688. https://doi.org/10.1016/S1097-2765(04)00083-8.

Zahn, R., Stevenson, B.J., Schröder-Köhne, S., Zanolari, B., Riezman, H., Munn, A.L., 2001. End13p/Vps4p is required for efficient transport from early to late endosomes in Saccharomyces cerevisiae. J. Cell Sci. 114,

1935–47.

Zhang, L.-B., Tang, L., Ying, S.-H., Feng, M.-G., 2017. Two eisosome proteins play opposite roles in autophagic control and sustain cell integrity, function and pathogenicity in Beauveria bassiana. Environ. Microbiol. 19, 2037–2052. https://doi.org/10.1111/1462-2920.13727.

Zhang, X., Lester, R.L., Dickson, R.C., 2004. Pil1p and Lsp1p negatively regulate the 3-phosphoinositide-dependent protein kinase-like kinase Pkh1p and downstream signaling pathways Pkc1p and Ypk1p. J. Biol. Chem. 279, 22030–22038. https://doi.org/10.1074/jbc.M400299200.

Zinser, E., Daum, G., 1995. Isolation and biochemical characterization of organelles from the yeast, Saccharomyces cerevisiae. Yeast 11, 493–536. https://doi.org/10.1002/yea.320110602.

Zinser, E., Paltauf, F., Daum, G., 1993. Sterol composition of yeast organelle membranes and subcellular distribution of enzymes involved in sterol metabolism. J. Bacteriol. 175, 2853–8. https://doi.org/10.1128/jb.175.10.2853-2858.1993.

Ziółkowska, N.E., Karotki, L., Rehman, M., Huiskonen, J.T., Walther, T.C., 2011. Eisosome-driven plasma membrane organization is mediated by BAR domains. Nat. Struct. Mol. Biol. 18, 854–856. https://doi.org/10.1038/nsmb.2080.

9. Appendices

Appendix 1:

Vaskovicova K., Stradalova V., Efenberk A., Opekarova M., and Malinsky J. (2015)

Assembly of fission yeast eisosomes in the plasma membrane of budding yeast: import of foreign membrane microdomains.

Eur J Cell Biol 94(1): 1-11.

PMID: 25457676.

DOI: 10.1016/j.ejcb.2014.10.003.

Appendix 2:

Vaškovičová K., Awadová T., Veselá P., Balážová M., Opekarová M., and Malinsky J. (2017)

mRNA decay is regulated via sequestration of the conserved 5'-3' exoribonuclease Xrn1 at eisosome in yeast.

Eur J Cell Biol 96(6) 591-599.

PMID: 28501103.

DOI: 10.1016/j.ejcb.2017.05.001.